MASSACHUSETTS INSTITUTE OF TECHNOLOGY

APOLLO

GUIDANCE, NAVIGATION AND CONTROL

E-1982

LEM PGNCS AND LANDING RADAR OPERATIONS DURING THE POWERED LUNAR LANDING MANEUVER

by

B. Kriegsman*

N. Sears

August 1966

MIT INSTRUMENTATION LABORATORY

CAMBRIDGE 39, MASSACHUSETTS

MASSACHUSETTS INSTITUTE OF TECHNOLOGY

APOLLO

GUIDANCE, NAVIGATION AND CONTROL

Approved: D. G. Hoag Date: 18 Aug 66
for RICHARD H. BATTIN, DIRECTOR, MISSION DEVEL.
APOLLO GUIDANCE AND NAVIGATION PROGRAM

Approved: D. G. Hoag Date: 18 Aug 66
DAVID G. HOAG, DIRECTOR
APOLLO GUIDANCE AND NAVIGATION PROGRAM

Approved: Ralph R. Ragan Date: 18 Aug 66
RALPH R. RAGAN, DEPUTY DIRECTOR
INSTRUMENTATION LABORATORY

E-1982

LEM PGNCS AND LANDING RADAR OPERATIONS DURING THE POWERED LUNAR LANDING MANEUVER

by
B. Kriegsman*
N. Sears

August 1966

MIT INSTRUMENTATION LABORATORY
CAMBRIDGE 39, MASSACHUSETTS

*Raytheon Resident

COPY # 133

ACKNOWLEDGEMENT

This report was prepared under DSR Project 55-238, sponsored by the Manned Spacecraft Center of the National Aeronautics and Space Administration through Contract NAS 9-4065.

E-1982

LEM PGNCS AND LANDING RADAR OPERATIONS DURING THE POWERED LUNAR LANDING MANEUVER

ABSTRACT

This report summarizes the results of a study of the LEM primary guidance, navigation, and control system during automatic controlled powered landing maneuvers prior to touchdown on the moon. The navigation system employs an inertial-measurement unit as the primary sensor, updated at discrete intervals of time by landing-radar altitude and velocity measurements. The vehicle steering commands are based on the difference between the present and desired terminal state of the vehicle. Both the navigation and guidance systems are described in detail, including key mathematical relations. Particular attention is given to the development and selection of weighting functions to use in the updating of the navigation system by the landing-radar measurements. Extensive data are presented from a digital-simulation study of the guidance-and-navigation system performance in the presence of initial-condition errors, propulsion-system uncertainties, random and bias sensor errors, and lunar terrain altitude variations.

by B. A. Kriegsman*
N. E. Sears

June 15, 1966

* Raytheon Resident Staff

TABLE OF CONTENTS

TABLE OF CONTENTS (Cont'd)

CHAPTER 1

GENERAL INFORMATION

1.1 Definition of Guidance and Navigation Problem

This report is concerned with the primary guidance, navigation, and control system (PGNCS) of the LEM during the powered landing prior to touchdown on the moon. The particular phase of interest here begins when the LEM's descent engine is ignited, at which time the LEM is travelling at an essentially horizontal velocity of about 5600 ft/sec at an altitude of about 50,000 feet above the lunar surface. Typically this occurs about 60 minutes after the descent orbit injection of the LEM from the CSM 80-mile-altitude lunar orbit. The landing maneuver to be studied here nominally lasts for about 10 minutes. During this period the LEM's velocity is reduced from the initial value of 5600 ft/sec to a final value of about 3 ft/sec, while at the same time the LEM's altitude is decreased from 50,000 to about 115 feet. Specifically, this report deals with the completely automatic mode of operation of the LEM guidance and navigation system from the start of the landing maneuver to the point at which the hover maneuver begins (Low-Gate point).

The basic objective for the guidance and navigation system considered here is to control the LEM in such a manner that the preselected Low-Gate conditions (altitude and velocity) are achieved within a desired accuracy. In the process of meeting this objective, the guidance and navigation system must satisfy many different constraints and requirements imposed both by the nature of the mission and the characteristics of the existing subsystems. A detailed discussion of the trajectory constraints at the time this study was made are given in Appendix A, including the requirements for site redesignation.[1*] The most important objectives for the guidance and navigation system can be summarized as follows:

1) Propellant must be utilized as efficiently as possible during the deceleration phase, i.e. the required characteristic velocity (ΔV) should be as low as possible.

---

*Numerical superscripts refer to similarly numbered references in the Bibliography.

2) The selected landing site should lie at least 10 degrees above the edge of the LEM's window for a minimum of 75 seconds just prior to arrival at the Low-Gate point.

3) To minimize descent engine throat erosion, the descent propulsion system (DPS) must either be operated at a specified fixed high-throttle settting of 92.5 percent of the maximum specified thrust (10,500 lbs), or over a range of lower throttle positions from 10 to 60 percent of maximum thrust. There is a range of throttle settings over which the engine should not be operated, e.g. 60 to 92.5 percent of nominal thrust. To minimize vehicle attitude transients, switching the throttle back and forth from the 10-60 percent operating region to the fixed 92.5-percent setting is not desirable.

4) The powered landing maneuver is an extremely critical phase of the landing with regard to LEM computation-time requirements. It is therefore important that the computation times for the landing-maneuver guidance and navigation computations be compatible with the various other functions that must be performed on the LEM during the landing maneuver.

The general approach to the problem of LEM guidance and navigation during the landing maneuver will next be discussed. Before doing this, it is appropriate to distinguish between the basic functions of the guidance and navigation systems. The navigation system basically determines (estimates) the state of the vehicle, i.e. its position and velocity. The guidance system uses the navigation information to steer the vehicle such that the desired mission objectives are achieved. The relationship between the guidance and navigation systems is shown in the simplified functional diagram of Fig. 1.1. The emphasis in this report is on the navigation system, in particular on the landing-radar (LR) sensor-information processing techniques and on operations in the LEM PGNCS computer (LGC).

1.2 Navigation Concept for the Landing Maneuver

To accomplish the navigation of the LEM, an inertial measurement unit (IMU) and a landing radar are provided on-board the vehicle. The IMU, which is the primary navigation sensor, measures the net specific force (thrust acceleration and nongravitational field forces) acting on the vehicle. The IMU operates continuously throughout the landing maneuver. The landing radar provides data of the velocity of the vehicle relative to the lunar surface (doppler frequency-shift data), and vehicle altitude data above the local terrain. These doppler-velocity and altitude* measurements are used to update the IMU at discrete intervals of time during the powered landing maneuver. The time at which the updating process is begun and the spacing between successive updatings are strongly dependent on the performance characteristics of the landing

*The physical quantity actually measured by the LR is the range from the vehicle to a point on the lunar surface, along the direction of the landing-radar range beam. The primary navigation information derived from this measurement is the altitude of the vehicle above the local terrain. For this reason the range measurement is loosely referred to throughout this report as an altitude rather than a range measurement.

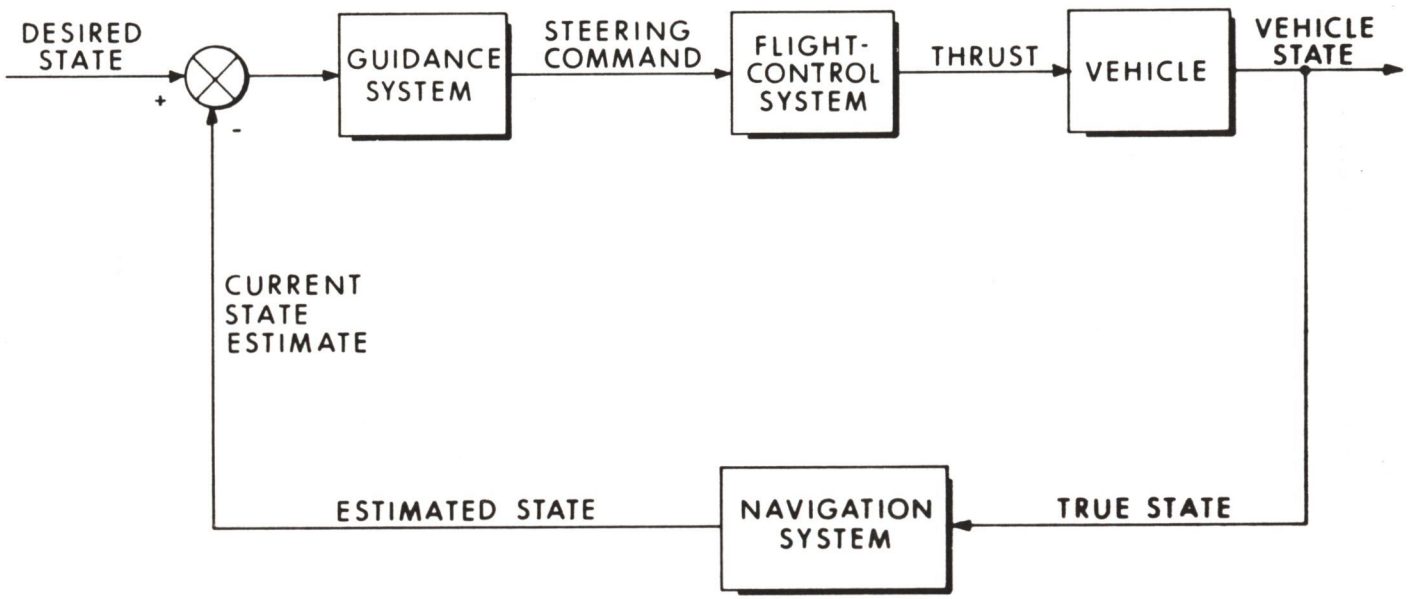

Fig. 1.1 Functional Diagram Showing Relationships between Guidance and Navigation Systems for LEM

radar and the time required for processing the given measurement. Typically, altitude measurements are initially taken when the LEM is at an estimated altitude of 25,000 ft; velocity measurements are begun when the LEM is at an estimated altitude of 15,000 ft. The spacing between successive altitude updatings is typically 2 seconds. For velocity updatings, on the other hand, the spacing between successive updatings is typically 6 to 8 seconds. As will be shown later, in order for the LEM to meet Low-Gate conditions with a satisfactory accuracy, within desired propellant limits, and with adequate site visibility enroute, it is very important to achieve effective LR updating of the IMU.

The actual estimates of vehicle position and velocity generated in the navigation system are based on the optimum linear estimators developed by Kalman[2] and Battin[3]. Up-to-date estimates of the vehicle's state are obtained by comparing landing-radar measurements with IMU-derived estimates of the same physical quantities. This measurement difference properly weighted is used to update the a-priori* vehicle state estimates. In between updatings, the state estimates are extrapolated forward by integrating the two-body equations of motion for the vehicle, with the IMU providing the required specific force data.

The key to the updating process is the choice of weighting functions used in the incorporation of each new measurement into the state estimate. For the processing of altitude information a single weighting function (w_h) is used in the computer. The velocity information, on the other hand, is processed as three individual components along the orthogonal set of landing-radar antenna axes (XA, YA, and ZA). Hence, three weighting functions (w_{VXA}, w_{VYA}, and w_{VZA}) are used in the velocity updating process. All of these weighting functions are precomputed and stored for in-flight use in the LGC. The altitude weighting function is stored as a linear function of vehicle altitude. The velocity weighting functions are stored as linear functions of vehicle speed. The factors involved in the selection of navigation-system weighting functions are discussed in Sec. 1.4 and in Chapter 4 of this report.

1.3 Guidance Concept for the Landing Maneuver

To accomplish the landing-maneuver mission in an efficient manner, it is desirable to separate the landing maneuver into two major phases. For convenience these two phases will be referred to as the braking and visibility phases, as shown in Fig. 1.2. The basic function of the braking phase is to efficiently decelerate the vehicle to the High-Gate terminal conditions. The High-Gate conditions must be met with a reasonable accuracy in order that the visibility phase be successfully accomplished. The basic

*The terminology of an "a-priori estimate" is used in this report to refer to an estimate of the state prior to the incorporation of the new measurement. The estimate of the state immediately after the processing of the new measurement is referred to as the "up-to-date" or "updated" estimate.

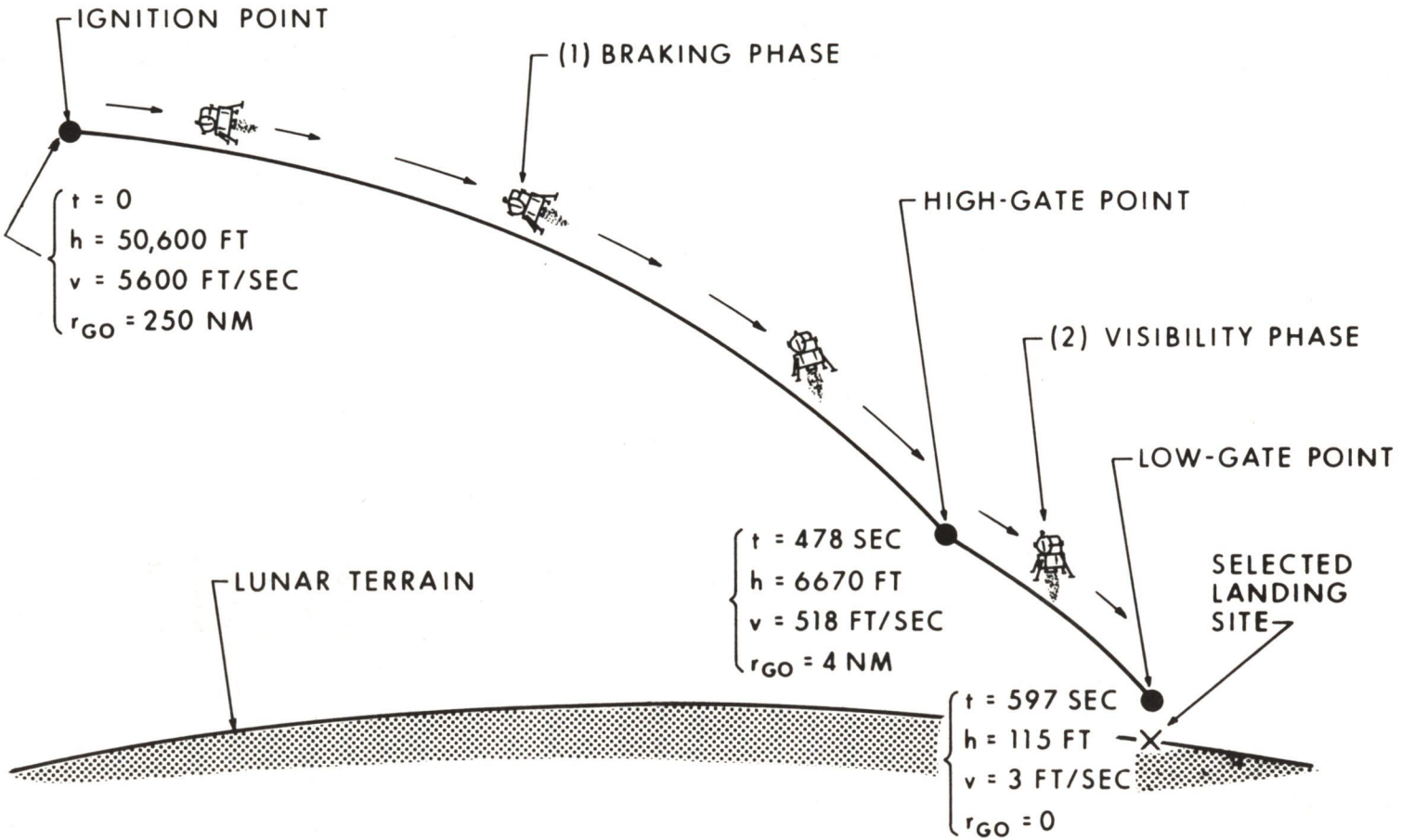

Fig. 1.2 Geometry and Terminology for Landing Maneuver

function of the visibility phase is to allow the astronaut to observe the selected landing site for a reasonable interval of time prior to arrival at the Low-Gate point. The powered landing trajectory used for this study was than considered by MSC for the Design Reference Mission-Two (DRM-2) when this report was prepared.

The desired terminal conditions for the braking and visibility phases are shown in Table 1.1 for the reference landing trajectory. In this trajectory the visibility phase is only about 2 minutes in duration; the braking phase, on the other hand, lasts for about 8 minutes. It is interesting to note that at the High-Gate point, the LEM is 6600 feet above the lunar surface; at the Low-Gate point, on the other hand, the vehicle is only 115 feet above the surface. At the start of the braking phase the LEM is typically about 250 nautical miles from the desired landing site; at the start of the visibility phase, on the other hand, the LEM is generally only 4 mi from the site. The selection of initial and terminal conditions for the braking and visibility phases strongly determine the manner and efficiency with which the guidance system objectives are achieved.

Although the steering profiles are different for the braking and visibility phases, the overall guidance concepts for the two phases are similar. The required specific force (magnitude and direction) at any given time is computed as an explicit function of the difference between the present vehicle state ($\underline{x}$)* and the desired terminal state ($\underline{x}_D$) using the guidance laws presented in Refs. 1 and 4. The values of the present vehicle state used in the guidance computations are the up-to-date estimated values determined in the navigation system. The values used for the desired terminal state are different for the braking and visibility phases: in the braking phase the High-Gate terminal conditions are used; in the visibility phase the Low-Gate terminal conditions are used. The overall landing-maneuver guidance problem in essence is solved as two successive two-point boundary-value guidance problems.

Because of the difference in requirements between the braking and visibility phases, the steering profiles (time histories of thrust magnitude and orientation) are quite different for the two phases. During the braking phase the thrust vector is for the most part in a nearly horizontal orientation; at the same time, the throttle remains fixed at the selected high-thrust operating position (92.5 percent of nominal thrust) except for a short period at the end of the braking phase. During the visibility phase, on the other hand, the vehicle is pitched up to a more nearly vertical orientation, i.e. the thrust vector is typically oriented between 50 and 90 degrees above the local horizontal; at the same time, the throttle is operated in the permissible variable-thrust region (10-60 percent of nominal thrust).

---

*Lower case letters and Greek symbols will generally be reserved for vectors and scalars in this paper. Vectors will be indicated by underlining the symbol, e.g. $\underline{x}$. Upper case letters will be reserved for matrices.

Table 1.1

Desired Terminal Conditions for Braking and Visibility Phases

			Braking Phase (High-Gate Point)	Visibility Phase (Low-Gate Point)
1)	Position	X	-23920 ft	-3.3 ft
		Y	6667 ft	115 ft
		Z	0	0
2)	Velocity*	X	501 ft/s	2.5 ft/s
		Y	-132 ft/s	-1.4 ft/s
		Z	0	0
3)	Acceleration	X	-8.56 f/s^2	-1.25 f/s^2
		Y	-1.33 f/s^2	0.70 f/s^2
		Z	0	0
4)	Jerk	X	-0.010 f/s^3	0.0789 f/s^3
		Y	0.0074 f/s^3	0

Coordinate Axes: Origin at selected landing site location at the nominal landing time.

X = horizontal and forward in plane of nominal trajectory.

Y = vertical and upward in plane of nominal trajectory.

Z = normal to plane of trajectory and directed to form a right-handed X-Y-Z system.

*The velocity data here are presented relative to the rotating lunar terrain.

The guidance system has the capability of steering the vehicle to landing sites changed from the originally-selected site by the astronaut during the visibility phase. A detailed description of the site-redesignation techniques is given in a separate report[1]. This present report is concerned with guidance and navigation of the LEM for the automatic mode of operation with no site redesignations. A more detailed discussion of the guidance system for this mode of operation is given in Chapter 3 of this report, including the basic steering equations.

1.4 Navigation-System Design Considerations

The key to the operation of the navigation system is the selection of weighting functions to use in the processing of each new navigation measurement. This section discusses some of the important factors involved in the determination of the weighting functions and the reasons for the mechanizations finally selected for them.

The choice of weighting functions for a given measurement is basically determined by comparing the expected accuracy of the a-priori state estimates with the expected accuracy of the measurement. Statistical data must, of course, be used in this procedure since the absolute accuracy of a navigation system or a particular navigation measurement at a given time is not usually known. The most widely used procedure for computing weighting functions is to minimize the sum of mean-squared errors in the quantities being estimated, as developed by Kalman[2] and Battin[3]. Estimates of this type are normally referred to as least-squares or minimum-variance estimates, and are generally equivalent to maximum-likelihood estimates.

In order to make a meaningful least-squares or maximum-likelihood estimate of the vehicle's state, it is necessary, ideally, to keep track of the accuracy of the navigation system (statistical errors) throughout the landing maneuver. To accomplish this in the problem under investigation, several factors must be considered. First of all, initial-alignment errors of the inertial platform, gyro drift, accelerometer bias, and accelerometer scale-factor errors cause the navigation information derived from the IMU to become degraded with time. These IMU errors can reasonably be assumed to be predominantly time-invariant bias errors. Second of all, the velocity-measurement accuracy of the landing radar is limited by random errors (noise) in the measurement of vehicle speed; the rms value of these errors is assumed to vary as a function of the speed in the vehicle. Likewise, uncertainties in the knowledge of the orientation of the radar beams with respect to the IMU reference axes limit the accuracy with which vehicle velocity in IMU coordinates can be determined from the radar measurements. Landing-radar altitude measurements, moreover, are limited in accuracy by random errors (noise) whose rms values are dependent upon the altitude of the vehicle above the lunar surface. Finally, variations in the local terrain, i.e. slopes, hills, valleys, and craters, can cause altimeter measurements of local vehicle altitude to be significantly different from the a-priori estimated values in the navigation computer.

To properly determine the accuracy of the navigation system (statistically) during the landing maneuver, a navigation-system model should be used with all of the above-mentioned error sources included. Under these conditions the in-flight computation is not an easy job because of the large number of covariance-matrix terms that must be included in the computer to account for correlations between navigation-sensor and state-vector estimate errors. A particularly difficult problem in this statistical analysis is the treatment of measurement bias errors and terrain-slope variations.

The minimization and simplification of guidance-and-navigation system computations during the LGC time-critical landing maneuver are extremely important. For this reason it was decided not to compute the navigation-system weighting functions in flight. Instead, it was decided to precompute weighting functions for the nominal reference trajectory, based on the most accurate and complete simulations available for the landing maneuver. These weighting functions would then be stored in the LGC as functions of altitude for the altitude measurement data, and as functions of speed for the doppler-velocity measurement data. Theoretically it is possible to update all components of the state vector with the information from each new measurement. To further simplify the navigation computations, however it was decided to update only the component of the state vector corresponding to the measurement quantity with the data from a given measurement; e.g. an altitude measurement is used only to update altitude, and an XA-component velocity measurement is used only to update the XA-component of velocity. For convenience in the report this type of weighting function is referred to as an "uncoupled" weighting function. The end result is that only four weighting functions need to be stored in the on-board computer; one for altitude, and one for each of the three components of velocity being processed. To simplify the required AGC computations still more, these weighting functions will be stored in the computer as simple linear functions of altitude or speed.

In concluding this section, it should be noted that errors in the IMU-derived estimates of the vehicle's state will increase with time during the landing maneuver. Accordingly, in order to accomplish the landing-maneuver objectives successfully (including the capability for site redesignation), the navigation data from the IMU must be updated during the landing maneuver with velocity and altitude information from the landing radar.

CHAPTER 2

PGNCS NAVIGATION SYSTEM DESCRIPTION

2.1 Introduction

In the preceeding chapter the mission objectives for the landing maneuver were discussed, and the proposed guidance-and-navigation-system concepts to accomplish these objectives were described. In the present chapter a more detailed discussion will be given of the navigation system. Included here are the basic equations to be used for extrapolating and updating the state-vector estimates. Also presented are the relations for the weighting functions to be used in the processing of the landing-radar measurement data.

2.2 Method of Operation of Navigation System

The navigation system's basic function is to provide information on the current state of the vehicle, i.e. its position and velocity. This information is then used in the guidance system to steer the vehicle in such a way that the mission objectives are accomplished.

The primary navigation sensor is the inertial measurement unit (IMU) which provides a continuous measurement of the specific force acting on the vehicle during the powered flight. The landing radar provides measurements of the vehicle's altitude and velocity. The LR velocity measurements are of the vehicle's velocity relative to the rotating lunar surface. These landing-radar measurements are used to update the IMU - derived state - vector estimates at discrete intervals of time during the landing maneuvers.

If the IMU were used by itself to navigate the vehicle, the resultant errors in the estimates of vehicle altitude and velocity would build up in time to unacceptably large values. For this reason it is necessary to update the IMU-derived state-vector estimates during the landing maneuver with altitude and velocity data from the landing radar. This is especially advantageous because the errors in the landing-radar measurements tend to decrease as the vehicle approaches the landing site with a reduced velocity.

The landing-radar velocity-measurement data are basically obtained as components along an orthogonal set of axes (XA, YA, and ZA) fixed with respect to

the landing-radar antenna, as shown in Fig 2.1. Each radar beam experiences a doppler-frequency shift proportional to the component of vehicle velocity (relative to the moon) projected along the beam axis. By taking the sums and differences of the frequency shifts from the three beams (f_1, f_2, and f_3), the following relations are obtained for the velocity-component measurements* ($\tilde{v}_{XA}$, $\tilde{v}_{YA}$, and $\tilde{v}_{ZA}$):

$$\tilde{v}_{XA} = \frac{-\lambda (f_1 + f_3)}{4 \sin\theta_v \cos\phi_v} \tag{2-1}$$

$$\tilde{v}_{YA} = \frac{\lambda (f_1 - f_2)}{4 \cos\theta_v} \tag{2-2}$$

$$\tilde{v}_{ZA} = \frac{\lambda (f_3 - f_2)}{4 \sin\theta_v \sin\phi_v} \tag{2-3}$$

where λ is the wavelength of the transmitted radar signals. The quantities θ_v and ϕ_v represent the orientation angles of the doppler-radar beams with respect to the XA-YA-ZA coordinate frame, as shown in Fig. 2.1. The XA-YA-ZA frame, it should be noted, is fixed with respect to the vehicle. Accordingly, this coordinate frame will rotate in inertial space as the vehicle attitude changes during the landing maneuver.

It might be noted that the LGC computes the velocity components of the above equations 2-1 through 2-3 by the following procedure. Upon LGC command, the LR will provide one of the three following sum-or-difference frequencies by allowing the selected LR velocity signal to accumulate in the radar high-speed counter for an 80-millisecond count interval controlled by the LGC. This frequency sample is then transferred to the LGC as

$$s_{XA} = (f_1 + f_3) + f_B \tag{2-4}$$

$$s_{YA} = (f_1 - f_2) + f_B \tag{2-5}$$

$$s_{ZA} = (f_3 - f_2) + f_B \tag{2-6}$$

where s_{XA}, s_{YA}, and s_{ZA} are the signals transferred across the LR-LGC interface, and f_B is a bias frequency. Within the LGC, a digital number corresponding to the numerical value of f_B is subtracted from each of the LR signals, and the velocity along each antenna coordinate axis is computed by

$$\tilde{v}_{XA} = -k_X (f_1 + f_3) \tag{2-7}$$

* A tilda ($\sim$) over a quantity is used to indicate a raw measurement which may have both random and bias errors.

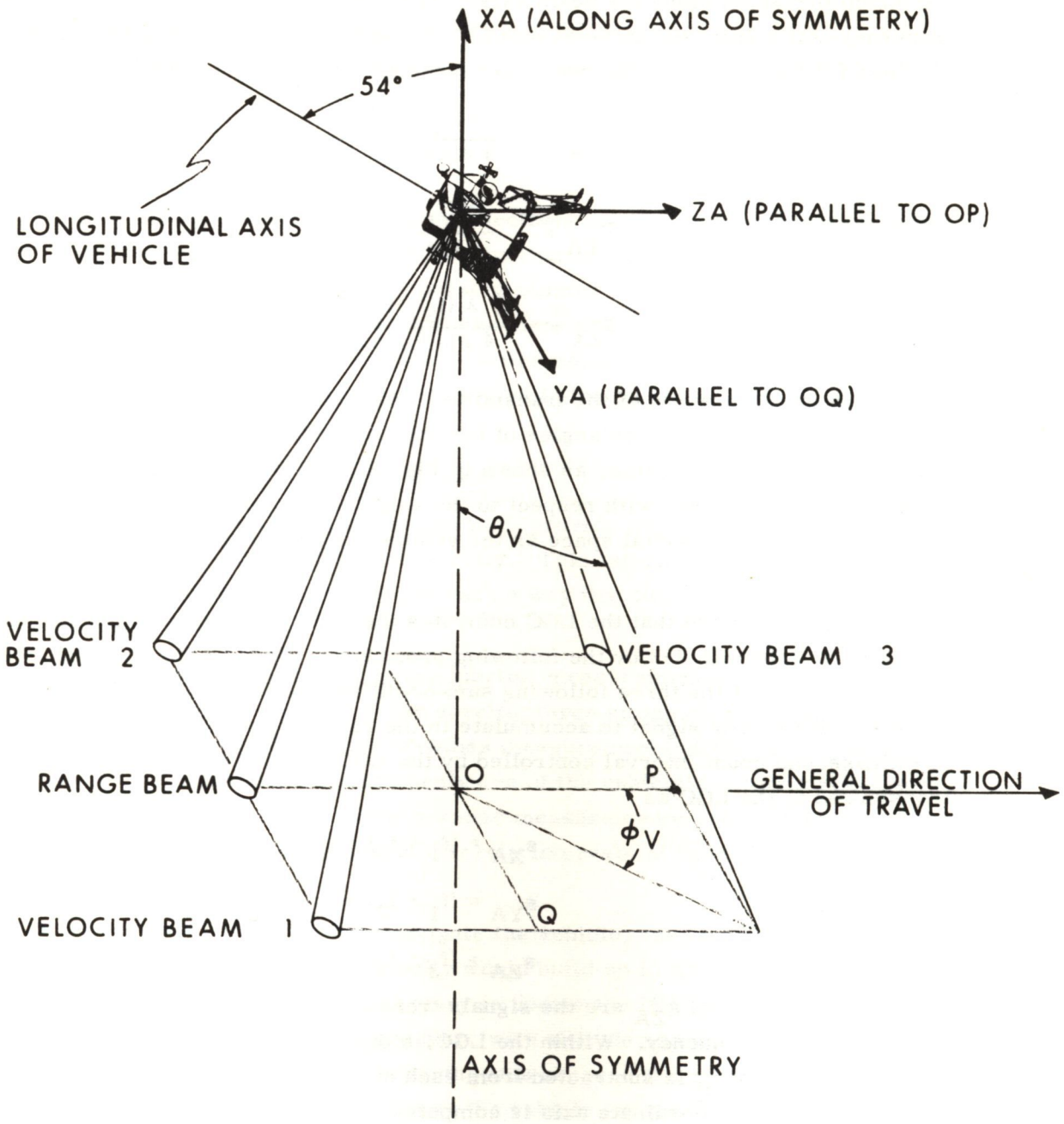

Fig. 2.1 Geometrical Relations for Landing Radar

$$\tilde{v}_{YA} = k_Y (f_1 - f_2) \tag{2-8}$$

$$\tilde{v}_{ZA} = k_Z (f_3 - f_2) \tag{2-9}$$

where k_X, k_Y and k_Z are positive constant scale factors determined by the LR operating frequency and alignment relative to the spacecraft as indicated in equations 2-1 to 2-3. Successive 80-millisecond LR velocity samples along the same antenna axis can be made to provide effective data smoothing to improve LR performance if required.

The landing-radar altitude data are obtained from actual measurements of the range from the vehicle to the lunar surface, directed along the range beam as shown in Fig. 2.1. To obtain altitude data ($\tilde{h}$) from the range data ($\tilde{r}_{LR}$), the range data are simply projected along the direction of the local vertical ($\underline{u}_r$). The mathematical relation is:

$$\tilde{h} = \tilde{r}_{LR} \cos (\theta_R) \tag{2-10}$$

where θ_R is the angle between the direction of the local vertical (estimated) and the range-beam axis. For convenience in this report the range measurement is loosely referred to as an altitude measurement, since the data used in the navigation-system updatings are for updating altitude rather than range.

Each of the three velocity components ($\tilde{v}_{XA}$, $\tilde{v}_{YA}$, and $\tilde{v}_{ZA}$) and the landing-radar altitude measurement ($\tilde{h}$) are incorporated into the state-vector estimate as an individual measurement. In order to utilize the velocity measurement data most efficiently, they are prefiltered or smoothed before incorporation into the estimate.

A typical measurement schedule for processing the altitude and velocity-component data is presented in Fig. 2.2. Each altitude measurement is processed at 2-second intervals, starting when the estimated vehicle altitude is 25,000 feet. The velocity-component measurements are processed with a 2-second interval between the different components, and an 8-second interval between successive measurements for the same velocity component. The first velocity measurement is processed when the estimated vehicle altitude is 15,000 feet. In the particular schedule shown in Fig. 2.2 the velocity-component measurements are processed at essentially the same times as the altitude measurements, with the altitude measurements being processed first.

The basic vehicle state vector ($\underline{x}_n$) contains the three components of vehicle position ($\underline{r}_n$) and velocity ($\underline{v}_n$) in an inertially-fixed rectilinear coordinate frame. The arrangement of the position and velocity elements is by definition:

$$\underline{x}_n \equiv \begin{bmatrix} \underline{r}_n \\ \hline \underline{v}_n \end{bmatrix} \tag{2-11}$$

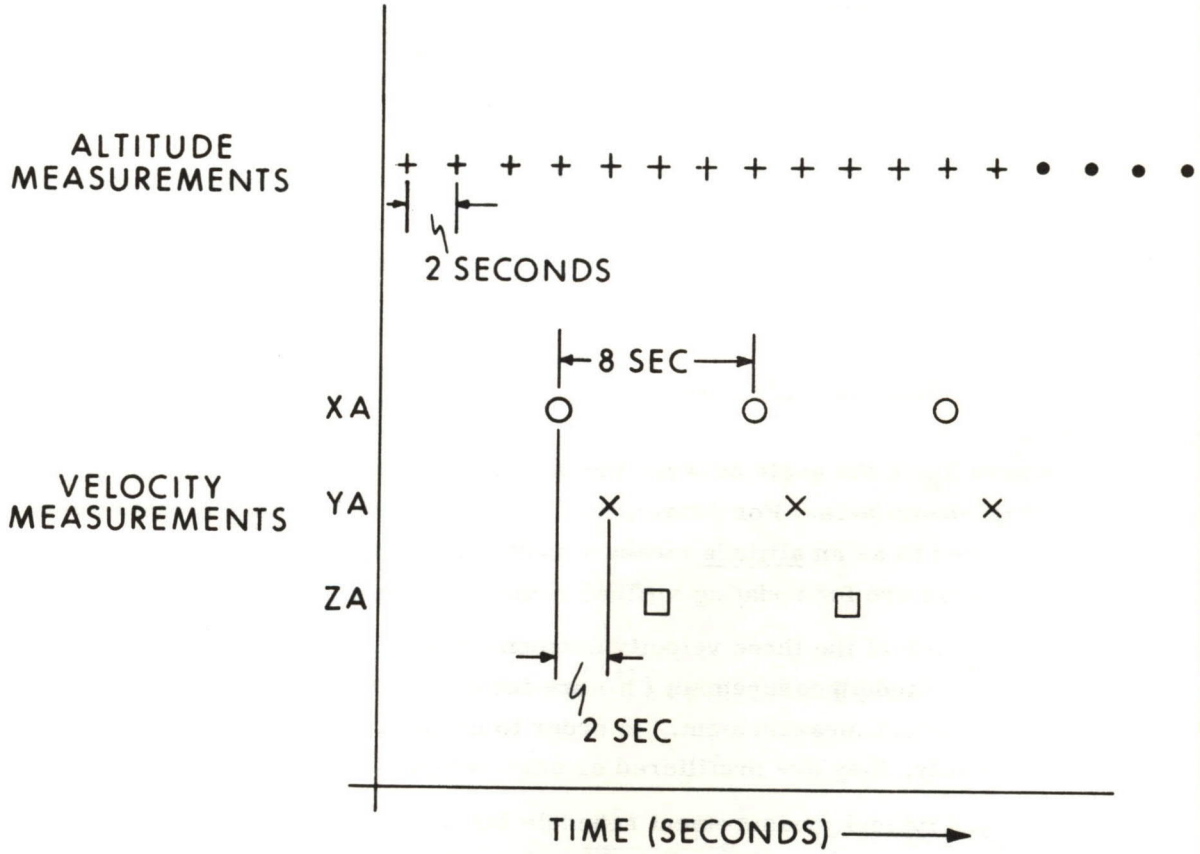

INITIAL ALTITUDE UPDATING : h = 25,000 FT
(t≈290 SEC)

INITIAL VELOCITY UPDATING : h = 15,000 FT
(t≈350 SEC)

Fig. 2.2 A Typical Measurement Schedule for Landing-Radar Updatings

where it should be noted that $\underline{v}_n$ represents the absolute velocity of the vehicle with respect to an inertial point (not relative to the moon). The subscript n indicates quantities at time t_n.

The updated estimate of the state vector is obtained by first making a comparison between the raw measurement (e.g. $\tilde{h}$ or $\tilde{v}_{XA}$) and the a-priori estimate of the measurement quantity (e.g. h' or v'_{XA}).* Based on this measurement difference, a correction to the estimated state vector ($\delta \underline{x}_n$) is computed. Only the component of the state vector corresponding to the measurement being processed is updated by data from the measurement, i.e. only h' is updated by the measurement $\tilde{h}$, and only v'_{XA} is updated by the measurement $\tilde{v}_{XA}$.

Accordingly, the relation for correcting the state estimate by use of an altitude measurement is**:

$$\delta \underline{r} = w_h \left(\tilde{h} - h' \right) \underline{u}_r \tag{2-12}$$

where $\underline{u}_r$ is a unit vector directed along the estimated vehicle position vector ($\underline{r}'$) and w_h is the altitude-measurement weighting function. Similarly, for the velocity-component measurements, the corrections to the estimate for the XA, YA and ZA measurements are:

$$\delta \underline{v} = w_{VXA} \left(\tilde{v}_{XA} - v'_{XA} \right) \underline{u}_{XA} \tag{2-13}$$

$$\delta \underline{v} = w_{VYA} \left(\tilde{v}_{YA} - v'_{YA} \right) \underline{u}_{YA} \tag{2-14}$$

and

$$\delta \underline{v} = w_{VZA} \left(\tilde{v}_{ZA} - v'_{ZA} \right) \underline{u}_{ZA} \tag{2-15}$$

where w_{VXA}, w_{VYA}, and w_{VZA} represent the velocity-component measurement weighting functions. The quantities $\underline{u}_{XA}$, $\underline{u}_{YA}$, and $\underline{u}_{ZA}$ represent unit vectors along the XA, YA, and ZA axes. As can be seen, the position estimate ($\underline{r}'$) is corrected only along the direction of the computed local vertical ($\underline{u}_r$). The estimate ($\delta \underline{v}$), on the other hand, is sequentially corrected along the computed XA, YA, and ZA axes as the different component measurements are incorporated into the estimate.

The corrections to the a-priori state estimates, as given in Eqs. 2-12 through 2-15, are applied to the a-priori estimate ($\underline{x}_n'$) to provide the up-to-date estimate ($\delta \hat{\underline{x}}_n$).*** Mathematically this can be stated as:

$$\hat{\underline{x}}_n = \delta \underline{x}_n + \underline{x}_n' \tag{2-16}$$

where the subscript n is used to indicate the values of the quantities at time t_n.

---

*The superscript of a prime (') will be used to indicate the estimated value prior to the incorporation of the current measurement, i.e. the a-priori estimate.

**The subscript n, which indicates values at time t_n, has been left off the quantities here to simplify notation.

***The notation of a caret (^) over a quantity will be used to indicate the estimated value after the current measurement is processed, i.e. the updated estimate.

During the intervals of time when no landing radar measurements are being processed, the state of the vehicle is determined by integrating the two-body equations of motion for the vehicle:

$$\frac{d\underline{v}'}{dt} = \tilde{\underline{s}} - \frac{\mu\,\underline{r}'}{r'^3} \tag{2-17}$$

and

$$\frac{d\underline{r}'}{dt} = \underline{v}' \tag{2-18}$$

where $\underline{r}'$ and $\underline{v}'$ represent the current estimates of vehicle position and absolute velocity, respectively. The quantity μ represents the lunar gravitational constant and $\tilde{\underline{s}}$ represents the specific force measured by the IMU accelerometers. The operations in Eqs. 2-17 and 2-18, it should be noted, are carried out in an inertially-fixed coordinate system.

2.3 Weighting-Function Computations

The key elements in the navigation system are the weighting functions (w) to be applied to the measurement difference to obtain the correction to the a-priori state estimate ($\delta\underline{x}_n$). In a typical optimum linear estimator a weighting vector ($\underline{w}_n$) is computed so as to minimize the mean-squared errors in the quantities being estimated. The updating relation for processing a measurement $\tilde{\underline{q}}_n$ is given as:

$$\delta\underline{x}_n = \underline{w}_n\,(\tilde{\underline{q}}_n - \underline{q}_n') \tag{2-19}$$

The information from each measurement in this type of estimator is used to update all six state-vector components. Different sets of weighting functions are required for each type of measurement being processed. If this type of an estimator were to be used for the landing maneuver, it would probably be necessary to perform in-flight computations to determine the proper weighting functions. As mentioned earlier, the computation requirements to do this appear to be quite formidable for the landing maneuver, where the minimization of computation time is of prime importance.

As an initial means of simplifying the navigation computations it was decided to update only the component of the state vector corresponding to the measurement being processed, as indicated in Eqs. 2-12 through 2-15. Under these conditions only four weighting functions are required, one for each of the four types of measurements processed in the navigation system. For convenience, these weighting functions will be referred to as w_h, w_{VXA}, w_{VYA}, and w_{VZA}.

To further simplify the required in-flight navigation computations, these altitude and velocity-component weighting functions are precomputed on the ground prior to the mission, using data from the best available computer simulations. The precomputed weighting functions are then stored in the navigation computer as linear

functions of altitude and speed, with a typical example shown in Fig. 2.3. These linearized weighting functions are approximations to weighting functions derived for a reference trajectory to give least-squares state-vector estimates. The weighting functions are stored in the computer in terms of altitude and speed rather than as functions of time, in order to provide better operational capability in the presence of landing site redesignations.

The linearized altitude-measurement weighting function (w_h) of Fig. 2.3 would be stored as:

$$w_h = 0.55 \left(1 - \frac{h'}{25,000}\right) \tag{2-20}$$

where h' is the estimated altitude of the vehicle, expressed in feet. When h' is greater than 25,000 feet, the altitude weighting function (w_h) is zero. Likewise, the linearized weighting functions for the velocity-component measurements would be stored as:

$$w_{VXA} = 0.40 \left(1 - \frac{v'}{1,550}\right) \tag{2-21}$$

$$w_{VYA} = 0.70 \left(1 - \frac{v'}{1,550}\right) \tag{2-22}$$

and

$$w_{VZA} = 0.70 \left(1 - \frac{v'}{1,550}\right) \tag{2-23}$$

where v' is the estimated speed of the vehicle, expressed in feet/second. When the estimated speed v' is greater than 1,550 ft/sec, the velocity-component weighting functions have zero values.

2.4 Operations Required in a Typical Velocity-Component Updating

In the process of updating the navigation system with landing-radar measurements, certain coordinate transformations must be performed. Likewise, in the processing of velocity data, the rotational velocity of the moon must be considered. This section will show how the coordinate transformations and lunar-velocity corrections enter into the updating procedure. To illustrate the method, the processing of an XA-component velocity measurement will be considered here.

Certain coordinate transformations are required in the navigation system because the basic information from the IMU is in an inertially-fixed frame, whereas the doppler-velocity measurements are in the body-fixed radar-antenna coordinate frame. Also, the rotational velocity of the moon must be accounted for in the updating process, since the landing radar measures velocity relative to the moon whereas the IMU data determine the absolute inertial velocity of the vehicle. Finally, a coordinate transformation is required because the guidance-system input data must be provided in a rotating coordinate frame, whereas the state-vector computations from the IMU are in an inertially-fixed frame.

Detailed functional diagrams for the guidance-and-navigation system are given in Ref. 5, including all coordinate transformations and lunar-rotation velocity corrections. To illustrate the transformations and lunar-rotation corrections present in the navigation system, a simple functional diagram is presented in Fig. 2.4 for

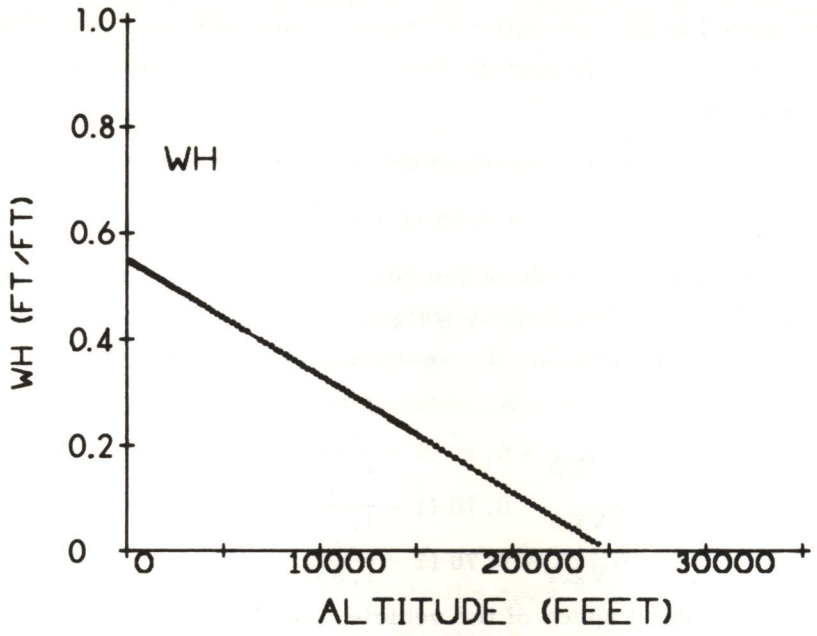

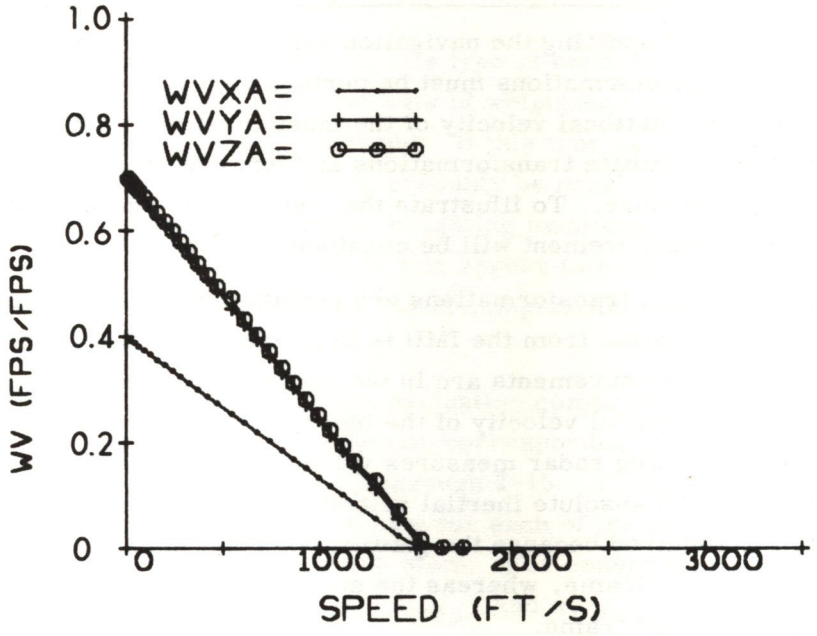

Fig. 2.3 Simplified Linearized Weighting Functions

the processing of an XA-component velocity measurement. The superscripts (I), (B), and (L) are used to indicate components in the inertially-fixed, body-fixed, and lunar-fixed frames, respectively. The subscript L on the velocity $\underline{v}$ is used to indicate velocity relative to the moon, the subscript I is used to indicate absolute velocity.

The first step in the updating process, as indicated in Fig. 2.4, is to take the absolute vehicle velocity from the IMU ($\underline{v}_I$) and remove the lunar-rotation velocity to obtain vehicle velocity relative to the moon ($\underline{v}_L$). This operation is performed in the inertially-fixed frame, i.e. with inertial components of the quantities involved. Then, using orientation-angle information from the inertial package, unit vectors are computed in inertial-frame coordinated to specify the radar-antenna axes ($\underline{u}_{XA}$, $\underline{u}_{YA}$, and $\underline{u}_{ZA}$).

The a-priori estimate of the measurement quantity(e.g. v'_{XA}) is next obtained by projecting the velocity $\underline{v}_L^{(I)}$ along the antenna-axis direction appropriate for the measurement being processed. This simply involves for an XA-component measurement the dot-product operation:

$$v'_{L,XA} = \underline{v}'^{(I)}_L \cdot \underline{u}^{(I)}_{XA} \qquad (2\text{-}24)$$

where the superscript (I) is used to emphasize the fact that inertial-frame components are used for $\underline{v}'_L$ and $\underline{u}_{XA}$. A comparison is next made between the velocity-component measurement ($\tilde{v}_{L,XA}$) and the a-priori estimate of the measurement ($v'_{L,XA}$), both of which are scalar quantities. The magnitude of the correction to the a-priori estimate is then computed as the weighted difference between the raw measurement and the a-priori estimate of the quantity being measured. This computed correction is then applied to the component of a-priori estimated velocity along the direction of the measurement ($\underline{u}_{XA}^{(I)}$) to yield the updated velocity estimate $\hat{\underline{v}}_I^{(I)}$. The updating relation used here is:

$$\hat{\underline{v}}_I^{(I)} = \underline{v}'^{(I)}_I + w_{VXA}\,(\tilde{v}_{L,XA} - v'_{L,XA})\,\underline{u}^{(I)}_{XA} \qquad (2\text{-}25)$$

where w_{VXA} is the XA-component velocity weighting function. The updating relations are similar for the other velocity components.

To obtain the required navigation-system input data, the lunar-rotational velocity is removed from $\underline{v}_I^{(I)}$, as shown in Fig. 2.4 to yield the relative velocity $\underline{v}_L^{(I)}$. The updated relative-velocity estimate $\underline{v}_L^{(I)}$ and the vehicle-position estimate $\underline{r}^{(I)}$ are then transformed from inertially-fixed to lunar-fixed coordinates, as indicate on Fig. 2-4 by the transformation matrix $C_{I\text{-}L}$. These components of vehicle position and velocity (in lunar-fixed coordinates) are used to generate vehicle steering commands in the guidance system, as will be described in Chapter 3 of this report.

In concluding this section, it should be noted that the operation of projecting the vehicle's estimated velocity along radar-antenna axes, as indicated by Eq. 2-24,

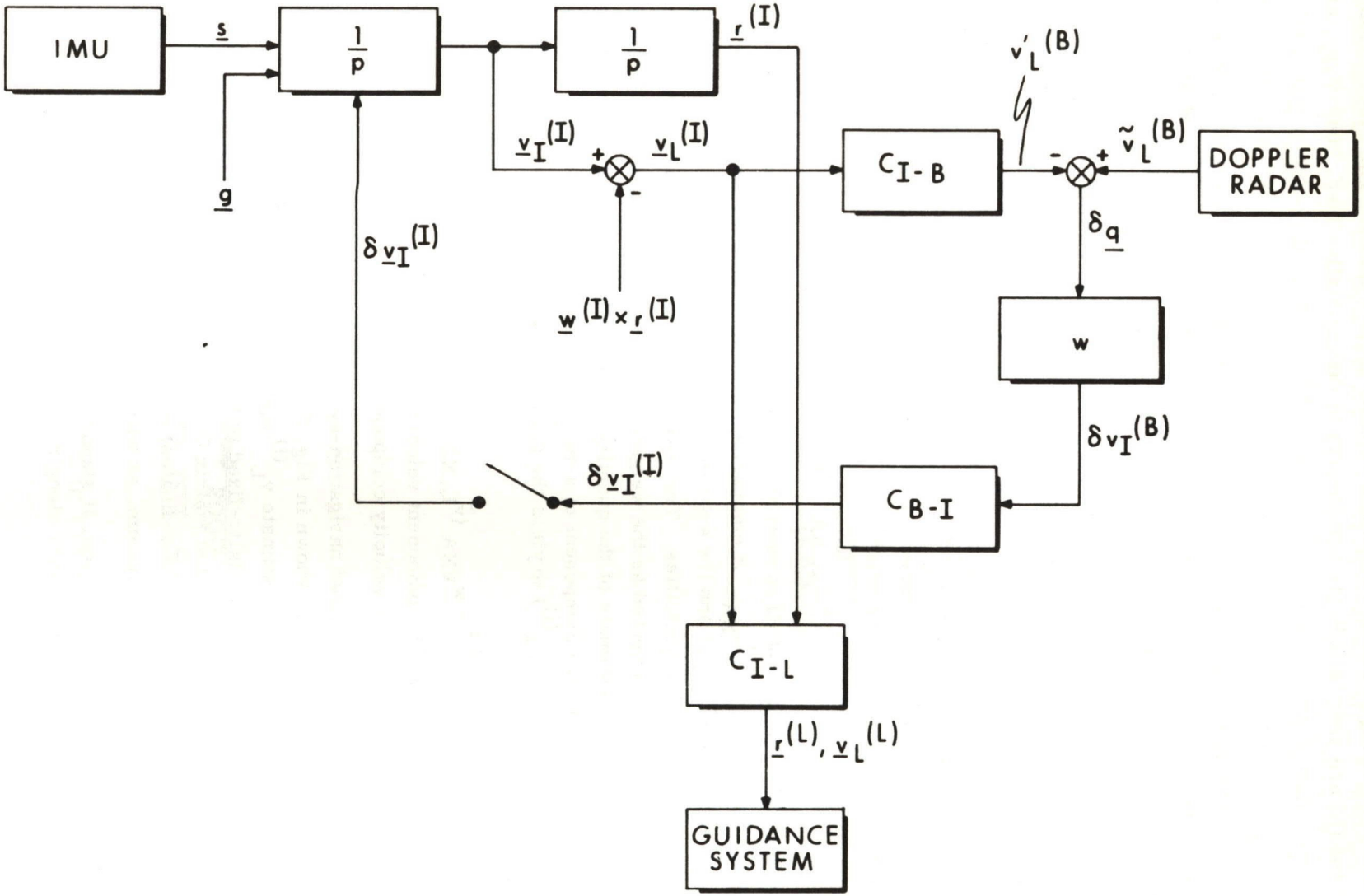

Fig. 2.4 Functional Diagram for Velocity-Component Updating Process

requires the same basic computations as a transformation from inertial to body coordinates. The row vectors of the matrix that would be required to accomplish this transformation are the unit vectors $\underline{u}_{XA}^{(I)}$, $\underline{u}_{YA}^{(I)}$, and $\underline{u}_{ZA}^{(I)}$. Likewise, the operation of applying the correction to the estimate along the measurement direction, as indicated in Eq. 2-25, can be thought of as a transformation of the correction from body to inertial coordinates. All the basic navigation computations, however, as indicated in Eqs. 2-24 and 2-25 and Fig. 2.4, are really carried out as components in an inertially-fixed frame.

CHAPTER 3

LANDING MANEUVER

3.1 General Considerations

The mission objectives for the landing maneuver, as mentioned earlier, are that the vehicle satisfy certain preselected Low-Gate terminal conditions. These objectives require that the vehicle be decelerated from an initial value of about 5600 feet/sec down to about 3 feet/sec, while the vehicle's altitude is reduced from 50,000 feet to about 115 feet. All of this must be accomplished on a trajectory that makes efficient use of the vehicle's propellant, and at the same time permits adequate landing-site visibility. The capability for changing landing sites during the descent phase, i.e. site-redesignation capability, must also be provided.

To accomplish the mission objectives efficiently, the landing maneuver, as mentioned in Chapter 1, is divided into two separate phases called the "braking" and "visibility" phases. The overall guidance problem is then solved as two successive two-point boundary-value guidance problems, separated by a short transition phase. The terminal conditions for the braking-phase problem are referred to as the High-Gate conditions; the terminal conditions for the visibility-phase problem are referred to as the Low-Gate conditions.

Both the braking-phase and visibility-phase guidance systems compute vehicle steering commands based on the difference between the present estimate of the vehicle's state ($\underline{x}'$) and the desired terminal state for the phase ($\underline{x}_D$). Because of the difference in objectives for the braking and visibility phases, the important system design considerations are different for the two phases. In the braking phase, for example, where it is desirable to decelerate at a high-thrust level, the limited throttling range characteristic of the descent engine is a major factor. In the visibility phase, on the other hand, it is of prime importance that the vehicle thrust attitude be pitched up sufficiently high so that adequate landing-site visibility is obtained.

In this chapter the guidance concepts for both the braking and visibility phases will be described for the automatic mode of operation without site redesignations.

Included here are the basic relations for the steering commands, i.e. the command specific force* (s_c) and the command thrust (f_c). In a rigorous description of the guidance system[1, 5] five different coordinate frames are required. To simplify the discussion here and to clarify the overall guidance concept, the different coordinate frames have for the most part been suppressed in the discussions of this chapter. A detailed description of the guidance system is given in Refs. (1) and (5), including a discussion of the site-redesignation mode of operation.

3.2 Braking-Phase Guidance System

The basic objective in the braking phase is to accomplish the major deceleration of the vehicle on a trajectory that permits efficient propellant utilization. In order that the visibility-phase objectives be successfully accomplished, however, the vehicle must satisfy certain preselected terminal conditions at the end of the braking phase. These conditions, which are called the High-Gate conditions, specify the vehicle's altitude and velocity, and its down-range distance from the visibility-phase terminal point.

Under idealized conditions, where it is assumed that the descent engine's thrust can be varied continuously over the desired operating range, the guidance objectives can be accomplished reasonably well by computing specific-force commands** ($\underline{s}_c$) according to the relation:

$$\underline{s}_c = \underline{c}_0 + \underline{c}_3 (t - t_f) + \underline{c}_6 \frac{(t - t_f)^2}{2} + \frac{\mu \underline{r}'}{r'^3} \tag{3-1}$$

where t is the present time, and t_f is the predicted (or preselected) final time for the phase. The quantity μ represents the lunar gravitational constant and $\underline{r}'$ represents the vehicle's position vector relative to the center of the moon (estimated from the navigation system). The coefficients $\underline{c}_0$, $\underline{c}_3$, and $\underline{c}_6$, which are three-dimensional vectors, are computed[4, 6] based on the difference between present vehicle state ($\underline{x}$) and the desired terminal state ($\underline{x}_D$). The basic relations for these coefficients are:

$$\underline{c}_0 = \underline{a}_D \tag{3-2}$$

$$\underline{c}_3 = \left(\frac{6}{t_{GO}}\right) \underline{a}_D - \left(\frac{18}{t_{GO}^2}\right) (\underline{v}_D - \underline{v}') + \left(\frac{24}{t_{GO}^3}\right) (\underline{r}_D - \underline{r}' - \underline{v}' t_{GO}) \tag{3-3}$$

$$\underline{c}_6 = \left(\frac{12}{t_{GO}^2}\right) \underline{a}_D - \left(\frac{48}{t_{GO}^3}\right) (\underline{v}_D - \underline{v}') + \left(\frac{72}{t_{GO}^4}\right) (\underline{r}_D - \underline{r}' - \underline{v}' t_{GO}) \tag{3-4}$$

*Specific force is defined as thrust per unit mass.

**Specific force and thrust acceleration are used interchangeably in this report.

where $\underline{a}_D$, $\underline{v}_D$, and $\underline{r}_D$ represent the desired terminal acceleration, velocity, and position. The quantity t_{GO} represents the time-to-go to the end of the phase, i.e. $t_f - t$. The quantities $\underline{r}'$ and $\underline{v}'$ represent the estimated values of vehicle position and velocity.

The inertial acceleration of the vehicle under these conditions is given by the relation:

$$\frac{d^2\underline{r}}{dt^2} = \underline{c}_0 + \underline{c}_3 (t - t_f) + \underline{c}_6 \frac{(t - t_f)^2}{2} \qquad (3\text{-}5)$$

As can be seen, the inertial acceleration of the vehicle in this case is a quadratic function of time. The coefficients $\underline{c}_0$, $\underline{c}_3$, and $\underline{c}_6$ correspond respectively to the final acceleration, final jerk (time-rate-of-change of acceleration), and the final snap (second derivative of acceleration) for the braking phase. By using a quadratic function of time for the command specific force ($\underline{s}_c$), there are nine available coefficients (c_0, c_1, ... c_8) which permit the terminal position, velocity, and acceleration to be specified.

Under ideal conditions where the errors in the estimates of $\underline{r}$ and $\underline{v}$ are small, the coefficients c_0, c_1, ... c_8 do not change rapidly with time. As a result, the coefficient computations (Eqs. 3-2 through 3-4) can be performed at a much slower rate than the specific-force computation (Eq. 3-1). Under conditions where radar updates or site redesignations are made, on the other hand, there will be changes in the coefficients corresponding to the changes in the state estimates and desired terminal conditions.

The actual trajectory that the vehicle will fly if the specific force provided by the descent engine ($\underline{s}$) is equal to the command specific force ($\underline{s}_c$) is dependent upon the state of the vehicle at the ignition point ($\underline{r}$, $\underline{v}$), the desired terminal conditions ($\underline{r}_D$, $\underline{v}_D$, and $\underline{a}_D$), and the terminal time (t_f). This can be seen from Eqs. 3-3 and 3-4 where the final jerk and snap are computed. The terminal time for the deboost phase (t_f) can be preselected for use in the steering relations of Eqs. 3-1 through 3-4. It has been found[1, 6], however, that it is more useful to specify the desired final downrange component of jerk (j_{DX}) rather than the terminal time (t_f). The time-to-go (t_{GO}) is then obtained by an iteration process, using the reciprocal of time-to-go (t_{GO}) as the iteration quantity. The basic relation for t_{GO}^{-1} is:

$$(t_{GO}^{-1})_k = (t_{GO}^{-1})_{k-1} + \frac{(j_{DX} - j_{FX})_{k-1}}{\left(\frac{dj_{FX}}{dt_{GO}^{-1}}\right)_{k-1}} \qquad (3\text{-}6)$$

where the subscripts k and k-1 are used to indicate the k'th and (k-1)' th iterations. The quantity j_{FX} is the computed down-range component of terminal jerk, and $\frac{dj_{FX}}{dt_{GO}^{-1}}$ is the derivative with respect to reciprocal time-to-go. The computed down-range terminal jerk j_{FX} is given by:

$$j_{FX} = 6\, a_{DX} (t_{GO}^{-1}) - 18\, v_{DX} (t_{GO}^{-1})^2 - 6\, v_X (t_{GO}^{-1})^2 - 24\, r_X (t_{GO}^{-1})^3 \qquad (3\text{-}7)$$

where a_{DX} and v_{DX} are the desired terminal down-range components of vehicle acceleration and velocity. The quantities v_X and r_X represent the down-range components of vehicle velocity and position. The time-rate-of-change of final jerk with respect to t_{GO}^{-1} is given by:

$$\frac{dj_{FX}}{dt_{GO}^{-1}} = 6\, a_{DX} - 36\, v_{DX} (t_{GO}^{-1}) - 12\, v_X (t_{GO}^{-1}) - 72\, r_X (t_{GO}^{-1})^2 \qquad (3\text{-}8)$$

where a_{DX}, v_{DX}, v_X, and r_X represent the same quantities as in Eq. 3-7. The iterative process in Eqs. 3-6 through 3-8, it should be noted, is carried out in terms of the reciprocal of time-to-go, i.e., (t_{GO}^{-1}) rather than t_{GO} itself, because of numerical computation advantages in the iteration computations.

The guidance laws presented in Eqs. 3-1 through 3-4 have been investigated for lunar-landing applications in Refs. (4) and (6). Other functional forms can be found for the coefficients c_0, c_1, --- c_8 which will permit the terminal-point boundary conditions to be satisfied. The best results to date, however, have been obtained using the coefficients given by Eqs. 3-2 through 3-4.

In the actual physical problem the descent engine is not continuously throttleable over the desired operating range. Instead, it must be operated either at a fixed high-throttle setting (92.5 percent of nominal thrust), or it can be operated over a range of lower-throttle settings (between 10 and 60 percent of nominal thrust). To achieve effective propellant utilization during the braking phase, it is desirable to accomplish the major deceleration at the high-throttle setting. In order to satisfy the terminal boundary conditions, on the other hand, it is necessary that the command thrust be in the continuously throttleable lower-thrust region (10-60 percent of nominal thrust) during the latter part of the braking phase. If the command thrust is not in the throttleable region, then the propulsion system will not be able to provide the required thrust (unless by chance it is 92.5 percent of the nominal thrust).

To accomplish the deboost-phase objectives in the presence of the above-mentioned propulsion-system constraints, the guidance relations of Eqs. 3-1 through 3-4 have been applied with certain special modifications. These modifications are necessary because the engine cannot be throttled except over the low 10-60 percent range. To minimize vehicle-attitude transients, moreover, the throttle is not permitted to return to the high setting (92.5 percent) once it has dropped to the low range* (10-60 percent).

The basic guidance philosophy adopted in this situation was to operate the vehicle at the high-throttle setting for about the first 380 seconds of the braking phase, as shown in Fig. 3.1 for the nominal reference trajectory. Then, during the last 80 seconds of the initial braking phase, the throttle is operated in the 10-60 percent throttleable region. To accomplish this, thrust commands are obtained from Eq. 3-1 by using the relation:

$$f_c = s_c m \tag{3-9}$$

where f_c is the thrust command, s_c is the specific force command (magnitude), and m is the estimated mass of the vehicle. The following logic is then used on the thrust command (f_c) to determine the proper throttle setting, starting with the throttle at the 92.5-percent position and Flag_A at zero:

$$\text{If } \text{Flag}_A = 0 \text{ and } f_c \geq .52\, f_{nom}, \text{ then } f_c = .925\, f_{nom} \tag{3-10}$$

$$\text{If } \text{Flag}_A = 0 \text{ and } f_c < .52\, f_{nom}, \text{ then } \text{Flag}_A = 1 \tag{3-11}$$

$$\text{If } \text{Flag}_A = 1 \text{ and } f_c > .60\, f_{nom}, \text{ then } f_c = .60\, f_{nom} \tag{3-12a}$$

$$\text{If } \text{Flag}_A = 1 \text{ and } .60\, f_{nom} \geq f_c \geq .10\, f_{nom}, \text{ then } f_c = f_c \tag{3-12b}$$

$$\text{If } \text{Flag}_A = 1 \text{ and } f_c < .10\, f_{nom}, \text{ then } f_c = .10\, f_{nom} \tag{3-12c}$$

where f_{nom} represents the nominal maximum thrust of the descent engine. The relations of Eqs. 3-10 through 3-12 say that as long as the initial command thrust is greater than 52 percent of the nominal thrust, keep the throttle at the 92.5-percent position. As soon as the command thrust drops below 52 percent of the nominal thrust, however, the throttle should follow the command thrust, provided that it remains below 60 percent of nominal thrust (which it will do under normal conditions). Once the DPS has been throttled down to the 10-60 percent region, the logic will not permit the throttle to return to the 92.5-percent position.

*The 26-second low-thrust DPS trim period at the start of the braking phase is not included here.

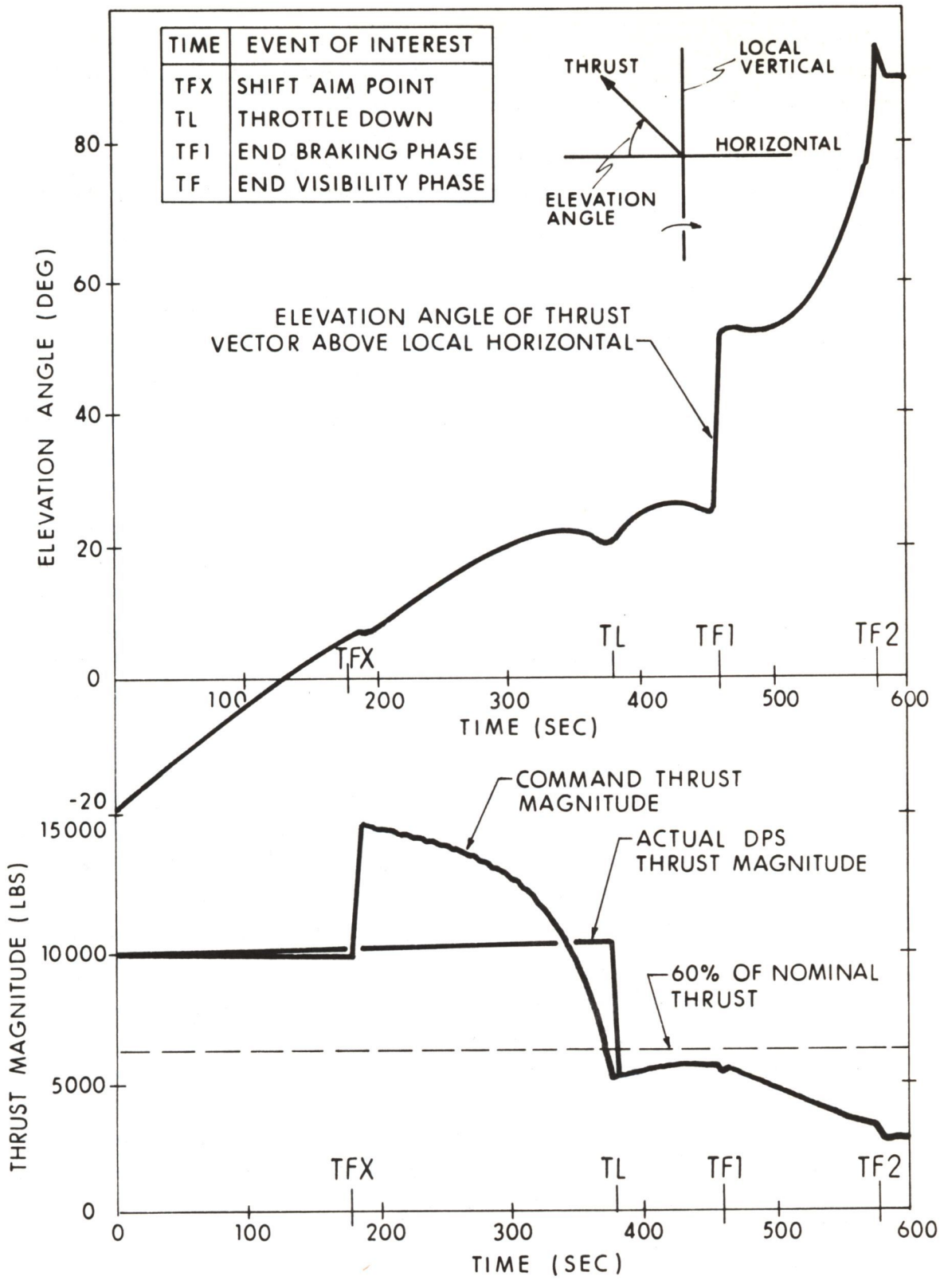

Fig. 3.1 Thrust Profiles for Reference Trajectory

The profile of command thrust as a function of time on a typical descent-phase trajectory is shown in Fig. 3.1 along with a curve of the actual thrust provided by the descent-stage engine. The 26-second low-thrust DPS trim period immediately after engine ignition is not shown here. This general type of command-thrust profile has been found by extensive simulation studies to provide efficient propellant utilization, to provide satisfactory propulsion-system throttling characteristics, and to allow the braking-phase terminal conditions to be met with a satisfactory accuracy.

To obtain command-thrust profiles which provide satisfactory guidance-system performance, like the one in Fig. 3.1, is not a simple task. The procedure that was adopted to accomplish this is presented in detail in Ref. (6). In essence, the desired command-thrust profile is obtained by the following procedures.

(1) The DPS ignition is controlled to place the vehicle initially on a trajectory to a preselected dummy aim-point, with preselected values of terminal velocity, acceleration, and down-range jerk.

(2) For a preselected interval after ignition (typically 180 seconds)*, specific force commands are generated on the basis of Eqs. 3-1 through 3-4 and Eqs. 3-6 through 3-8, using the dummy aim-point conditions as required. During this period the thrust vector ($\underline{f}$) of the vehicle is oriented along the direction of the command thrust ($\underline{f}_c$). The throttle remains at the high-thrust position throughout this interval, as required by the thrust-control logic (Eqs. 3-10 through 3-12).

(3) At a preselected time (about 180 seconds after ignition)* during the braking phase, the desired terminal conditions used in Eqs. 3-1 through 3-4 and Eqs. 3-6 through 3-8 are changed to those corresponding to the braking-phase terminal point (the High-Gate point). The same method of thrust-vector control is still employed, i.e., the orientation of the thrust-vector is along the direction of the command thrust (f_c) and the throttle setting is determined by the logic of Eqs. 3-10 through 3-12.

(4) When the time remaining for the braking phase has dropped to about 80 secs, the command thrust will for the first time (nominally) drop below the level corresponding to 52 percent of the nominal thrust. The throttle will then be permitted to move from its 92.5-percent setting into the throttleable 10-60 percent region. Thereafter, during the braking phase, the propulsion system will provide a thrust vector ($\underline{f}$) oriented in the direction of and equal in magnitude to the command thrust ($\underline{f}_c$).

*180 seconds after the initial 26-second DPS trim period.

Of particular importance in this guidance scheme is the selection of the trajectory parameters for both the dummy aim-point and the High-Gate terminal point. This can best be accomplished by a careful and accurate simulation of the braking-phase guidance problem.

The vehicle steering commands, as mentioned earlier, are basically derived from the command specific force ($\underline{s}_c$), as given by Eq. 3-1. In the computation of $\underline{s}_c$ it is required that nine coefficients (c_0, c_1, ... c_8) be computed using the relations of Eqs. 3-2 through 3-4. These coefficients, as mentioned previously, will remain essentially constant throughout the braking phase under ideal, error-free operating conditions. Under realistic conditions, however, where guidance-and-navigation-system errors are present and landing-radar updatings are made, some of these coefficients will tend to increase very rapidly at the end of the braking-phase. This can be seen from Eqs. 3-3 and 3-4 where the various terms have time-to-go (t_{GO}) in their denominator. To guard against the rapid buildup of $\underline{c}_3$ and $\underline{c}_6$ at the end of the phase, the coefficient computations (Eqs. 3-2 through 3-4) and final-time predictions (Eqs. 3-6 through 3-8) are stopped for the braking phase when the time-to-go (t_{GO}) has dropped to 20 seconds. The command specific force thereafter is obtained simply from Eq. 3-1, using the last computed values for the coefficients (c_0, c_1, ... c_8) and the terminal time (t_f).

In concluding this section it should be noted that the reference trajectory and guidance operation have been predicated on DPS acceleration uncertainties of ±1% in the high-throttle-setting position. On the basis of simulation studies it has been found that even with throttle-setting uncertainties of this magnitude, the above-mentioned guidance system will satisfy all the braking-phase guidance objectives. The length of time during which the throttle is in the 10-60 percent throttleable region will, however, change about 30 seconds for a 1-percent acceleration uncertainty. It will increase when the DPS acceleration is high, and it will decrease when the acceleration is low.

3.3 Visibility-Phase Guidance System

The basic guidance objective of the visibility phase is to accomplish the final deceleration of the LEM in such a way that the selected site is visible to the astronaut through the window for a predetermined interval of time. Of prime importance here is that the longitudinal X-axis of the vehicle (which is essentially the direction of applied thrust) be elevated at a sufficiently high angle for the landing site to be visible through the window. It is desirable, moreover, for the line-of-sight to the selected landing site to be at least 10 degrees above the window edge for at least 75 seconds. At the same time, it is undesirable from the viewpoint of efficient propellant utilization to keep the thrust vector at the high elevation angle (required for site visibility) for any longer than the minimum required time.

The visibility-phase guidance concept must, of course, steer the vehicle to the Low-Gate-point terminal conditions (position and velocity) with a satisfactory terminal accuracy. In addition, the visibility-phase system must provide the capability of site redesignation without violating the specified trajectory constraints for the visibility phase. The trajectory constraints which were used in the study reported here are presented for the convenience of the reader of Appendix A, as stated in Ref. (1), and a detailed description of the site-redesignation mode of operation of the visibility-phase guidance system is given in that reference. Accordingly, the discussion here will be restricted to the automatic mode of operation with no landing-site redesignations.

Under these conditions, the guidance problem can be solved quite simply by a straight-forward application of Eq. 3-1 to obtain the command specific force ($\underline{s}_c$). The command thrust ($\underline{f}_c$) is obtained by multiplying $\underline{s}_c$ by the estimated vehicle mass (m). The coefficients $c_0, c_1, \ldots c_8$ required in the computation of $\underline{s}_c$ are obtained from Eqs. 3-2 through 3-4, using the Low-Gate-point values for $\underline{a}_D$, $\underline{v}_D$, and $\underline{r}_D$, as given in Table 1.1. Likewise, the time-to-go (t_{GO}), used in Eqs. 3-2 through 3-4, is computed iteratively from Eqs. 3-6 through 3-8, using Low-Gate-point quantities as required here.

By carefully selecting the desired terminal quantities for the visibility phase ($\underline{a}_D$, $\underline{v}_D$, and $\underline{r}_D$), the down-range terminal jerk (j_{DX}), and the time duration of the phase, it is possible to guide the vehicle in such a way that all the major objectives are satisfied, using Eqs. 3-1 through 3-4 and 3-6 through 3-8. The commanded vehicle thrust on a typical trajectory will remain in the throttleable (10-60 percent) region throughout the visibility phase, as shown in Fig. 3.1. Accordingly, the descent engine will be able to provide the commanded specific force ($\underline{s}_c$) throughout the entire visibility phase. In order to achieve the required visibility-phase objectives, the vehicle must have previously satisfied the braking-phase (High-Gate-point) terminal conditions with a reasonable accuracy.

As the visibility phase nears completion, certain guidance coefficients ($c_3, c_4, \ldots c_8$) will tend to increase rapidly as time-to-go becomes small. As mentioned earlier in conjunction with the braking-phase system, this is caused by the presence of t_{GO} in the denominator of various terms in the coefficient relations Eqs. 3-3 and 3-4. To circumvent this problem in the visibility phase, the coefficient computations (Eqs. 3-2 through 3-4) and terminal time computations (Eqs. 3-6 through 3-8) are stopped when the estimated time-to-go to the end of the phase is less than 5 seconds. The specific force is computed thereafter simply from Eq. 3-1, using the last computed values for $c_0, c_1, \ldots c_8$ and t_f.

3.4 Alternate Formulation of Certain Guidance Relations

The guidance-system studies presented in this report have employed the guidance laws as formulated in Sections 3.2 and 3.3. In the actual mechanization of the guidance laws for use in the LGC, a somewhat different though equivalent formulation will be used for Eqs. 3-1 through 3-4. This formulation, which is simpler to mechanize, will next be described.

The command specific force ($\underline{s}_c$) in this new formulation is given by the relation:

$$\underline{s}_c = \underline{a}_D - \frac{6}{t_{GO}} (\underline{v}_D - \underline{v}') + \frac{12}{t_{GO}^2} (\underline{r}_D - \underline{r}' - \frac{\underline{v}'}{t_{GO}}) + \frac{\mu \underline{r}'}{r'^3} \quad (3\text{-}13)$$

where $\underline{a}_D$, $\underline{v}_D$, and $\underline{r}_D$ represent the desired terminal vehicle acceleration, velocity, and position. The quantities $\underline{v}$ and $\underline{r}$ represent the estimated values of the present vehicle velocity and position. The time-to-go (t_{GO}) is given by the relation:

$$t_{GO} = t_f - t \quad (3\text{-}14)$$

where t is the present vehicle time and t_f is the final terminal time. The formulation of Eq. 3-13 is identical to Eqs. 3-1 through 3-4 and can be obtained from Eq. 3-1 by substituting the relations of Eqs. 3-2 through 3-4 to eliminate $\underline{c}_0$, $\underline{c}_3$, and $\underline{c}_6$. The relations of Eqs. 3-6 through 3-8 provide the means for computing $\frac{1}{t_{GO}}$ as required in Eq. 3-13.

Under conditions when the time-to-go for the guidance phase of interest becomes small, the command specific force ($\underline{s}_c$) as computed from Eq. 3-13 can become badly behaved, i.e. it may get very large as time-to-go becomes small. To circumvent this difficulty, an alternate expression is used for $\underline{s}_c$ when t_{GO} is less than 20 second during the braking phase, and less than 5 seconds during the visibility phase. This alternate relation for small values of t_{GO} is:

$$\underline{s}_c = \underline{a}_L + (\underline{a}_D - \underline{a}_L) \left(\frac{t_{GO}}{t_f - t_L}\right) + \frac{\mu \underline{r}'}{r'^3} \quad (3\text{-}15)$$

where t_L represents the time at which Eq. 3-15 is first used in a given phase. The quantity $\underline{a}_L$ represents the vehicle's acceleration at time t_L. In effect, the relation of Eq. 3-15 causes the vehicle's acceleration to change linearly with time from its value at the time Eq. 3-13 is abandoned (i.e. $\underline{a}_L$) to its final desired value for the phase of interest ($\underline{a}_D$).

In concluding this section, it should be noted that Eq. 3-13 provides a much simpler mechanization for the LGC than Eqs. 3-1 through 3-4, which is a very strong recommendation for its use. Also, it is felt that the use of Eqs. 3-13 and 3-15 for computation of the specific force ($\underline{s}_c$) will give system performance not significantly different from Eqs. 3-1 through 3-4. Simulation studies are currently being made to substantiate this point.

3.5 Guidance-System Operation on the Reference Landing Trajectory

To illustrate the operation of the landing-maneuver guidance system under ideal error-free conditions, the reference-trajectory data of Fig. 3.2 through 3.5 are presented. It is assumed here that there are no initial-condition errors (i.e. errors in the initial estimates of $\underline{r}$ and $\underline{v}$), there are no errors in the IMU, there are no propulsion-system uncertainties, and the thrust vector is always oriented along the direction of the command-thrust vector. It is assumed, of course, that the descent engine must be operated either at 92.5 percent of nominal thrust or in the throttleable 10-60 percent region. All of the data presented here start at a time 200 seconds after the initial 26-second low-thrust DPS trim period following engine ignition. No landing-radar updatings are taken or required on this idealized trajectory.

The particular trajectory shown in the data of Figs. 3.2 through 3.5 goes to a High-Gate point at an altitude of 6,667 feet above the surface of the moon. The initial, High-Gate, and Low-Gate-point conditions for the trajectory are summarized in Table 3.1. For convenience the data here are presented as altitude, speed, flight-path angle, and range-to-go to the selected site. (Table 1.1 presents High-Gate and Low-Gate-point data in an inertial frame.)

The orientation of the thrust vector with respect to the local horizontal during the landing maneuver is shown in Fig. 3.2 as a function of time. As expected, the thrust vector remains within 25 degrees of the horizontal during the major part of the braking-phase, in order to accomplish the deceleration with efficient utilization of fuel. During the visibility phase, the vehicle's attitude is pitched upward so that the selected site can be seen from the vehicle. There are small discontinuities in thrust-vector orientation curves, as can be seen in Fig. 3.2. These occur at the time the throttle is switch down from the 92.5-percent position into the 10-60 percent region, and at the transition points between the braking and visibility phases. These discontinuties do not constitute a serious problem in the actual operation of the system, and will be smoothed out by the normal dynamic lag in the response of the vehicle and propulsion system to steering commands.

Superposed on the thrust-vector orientation curve of Fig. 3.2 is a curve of visibility angle during the landing maneuver. The visibility angle, as presented here, is the angle by which the line-of-sight to the selected site is visible above the edge

of the LEM window. When the landing site is not visible through the window, the visibility angle as shown has a zero value. The selected landing site is taken here as a point 3.3 feet down range from the Low-Gate point. In order for the landing site to be visible through the window in the LEM, the line-of-sight to the landing site must be at least 25 degrees above the longitudinal axis of the vehicle. Examination of the visibility-angle curve indicates that the visibility requirements for the landing maneuver, i. e. a visibility angle of at least 35 degrees (10 degrees above the window edge) for at least 75 seconds, are satisfied on this reference trajectory.

The required velocity increment for the reference trajectory, as indicated in Fig. 3.2,is 6281 ft/sec. Included here are 37 ft/sec expended during the 26-second low-thrust interval immediately after ignition.

The important characteristics of the reference landing trajectory are given in Figs. 3.3 and 3.4 and 3.5. Data are given in Fig. 3.3 of the vehicle altitude as a function of the down-range distance travelled from the start of the braking phase. Time histories of vehicle altitude, vertical velocity, speed, and flight-path angle are shown in Figs. 3.4 and 3.5.

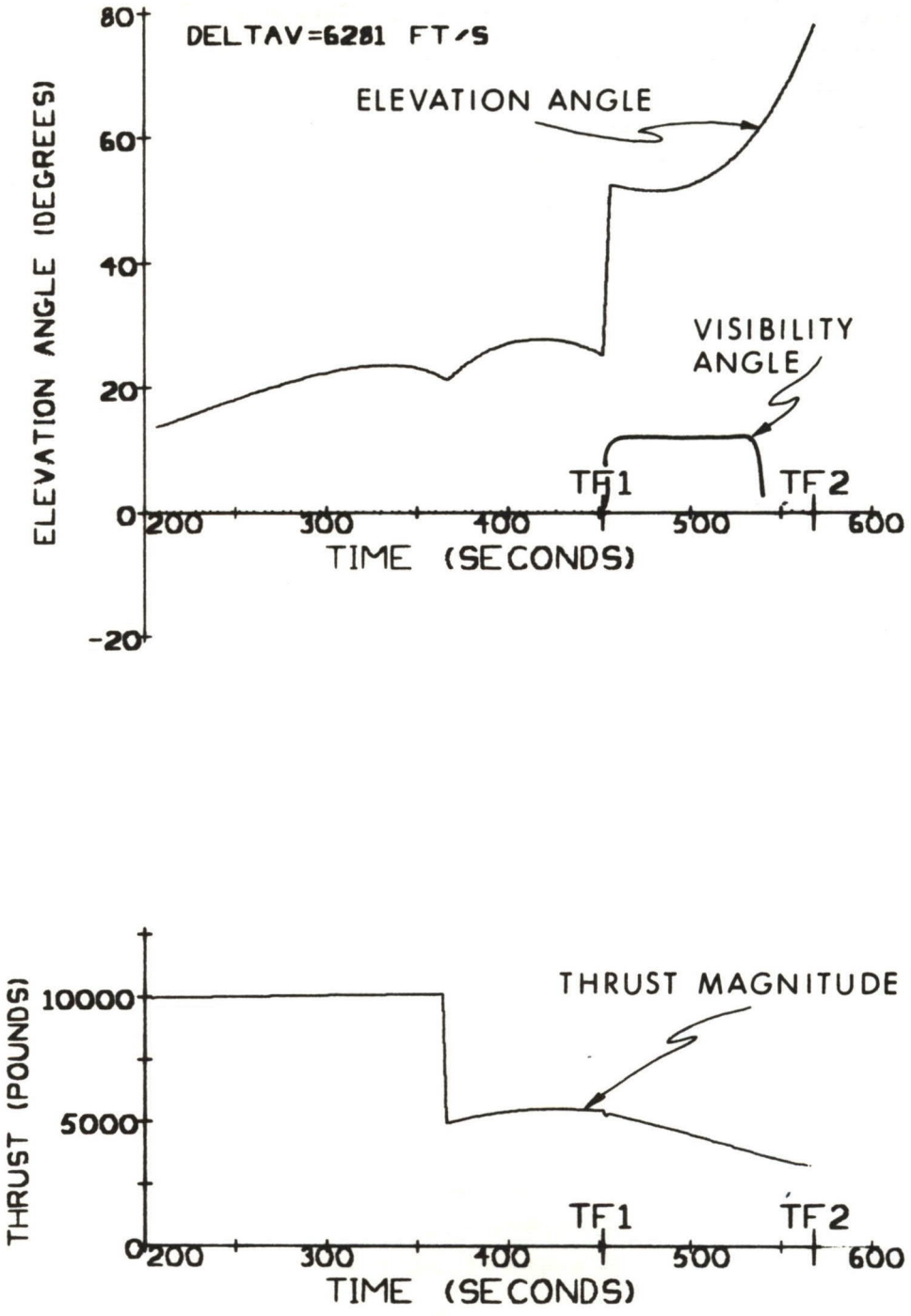

Fig. 3.2 Thrust Profiles for Reference Trajectory

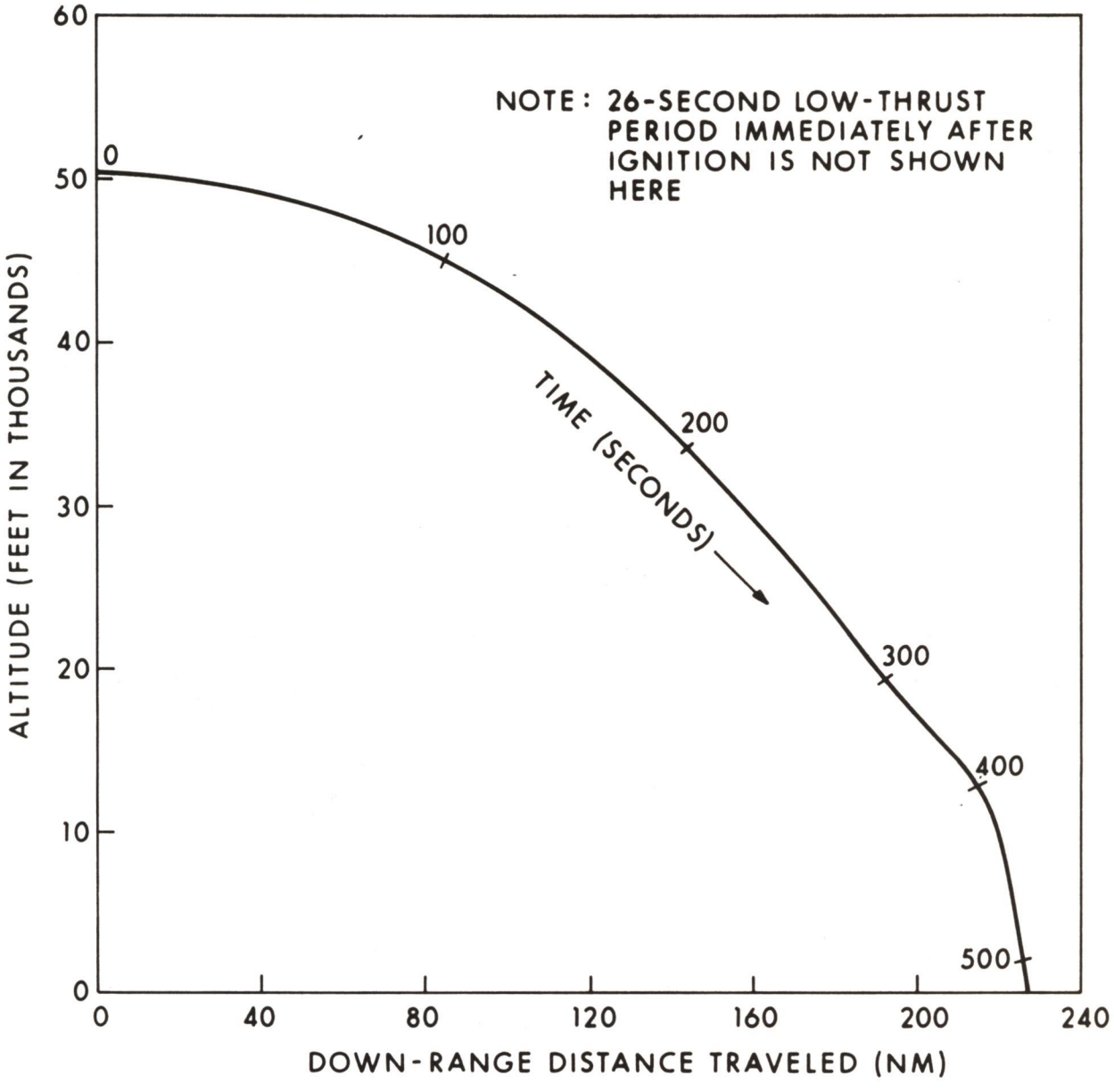

Fig. 3.3 Altitude vs Down-Range Distance Traveled on Reference Trajectory

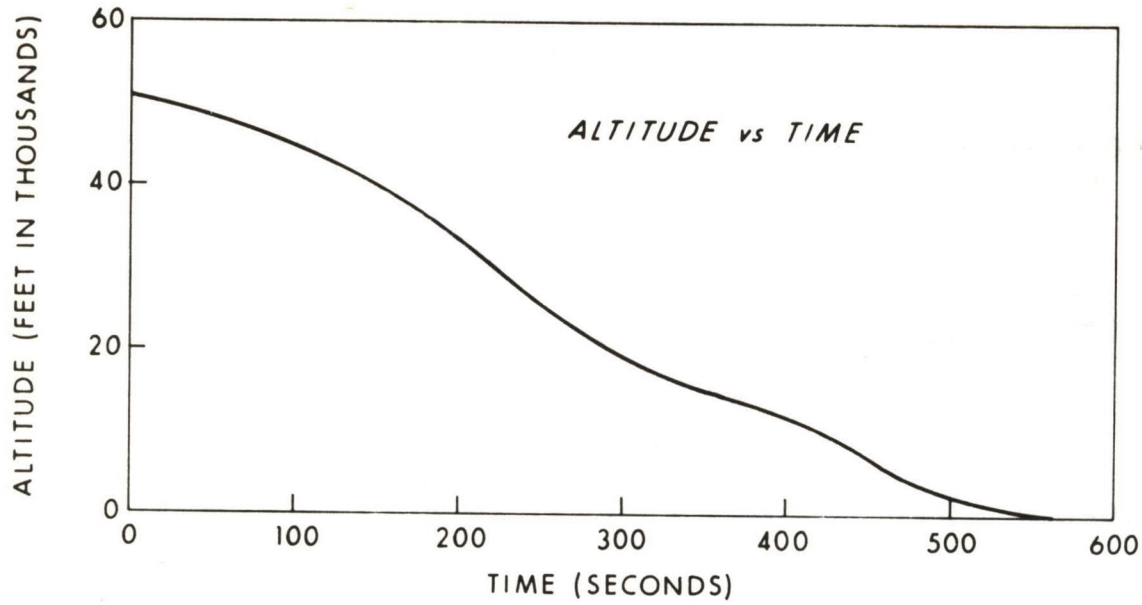

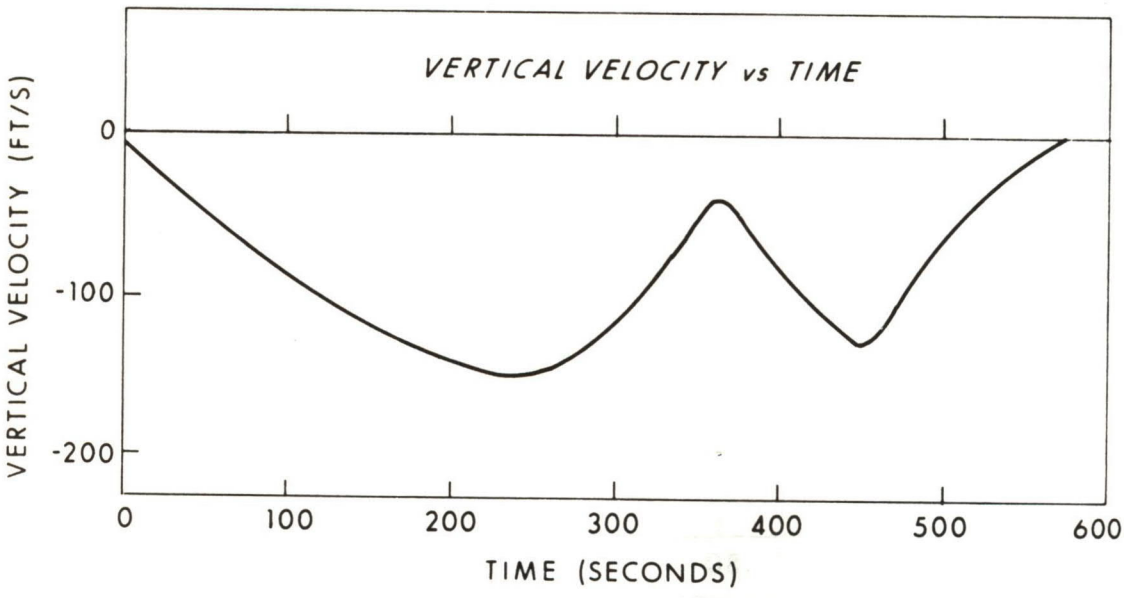

Fig. 3.4 Altitude and Vertical Velocity vs Time on Reference Trajectory

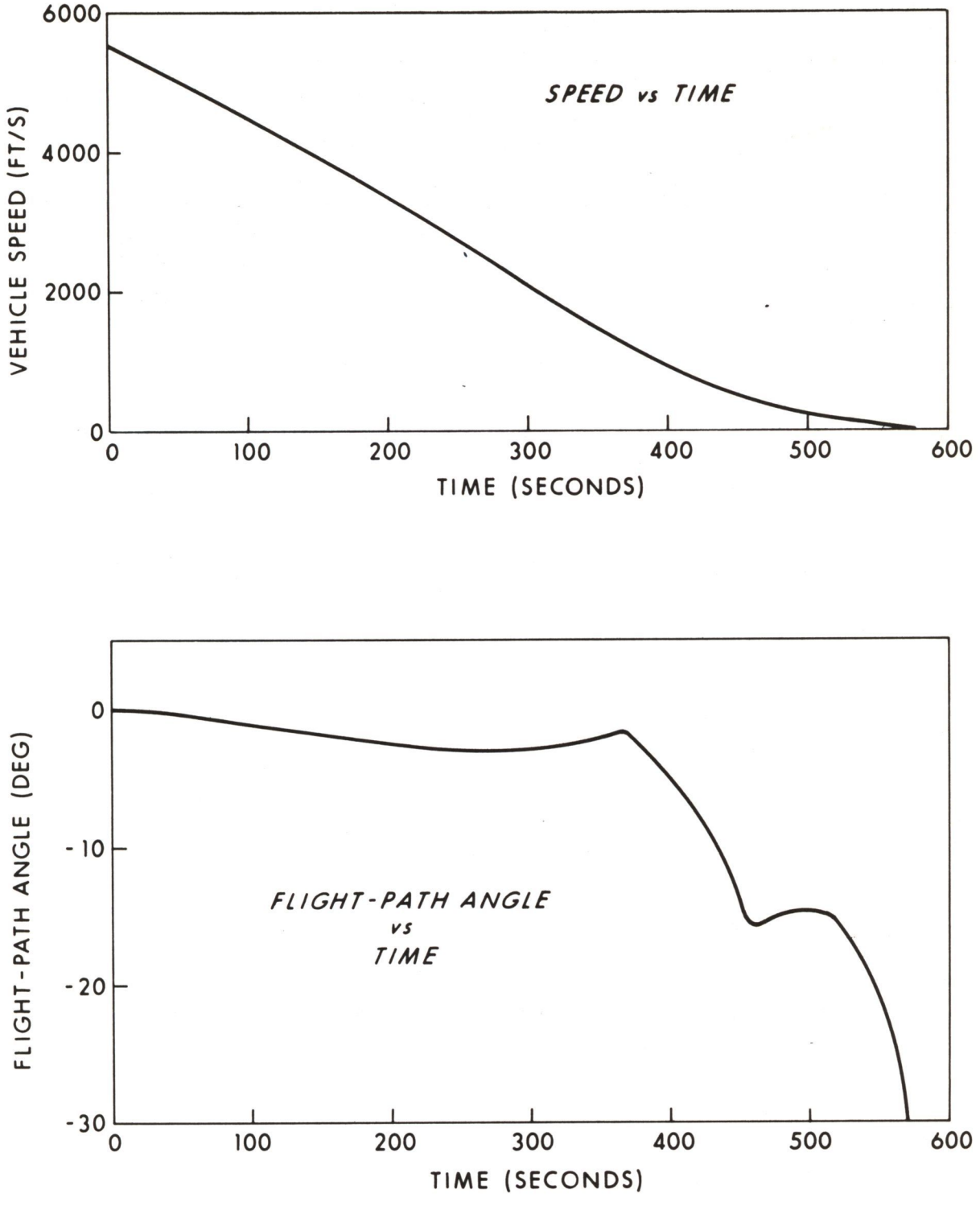

Fig. 3.5 Speed and Flight-Path Angle vs Time on Reference Trajectory

Table 3.1

Terminal Conditions for Reference Trajectory

	Initial Point	High-Gate Point	Low-Gate Point
Time after ignition	26 sec	452 sec	568 sec
Altitude	50,355 ft	6667 ft	114 ft
Speed	5563 ft/sec	518 ft/sec	2.8 ft/sec
Flight-Path Angle	-.08 deg.	-15.0 deg.	-29.2 deg.
Range-to-go to site	227 nm	4.1 nm	3.3 ft

CHAPTER 4

DEVELOPMENT OF LANDING-RADAR WEIGHTING FUNCTIONS

4.1 Introduction

A detailed description of the navigation system has been given in Chapter 2. Included there were the relations for updating the state-vector estimates with range* and velocity data from the landing radar. As was mentioned earlier, the landing-radar weighting functions are to be precomputed and stored in the LEM Guidance Computer (LGC). The altitude weighting function is stored as a linear function of estimated vehicle altitude; the velocity-component weighting functions are stored as linear functions of the estimated vehicle speed. The equations for these linearized weighting functions are given in Chapter 2.

The present chapter is concerned with the development or evolution process that led to the weighting functions that were finally selected. First of all, the models formulated for the IMU and landing radar are presented. Then the various relations used in the statistical analysis of the navigation-system performance during the landing maneuver are presented. This statistical analysis is a necessary step in the process of determining landing-radar weighting functions. Included here is a discussion of the various methods investigated for the treatment of radar bias errors and terrain-slope variations in the estimation process. Finally, a description is given of the various weighting functions that have been considered for the landing radar, leading to the currently employed weighting functions.

4.2 Modeling of the Navigation Sensors

4.2.1 General Considerations

In order to properly model the navigation sensors for the purpose of determining estimator weighting functions, two different types of information are required:

1) the statistical characteristics of the errors to be expected in the measurements from all the sensors, and
2) the sensitivities of the various landing-radar measurements to small changes in the state vectors.

* The landing radar provides data on the range from the vehicle to the lunar terrain, measured along the direction of the range beam. Inasmuch as this measurement is useful primarily in updating altitude estimates, it is often referred to in this report as an "altitude" measurement rather than a "range" measurement.

With regard to the statistical description of the measurement errors, it must first be decided whether to model the error as a white noise (uncorrelated in time), as a bias error (completely correlated), or as a colored noise (intermediate correlation-time intervals). Then, it is necessary to determine the first and second moments of the probability distributions (mean and mean-squared values), including the correlations between the different measurement errors. In many cases it is necessary to use a combination of white noise, bias errors, and colored noise to properly represent the errors from a given measurement.

The sensitivity of the different landing-radar measurements, as required in the navigation-system design, is defined for a given measurement (q_n) by the relation:

$$\delta q_n = \underline{b}_n \cdot \delta \underline{x}_n \tag{4-1}$$

where $\underline{b}_n$ represents the sensitivity of the measurement (q_n) at the time t_n to small changes in the state vector ($\delta \underline{x}_n$). The elements of $\underline{b}_n$ are the first-order terms of a Taylor series expansion about the reference state, relating small changes in q_n to small changes in $\underline{x}_n$, i e, $\frac{\partial q}{\partial x_0}, \frac{\partial q}{\partial x_1}, \ldots \frac{\partial q}{\partial x_i}$.

4.2.2 Inertial Measurement Unit

The inertial measurement unit or IMU measures the total specific force acting on the vehicle. By integrating the basic equations of vehicle motion, it is possible to compute the changes in vehicle position and velocity from their values at the start of the integration interval. The gravitational force term required in these computations can be based on the current estimate of vehicle position.

Some of the important sources of error in the IMU measurements used for navigation during the landing maneuver are the following:

1) initial alignment uncertainty of the inertial package,
2) drift of the stabilization gyros,
3) accelerometer output bias errors,
4) accelerometer scale factor errors.

In order to obtain a reasonably accurate model for the IMU, it was decided to represent the performance uncertainties by the combination of a random error in the measurement of specific force ($\underline{\alpha}_I$), and bias errors corresponding to the initial misalignment ($\underline{\gamma}_{AL}$), the gyro drift rate ($\underline{\gamma}_{DR}$), the accelerometer bias ($\underline{\gamma}_{BI}$), and the accelerometer scale-factor uncertainty ($\underline{\gamma}_{SF}$).

The vectors $\underline{\alpha}_I$, $\underline{\gamma}_{BI}$, and $\underline{\gamma}_{SF}$ in this case represent components of error in the measurement of specific force along the three orthogonal inertial-package reference axes. Likewise, the vectors ($\underline{\gamma}_{AL}$) and ($\underline{\gamma}_{DR}$) represent

small angular displacements and angular rates of rotation about the inertial-package reference axes. The magnitudes of each of these errors for an ensemble of inertial units are assumed to follow a Gaussian distribution about a zero mean value.

In order to obtain a model for the IMU errors that was reasonably accurate and at the same time not unduly complex, it was decided to represent the error in measured specific force ($\tilde{\underline{e}}_s$) as a linear combination of the above-mentioned measurement errors. By using this type of linear model for the IMU, the statistical error analysis of the navigation-system performance during the landing maneuver (which is useful in determining weighting functions) is greatly simplified. This linear error model for the IMU is most conveniently described by the relation[8]:

$$\tilde{\underline{e}}_s = M_{AL}\,\underline{\gamma}_{AL} + M_{DR}\,\underline{\gamma}_{DR} + M_{BI}\,\underline{\gamma}_{BI} + M_{SF}\,\underline{\gamma}_{SF} + \underline{\alpha}_I \tag{4-2}$$

where M_{AL}, M_{DR}, M_{BI}, and M_{SF} are 3 x 3 matrices. The measurement bias errors $\underline{\gamma}_{AL}$, $\underline{\gamma}_{DR}$, $\underline{\gamma}_{BI}$, and $\underline{\gamma}_{SF}$, and the measurement random errors $\underline{\alpha}_I$ are all three-dimensional vector quantities.

If the inertial-package alignment errors are reasonably small, it can be shown[8] that M_{AL} is given by the relation:

$$M_{AL} = \begin{bmatrix} 0 & -s_z & s_y \\ s_z & 0 & -s_x \\ -s_y & s_x & 0 \end{bmatrix} \tag{4-3}$$

where s_x, s_y, and s_z are the components of specific force ($\underline{s}$) measured along the inertial-package axes. Likewise, for the assumed conditions of constant drift-rate components of $\underline{\gamma}_{DR}$ and small angular displacements of the inertial package, it can be seen that M_{DR} is given by:

$$M_{DR} = tM_{AL} \tag{4-4}$$

where t represents the time after the start of the braking phase. It can also readily be seen that M_{BI} is equal to the 3 x 3 unit matrix I. Finally, if the elements of $\underline{\gamma}_{SF}$ are expressed as fractions of the total specific force, it can be shown that M_{SF} is given by:

$$M_{SF} = \begin{bmatrix} s_x & 0 & 0 \\ 0 & s_y & 0 \\ 0 & 0 & s_z \end{bmatrix} \tag{4-5}$$

where s_x, s_y, and s_z again represent the components of specific force measured along the inertial-package axes.

The accuracy of the navigation system during the landing maneuver is most conveniently described by the covariance matrix of the errors in the estimates of the state vector. The relation of Eq. 4-2, as will be shown later in this chapter, is extremely useful for computing this covariance matrix during the powered landing maneuver.

4.2.3 Doppler-Velocity Measurement Unit

As a basis for modeling the doppler radar, a three - beam configuration, as shown in Fig. 2-1, has been assumed. The doppler-frequency shift experienced by each beam is proportional to the component of vehicle velocity (relative to the lunar terrain) along the particular beam. By adding and subtracting the doppler-frequency shifts for the different pairs of beams, it is possible to determine the components of vehicle velocity in an orthogonal coordinate frame fixed with respect to the radar-antenna axes. This coordinate frame is for convenience referred to as the XA-YA-ZA frame, and the corresponding velocity components are referred to as v_{XA}, v_{YA}, and v_{ZA}. The relations between these velocity components and the doppler frequency shifts have been presented in Chapter 2, (Eqs. 2-1 through 2-3).

In order to utilize the velocity-measurement data (v_{XA}, v_{YA}, and v_{ZA}) for navigation of the landing vehicle, it is necessary to determine the geometrical relationship between the basic velocity-measurement frame (XA, YA, and ZA axes) and the inertial-reference frame (XI, YI, and ZI axes). The desired relationship is most conveniently represented by a matrix M_{IA}, which transforms velocity data from components in inertial coordinates ($\underline{v}_I$) to components in antenna coordinates ($\underline{v}_A$) according to the expression

$$\underline{v}_A = M_{IA}\,\underline{v}_I \tag{4-6}$$

The row vectors of M_{IA} are the unit vectors along the antenna axes ($\underline{u}_{XA}$, $\underline{u}_{YA}$, and $\underline{u}_{ZA}$) expressed in terms of inertial-frame components. The relation for M_{IA} is :

$$M_{IA} = \begin{bmatrix} \underline{u}^T_{XA} \\ \hline \underline{u}^T_{YA} \\ \hline \underline{u}^T_{ZA} \end{bmatrix} \tag{4-7}$$

where the superscript T is used to indicate the transpose operation.

Using the relations of Eqs. 4-6 and 4-7, the sensitivity vector ($\underline{b}$) relating changes in the doppler-velocity measurements to changes in the state vector can readily be determined. The desired relations for $\underline{b}$, shown for convenience transposed, are:

$$\underline{b}^T_{VXA} = \left[\underline{0}^T \;\vdots\; \underline{u}^T_{XA}\right] \tag{4-8}$$

$$\underline{b}^T_{VYA} = \left[\underline{0}^T \;\vdots\; \underline{u}^T_{YA}\right] \tag{4-9}$$

$$\underline{b}^T_{VZA} = \left[\underline{0}^T \;\vdots\; \underline{u}^T_{ZA}\right] \tag{4-10}$$

where the vector $\underline{0}$ is a 3-dimensional vector having all zero-valued elements. The sensitivity vectors $\underline{b}_{VXA}$, $\underline{b}_{VYA}$, and $\underline{b}_{VZA}$ are each 6-dimensional vectors containing terms corresponding to all six state-vector components. The subscript "n", which is used to indicate values at time t_n, has been left off the quantities in Eqs. 4-8 through 4-10 to simplify notation. The first three elements of these vectors are zero, as would be expected, since the doppler-velocity measurements are to first order insensitive to changes in the position of the vehicle.

The modeling of errors present in the doppler radar will next be considered. Some of the errors typically found in doppler radars[9-12] are the following:

1) actual frequency-measurement error (frequency tracker)
2) conversion of frequency data to electrical signals
3) transmission-frequency errors
4) terrain-reflectivity variation errors
5) orientation of radar-antenna coordinate frame (XA, YA, and ZA axes) with respect to the inertial-reference frame (XA, YI, and ZI axes).

These errors lead to both random and bias errors in the measurement of vehicle velocity.

As might be expected, it is difficult to model the doppler radar in sufficient detail so that each of the above-mentioned errors is explicitly accounted for in the model. Accordingly, in order to obtain a relatively simple model that at the same time was somewhat representative of radar performance, it was decided to model the radar by the following combination:

1) a random error (Gaussian white noise) whose rms value is proportional to the magnitude of the vehicle's velocity ($\underline{\alpha}_D$)
2) a bias error corresponding to the uncertainties in the knowledge of the orientation of the radar-antenna coordinate frame with respect to the inertial-reference frame ($\underline{\gamma}_D$)

Under these conditions the components of vehicle velocity as measured by the doppler radar and then transformed to the inertial reference coordinate frame

will be in error by the amount:

$$\tilde{\underline{e}}_{VA} = \underline{\alpha}_D + M_{RD}\,\underline{\gamma}_D \tag{4-11}$$

where $\tilde{\underline{e}}_{VA}$ is a 3-dimensional vector containing the errors in the XA, YA, and ZA components of velocity. If the angular displacement components of $\underline{\gamma}_D$ are small angles then it can be shown that M_{RD} is given by the relation:

$$M_{RD} = \begin{bmatrix} 0 & -v_{ZA} & v_{YA} \\ v_{ZA} & 0 & -v_{XA} \\ -v_{YA} & v_{XA} & 0 \end{bmatrix} \tag{4-12}$$

where v_{XA}, v_{YA}, and v_{ZA} represent the components of vehicle velocity along the XA, YA, and ZA axes.

It should be noted the magnitudes of the components of both $\underline{\alpha}_D$ and $\underline{\gamma}_D$ are assumed to be normally distributed about a zero mean value, even though $\underline{\alpha}_D$ represents a random error and $\underline{\gamma}_D$ a bias error. Also, the rms values of the components of $\underline{\alpha}_D$ are varied during the landing maneuver as the vehicle's velocity is changed, whereas the rms value for the components of $\underline{\gamma}_D$ will remain fixed throughout the landing maneuver.

4.2.4. Range Measurement Unit

The landing radar provides data on the range from the vehicle to a point on the lunar terrain below, measured along the direction of the range beam. The range beam, as can be seen from Fig. 2.1, is located half-way between the two rear doppler-velocity beams. The range beam is fixed with respect to the vehicle body, i.e. its orientation with respect to the inertial-reference axes will change during the landing maneuver as the orientation of the thrust vector is changed.

Inasmuch as the range measurement is simply to the lunar surface along the range-beam direction rather than to a preselected known point on the surface, the primary useful navigation data from the measurement are of vehicle altitude. For this reason the range measurement is frequently referred to in this report as an "altitude" rather than a "range" measurement. The angular displacement of the range beam from the local vertical must, of course, be determined to obtain useful altitude data from the range measurement.

The sensitivity of the range measurement to changes in the state vector ($\underline{b}$) is given simply by the relation:

$$\underline{b}^T = \left[\underline{u}^T{}_r / \cos\phi_H \;\vdots\; \underline{0}^T \right] \tag{4-13}$$

where $\underline{u}_r$ is a unit vector along the local vertical, and ϕ_H is the angle between the direction of the local vertical and range beam. The quantity $\underline{0}$ is a 3-dimensional vector containing all zero-valued elements. The last three elements of $\underline{b}$ are represented by $\underline{0}$, since the range measurement is insensitive to first order to changes in vehicle velocity. It should also be noted that the position-sensitive part of the $\underline{b}$-vector is directed along the local vertical ($\underline{u}_r$) rather than along the range beam. The reason for this is that to first order the measurement is insensitive to changes in position in the horizontal direction.

An important source of error in the use of landing-radar measurements to update the state vector is the uncertainty or variation in the characteristics of the lunar terrain. Of particular concern here are differences in altitude (relative to the lunar sphere) between the selected landing site and the point to which the range measurements are made. It is expected that hills, craters, and slopes of significant magnitude may be encountered during the landing maneuver.

The basic model selected to represent the errors in the landing-radar range measurements consists of the following combination:

1) a random white noise whose rms value is proportional to the altitude of the vehicle down to a specified minimum altitude below which it remains fixed (α_h).
2) a constant slope away from the landing site (γ_h) causing a measurement bias error proportional to the ground-range distance from the vehicle to the site.

The measurement error ($\tilde{e}_h$) under these conditions is given by the relation:

$$\tilde{e}_h = \alpha_h + r_{GO}\gamma_h \qquad (4\text{-}14)$$

where r_{GO} represents the down-range distance from the vehicle to the landing site. Both α_h and γ_h are assumed to have Gaussian distributions about zero mean values,* even though the rms value of α_h is varied as a function of altitude whereas the rms value of γ_h remains fixed.

In the basic navigation system investigated in this report the IMU-derived estimates of vehicle position are updated only along the direction of the local vertical, as was indicated in Eq. 2-12 of Section 2. Under these conditions it is possible for the vehicle to be as much as 5,000-6,000 feet down range from the Low-Gate point at the end of the visibility phase. It is particularly important that the vehicle be at the proper altitude at the point where the vehicle actually arrives at the end of the visibility phase. For this reason the proper values of range-to-go (r_{GO}) to use in the navigation-system error models are the values estimated in the navigation system rather than the true values.

*Viewed on an ensemble basis at a given time.

An alternate model currently under investigation for representing terrain-slope variations as a correlated noise [13, 14] whose rms value is varied as a function of the distance from the vehicle to the selected site. The correlated noise is obtained by passing white noise through a first-order filter. The results of this study will be reported at a later date.

4.2.5 Summary of Sensor Models

The IMU has been modeled to include platform alignment ($\underline{\gamma}_{AL}$), gyro drift ($\underline{\gamma}_{DR}$), accelerometer bias ($\underline{\gamma}_{BI}$), and accelerometer scale-factor errors ($\underline{\gamma}_{SF}$). All of these errors are represented as time-invariant bias errors. A random error in the measurement of specific force ($\underline{\alpha}_{I}$) was also included. The basic errors in the measurement of specific force ($\underline{\tilde{e}}_{S}$) from all of these sources are given by Eq. 4-2.

The doppler-velocity measurement unit has been modeled to include a random error whose rms value is proportional to the magnitude of vehicle velocity ($\underline{\alpha}_{D}$), and a bias error corresponding to the uncertainty in knowledge of the relative orientation of the radar-antenna and inertial-reference frames ($\underline{\gamma}_{D}$). The velocity measurement errors are given by Eq. 4-11, the measurement-sensitivity vectors are given by Eqs. 4-8 through 4-10.

The range (altitude) measurement unit has been modeled to include a random error whose rms value is proportional to the altitude of the vehicle. The difference in altitude of the local terrain and the selected landing site (relative to the lunar sphere) has been modeled as a constant-slope bias (i e, the difference in altitude is proportional to the range-to-go to the site). The altitude-measurement errors are given by Eq. 4-14; the measurement-sensitivity vector is given by Eq. 4-13.

4.3 Statistical Analysis of Navigation-System Performance

4.3.1 General Considerations

In the selection of landing-radar weighting functions it is important to determine the accuracy of the navigation-system state-vector estimates prior to the incorporation of a new measurement. By properly comparing the accuracy of the a-priori estimates with the expected accuracy of the new measurement, a suitable measurement weighting funtion can be determined. The accuracies of the navigation system and the measurement sensor must, of course, be represented in statistical terms, since only the statistical characteristics of the errors of a given navigation system or navigation sensor are generally known before the actual operation of the system.

The accuracy of the navigation system can best be described by the covariance matrix of the errors in the estimate of the state vector (E). This

covariance matrix is defined mathematically by the relation:

$$E = \overline{\underline{e}\underline{e}^T} \tag{4-15}$$

where the quantity $\underline{e}$ represents the errors in the estimates of vehicle position ($\underline{e}_r$) and velocity ($\underline{e}_v$), i.e. it is a 6-dimensional vector quantity. The bar over $\underline{e}$ and its transpose $\underline{e}^T$ is used to indicate the operation of an ensemble average.

The estimation-error covariance matrix (E), which is a 6 x 6 symetrical matrix, can be partitioned into four 3 x 3 submatrices as indicated by:

$$E = \left[\begin{array}{c|c} \overline{\underline{e}_r\underline{e}_r^T} & \overline{\underline{e}_r\underline{e}_v^T} \\ \hline \overline{\underline{e}_v\underline{e}_r^T} & \overline{\underline{e}_v\underline{e}_v^T} \end{array}\right] \tag{4-16}$$

The upper-left submatrix represents the covariance matrix of the errors in position, and the lower-right submatrix represents the covariance matrix of the errors in velocity. The lower-left and upper-right submatrices represent the cross-correlation between position and velocity errors. The elements along the principal diagonal of E represent the mean-squared errors in the estimates of vehicle position and velocity.

The basic equations for computing the estimation-error covariance matrix (E) during the landing maneuver are quite complex, even with the relatively simple sensor models described in Sections 4.2.2 through 4.2.4. For this reason it is felt that a continuous in-flight computation of E during the powered landing maneuver is not desirable. On the other hand, it is important in ground-based simulation studies of the navigation system to determine E so that weighting functions are most intelligently selected. It is for this latter purpose that the relations for E presented in this section are intended.

4.3.2 Propagation of Estimation-Error Covariance Matrix

In this section the relations will be given for computing the covariance matrix of the errors in the estimates of the state vector (E) during the period when no landing-radar updatings take place. The important navigation sensor during this time is the IMU. The following section will show how E is updated after the processing of a landing-radar measurement.

Before presenting the relations for E, it is useful to describe the IMU in a more compact notation. Accordingly, let us make the following definitions:

$$\underline{\gamma}_I^T \triangleq \left[\begin{array}{c|c|c|c} \underline{\gamma}_{AL}^T & \underline{\gamma}_{DR}^T & \underline{\gamma}_{BI}^T & \underline{\gamma}_{SF}^T \end{array}\right] \tag{4-17}$$

and

$$M_I \triangleq \left[\begin{array}{c|c|c|c} M_{AL} & M_{DR} & M_{BI} & M_{SF} \end{array}\right] \tag{4-18}$$

where $\underline{\gamma}_I$ is a 12-dimensional vector and M_I is a 3 x 12 rectangular matrix. Using these definitions, the relation of Eq. 4-1 for the error in the measurement of specific force can be written simply as

$$\underline{\tilde{e}}_s = M_I \underline{\gamma}_I + \underline{\alpha}_I \tag{4-19}$$

Next, let the 3 x 3 symetrical matrix G represent the gradient with respect to position of the gravitational force from the moon acting on the vehicle, evaluated on the reference trajectory. It can be shown[3] that G is given by the relation:

$$G = \frac{\mu}{\rho^5} (3 \underline{\rho}\underline{\rho}^T - \rho^2 I) \tag{4-20}$$

where μ is the lunar gravitational constant, I is the 3-dimensional unit matrix, and $\underline{\rho}$ is the position of the vehicle with respect to the center of the moon.

Finally, let us define the matrices K, F and M in the following manner:

$$K \triangleq \left[\begin{array}{c|c} O & I \end{array}\right] \tag{4-21}$$

$$F \triangleq \left[\begin{array}{c|c} O & I \\ \hline G & O \end{array}\right] \tag{4-22}$$

$$M \triangleq \left[\begin{array}{c|c|c|c} O & O & O & O \\ \hline M_{AL} & M_{DR} & M_{BI} & M_{SF} \end{array}\right] \tag{4-23}$$

where O represents a 3 x 3 matrix having all zero-valued elements, and I represents the 3-dimensional unit matrix, F is a 6 x 6 square matrix, and M is a 6 x 12 rectangular matrix.

The computation of E during the landing maneuver is most easily accomplished by integrating the differential equation for the time-rate-of-change of E, starting from an initial value E_0. It can be shown[8] that the time-rate-of-change of E, i.e. $\dot{E}$, is given by:

$$\dot{E} = FE + EF^T + MC^T + CM^T + KQ_I K^T \tag{4-24}$$

where K, F, and M are defined by Eqs. 4-21 through 4-23. The random errors in measurement of specific force ($\underline{\alpha}_I$) are represented by a Gaussian white noise having a zero mean value and a covariance matrix $Q_I(t)\,\delta(t - \tau)$.* The matrix C represents the correlation between the errors in the estimate of the state vector and the IMU bias errors, that is:

$$C = \overline{\underline{e}\underline{\gamma}_I^T} \tag{4-25}$$

where the 12-dimensional vector $\underline{\gamma}_I$ has been defined in Eq. 4-17. The matrix C is most easily computed by integrating the differential equation for the time-rate-of-change of C, starting from an initial value C_0. It can be shown[8] that

* The quantity $\delta(t - \pi)$ represents the delta or unit impulse function.

the required equation for the time-rate-of-change of C, i.e. $\dot{C}$, is given by:

$$\dot{C} = FC + M\Gamma \tag{4-26}$$

where Γ represents the covariance matrix $\overline{\underline{\gamma}_I \underline{\gamma}_I^T}$ of the IMU bias errors.

The relation of Eq. 4-24 permits computation of the navigation-system estimation-error covariance matrix (E) during the periods in-between (and before) landing-radar measurements when the IMU is the primary navigation sensor. Simultaneously with the computation of E, the matrix C must also be computed, as indicated in Eq. 4-26.

4.3.3 Updating of Estimation-Error Covariance Matrix

It will be next shown how the covariance matrix E is changed after a new measurement is processed in the navigation system. The basic relation will be presented in terms of the measurement weighting vector $\underline{w}$. For convenience, the covariance matrix of the estimation errors prior to the processing of the new measurement at time t_n will be referred to as E'_n; the covariance matrix immediately after the processing of the measurement will simply be referred to as E_n.

Consider first of all the processing of a range (altitude) measurement at time t_n. Using the sensitivity for the range measurement (Eq. 4-13) and the measurement error model (Eq. 4-14), it can be shown[8] that the error in the state estimate immediately after the processing of the measurement ($\hat{\underline{e}}_n$) is given by:

$$\hat{\underline{e}}_n = (I - \underline{w}_h \underline{b}_n^T)\, \underline{e}_{n'} + \underline{w}_n (\alpha_{h,n} + r_{GO,n}\, \gamma_h) \tag{4-27}$$

where $\underline{e}'_n$ represents the error in the estimate at time t_n prior to the incorporation of the new range measurement. The quantity I represents the 6-dimensional unit matrix, and the quantities of α_h, r_{GO}, and γ_h have the same meanings as in Eq. 4-14 where the altitude-measurement error is modeled. The quantity $\underline{w}_n$, which is a 6-dimensional vector here, represents the weightings to be used on the altitude-measurement data in updating the six state-vector elements. The basic updating relation, as stated in Chapter 2 is:

$$\hat{\underline{x}}_n = \underline{x}'_n + \underline{w}_n (\tilde{h}_n - h'_n) \tag{4-28}$$

where $\tilde{h}$ and h' represents the measured and a-priori estimate of the altitude from the vehicle to the lunar surface.

Using the relation of Eq. 4-27, it can be shown that the estimation-error covariance matrix after the measurement has been processed (E_n) is related to the covariance matrix prior to the processing of the measurement (E'_n) by the expression:

$$E_n = S_n E'_n S_n^T + \underline{w}_n \underline{w}_n^T \left(\overline{\alpha_{h,n}^2} + r_{GO,n}^2 \overline{\gamma_h^2} \right) + r_{GO,n} \left(S_n \underline{c}_n \underline{w}_n^T + \underline{w}_n \underline{c}_n^T S_n^T \right) \tag{4-29}$$

where the symbol S_n has been used for convenience to represent the quantity $(I - \underline{w}_n \underline{b}_n^T)$. The quantities $\overline{\alpha_h^2}$ and $\overline{\gamma_h^2}$ represent the mean-squared values of the random error (α_h) and the slope-bias coefficient (γ_h) used in modeling the altitude-measurement errors. The vector $\underline{c}_n$, which is required in the computation of E_n (i.e. in the updating of E'_n), represents the correlation between the error in the estimate ($\underline{e}_n$) and the terrain slope-bias coefficient (γ_h). It is given by the relation:

$$\underline{c}_n = \overline{\underline{e}_n \gamma_h} \tag{4-30}$$

where the bar over $\underline{e}_n \gamma_h$ is used to indicate the operation of taking an ensemble average.

The vector $\underline{c}_n$ is most easily obtained by integrating the differential equation for $\underline{c}_n$, starting from an initial value $\underline{c}_0$. The desired relation is[8]:

$$\dot{\underline{c}}_n = F \underline{c}_n \tag{4-31}$$

where F represents the 6 x 6 matrix defined in Eq. 4-22. The relation of Eq. 4-31 essentially propagates $\underline{c}_n$ in-between (and before) the landing-radar updatings. The vector $\underline{c}_n$ must also be updated after each new measurement is processed. For the case when an altitude measurement is processed, the updating relation is[8]:

$$\underline{c}_n = (I - \underline{w}_{h,n} \underline{b}_{h,n}^T) \underline{c}'_n + \underline{w}_{h,n} r_{GO,n} \overline{\gamma_h^2} \tag{4-32}$$

where the quantity $\underline{c}_n'$ represents the value of $\underline{c}_n$ prior to the incorporation of the new measurement into the estimate. The subscript "h" is attached to $\underline{w}_n$ and $\underline{b}_n$ to indicate that these quantities are for the altitude measurement being processed at time t_n. For the case when a velocity component measurement is processed, on the other hand, the updating relation is simply:

$$\underline{c}_n = (I - \underline{w}_{v,n} \underline{b}_{v,n}^T) \underline{c}_n' \tag{4-33}$$

where the subscript "v" is used to indicate that the values of w_n and b_n are for the velocity-component measurement being processed.

Consider next the updating of E'_n after a velocity-component measurement v_{XA} has been processed in the navigation system. The measurement bias error in this case (γ_{VXA}) is given by the relation:

$$\gamma_{VXA} = \underline{m}_{VXA}^T \underline{\gamma}_D \tag{4-34}$$

where the vector $\underline{m}_{VXA}^T$ represents the top row-vector of the matrix M_{RD} (defined in Eqs. 4-11 and 4-12). The vector $\underline{\gamma}_D$ represents the uncertainties

in knowledge of the orientation of the XA-YA-ZA radar-antenna coordinate frame relative to the XI-YI-ZI inertial-reference frame. Likewise, the random component of the measurement error α_{VXA} is the top element of the vector $\underline{\alpha}_D$ (Eq. 4-11). Using the above relations, it can be shown[8] that the error in the state estimate after processing the velocity-component measurement is given by the relation:

$$\hat{\underline{e}}_n = (I - \underline{w}_n \underline{b}_n^T)\, \underline{e}_n' + \underline{w}_n (\alpha_{VXA} + \underline{m}_{VXA}^T \underline{\gamma}_D) \tag{4-35}$$

where the weighting vector ($\underline{w}_n$) and the measurement sensitivity ($\underline{b}_n$) are those corresponding to the velocity-component measurement being processed.

Using the relation of Eq. 4-35 it can be shown[8] that E_n is given by the expression:

$$E_n = S_n E_n' S_n^T + \underline{w}_n \underline{w}_n^T (\overline{\alpha^2}_{VXA} + \underline{m}_{VXA}^T \Gamma_D \underline{m}_{VXA})$$
$$+ \underline{w}_n \underline{m}_{VXA}^T C_n^T S_n^T + S_n C_n \underline{m}_{VXA} \underline{w}_n^T \tag{4-36}$$

where the 6 x 3 matrix C_n represents the correlation between the state-vector estimation errors ($\underline{e}_n$) and the radar-antenna coordinate-frame alignment errors ($\underline{\gamma}_D$). The relation defining C_n is:

$$C_n = \overline{\underline{e}_n \underline{\gamma}_D^T} \tag{4-37}$$

where the bar over $\underline{e}_n \underline{\gamma}_D^T$ is used to indicate an ensemble average.

The matrix C_n is most easily obtained by integrating the differential equation for C_n, starting from the initial value C_0. The basic differential equation is:

$$\dot{C}_n = F C_n \tag{4-38}$$

where the matrix F is as defined as in Eq. 4-22. The relation for updating C_n after a v_{XA} measurement has been processed is[8]:

$$C_n = (I - \underline{w}_{VXA,n} \underline{b}_{VXA,n}^T)\, C_n' + \underline{w}_{VXA,n} \underline{m}_{VXA,n}^T \Gamma_D \tag{4-39}$$

where the subscript "VXA" is used to indicate that the quantities $\underline{w}$, $\underline{b}$, and $\underline{m}$ are associated with the v_{XA} measurement. The relations for updating C_n after v_{YA} and v_{ZA} measurements are similar to Eq. 4-39, except that the values of $\underline{w}$, $\underline{b}$, and $\underline{m}$ corresponding to the v_{YA} and v_{ZA} measurements are used. For the case of an altitude updating, the relation for updating C_n is simply:

$$C_n = (I - \underline{w}_{h,n} \underline{b}_{h,n}^T)\, C_n' \tag{4-40}$$

where $\underline{w}_h$ and $\underline{b}_h$ are associated with the altitude measurement.

The relations have been presented for updating E_n for a v_{XA}-component measurement (Eqs. 4-36 through 4-40). The basic relations for the v_{YA} and v_{ZA} component measurements are similar to these, except that the measurement errors and sensitivities associated with the v_{YA} and v_{ZA} measurements are used.

In concluding this section it should be noted that the updating relations presented here are valid for any functional form of the 6-dimensional weighting vector ($\underline{w}_n$). No simplifying assumptions have been made in regard to the form of the weighting functions (e.g. optimum least-squares) in the derivation of these relations.

4.3.4 Application of Statistical-Analysis Techniques

The relations presented in the preceding sections (Secs. 4.3.2 and 4.3.3) provide a means for computing the estimation-error covariance matrix for the navigation system (E) during the landing maneuver. The statistical relations, as mentioned earlier, are valid for any 6-dimensional weighting vector ($\underline{w}_n$); the extension of these relations to higher-order weighting vectors and state vectors is a simple matter. It should be noted, however, that the relations for the covariance matrix (E) are predicated on an IMU model as described by Eq. 4-2 and a landing-radar model as given by Eqs. 4-6 through 4-14.

The statistical estimation-error data are extremely useful in evaluating navigation-system performance for different types of weighting vectors. A set of typical, statistical estimation-error data are presented in Fig. 4.1 for the uncoupled weighting functions shown in Fig. 2.3. Additional statistical data are given in Chapter 6 for the other weighting functions investigated.

The curves of Fig. 4.1 show the rms errors in the estimates of vehicle position and velocity as a function of time during the landing maneuver. These data were obtained from a digital-computer simulation of the landing maneuver, using the sensor models and statistical error relations given earlier in this chapter. The initial and desired terminal conditions used here were as given in Tables 1.1 and 3.1; the measurement schedule was as shown in Fig. 2.2.

Examination of the data of Fig. 4.1 indicates that the landing-radar updatings, viewed on an ensemble-average basis, significantly improve the accuracy of the navigation system. As can be seen, the final values of the rms errors in altitude and velocity are much smaller than their values prior to the start of the updatings. No position updatings (other than altitude) are made in these data, with the result that the final values of the rms errors in the estimates of position are larger than the initial values. The simplified linearized weighting functions used in the data of Fig. 4.1 are not the optimum weighting functions

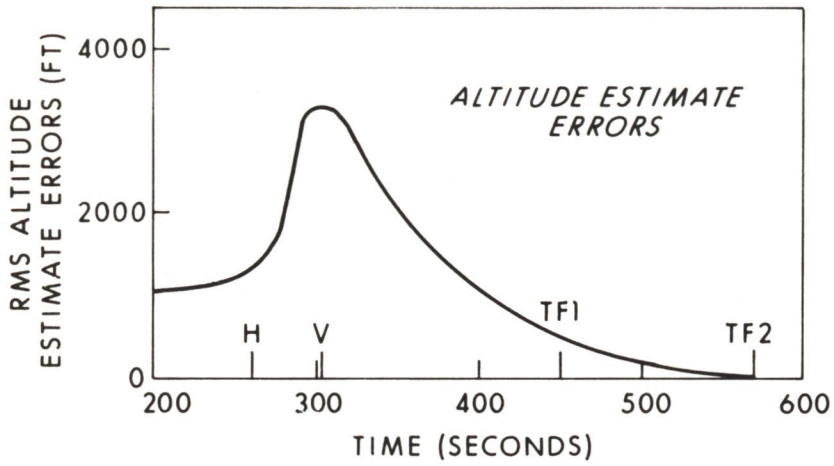

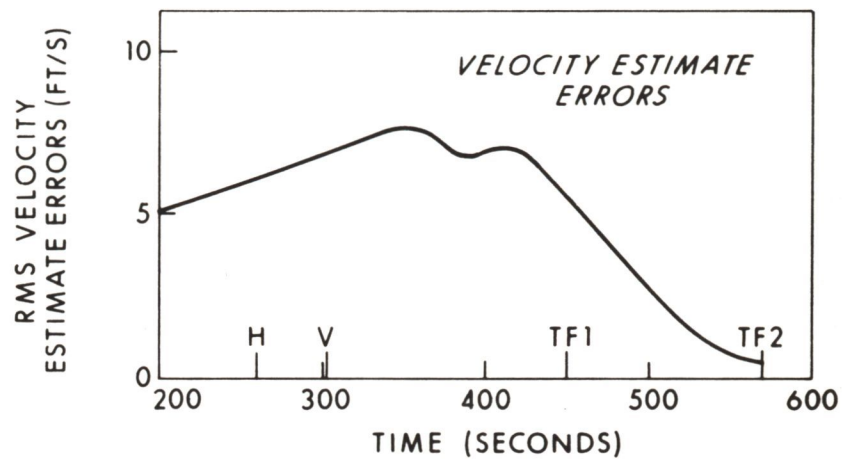

- *NOTES* -

1. LINEARIZED WEIGHTING FUNCTIONS ARE USED HERE
2. H = TIME OF INITIAL ALTITUDE UPDATING
3. V = TIME OF INITIAL VELOCITY UPDATING
4. TF1 = END OF BRAKING PHASE
5. TF2 = END OF VISIBILITY PHASE

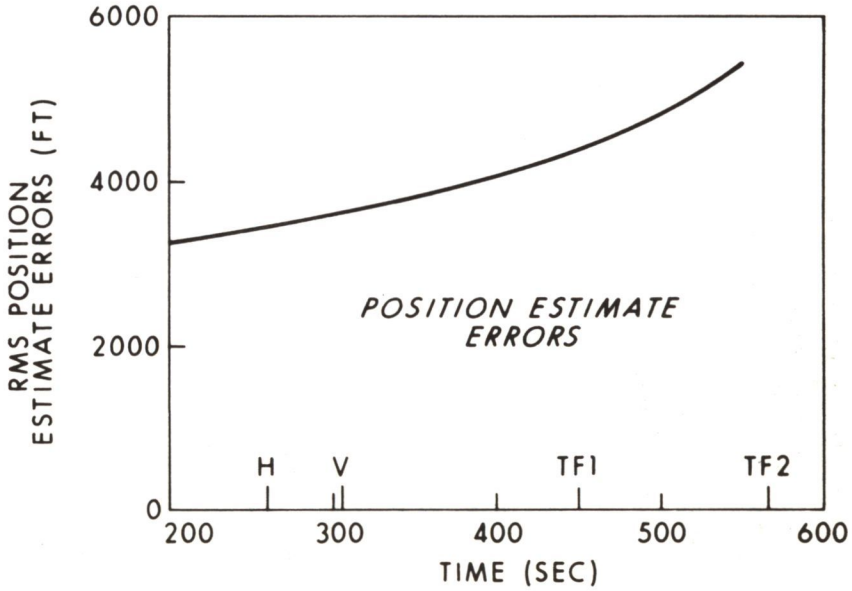

Fig. 4.1 RMS Altitude, Velocity, and Position Estimate Error on Typical Landing Trajectory

for the navigation problem investigated here. This can be seen from the portion of the altitude error curve immediately after the start of the updatings, during which the rms errors initially appear to increase at a more rapid rate than before the start of the updating.

4.4 Evolution Process for Landing Radar Weighting Functions

4.4.1 General Information

Several different types of weighting functions have been investigated for processing the landing-radar data in the navigation system during the landing maneuver. The present section will describe these weighting functions, leading to the currently employed set. Statistical data will be presented to show the navigation-system accuracy attainable with the different weighting functions.

An important source of differences between the various weighting functions is the way in which doppler-velocity bias errors and terrain-slope variations are handled in the derivation of the weighting functions. The bias-type error , for example, could either be completely ignored, could be estimated as an additional state-vector element, could be treated as white noise, or could be accounted for partially in the estimator design.

Also, the computations required to implement the weighting functions in the LGC are a very important consideration here. Computation time is particularly critical during the powered landing maneuver.

For convenience in presentation, the weighting functions are divided in two classifications, referred to as "coupled" and "uncoupled" weighting functions. The coupled weighting functions update all components of the state vector with the data from each measurement. The uncoupled weighting functions update only the components of the state-vector corresponding to the measurement being processed. The computation requirements for the coupled weighting vectors are relatively complex; the requirements for the uncoupled weighting vectors are relatively simple.

4.4.2 Coupled Weighting Functions

In the earlier studies of landing-radar weighting functions, serious consideration was given to the possibility of using the so-called "coupled" weighting functions wherein all components of the state vector are updated by the data from each measurement. These weighting functions are referred to as "coupled" weighting functions because information is taken from all elements of the estimation-error covariance matrix in determining the proper weightings for each new measurement. Altitude information, for example, is used to update velocity (as well as altitude). Also, velocity information is used to update position (as well as velocity).

A potential advantage in the use of coupled weighting functions is that the down-range position estimates can be improved to a certain extent by virtue of data from the altitude and velocity measurements. This improvement will occur even though no down-range measurements per se are taken. The computational requirements for the coupled weighting functions, however, are much greater than for the uncoupled weighting functions. It is for this reason that they are not being seriously considered at the present time.

The distinguishing characteristics of various coupled weighting functions that have been considered for the landing maneuver are summarized in Table 4-1. All of these weighting functions are designed to give optimum linear least-squares or minimum-variance state-vector estimate errors, using the techniques of Kalman[2] and Battin[3]. The differences between the weighting functions, as indicated in the table, are basically in the treatment of doppler-velocity bias errors and terrain-slope variations in the weighting-function computations.

The first weighting functions considered, W-1, of Table 4-1, are based on the assumption that no doppler-velocity bias errors or terrain-slope variations are present. This is not a good assumption in view of the expected magnitudes of these errors. Using this assumption, however, it can be shown[8] that the weighting functions for a least-squares estimation error is given by:

$$\underline{w}_n = \frac{\overset{*}{E}_n' \underline{b}_n}{\underline{b}_n^T \overset{*}{E}_n' \underline{b}_n + \overline{\alpha_n^2}} \qquad (4\text{-}41)$$

where $\underline{b}_n$ and $\overline{\alpha_n^2}$ represent the sensitivity and mean-squared random error for the measurement being processed. The quantity $\overset{*}{E}_n'$ represents the covariance matrix of the errors in the state-vector estimates prior to the incorporation of the new measurement, assuming that no doppler-velocity bias or terrain-slope variations are present. In effect, $\overset{*}{E}_n'$ is the estimator's own idea of what the estimation-error covariance E_n' is; the estimator's idea in this case is not very good because its model here has ignored the bias and terrain variations.

It should be noted here that, in the most general case, an in-flight computation of $\underline{w}_n$ from Eq. 4-41 would require the propagation and updating of a 6 x 6 estimation-error covariance matrix throughout the landing maneuver. Also, the vector-matrix product operations in Eq. 4-41 would have to be performed for each new measurement. Alternately, if the approach of precomputing and storing were used instead, a total of 24 different weighting functions would be required (six for each of the four types of measurements being processed).

Table 4.1 Coupled Weighting Function Characteristics

Type	Treatment of Doppler-Velocity Bias Errors	Treatment of Terrain-Slope Variations
W-1	Ignored completely	Ignored completely
W-2	Treated as white noise	Treated as white noise
W-3	Account for in computation of E-matrix as bias error	Account for in computation of E-matrix as bias error
W-4	Account for in computation of E-matrix as bias error	Estimate a constant-slope bias error

The second weighting functions considered, W-2 of Table 4.1, are based on the idea of modeling the doppler-velocity bias errors and the terrain-slope variations as random errors (Gaussian white noise) in the derivation of estimator weighting functions. This is not a particularly good modeling scheme, but it is certainly better than ignoring the velocity-bias and terrain-variation errors completely. Under these conditions it can be shown that the weighting function for a least-squares estimation error is given by:

$$\underline{w}_n = \frac{\overset{*}{E}_n' \underline{b}_n}{\underline{b}_n^T \overset{*}{E}_n' + \overline{\alpha_n^2} + \overline{\gamma_n^2}} \tag{4-42}$$

where $\overline{\alpha_n^2}$ and $\overline{\gamma_n^2}$ represent the mean-squared values of the random and bias errors in the measurement being processed. The quantity $\overset{*}{E}_n'$ represents the computed E_n' in the estimator, assuming here a white-noise model for the velocity-bias and terrain-slope variation errors.

The third weighting functions considered, W-3 of Table 4.1, are based on the idea of accounting for the doppler-velocity bias and terrain-slope variation errors in the weighting-function computations as modeled in the earlier part of this chapter. No attempt is made here to estimate either of these bias-type errors. The weighting-function relations under these conditions are more complex than in Eqs. 4-41 and 4-42. For the case of an altitude-measurement updating, the weighting functions are[8]:

$$\underline{w}_n = \frac{E_n' \underline{b}_n - r'_{GO,n} \underline{c}_n'}{\underline{b}_n^T E_n' \underline{b}_n + \overline{\alpha_n^2} + \overline{\gamma_n^2} r_{GO}'^2 - 2 \underline{b}_n^T \underline{c}_n'} \tag{4-43}$$

where $\overline{\alpha_n^2}$ and $\overline{\gamma_n^2}$ represent the mean-squared values of the random component of the measurement error and the assumed slope-bias coefficient, respectively. The quantity r'_{GO} represents the current estimate of the down-range distance to the landing site. The vector $\underline{c}_n'$ is the estimated correlation between terrain-slope-bias coefficient and estimation error, as defined in Eq. 4-30 and computed in Eqs. 4-31 through 4-33. Similarly, for a velocity-component updating such as with v_{XA}, the weighting functions are[8]:

$$\underline{w}_n = \frac{E_n' \underline{b}_n - C_n' \underline{m}_{VXA,n}}{\underline{b}_n^T E_n' \underline{b}_n + \overline{\alpha^2}_{VXA,n} + \underline{m}_{VXA,n}^T \Gamma_D \underline{m}_{VXA,n} - 2 \underline{b}_n^T C'_n \underline{m}_{VXA,n}} \tag{4-44}$$

where the 6 x 3 matrix C_n is used to represent the correlations between the errors in the state-vector estimates and the velocity-measurement bias errors. The defining relation for C_n is Eq. 4-37; the relations for computing C_n are

Eqs. 4-38 and 4-39. The vector $\underline{m}_{VXA}$, which is used in the modeling of the velocity-bias errors, contains the elements in the top row of the matrix M_{RD} (See Eq. 4-12). The quantity Γ_D represents the covariance matrix of the radar alignment bias error, that is, $\overline{\underline{\gamma}_D \underline{\gamma}_D^T}$.

It is evident from a cursory examination of Eqs. 4-43 and 4-44 that the computational requirements for an in-flight mechanization of these equations in the LGC are quite severe. In particular, not only would the 6 x 6 covariance matrix (E_n) have to be computed throughout the landing maneuver, but also the 6 x 1 vector ($\underline{c}_n$) and the 6 x 3 matrix (C_n) would be required. Alternately, if the landing-radar weighting functions were to be precomputed and stored in the LGC, twenty-four different functions would be required in the general case.

The fourth weighting functions considered, W-4 of Table 4.1, estimate a constant-slope bias for the terrain-slope variations. To accomplish this, the state vector is augmented to be a 7-dimensional vector, as described in Ref.8, with the slope bias coefficient* to be estimated as the 7-th element. The doppler-velocity bias errors here are treated in the same manner as for the weighting-function set W-3. The weighting functions for the altitude updatings in this case are given by the relation:

$$\underline{w}_n = \frac{E_n' \underline{b}_n}{\underline{b}_n^T E_n' \underline{b}_n + \overline{\alpha_n^2}} \qquad (4\text{-}45)$$

which is similar in form to Eq. 4-41. It should be noted, however, that the vectors $\underline{b}_n$ and $\underline{w}_n$ in Eq. 4-45 are 7-dimensional vectors. Likewise, the covariance matrix E_n' in Eq. 4-45 is a 7 x 7 matrix. It should also be noted that, even though it is not shown explicitly in Eq. 4-45, the down-range distance from the vehicle to the desired site (r_{GO}) must be computed continuously in this bias-estimation scheme.

The technique of estimating a constant-slope bias is not being strongly considered at the present time for two different reasons. First, the computational requirements for mechanizing the bias-estimation process in the LGC appear to be too severe. Second, although the idea of estimating a constant-slope bias has been found by simulation runs to work quite well when the actual terrain slope is reasonably close to being constant throughout the landing maneuver, it has not worked out as well for other types of terrain variations. The reason for this is that the later altitude measurements tend to be weighted relatively lightly, on the assumption that the slope-bias coefficient has already been well estimated. An alternate approach currently under investigation is to estimate the terrain variations as a correlated noise, i.e. a white noise

*The quantity being estimated here is not the terrain deviation but rather its rate of change (which is assumed to be constant).

passed through a filter, rather than as a constant slope. This work will be reported at a later date.

4.4.3 Uncoupled Weighting Functions

In order to simplify computational requirements in the LGC, the basic philosophy has been to use simple uncoupled weighting functions. The information from each new measurement here is used to update only that component of the state vector corresponding to the measurement quantity, i.e. an altitude measurement is used to update altitude only and not velocity or down-range position. This type of weighting function is precomputed from a digital simulation of the landing maneuver for a reference trajectory, and then stored in the LGC for in-flight use. A total of four different functions are required: one for altitude measurements, and one for each of the three components of doppler-velocity measurements being processed. The altitude weighting functions would be stored in the LGC as a function of estimated vehicle altitude; the velocity-component weighting functions would be stored as functions of the estimated speed of the vehicle.

Several different types of uncoupled weighting functions have been investigated for use during the landing maneuver. The important characteristics of these weighting functions are summarized in Table 4.2. For convenience these weighting functions are referred to by the notation W-5, W-6, . . . W-11.

The first set of weighting functions, W-5 of Table 4.2, are the original set of uncoupled weighting functions considered for the landing radar. The basic reasoning behind the choice of these particular functions can best be described as heuristic or intuitive in nature. The characteristics of these weighting functions are shown in Fig. 4.2 as functions of estimated vehicle altitude and speed.

The second, third, and fourth weighting functions of Table 4.2, i.e. W-6 W-7, and W-8, are essentially constant in value throughout the operating-time interval of the landing radar. For the set W-6 all four weighting functions are held at 0.1, for set W-7 they are held at 0.5, and for set W-8 they are held at 0.9.

The fifth set of weighting functions, W-9 of Table 4.2, are based on an optimum least-squares or minimum-variance estimate of the state vector. The doppler-velocity bias errors and terrain-slope variations are accounted for in the computation of E_n' as required to determine $\underline{w}_n$. The procedure here is similar to that for weighting-vector set W-3 except that only the component of $\underline{w}_n$ corresponding to the measurement being processed is retained. No bias errors are estimated here. The characteristics of these weighting functions are shown in Fig. 4.3 as functions of estimated vehicle altitude and speed.

Table 4.2 Uncoupled Weighting Functions

Type	General Characteristics
W-5	Original set, intuitively selected from sensor performance data.
W-6	Set at .1 for all measurements.
W-7	Set at .5 for all measurements.
W-8	Set at .9 for all measurements.
W-9	Optimum least-squares estimates, account for bias errors in computation of E
W-10	Linear-segment fit to W-9.
W-11	Single Linear-fit to W-9.

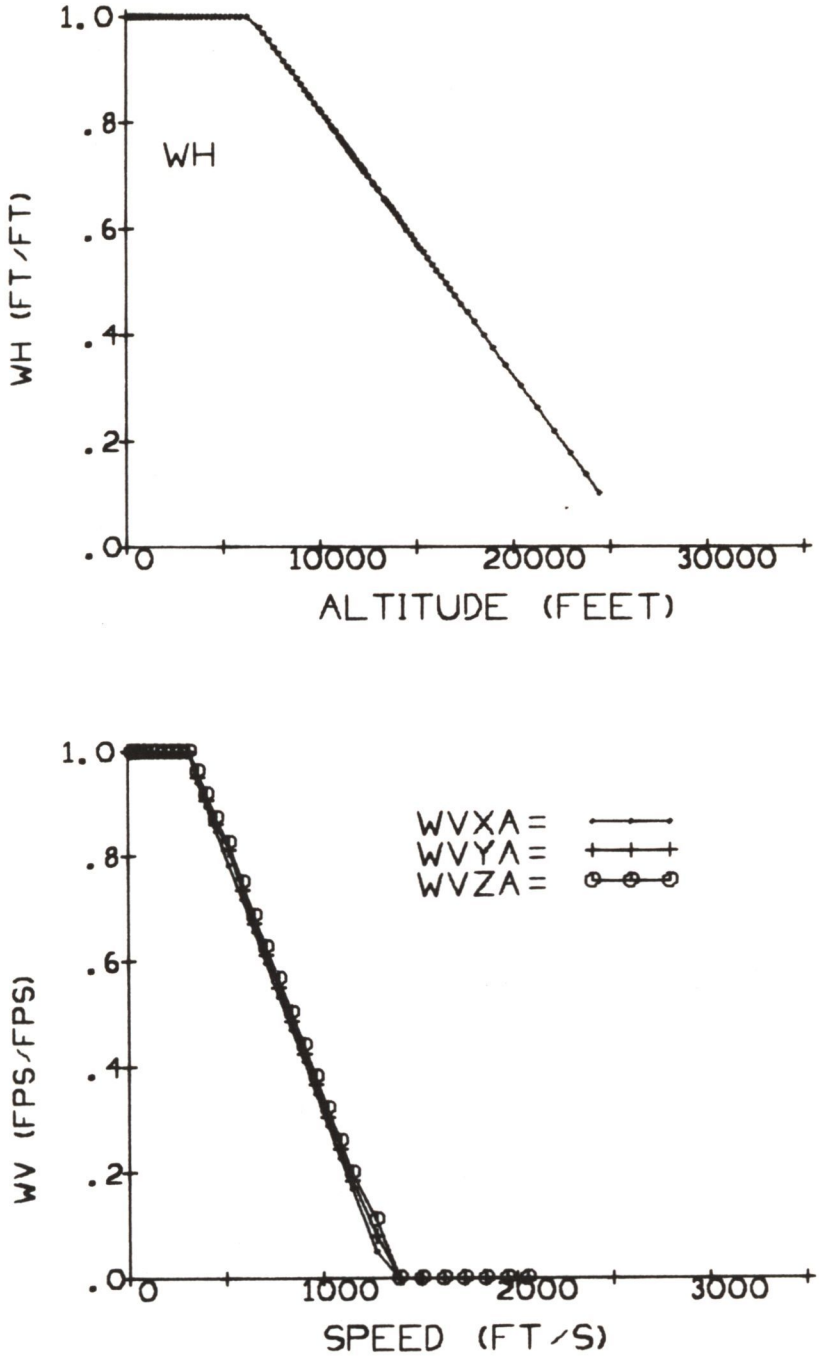

Fig. 4.2 Original Linear Weighting Functions

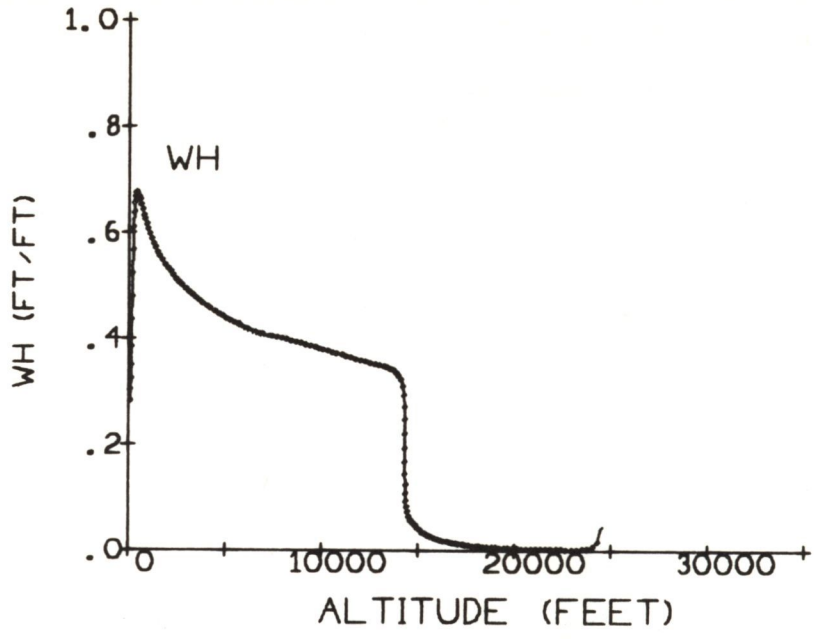

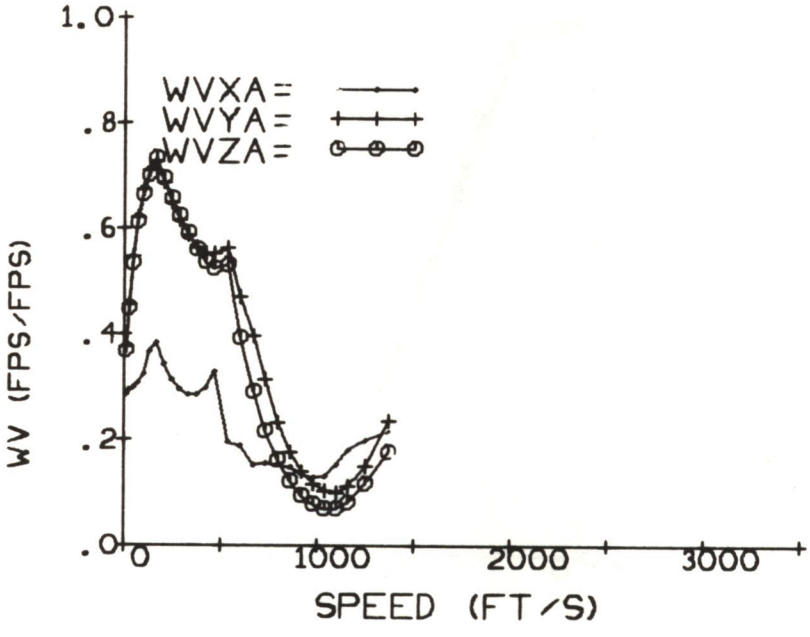

Fig. 4.3 Optimum Uncoupled Weighting Functions

The sixth and seventh sets of weighting functions, W-10 and W-11 of Table 4.2, are linearized approximations to the set W-9. The set W-10 attempts to fit the data with straight-line segments, as indicated in Fig. 4.4. The set W-11 simply approximates the weighting functions by single linear functions, as indicated in Fig. 2.3 of Chapter 2.

Statistical and Monte-Carlo data on navigation-system performance will be presented in Chapter 6 for all the uncoupled and coupled weighting functions described in this chapter.

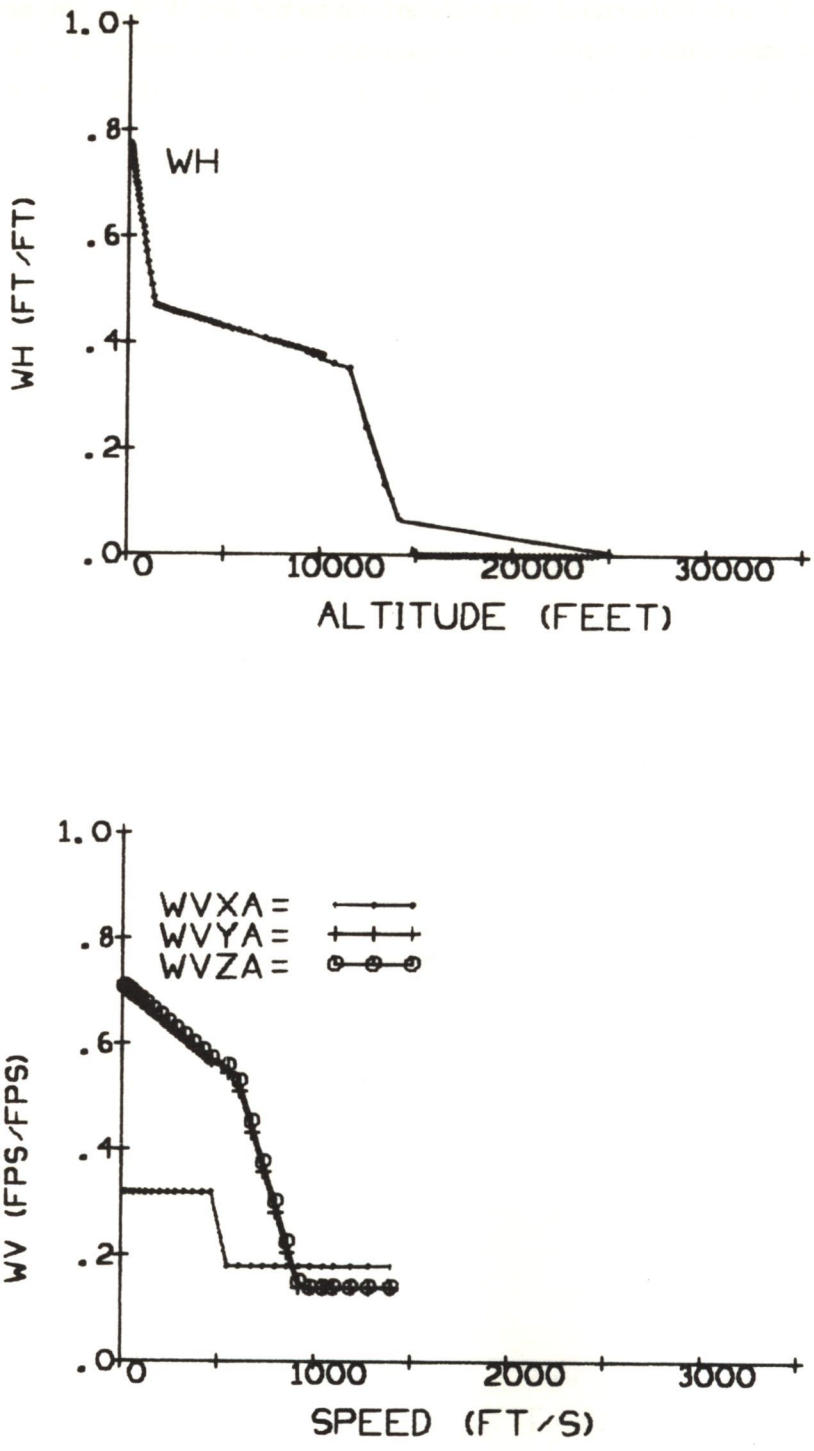

Fig. 4.4 Linearized Weighting Functions

CHAPTER 5

PGNCS LUNAR LANDING MANEUVER SIMULTATIONS

5.1 General Comments

In order to study the performance characteristics of the primary guidance and navigation system used in the LEM during the powered landing maneuver, an extensive simulation of the landing problem has been built using a Honeywell-1800 digital computer. The present chapter will present a general description of this simulation and its capabilities. Also included are the standard performance numbers used in the modeling of the IMU and the landing radar. The assumed initial-condition errors for the state estimates and the actual terrain models used in the simulation are also discussed.

The simulation basically has the capability of providing the following types of information on a given run:

1) Vehicle trajectory data, such as position, velocity, acceleration, altitude, attitude, down-range distance travelled, and flight-path angle.

2) Propulsion-system data, such as thrust magnitude, thrust-vector orientation, specific force, characteristic velocity increment (ΔV), and weight of propellant expended.

3) Statistical performance data for the navigation system, such as the rms errors in the estimates of vehicle position and velocity, the covariance matrix of the estimation errors, and principal axes of estimation-error ellipsoids.

4) Actual (Monte-Carlo) performance data for the navigation system, such as actual errors in the estimates of position and velocity, the magnitudes of the corrections used in the updatings of the state-vector estimates, and the estimated values of position and velocity.

5) Overall-performance data for the guidance and navigation system such as accuracy in achieving High-Gate and Low-Gate terminal conditions, total propellant expenditure or ΔV, and line-of-sight angle to landing site relative to edge of LEM window.

5.2 Simulation of Guidance and Control System

The steering of the vehicle in the simulation is accomplished by controlling the magnitude and direction of the specific force applied to the vehicle by the descent propulsion system engine. The required specific force ($\underline{s}_c$) and thrust vector ($\underline{f}_c$) are determined in the simulation by first computing a set of nine coefficients (c_0, c_1, ... c_8), using the relations of Eqs. 3-2 through 3-4. These coefficients, as was noted in Sec. 3.2, are based on the difference between the present state of the vehicle ($\underline{x}$) as determined from the navigation system, and the desired terminal state ($\underline{x}_D$). Then, the coefficients are used in the relation of Eq. 3-1 to command a vehicle acceleration which is a quadratic function of the time-to-go for the phase of interest. Under normal conditions, the coefficients c_0, c_1,... c_8 are recomputed in the simulation at 2-second intervals. When the computed time-to-go for the braking phase has dropped to 20 seconds, the recomputation of the coefficients for the braking phase is stopped; thereafter, during the braking phase, the command specific force is obtained simply from the relation of Eq. 3-1, using the last computed values for the coefficients. Similarly, during the visibility phase, the recomputation of the coefficients is stopped when the time-to-go has dropped to 5 seconds. It should be noted here that an alternate mechanization of the command specific-force equations, as described in Sec. 3.4, is currently under study and will be reported on at a later date.

In the simulation-study results presented in this report it is assumed that the throttle and attitude of the vehicle respond instantaneously to steering commands. The capability is provided in the simulation for including first-order dynamic time lags in both the response of the throttle to changes in command thrust, and in the response of the vehicle to orientation commands. In order to minimize computer running time, however, throttle and vehicle attitude dynamics have not been included in the performance-study runs of this report. It might be noted that when dynamic simulations involving vehicle attitude and DPS throttle were made on selected example runs presented in this report, no significant effects on the resulting performance profiles were noted.

The descent propulsion system (DPS) in the simulation is operated either at a fixed high-throttle setting (92.5 percent of nominal thrust) or over a range of variable throttle settings (10-60 percent of nominal thrust). The thrust applied to the vehicle at the high-throttle setting is assumed to increase as a function of burning time according to the relation:

$$f = 9710 + 1.18\,t \qquad (5\text{-}1)$$

where the units of thrust (f) are pounds and of time (t) are seconds. The specific impulse (I_{SP}) corresponding to this throttle setting is assumed to be given by:

$$I_{SP} = 303.4 - 0.007\,t \qquad (5\text{-}2)$$

where the units of I_{SP} and t are seconds. High-throttle acceleration uncertainties of ±1 percent are assumed to be possible in the propulsion-system simulation. The switching down from the high (92.5-percent) throttle setting to the throttleable (10-60-percent) region is assumed to take place when the command thrust falls below a level corresponding to 52 percent of the nominal thrust.

5.3 Simulation of Navigation System

The navigation system modeled in the simulation employs an IMU and a landing radar to obtain up-to-date estimates of vehicle position and velocity, as described in Chapter 2. The IMU is assumed to operate continuously throughout the powered landing maneuver to provide data on the specific force acting on the vehicle. Doppler-velocity and altitude data are used to update the IMU-derived state-vector estimates at discrete intervals of time. The typical updating schedule used for the simulation runs is as shown in Fig. 2.2.

Both the estimated and actual state of the vehicle are computed in the simulation by integrating the equations of motion of a point-mass vehicle acted on by engine thrust in an inverse-square gravitational field. The estimated quantities, of course, are computed from the estimated values of the lunar gravitational force and the measured specific force from the IMU. Also, these estimates are updated at discrete times by the landing-radar measurement data.

The modeling of the IMU and landing radar, as incorporated into the simulation, are essentially as described in Sec. 4.2. The error model for the IMU, which is described mathematically by Eq. 4-2, includes inertial-platform alignment, gyro drift rate, accelerometer bias, and accelerometer scale-factor errors. The error model for the LR velocity-measurement unit, which is described by Eq. 4-11, includes a random error whose rms value is proportional to the speed of the vehicle, and a bias error corresponding to uncertainties in the knowlege of the orientation of the radar-antenna axes relative to the IMU. The error model for the LR altitude-measurement data, which is described by Eq. 4-14, includes a random error whose rms value is proportional to the altitude of the vehicle, and an error related to the slope of the terrain.

In the simulation of the PGNCS, as mentioned earlier, both statistical and Monte-Carlo data on navigation-system performance are obtained simultaneously from each simulation run. Random-number generators are used to simulate the actual navigation-sensor errors and initial-estimate errors for each new run. At the same time, computations are made of the rms values of the estimation errors, using the sensor models of Sec. 4.2 and estimation-error relations of Sec. 4.3.

The important performance numbers used to represent the IMU and landing radar in the simulation are summarized in Table 5.1. With regard to this data the following points should be noted.

1) All of the errors (bias and random) are assumed to follow a Gaussian distribution about a zero mean value.

2) The rms values given in the last column of Table 5.1 are 1-sigma, not 3-sigma, values.

3) The values in the last column of Table 5.1 correspond to single error components, e.g. for platform alignment which is represented by a 3-dimensional vector ($\underline{\gamma}_{AL}$) the total rms error would be 1.73 mils.

4) There are lower limits on the rms values of the speed- and range-measurement errors, as indicated by the threshold values.

5) The primary IMU measurement errors in the simulation models are all assumed to be time-invariant bias errors.

6) The landing-radar performance figures listed in Table 5.1 were arbitrarily chosen to represent general LR performance. The combined random and bias errors of Table 5.1 represent an overall LR performance of about 2% (3σ). It should be noted that the actual detailed LR performance is currently being determined by MSC and the radar subcontractor. Future PGNCS simulations will use the official LR performance when available.

Up-to-date estimates of the state vector ($\hat{\underline{x}}_n$) are obtained in the simulation by computing a correction to the a-priori estimate ($\delta\underline{x}_n$), based on the weighted difference between the raw measurement ($\tilde{\underline{q}}_n$) and its a-priori estimate ($\underline{q}_n'$). The updating relation, repeated here for convenience, is:

$$\delta\underline{x}_n = \underline{w}_n (\tilde{\underline{q}}_n - \underline{q}_n') \qquad (5\text{-}3)$$

where $\underline{w}_n$ represents the weighting functions used on the measurement difference ($\tilde{\underline{q}}_n - \underline{q}_n'$) to update the state-vector estimates. Included in the simulation is the capability for incorporating each of the eleven weighting functions W-1, W-2, --- W-11 described in Tables 4.1 and 4.2 of Sec. 4.4 into the navigation-system model.

Table 5.1

Navigation-Sensor Performance Characteristics

Used in Landing Maneuver Simulation Study

Origin of Error	Symbol	Type	RMS Value
IMU:			
Stable Member Alignment	$\underline{\gamma}_{AL}$	Bias	1 mr
Gyro Drift Rate	$\underline{\gamma}_{DR}$	Bias	.15 deg/hr
Accelerometer Bias	$\underline{\gamma}_{BI}$	Bias	.006 ft/s^2
Accelerometer Scale-Factor Uncertainty	$\underline{\gamma}_{SF}$	Bias	.01 percent
LR Velocity Measurement:			
Speed Measurement	$\underline{\alpha}_{D}$	Random	.33 percent of speed
		Threshold	.5 ft/sec
Orientation of Radar-Antenna Coordinate Relative to IMU	$\underline{\gamma}_{D}$	Bias	6 mr
LR Altitude:			
Range Measurement	α_h	Random	.33 percent of altitude
		Threshold	5 ft
Terrain-Slope Variations	γ_h	Bias	100 ft/nm

Both Monte-Carlo and statistical data on navigation system performance are computed for all these cases.

The measurement schedule utilized in the majority of the simulation runs presented in this report is essentially as shown in Fig. 2.2. It is possible, however, to vary the starting times for the processing of measurements, the sequence of measurements, and the interval between successive measurements.

5.4 Initial Errors in State-Vector Estimates

The landing-maneuver simulation described in the preceding sections of this chapter generates both Monte-Carlo and statistical system-performance data. In order to obtain meaningful Monte-Carlo results, particular care must be given to the selection of initial-condition errors, i.e. the errors in the estimates of the state-vector components at the start of the landing maneuver. The correlations between the different components of the estimation error in navigation-system coordinates must be considered. This section will describe the method used in the simulation for the generation of the initial-condition errors. Then statistical data will be presented on the characteristics of these initial estimation errors. Finally, a table will be presented of typical error vectors for the initial-state estimates.

The method for generating initial-condition errors is based on the approach of Refs. (16) and (17). It is assumed here that the individual error components follow a Gaussian distribution about zero mean values. The statistical characteristics of the errors ($\underline{e}$) under these conditions can best be described by their covariance matrix (E), wh_ is equal to the ensemble average $\underline{e}\,\underline{e}^{T}$.

The first step in computing the initial-condition error vectors is to obtain a convariance matrix (E), which is representative of their statistical characteristics. In general, E will <u>not</u> be a diagonal matrix. Next, the 6×6 E-matrix must be transformed to principal coordinates. This requires that the eigenvalues ($\lambda_0, \lambda_1, \cdots \lambda_5$) and their 6-dimensional unit eigenvectors ($\underline{u}_{\lambda 0}, \underline{u}_{\lambda 1}, \cdots \underline{u}_{\lambda 5}$) be computed for the 6×6 convariance matrix (E). The required error vector ($\underline{e}$) is then obtained as the linear combination of errors (ϵ) directed along the principal axes(i.e. along the eigenvectors of E). The mathematical relation for the error ($\underline{e}$) is:

$$\underline{e} = \epsilon_0 \underline{u}_{\lambda 0} + \epsilon_1 \underline{u}_{\lambda 1} + \cdots \epsilon_5 \underline{u}_{\lambda 5} \qquad (5\text{-}4)$$

where $\underline{u}_{\lambda 0}, \underline{u}_{\lambda 1}, \cdots \underline{u}_{\lambda 5}$ represent the unit eigenvectors for the estimation-error covariance matrix (E). The error magnitudes $\epsilon_0, \epsilon_1, \cdots \epsilon_5$ represent randomly selected samples from Gaussian distributions (about zero mean values) whose standard deviations are respectively equal to $\sqrt{\lambda_0}, \sqrt{\lambda_1}, \cdots \sqrt{\lambda_5}$. In the simulation, random-number generators that provide numbers whose rms values are $\sqrt{\lambda_0}, \sqrt{\lambda_1}, \cdots \sqrt{\lambda_5}$ are used to obtain $\epsilon_0, \epsilon_1, \cdots \epsilon_5$.

As a means of identifying or classifying error vectors, the idea of computing constant probability-density hypersurfaces has been adopted. It can be shown[7, 17] that surfaces of constant probability density (equiprobability ellipsoids) are given by the relation:

$$k = \underline{e}^T E^{-1} \underline{e} \qquad (5\text{-}5)$$

where E^{-1} is the inverse of the estimation-error covariance matrix E, and $\underline{e}$ is a particular error vector. The quantity k is proportional to the probability density on the surface where $\underline{e}$ terminates. In effect, each value of k identifies an hyperellipsoid surface of constant probability density. Rather than working with probability density per se, it is more convenient to compute the probability (p) that an error vector lies in the hypersurface having the probability density corresponding to k. There is a direct correspondence between k and p, as given by the relation[17]:

$$p = 1 - \left(1 + \frac{k}{2} + \frac{k^2}{8}\right)\epsilon^{-k/2} \qquad (5\text{-}6)$$

where the quantity ϵ is here equal to 2.7828. The relation of Eq. 5-6, it should be noted, is based on the assumption of 6-dimensional error vectors and covariance matrices. Using the relations of Eqs. 5-5 and 5-6, each error vector can be identified by the probability (p) of an error vector being contained in the hyperellipsoid (k) for the given error vector.

Following the above line of reasoning, error vectors in the data to be presented in this report will frequently be referred to by nomenclature such as "80-percent-probability-ellipsoid" error vector or as "95-percent-probability-ellipsoid" error vector. The probability numbers used here, it should be noted, merely identify constant probability-density hyperellipsoid surfaces on which the error vectors lie. It should also be noted here that the fact that an error vector lies on a surface with a very high probability(e.g. a 99.5-percent-probability-ellipsoid error vector), does not necessarily imply that all components of the error vector are abnormally large. For example, an error vector can have a very large error in the estimation of velocity in combination with a very small (negligible) error in the estimation of position, and lie on a high-probability ellipsoid.

Statistical data used to describe the errors in the initial estimates of the state vector will next be presented. The initial estimation-error covariance matrix used in the simulation studies is given in Tables 5.2 and 5.3. The initial-condition covariance matrix present in Table 5.2 was generated by combining the PGNCS descent-orbit injection (DOI) uncertainties with a typical lunar-orbit-navigation covariance matrix at the DOI point, and then propagating this matrix 180 degrees over the Hohmann descent trajectory to the nominal DPS ignition point for the powered lunar-landing maneuver. The matrix listed in Table 5.2 is referenced to a local-vertical coordinate system at the DPS ignition point.

Table 5.2

Initial Estimation-Error Covariance Matrix in Perilune Point Coordinates

	RX	RY	RZ	VX	VY	VZ
RX	9.624421592 06	-2.634647308 06	7.561941888 03	1.842901184 03	-8.771383145 03	1.762149097 00
RY	-2.634646112 06	1.240815011 06	-1.248338281 04	-9.353684137 02	2.604251795 03	-5.574364374 00
RZ	7.561878330 03	-1.248338133 04	2.030286263 05	1.233743444 01	-7.279009286 00	1.693305349 02
VX	1.842901184 03	-9.353684137 02	1.233743444 01	7.158792700 -01	-1.849701616 00	5.442918871 -03
VY	-8.771383145 03	2.604241795 03	-7.279009286 00	-1.849703084 00	8.516400643 00	-6.219466844 -03
VZ	1.762149097 00	-5.574364374 00	1.693305349 02	5.442921776 -03	-6.219393946 -03	1.001034016 00

NOTE: Units in above matrix are feet (position) and ft/sec (velocity).

RMS VALUES OF INITIAL ERRORS

RX (ft)	RY (ft)	RZ (ft)	VX (ft/sec)	VY (ft/sec)	VZ (ft/sec)
3.102325191 03	1.113918763 03	4.505869797 02	8.460964897 -01	2.918287279 00	1.000516874 00

Table 5.3

Initial Estimation-Error Covariance Matrix in Landing Site Coordinates

	RX	RY	RZ	VX	VY	VZ
RX	1.036869755 07	-3.848151880 05	1.033021889 04	4.142453773 03	-8.392164282 03	3.045240383 00
RY	-3.843139925 05	4.965388449 05	-1.031040199 04	-5.561495504 02	3.046992047 02	-4.990512860 00
RZ	1.033015682 04	-1.031041576 04	2.030286263 05	1.372112914 01	-4.114228933 00	1.693305349 02
VX	4.142453772 03	-5.561495500 02	1.372112914 01	2.022594437 00	-3.450644691 00	6.773423364 -03
VY	-8.392164282 03	3.046992040 02	-4.114228933 00	-3.450646159 00	7.209685475 00	-4.735807172 -03
VZ	3.045240383 00	-4.990512860 00	1.693305349 02	6.773408736 -03	-4.735735698 -03	1.001034016 00

NOTE: Units in above matrix are feet (position) and ft/sec (velocity).

RMS VALUES OF INITIAL ERRORS

RX (ft)	RY (ft)	RZ (ft)	VX (ft/sec)	VY (ft/sec)	VZ (ft/sec)
3.220046202 03	7.046551247 02	4.505869797 02	1.422179467 00	2.685085747 00	1.000516974 00

The format for the error covariance matrix (E) is as indicated in Eqs. 4-15 and 4-16, with the upper part of $\underline{e}$ representing position-estimate errors, and the lower part velocity-estimate errors. Both sets of data are presented as components in a rectilinear X-Y-Z-coordinate frame, with the X-axis horizontal and directed forward, the Y-axis vertical and directed upward, and the Z-axis directed perpendicular to both the X-axis and Y-axis so as to form a right-handed coordinate system. In the data of Table 5.3 the X and Y axes are parallel to the horizontal and vertical directions at the location of the landing site at the nominal landing time (site-point, inertial, or reference coordinates). The basic navigation-system computations are carried out in the inertial site-point coordinates used in Table 5.3. Also presented in Tables 5.2 and 5.3 are the rms values of the errors in the different coordinate frames.

The correlation coefficients for the initial E-matrix of Table 5.3 are presented for reference in Table 5.4. These data are presented as components in the landing site reference-coordinate frame. The square-root of the eigenvalues of the 6-dimensional E-matrix are given in Table 5.5, along with the corresponding eigenvectors. The eigenvectors are presented here as row vectors in the reference-coordinate frame, i.e.,the first row corresponds to λ_0, the second row corresponds to λ_1, etc. The eigenvalues and eigenvectors of Table 5.5 are used in Eq. 5-4 to compute initial-condition error vectors in the landing-maneuver simulations.

Using the method described in this section, initial-condition estimation-error vectors have been computed for use in Monte-Carlo simulation runs. A series of representative error vectors are presented for general interest in Table 5.6. Included here are the particular error vectors that were used in the simulation runs given in this report. The error data are presented as components in the X-Y-Z landing site reference frame. Also presented in the table are the probability ellipsoid corresponding to the error vector (p). In the navigation system under study in this report, the major concern was on initial-position errors along the Y direction, i.e. essentially initial-altitude errors. For this reason the initial errors selected as "worst-case" errors were those having both a high probability-ellipsoid number (i.e. over 95-percent) and a large error component along the Y direction.

5.5 Lunar Terrain Variations

The function of the LEM PGNCS is to guide the vehicle to a preselected landing site, subject to fuel-management and visibility constraints imposed by the mission. The navigation of the vehicle, as mentioned earlier, is accomplished by using landing-radar velocity and altitude (range) data to update IMU-derived estimates of position and velocity.

The basic navigation information from the IMU is the measured specific force, from which changes in the estimates of vehicle position and velocity can be computed. The IMU output data are in an inertially-fixed coordinate frame. The landing radar, on the other hand, measures the altitude of the vehicle above the local terrain. As the

Table 5.4

Correlation Coefficients for Initial Estimation-Error Covariance Matrix in Landing Site Coordinates

	RX	RY	RZ	VX	VY	VZ
RX	1.000000000 00	-1.693748135 -01	7.119816206 -03	9.045678817 -01	-9.706300087 -01	9.452246951 -04
RY	-1.693748135 -01	1.000000000 00	-3.247284545 -02	-5.549585820 -01	1.610410326 -01	-7.078547433 -03
RZ	7.119816206 -03	-3.247284545 -02	1.000000000 00	2.141197904 -02	-3.400569510 -03	3.756057435 -01
VX	9.045678817 -01	-5.549585820 -01	2.141197904 -02	1.000000000 00	-9.036238381 -01	4.760246031 -03
VY	-9.706300087 -01	1.610410326 -01	-3.400569510 -03	-9.036238381 -01	1.000000000 00	-1.762834063 -03
VZ	9.452246951 -04	-7.078547433 -03	3.756057435 -01	4.760246031 -03	-1.762834063 -03	1.000000000 00

Table 5.5

Eigenvalues and Eigenvectors for Initial Estimation-Error Covariance Matrix in Landing Site Coordinates

SQUARE ROOT OF EIGENVALUES OF INITIAL E-MATRIX

3.222367965 03	6.942277767 02	4.501844047 02	7.514392177 -02	6.655115554 -01	9.272862405 -01

EIGENVALUES AS ROW VECTORS

9.992443979 -01	-3.884201370 -02	1.053262043 -03	4.007205040 -04	-8.087392401 -04	3.288954660 -07
3.885521749 -02	9.986146050 -01	-3.547479873 -02	-8.193994485 -04	-4.492943154 -05	-2.255881328 -05
3.261346776 -04	3.548893263 -02	9.993696637 -01	-2.306151175 -05	1.956447937 -05	8.341237182 -04
-1.605052068 -04	8.126736905 -04	-1.218309245 -05	9.699636872 -01	2.432453821 -01	1.194903533 -03
8.751216710 -04	-1.907397838 -04	-2.950799978 -05	-2.432384064 -01	9.698700138 -01	1.365348564 -02
-1.148191144 -05	-5.429140386 -06	-8.340597433 -04	2.162243516 -03	-1.353405411 -02	9.999057175 -01

Table 5.6

Error Vectors at Start of Landing Maneuvers in Landing Site Coordinates

No.	Prob. Ellipsoid (percent)	Position (feet)			Velocity (ft/sec)		
		RX	RY	RZ	VX	VY	VZ
2	63.89	-550	-1024	-821	0.59	0.63	-1.47
3	73.35	4972	-1226	358	2.62	-3.34	-0.37
4	38.68	-2116	-57	-288	-0.80	2.27	1.03
5	45.06	1154	134	13	0.18	-0.37	1.85
6	53.18	1814	-85	743	0.81	-1.46	0.64
7	52.40	3083	7	-555	0.89	-1.58	0.45
8	11.80	1639	-240	-526	0.92	-1.65	-0.67
9	74.26	1857	-1291	122	2.08	-2.26	-0.33
10	26.81	-3290	-577	-457	-0.83	3.03	-0.10
26	91.48	7664	-499	577	3.53	-7.36	-0.14
123	99.33	-10053	-61	248	-3.24	7.09	-0.76
203	90.91	-9652	-224	-125	-3.53	8.41	0.37
212	99.64	8089	-1048	-699	4.17	-7.10	-2.07
376	99.14	-10283	-90	163	-4.08	9.90	0.71
524	88.57	8556	-777	210	3.96	-7.19	1.00
539	98.07	4975	-1961	-746	3.42	-3.86	0.98
1089	52.08	-2763	421	-203	-1.14	1.03	-0.50
1120	93.09	2112	-1599	784	2.41	-2.48	1.33
1191	99.84	-6278	1906	43	-4.21	6.68	-1.88
1597	94.22	4683	1831	340	0.26	-4.05	1.16
828	46.61	4078	-748	147	2.08	-3.58	0.02
429	18.22	-542	87	553	-0.41	0.90	-0.30
1749	99.73	7258	2859	145	0.11	-7.36	-0.92
223	79.81	-7487	1123	-133	-3.77	6.56	-0.75
616	80.25	-6080	1130	728	-3.06	4.52	0.33
739	68.10	-5536	1309	21	-2.92	3.80	0.44
786	80.63	7782	-489	-470	3.49	-7.00	0.47
862	97.26	-8882	897	-541	-4.29	8.14	-1.83
887	99.67	10131	-1253	-945	4.55	-7.78	-1.64
1142	95.22	-4708	-1575	136	0.46	3.58	1.46
1154	4.39	-602	-577	369	0.23	0.53	0.60

vehicle approaches the selected site, this altitude measurement will essentially be that of vehicle altitude relative to the site.

In order to guide the vehicle to a safe landing on the moon, it is necessary to accurately determine vehicle altitude relative to the local terrain during the visibility phase of the descent maneuver. It is more important to know the local altitude of the vehicle at this time than the altitude relative to the selected site, since the vehicle may actually land several thousand feet away from the selected site due to down-range position-estimation errors.

On the basis of the information available at this time it is expected that there will be significant variations in the altitude of the local lunar terrain (relative to the mean lunar sphere) over the length of terrain for which the landing radar will operate. The PGNCS will begin taking landing-radar altitude data when the estimated altitude of the vehicle (relative to a mean lunar sphere) is 25,000 feet, at which time the vehicle is typically 50 n miles away from the site. In the navigation-system design, as mentioned earlier, it was assumed that the difference in altitude between the local terrain and the landing site was directly proportional to the distance from the site, i.e. a constant-slope terrain model was used. The numerical value used for the rms slope coefficient was 100 ft/n mi, which corresponds to a 1-degree slope.

In the digital simulation of the landing maneuver, several different models were used to represent altitude variations of the terrain below the vehicle. The general characteristics of the terrain models in the vicinity of the site are shown in Table 5.7 and the altitude-vs.-down-range-distance profiles are shown in Figs. 5.1 and 5.2. The first terrain model (T-1) is a constant slope of 100 ft/n mi. This is the same terrain model used in the derivation of navigation-system weighting functions. The next three terrain models (T-2, T-3, and T-4) are combinations of simple mathematical functions (straight lines and exponentials) which represent, in a simple manner, possible lunar-terrain variations. The final five terrain models (T-5, T-6, T-7, T-8, and T-9) represent data obtained from NASA[18] on the apparent lunar-terrain variations within 25 n mi of tentative landing areas. Terrain models T-6, T-8, and T-9 were selected as typical landing sites that would be chosen for a given lunar landing mission. The three landing sites would be selected as a function of launch time over the launch window such that one of the three would have suitable lighting conditions for landing at any time in the launch window. Terrain model T-7 is to the same landing site as T-6 but at a different approach angle, and was included in this group for general interest since it presented a more severe terrain profile than T-6. Terrain model T-9 is essentially zero slope or flat terrain over the final 25 n mi approach to the landing site and is therefore not illustrated in Fig. 5.2.

Table 5.7

General Characteristics of Terrain Models

Model	Description of Model	Terr.*
T-1	Constant Slope of 100 ft/nm	4
T-2	Combination of two constant slopes	1
T-3	Exponential from 0 to 2000 ft.	2
T-4	Combination of position and negative expontials	3
T-5	Landing Area: 0^{o} 00'N, 31^{o} 00'E; Approach angle: + 10 deg	5
T-6	Landing Area: 0^{o} 20'N, 12^{o} 50'E; Approach angle: -5 deg	7
T-7	Landing Area: 0^{o} 20'N, 12^{o} 50'E; Approach angle: +10 deg	8
T-8	Landing Area: 0^{o} 30'S, 1^{o} 28'W; Approach angle: -5 deg	9
T-9	Landing Area: 0^{o} 10'N, 24^{o} 10'E; Approach angle: -5 deg	0

*The Terr. numbers listed refer to the code used in identifying the terrain models in the figures of Chapter 6.

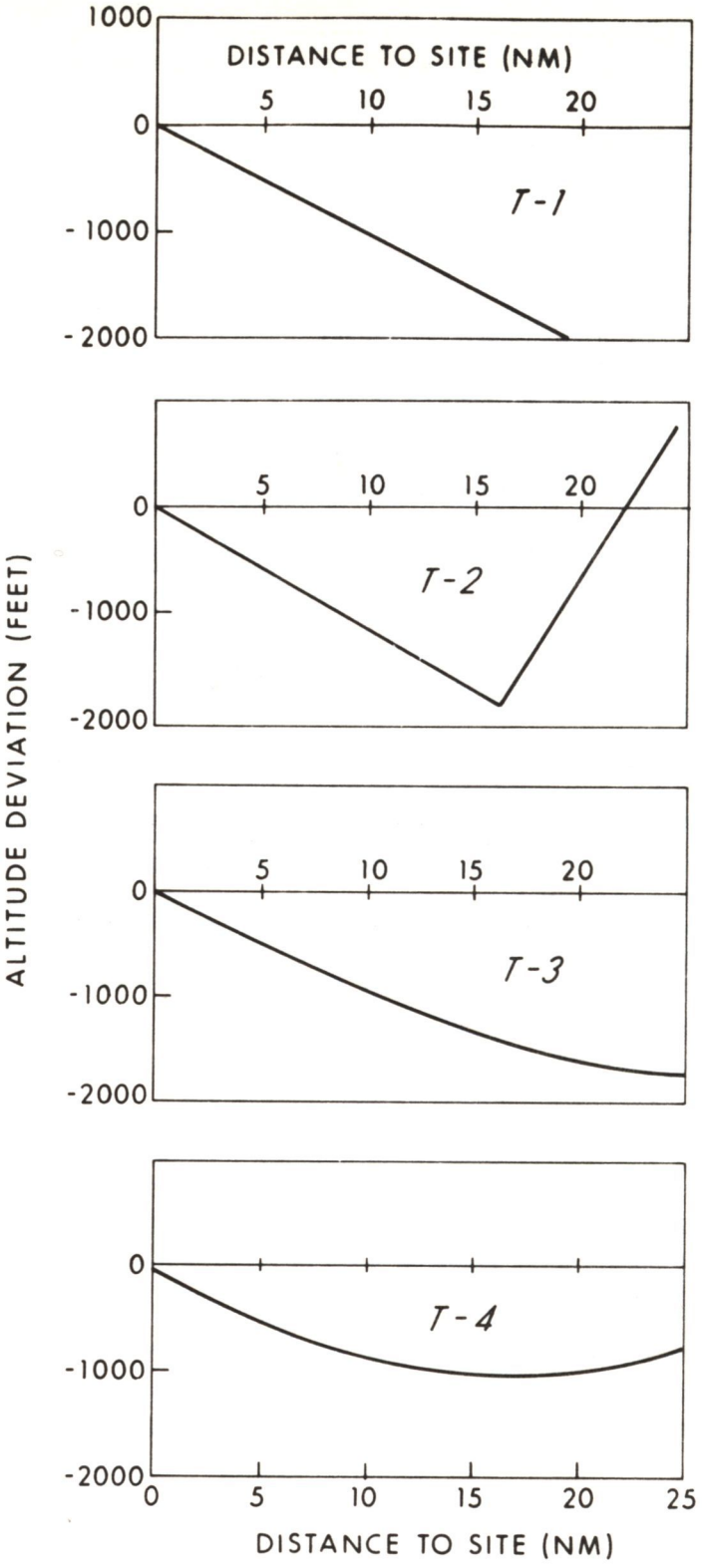

Fig. 5.1 Lunar Terrain-Variation Models

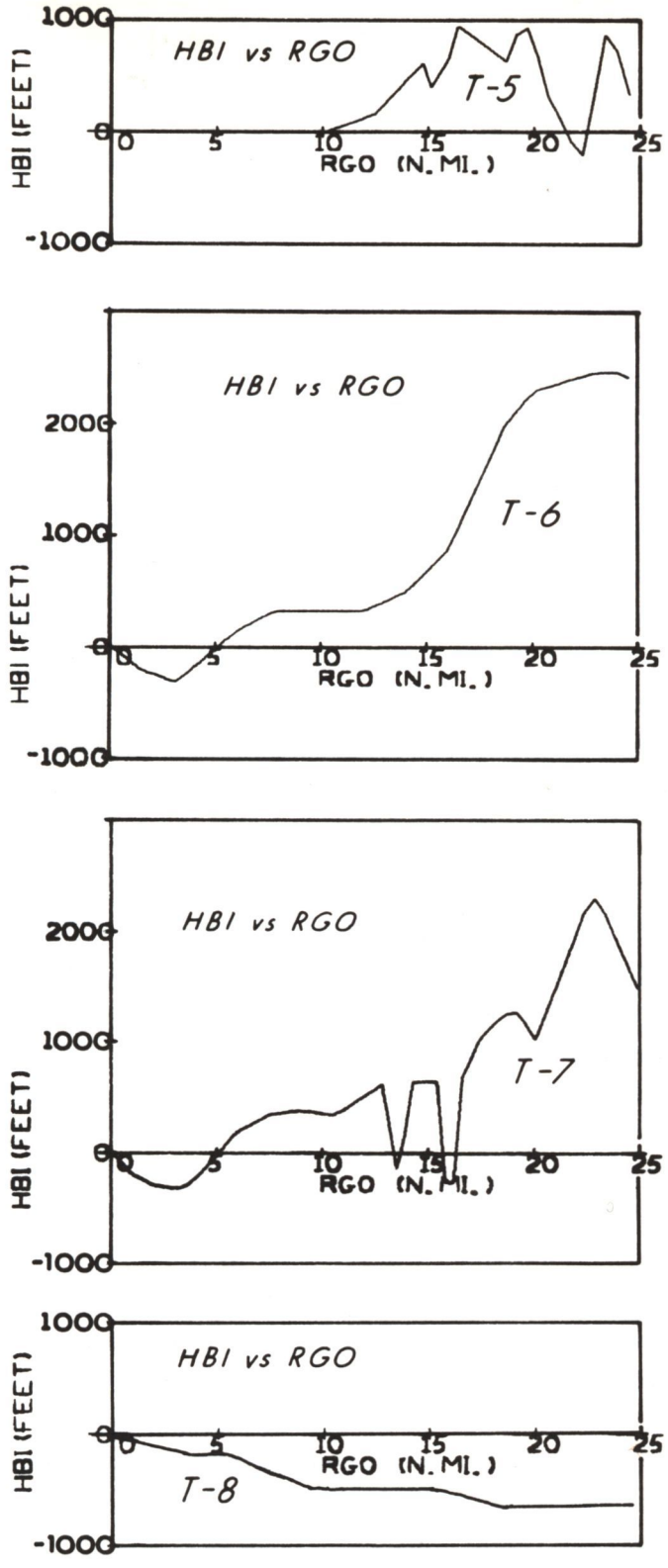

Fig. 5.2 Lunar Terrain-Variation Models

CHAPTER 6

PGNCS-LR LANDING RADAR MANEUVER PERFORMANCE STUDY

6.1 General Information

A digital simulation study has been made to investigate the performance of the PGNCS using LR updating during the powered landing maneuver. This chapter presents and discusses the important results of the study. Of particular interest from the study are the following items:

1) the time histories of vehicle attitude and thrust,
2) the required velocity increment (ΔV),
3) the interval during which the landing site is visible to the astronaut,
4) the accuracy with which Low-Gate point conditions are achieved.

The general characteristics of the simulation have been described in Chapter 5. The navigation and guidance concepts have been presented in Chapters 2 and 3. The modeling of the navigation sensors and lunar terrain have been discussed in both Chapters 4 and 5.

Unless specifically stated to the contrary, the following conditions will be assumed to apply to the simulation runs discussed in this chapter:

1) The initial, High-Gate, and Low-Gate point conditions are as given in Tables 1.1 and 3.1.
2) The measurement schedule is as indicated in Fig. 2.2, with the initial altitude and velocity updatings made at estimated vehicle altitudes of 25,000 and 15,000 feet respectively.
3) The thrust provided by the DPS at the high throttle setting (92.5 percent of nominal thrust) is as given by Eq. 5-1.
4) The throttle is switched from the high-throttle setting to the lower continuously-throttleable operating region (10-60 percent of nominal thrust) when the command thrust has dropped to 52 percent of the nominal thrust.
5) The performance characteristics for the IMU and landing radar are as given in Table 5.1.
6) The steering commands are computed from the relations of Eqs. 3-1 through 3-4, with the coefficients (c_0, c_1, ---c_8) normally recomputed at 2-second intervals from Eqs. 3-2 through 3-4.

7) The required velocity increment (ΔV) includes the requirements for DPS ullage, the DPS trim phase, the lunar-rotational velocity, and all maneuvers to the Low-Gate conditions.

8) The recomputation of steering coefficients (c_0, c_1, --- c_8) during the braking phase is stopped when the estimated time-to-go drops to 20 seconds; the recomputation during the visibility phase is stopped when the time-to-go drops to 5 seconds.

9) Uncoupled weighting functions based on an optimum least-squares estimate of the state vector (W-9, W-10, and W-11 of Table 4.2) are used.

The presentation and discussion of results in this chapter will procede in the following manner. First of all, thrust-vector profiles and navigation-system error data will be presented for a few selected typical landing trajectories, using the optimum uncoupled weighting functions of set W-9. Initial-condition errors, terrain-slope variations, DPS uncertainties, and landing-radar updatings will be included in these typical landing trajectories. Then, in the succeeding sections, more detailed information will be presented to show the effect on PGNCS performance of initial-condition errors, DPS uncertainties, and terrain-slope variations. Next, data will be presented comparing the PGNCS performance with the different weighting functions considered. Both statistical and Monte-Carlo data will be presented. Then, data are given to show the effect of changes in landing-radar parameters on overall PGNCS performance. Finally, data are presented for the conditions where the landing-radar measurements are interrupted at various times during the landing maneuver.

6.2 Typical Performance Data for Radar-Updated PGNCS

A large number of landing trajectories have been studied for the PGNCS using different assumed values for initial-condition errors, terrain-slope variations, DPS uncertainties, and landing-radar weighting functions. The present section shows data from selected examples of these trajectories, which are considered to be representative of normal system performance. The landing-radar weighting functions employed here are the optimum uncoupled set W-9, which are shown in Fig. 6.1 as functions of time on a typical trajectory. The landing-radar updating schedule used here is as shown in Fig. 2.2. The initial, High-Gate, and Low-Gate conditions are as given in Tables 1.1 and 3.1. Finally, the IMU and landing-radar performance numbers are as given in Table 5.1.

Before discussing the individual landing runs, it should be noted that the nominal landing trajectory used in this study was designed to throttle-down the DPS 80 seconds before the end of the braking phase. In view of the expected initial-condition errors, DPS uncertainties, and steering-coefficient freeze times (c_0, c_1, ---c_8), it was felt that this throttle-down time was reasonable in order to insure that High-Gate conditions be met. The ΔV penalty for increasing the interval during the braking phase

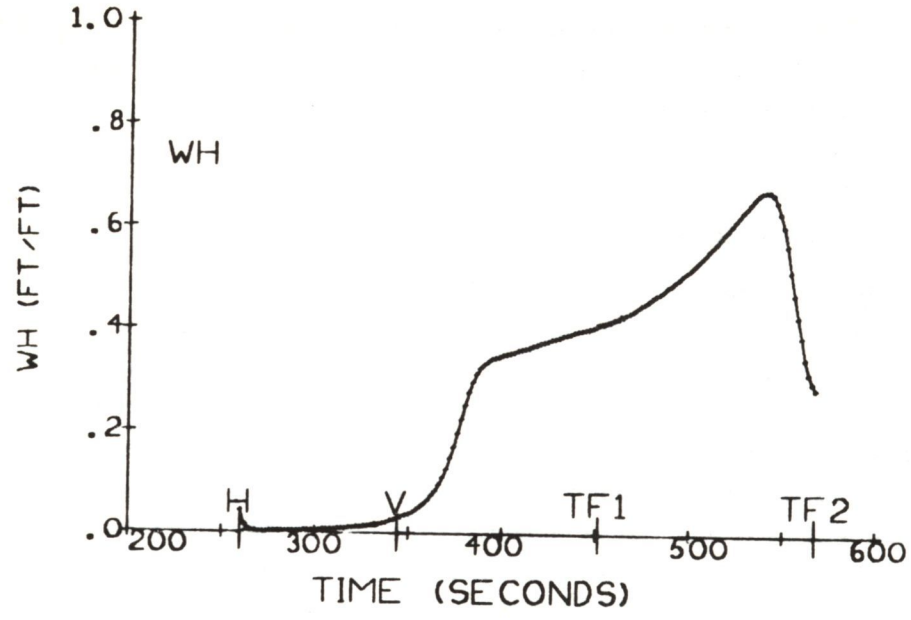

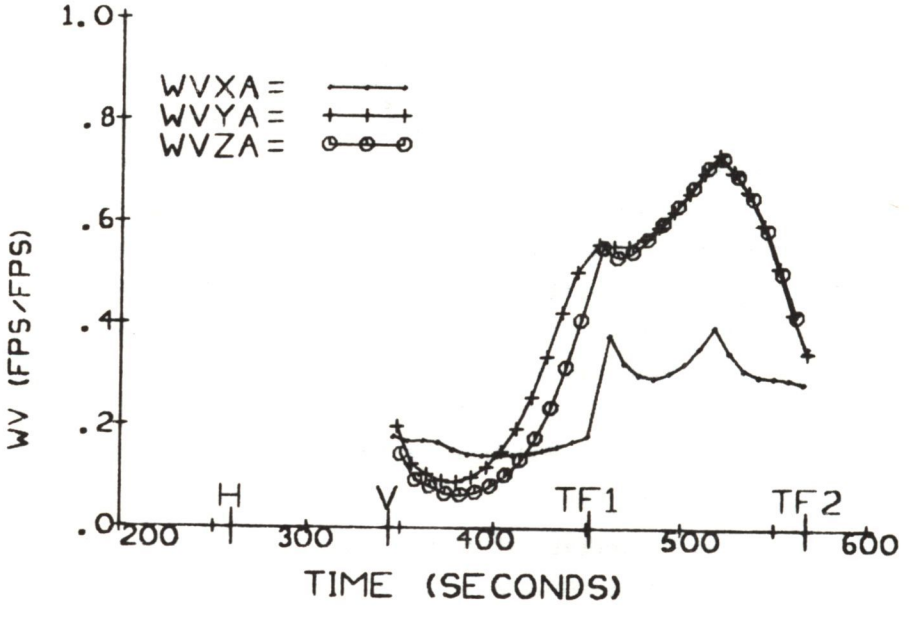

Fig. 6.1 Optimum Uncoupled Weighting Functions (W-9)

for which the DPS is in the throttleable region is typically 1 ft/sec/sec. It is important, however, that the High-Gate conditions be satisfied sufficiently well so that the visibility-phase objectives can be accomplished.

It should also be noted that the switching from the high-throttle setting (92.5 percent) to the low continuously-throttleable region (10-60 percent) is made when the command thrust (f_c) has dropped to 52 percent of nominal thrust. From the viewpoint of efficient propellant utilization it is desirable to operate the DPS at as high a thrust level as possible in the throttleable (10-60 percent) region. At the same time the operating region must be sufficiently low, so that the correction of navigation estimates for initial-condition and terrain-slope errors will not require thrust in excess of 60 percent of nominal thrust. The ΔV penalty for lowering the switching level at which the DPS is first throttled down under typical conditions was found to be about 3 ft/sec/percent. Based on the expected initial-condition errors and terrain models at the time this study was initiated, the switching level of 52 percent of nominal thrust was selected.

The important characteristics of the selected representative landing maneuver runs are given in Table 6.1. The first two cases (Runs 1 and 2) represent system performance with moderate initial-condition errors and realistic terrain models. The third case (Run 3) represents the case where the initial-error vector has very large vertical-velocity and altitude components. The fourth and fifth cases (Runs 4 and 5) present data for assumed DPS uncertainties of ±1 percent. The final case (Run 6) shows how the system performs when the initial-error vector is small and the lunar terrain is smooth. Thrust-vector profiles for these runs are given in Figs. 6.2 through 6.7.

In regard to the thrust-vector profile data presented in this report (e.g. Figs. 6.2 through 6.7) it should be noted that the times of the initial altitude and velocity updatings are indicated by the letters H and V, respectively, along the horizontal coordinate axes. Also, the times at which the braking and visibility phases terminate are indicated on the profiles by TF1 and TF2, respectively.

It should also be noted that the elevation angle shown in the various thrust-vector profiles is measured from the local horizontal plane to the thrust vector (vehicle longitudinal axis). At the start of the maneuver (t=0) the elevation angle will be negative, as indicated in Fig. 3.1. Then, as the landing maneuver progresses, the vehicle is pitched up until at the end of the visibility phase ($t \approx 570$ sec) the thrust-vector is directed upward within a few degrees of the local-vertical direction.

There are several points to be made from the data of Table 6.1 and Figs. 6.2 through 6.7. The most important of these are the following.

Table 6.1: Characteristics of Representative Landing Trajectories

Run No.	Fig. No.	Initial Error Vector			DPS Accel. Uncert. %	Terrain Model	ΔV (f/s)	Max Thrust 10-60% region (lbs)	Low-Gate Point Errors			High-Gate Point Errors		Max. Devs. Braking Phase	
		Type	No.	Probability Ellipsoid					Alt. (ft)	Vel. (f/s)	Hor. Pos (ft)	Alt. (ft)	Vel. (f/s)	El. Angle (deg)	Thrust (lbs)
1	6.2	Med.	1089	52.1%	0	T-6	6284	5461	-7	.4	2334	-34	9.1	3.6	160
2	6.3	Med.	828	46.6%	0	T-6	6288	5950	-11	.7	-5302	+14	7.5	8.9	411
3	6.4	Bad	1191	99.8%	0	T-7	6297	5563	+.1	.3	6781	-200	6.2	20.4	587
4	6.5	Bad	1142	95.2%	+1	T-7	6307	5872	+3	.7	3695	+158	1.8	10.4	298
5	6.6	Bad	1142	95.2%	-1	T-7	6258	5807	+4	.7	3810	+175	2.6	9.2	400
6	6.7	Low	1154	4.9%	0	T-9	6281	5589	3.2	.3	680	+ 20	1.0	1.8	85

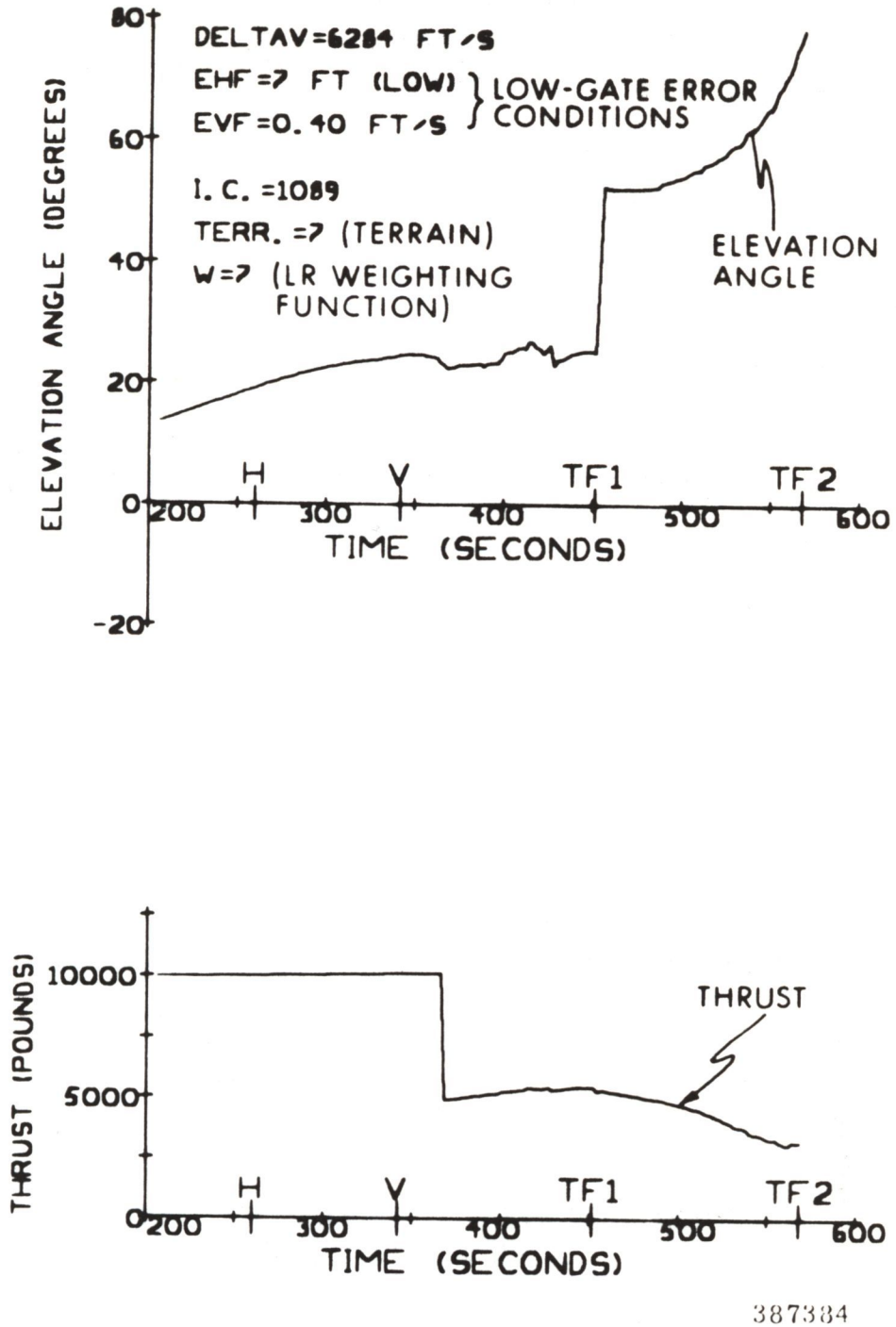

Fig. 6.2 Thrust-Vector Profiles: Moderate Initial Errors, No DPS Acceleration Uncertainty (Run 1 - Table 6.1)

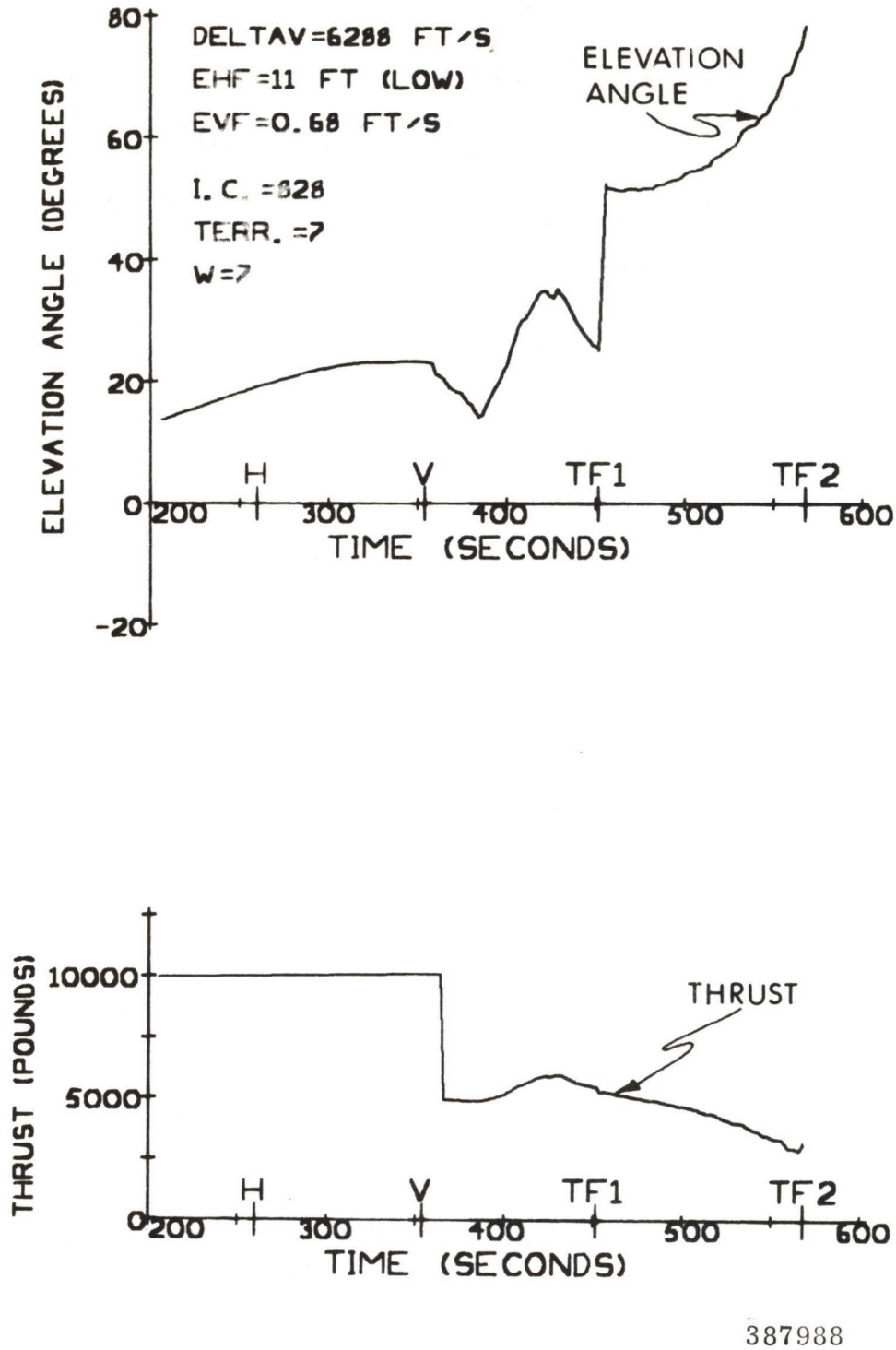

Fig. 6.3 Thrust-Vector Profiles: Moderate Initial Errors, No DPS Acceleration Uncertainty (Run 2 - Table 6.1)

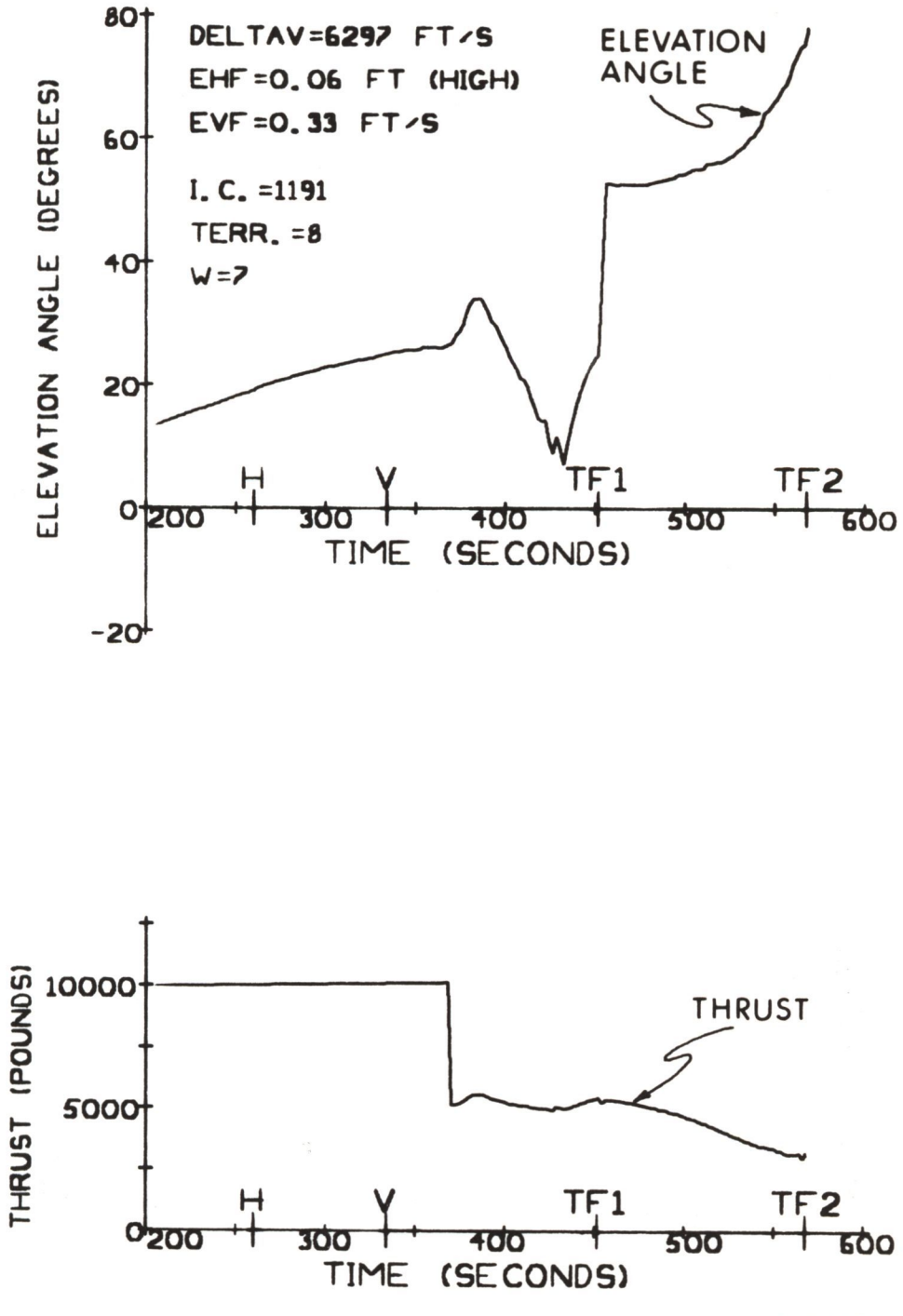

Fig. 6.4 Thrust-Vector Profiles: Severe Initial Errors, No DPS Acceleration Uncertainty (Run 3 - Table 6.1)

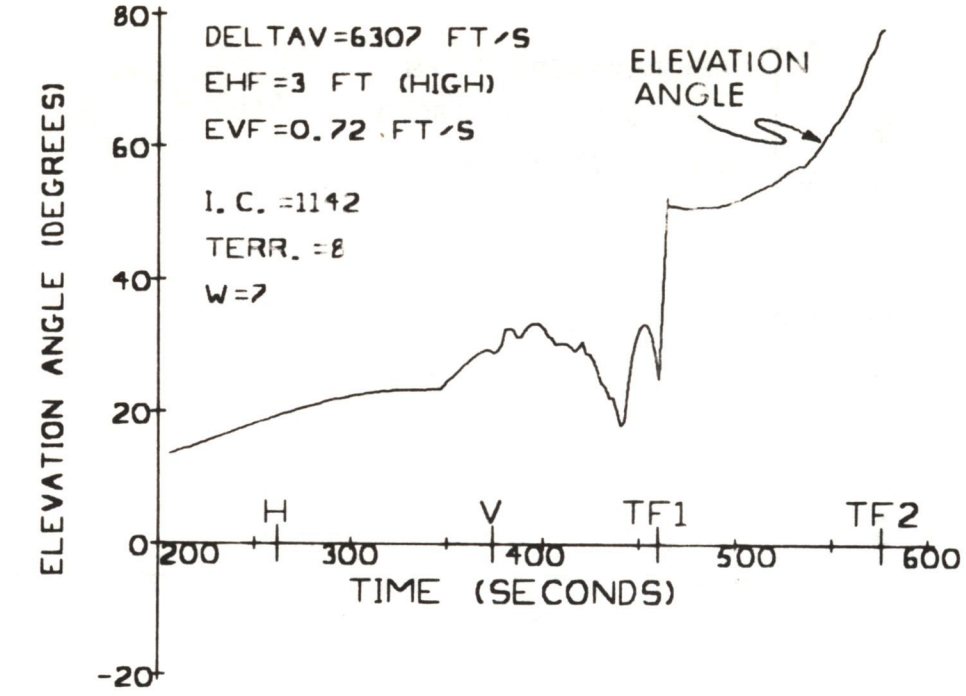

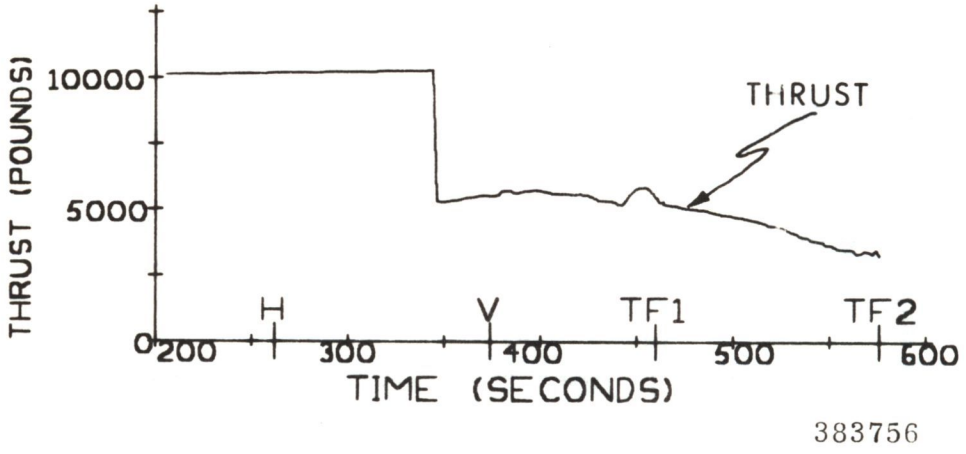

Fig. 6.5 Thrust-Vector Profiles: Severe Initial Errors, +1% DPS Acceleration Uncertainty at Max. Throttle Setting (Run 4 - Table 6.1)

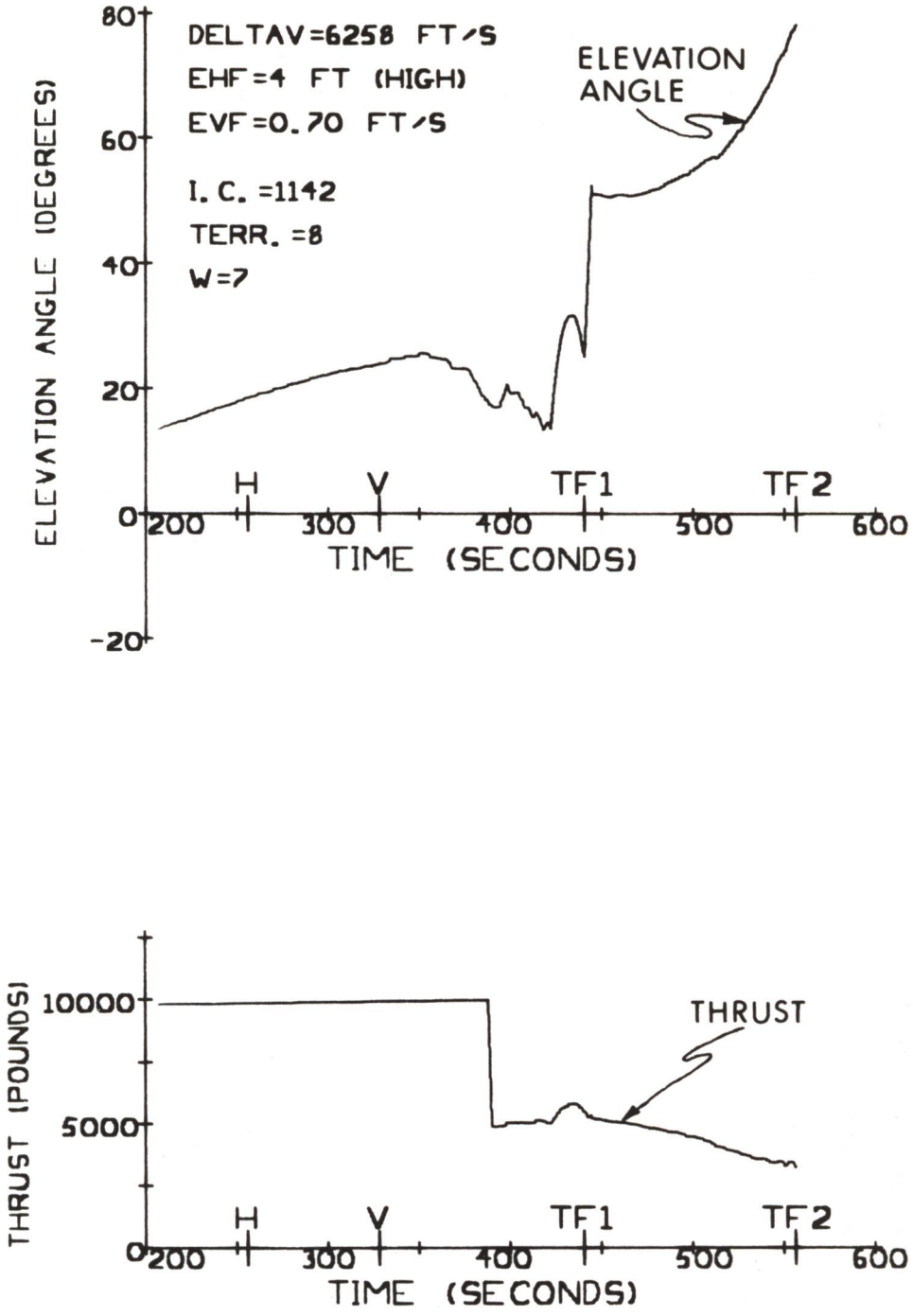

Fig. 6.6 Thrust-Vector Profiles: Severe Initial Errors, - 1% DPS Acceleration Uncertainty at Max. Throttle Setting (Run 5 - Table 6.1)

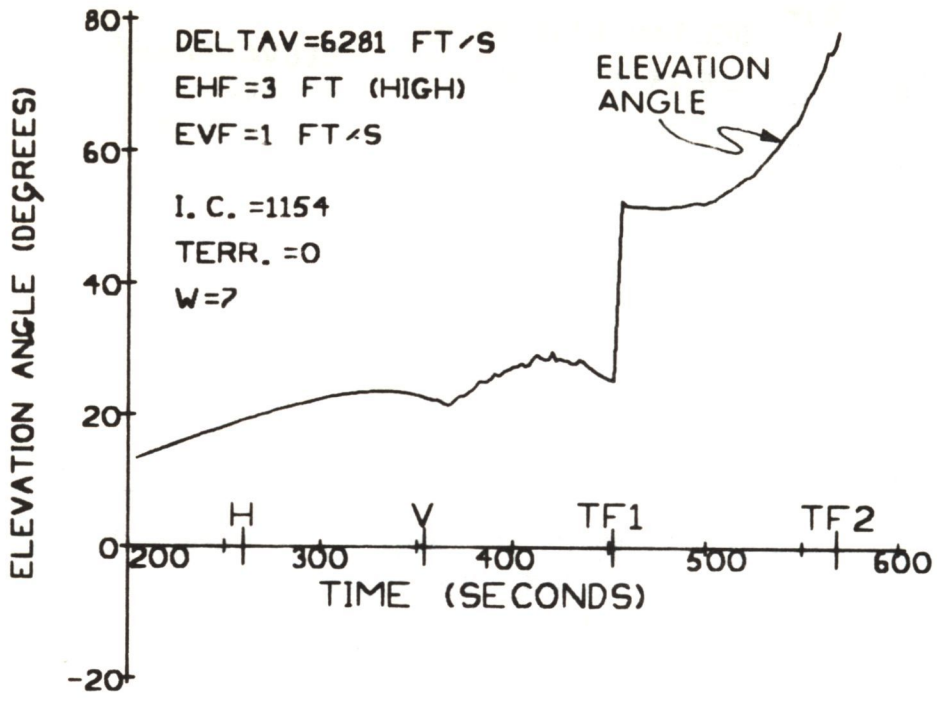

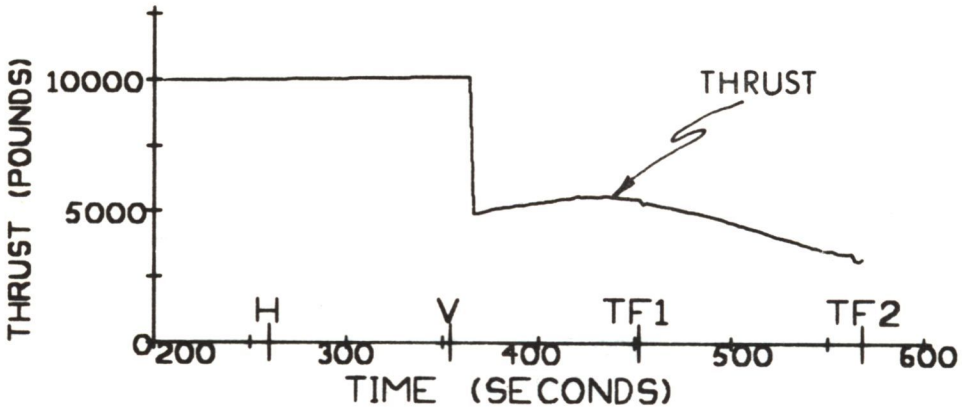

415681

Fig. 6.7 Thrust-Vector Profiles: Small Initial Errors
No DPS Acceleration Uncertainty
(Run 6 - Table 6.1)

1) The thrust-vector elevation-angle and thrust profiles are relatively smooth during the visibility phase in all cases shown. This is very important for effective LPD operation during the final approach or visibility phase.

2) The major trajectory corrections to handle initial-condition errors and terrain-slope variations are made during the last 100 seconds of the braking phase where the landing-radar data are given a reasonable weight in the estimation process. Trajectory corrections in this interval are important to establish the desired PGNCS-LR operation during the following visibility phase.

3) The PGNCS design philosophy is to accept and expect elevation-angle deviations (often of significant magnitude) during the braking phase in order to obtain a smooth elevation-angle profile during the visibility phase.

4) Low-Gate-point conditions are typically met with an accuracy of about 10 feet (or better) in altitude and about 0.7 ft/sec or better in velocity. The horizontal Low-Gate-point position errors are not updated by the LR data and may be as large as 7000 feet for some of the specific examples chosen. It should be noted that the results presented in this report are for completely automatic PGNCS operation, and that no landing-site redesignations with the LPD were made to correct horizontal-position uncertainties at Low-Gate point.

5) Positive or high DPS acceleration at the high-throttle setting tends to increase the required ΔV; negative or low DPS acceleration at the high-throttle setting tends to decrease the braking-phase time interval during which the DPS operates in the continuously-throttleable region.

6) After the DPS has been throttled down, the thrust magnitude remains below the maximum permissible value (6,300 pounds) during the remainder of the landing maneuver.

7) In all cases, adequate landing-site visibility is obtained below the Low-Gate point actually reached by the vehicle. The Low-Gate point actually attained will not necessarily be the desired Low-Gate point because of uncorrected down-range position errors in the navigation system.

In concluding this section it should be noted that additional thrust-vector profile data are given in the Appendices B, C, and D of this report. Also a more detailed look at the effects of initial-condition errors, terrain-slope variations, and DPS throttle-setting uncertainties will be given in the following sections of this chapter.

6.3 Effect of Landing-Maneuver Initial-Condition Errors on PGNCS Performance

Errors in the initial state-vector estimates, i.e. initial-condition errors, affect the PGNCS performance in three important ways.

1) Significant deviations in vehicle attitude, i.e. elevation angle, from that on an error-free trajectory may occur during the latter part of the braking phase.

2) Significant deviations in the magnitude of DPS thrust may also occur during the continuously-throttleable operating period at the end of the braking phase.

3) The required velocity increment (ΔV) will generally be larger than in the error-free case.

The thrust-vector deviations are caused to a large degree by the basic PGNCS design philosophy of correcting the major navigation errors during the braking phase, so as to insure a smooth visibility-phase trajectory. Accurate knowledge of navigation errors, e.g. initial-condition errors, moreover, is not obtained until 300-350 seconds after the start of the landing maneuver when the LR data are accurate enough to be given a reasonable weight in the estimation process.

In order to investigate the effects of initial-condition errors on navigation-system performance, a series of Monte-Carlo runs were made for a number of different initial-error vectors. The method for computing these error vectors has been described in Section 5.4. Some typical error vectors computed in this manner are presented in Table 5.6, including the various error vectors referred to in the data of this chapter.

An important objective in this study was to examine PGNCS performance in worst-case type situations. For this reason the majority of error vectors used here were those terminating on equiprobability ellipsoids corresponding to probabilities of 95 percent or more. For the purpose of this study the important error-vector position component is essentially along the direction of the landing-site local vertical (e_{RY}). Down-range and cross-range initial errors (e_{RX} and e_{RZ}) will not be corrected, in general, since only the altitude* component of vehicle position is updated by the landing radar. Referring to the rms errors in Table 5.3, it can be seen that the predominant velocity error component is the Y-component (rms value of 2.66 ft/sec). Also, the cross-range Z-component of initial-velocity error is much smaller than the Y-component (its rms value is 1.0 ft/sec). Finally, the X-component is only about one-half as large as the Y-component (rms value is 1.4 ft/sec).

Under these conditions, initial error-vectors for this study can quite properly be chosen primarily on the basis of errors in altitude* (e_{RY}) and vertical-velocity (e_{VY}). Down-range velocity errors (e_{VX}) are next in importance. An examination

*The terms "altitude" error and "Y-component" error are used interchangeably in this section. The Y-direction actually is displaced about 10 degrees from the initial-point vertical direction.

of the correlation coefficients for initial error vectors, which are given in Table 5.4 shows that the correlation between initial altitude errors (e_{RY}) and vertical-velocity errors (e_{VY}) is relatively small. The coefficient in this case is only 0.16. This implies that, for a given altitude error, the probability that the corresponding vertical-velocity error will have the same sign as the altitude error is essentially the same as the probability that it will have the opposite sign. Accordingly, to study worst-case situations it is reasonable to choose error vectors where the signs of the altitude and vertical-velocity errors are the same. With these error combinations the vertical-velocity errors (if uncorrected) will tend to increase the altitude-estimate errors during the landing maneuver.

On the basis of the preceding discussion, the error vectors shown in Table 6.2 were selected from a group of 2,000 to demonstrate PGNCS performance in worst-case situations. The first two error vectors, Nos. 123, and 1860, show cases where the predominant error component is vertical velocity (e_{VY}). The next two error vectors, Nos. 1907 and 1975, represent cases where the predominant error component is altitude (e_{RY}). The last three error vectors, Nos. 212, 1191, and 1749, represent cases where both vertical-velocity and altitude errors are extremely large. In the first two cases the vertical-velocity and altitude errors have the same algebraic sign, in the third case the errors have opposite signs.

Using the error vectors of Table 6.2, a series of Monte-Carlo runs were made to study PGNCS performance during the landing maneuver. Landing-radar measurements were used to update navigation-system estimates according to the schedule shown in Fig. 2.2. The weighting functions used in the processing of the radar data were the optimum uncoupled weighting functions W-9, which are shown in Fig. 6.1. A summary of the important results from the runs are shown in Table 6.3. Thrust-vector profiles for selected runs from these sets are shown in Figs. 6.8 through 6.11. Additional thrust-vector profiles for other initial-condition uncertainty conditions are shown in Appendix B for general reference.

The data presented in Table 6.3 are most conveniently considered in two separate parts. The first seven runs shown on the top of the table are for the assumed conditions of a smooth lunar terrain (Model T-9) except for IC-6, and no uncertainties in the DPS acceleration at the high-throttle-setting position. The last six runs, on the other hand, are for a more realistic terrain model (Model T-6) and with the maximum expected DPS acceleration uncertainties of ±1 percent. In regard to the thrust-elevation-angle and thrust-magnitude deviations referred to in Table 6.3, these are based on the ideal error-free reference trajectories shown in Fig. 3.2 as well as Figs. 6.15 and 6.16. Also, the maximum permissible DPS thrust in the continuously-throttleable region is 6,300 pounds (60 percent of nominal thrust).

Table 6.2: Error Vectors Selected to Study PGNCS Performance in Worst-Case Situations

Error Vector Number	Probability Ellipsoid (percent)	e_{RY} (feet)	e_{VY} (f/s)	e_{VX} (f/s)	e_{RX} (ft)	e_{RZ} (ft)	e_{VZ} (f/s)
123	99.33	- 61	7.09	-3.24	-10,053	248	-0.76
1860	87.80	- 2	-7.79	3.33	8,479	-151	-0.87
1907	93.65	-2225	0.44	1.63	- 512	-413	0.16
1975	91.67	2054	1.32	-2.30	- 1,728	346	1.54
212	99.64	-1048	-7.10	4.17	8,087	-699	-2.07
1191	99.84	1906	6.68	-4.21	- 6,278	43	-1.88
1749	99.73	1830	-7.37	1.74	8,196	- 90	-1.37

Table 6.3: Summary of Results from Study of PGNCS Performance with Severe Initial-Condition Errors

Run No.	Error Vector Number	Fig. No.	e_{RY} (ft)	e_{VY} (f/s)	Terrain Model	DPS Accel Uncert. %	ΔV (f/s)	Max. Thrust in 10-60 % region (pounds)	Max. Deviations during Braking Phase		High-Gate Point Errors		Low-Gate Point Errors	
									El. Angle (deg)	Thrust (lbs)	Alt. (ft)	Vel. (f/s)	Alt. (ft)	Vel. (f/s)
IC-1	123	B.1*	- 61	7.09	T-9	0	6289	5683	11.5	432	+ 87	2.5	- .94	.58
IC-2	1860	B.2	- 2	-7.79	T-9	0	6283	5882	6.0	320	+ 38	1.6	+10	.91
IC-3	1907	B.3	2045	1.32	T-9	0	6286	6020	8.8	264	-172	6.8	-4.7	.48
IC-4	1975	B.4	-2225	0.44	T-9	0	6282	5479	5.3	221	- 67	2.7	- .52	.42
IC-5	212	B.5	-1048	-7.10	T-9	0	6284	5974	4.0	460	+ 98	4.5	+2.9	.92
IC-6	1191	6.4	1906	6.68	T-8	0	6297	5506	18.7	350	-236	10.1	+ .06	.34
IC-7	1749	B.6	1830	-7.37	T-9	0	6280	5612	2.6	120	+ 97	3.7	+7	.44
IC-8	212	6.8	-1048	-7.10	T-6	+1	6306	6194	11.1	590	+442	4.6	+1.8	.49
IC-9	212	6.9	-1048	-7.10	T-6	-1	6261	6000	12.9	330	+453	5.0	+1.6	.49
IC-10	1191	6.10	1906	6.68	T-6	+1	6317	5973	10.8	805	- 29	9.4	-4.7	.64
IC-11	1191	6.11	1906	6.68	T-6	-1	6278	5458	26.0	575	- 38	9.6	-2.8	.55
IC-12	1749	B.7	1830	-7.37	T-6	+1	6305	5855	6.5	382	+339	1.8	+1.3	.65
IC-13	1749	B.8	1830	-7.37	T-6	-1	6256	5639	8.3	690	+367	3.7	+2.6	.30

* B-Numbered Figures refer to Appendix B.

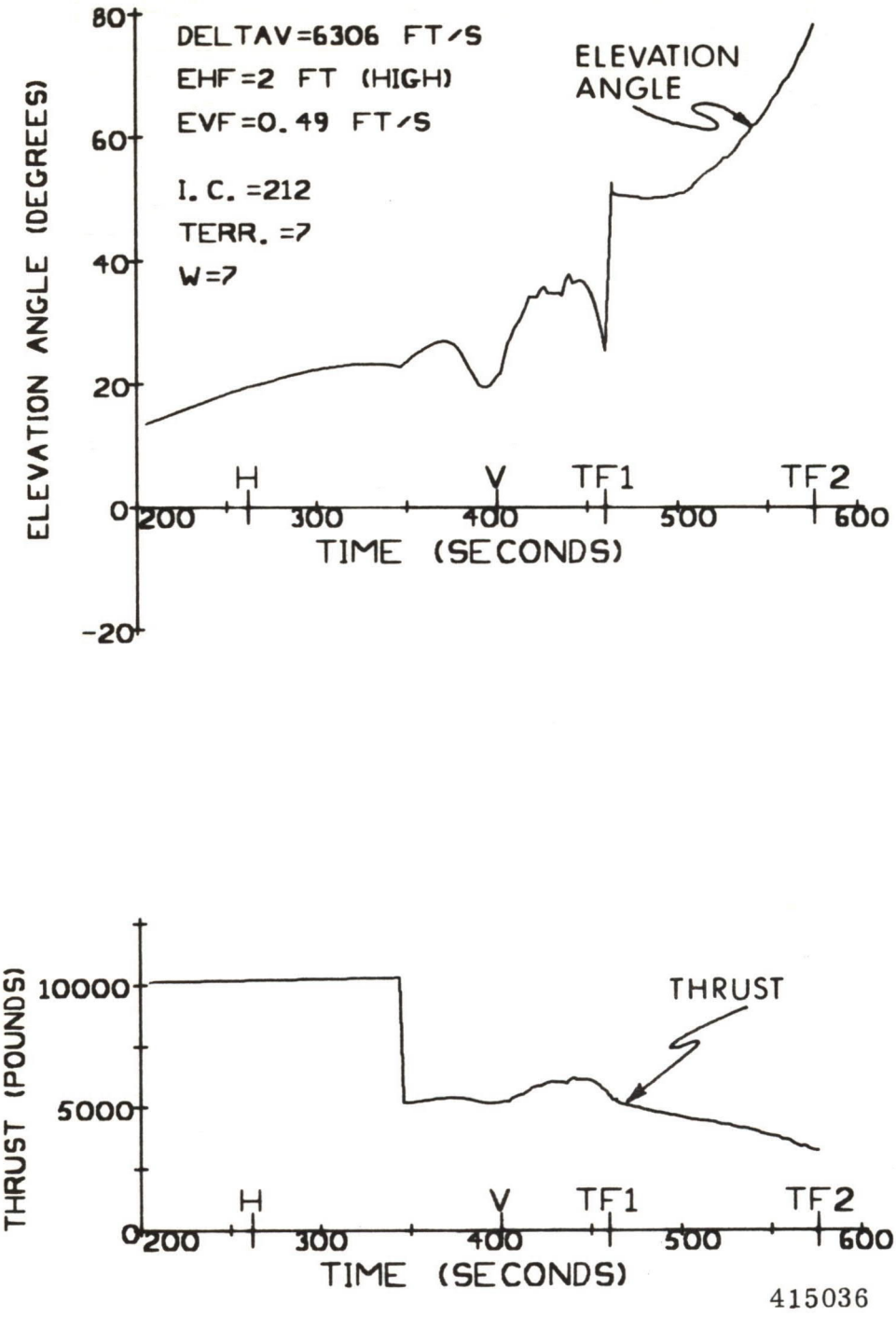

Fig. 6.8 Thrust-Vector Profiles: Very Severe Initial Errors, Realistic Terrain, +1% DPS Acceleration Uncertainty
(Case IC-8 Table 6.3)

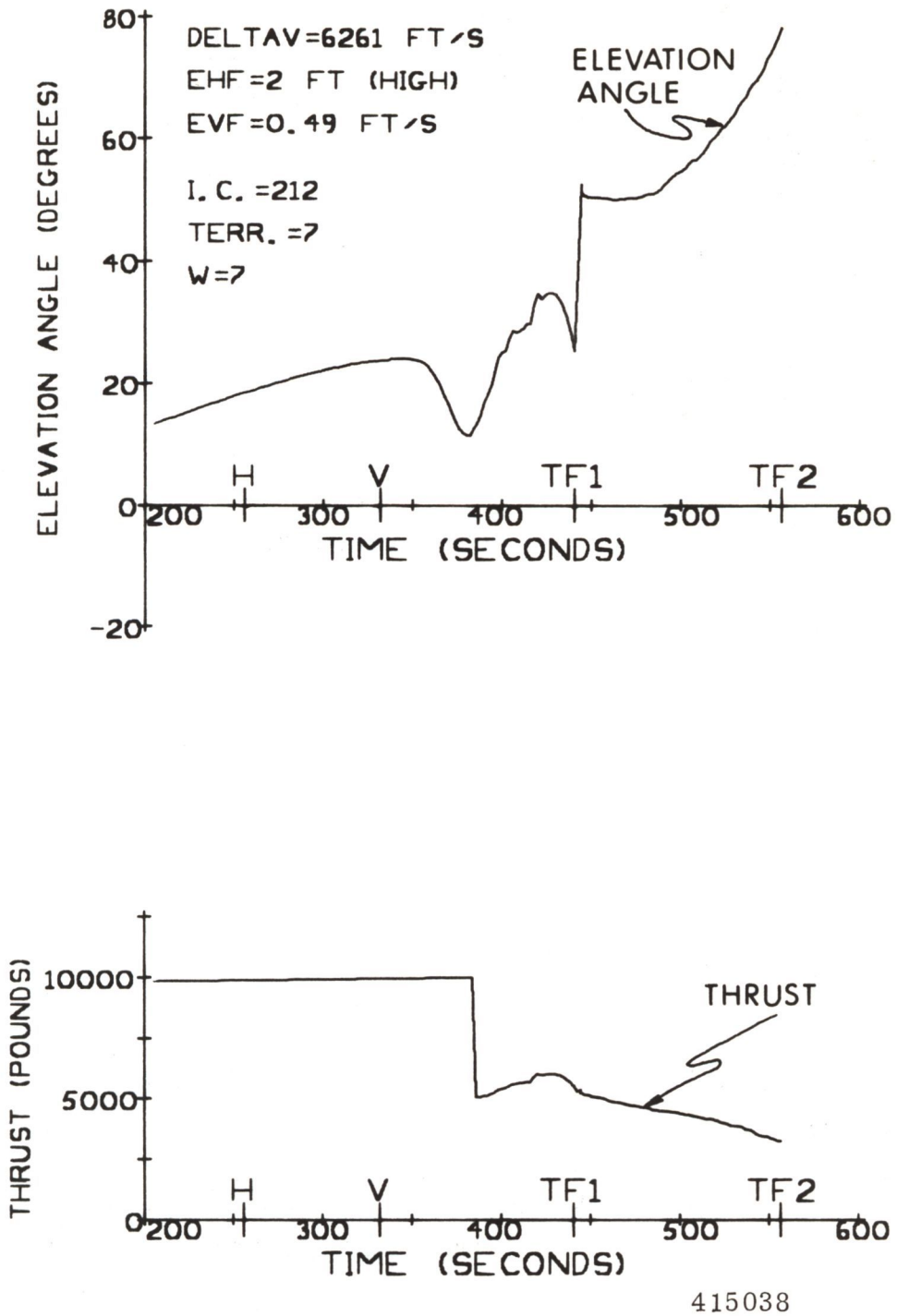

Fig. 6.9 Thrust-Vector Profiles: Very Severe Initial Errors, Realistic Terrain, -1% DPS Acceleration Uncertainty
(Case IC-9 Table 6.3)

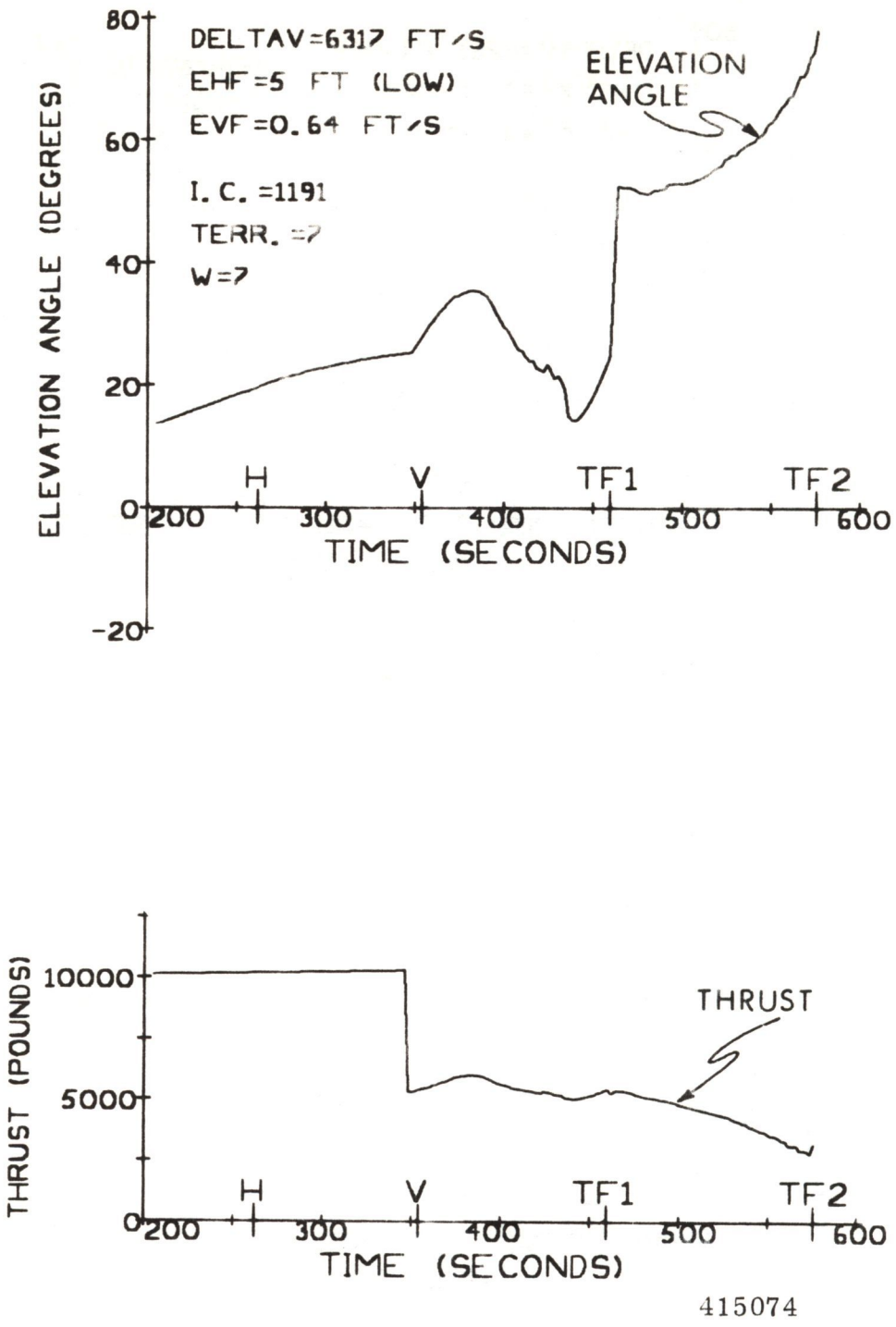

Fig. 6.10 Thrust-Vector Profiles: Very Severe Initial Errors, Realistic Terrain
+1% DPS Acceleration Uncertainty
(Case IC-10 Table 6.3)

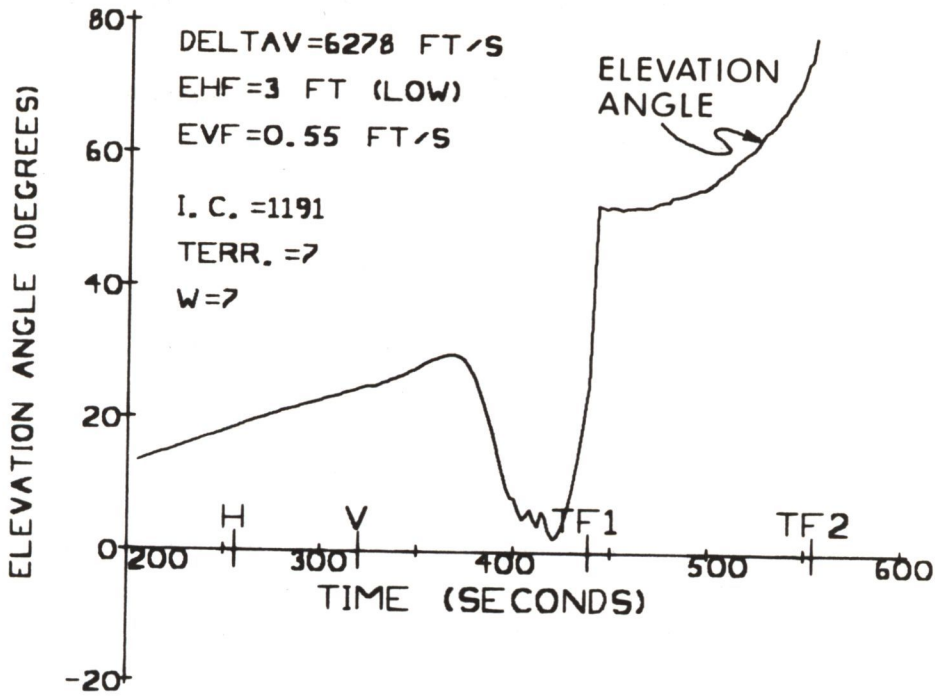

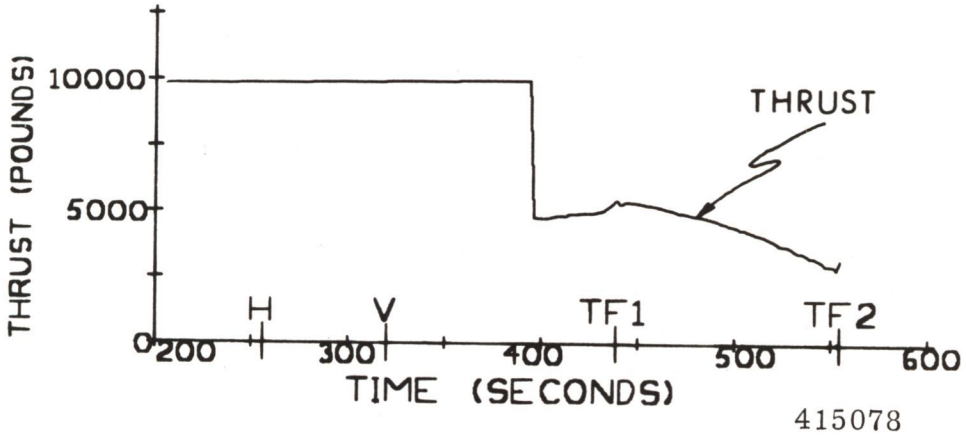

Fig. 6.11 Thrust-Vector Profiles: Very Severe Initial Errors, Realistic Terrain, -1% DPS Acceleration Uncertainty
(Case IC-11 Table 6.3)

From an examination of the data of Table 6.3 and Figs 6.8 through 6.11, the following important observations can be made in regard to PGNCS performance with severe initial-condition errors.

1) The increase in ΔV (above the reference-trajectory value of 6280 ft/sec) for the severe initial-condition errors is 17 ft/sec or less for the runs with no DPS acceleration uncertainties and no terrain-slope variations. In most of these cases the increase was less than 10 ft/sec.
2) The maximum permissible DPS thrust level for the continuously-throttleable region (6300 pounds) is not exceeded in any of the runs of Table 6.3. Included here are runs with the best available lunar-terrain models and with ± 1 percent DPS acceleration uncertainties.
3) The High-Gate conditions are met in all cases with an accuracy of 500 feet or better in altitude. As will be shown later, High-Gate altitude errors of this magnitude or less do not significantly affect the astronaut's visibility of the landing site in the following approach phase.
4) Fairly significant deviations in thrust-vector elevation angle (from nominal error-free case) can occur during the latter part of the braking phase. This is to be expected, however, since the major navigation errors are corrected at this time.
5) The visibility-phase thrust-vector profiles are very smooth in all cases. Low-Gate conditions are met with an accuracy of better than 10 feet in altitude and 1 ft/sec in velocity.

Referring to Figs. 6.8 and 6.9, it can be seen that the elevation angle is decreasing at a fairly rapid rate just prior to the end of the braking phase. The reason for this is that PGNCS is trying to bring the vehicle down to the High-Gate point at the end of the phase. Because of the severe initial errors, however, the vehicle is not able to get to the High-Gate point in time, as indicated by the corresponding High-Gate errors in Table 6.3. The High-Gate altitude errors, as will be shown in a later section of this chapter, make landing-site visibility more difficult for the astronaut.

In concluding this section it should be noted that the data presented here were based on the most severe initial-condition errors that can reasonably be expected for the landing maneuver at the present time. As such, these results represent limiting cases for PGNCS performance rather than average or typical cases. Additional data are presented, however, in Appendix B of PGNCS performance with less severe initial-condition errors.

6.4 Effect of Terrain Characteristics on PGNCS Landing Performance

In the development of landing-radar weighting functions, as mentioned in Chapter 4, the difference in altitude of the local terrain from the altitude of the selected site

was assumed to be proportional to the distance from the vehicle to the site, i.e. a constant-slope terrain model. The rms value of the slope coefficient was 100 ft/nmi (maximum slope of 3 degrees) which is the current MSC slope-uncertainty limit. In the study of PGNCS performance for the landing maneuver, on the other hand, several different terrain models were used to investigate terrain effects on the PGNCS-LR updating operation. These models, as indicated in Table 5.7, included terrain models based on combinations of simple mathematical forms, as well as models based on the best currently-available terrain data in the vicinity of currently considered landing sites.

A series of Monte-Carlo runs have been made to study the effect of terrain characteristics on PGNCS performance. To isolate the terrain effects more easily, these runs have been made with no initial-condition errors or DPS high-throttle-setting acceleration uncertainties present. The important results from these runs are summarized in Table 6.4. The first run (TER-1) is for a perfectly smooth moon with no terrain variations. The next two runs (TER-2 and TER-3) represent combinations of exponential terrain variations. The fourth and fifth runs (TER-4 and TER-5) are for constant slopes of ± 100 ft/nmi. The final four runs (TER-5,6,7,8) use terrain models based on the best data available at the time of this study of terrain variations near some expected landing sites. Thrust-vector profiles are given in Fig 6.12 for the case of a smooth lunar terrain (Run TER-1), and in Figs. 6.13 and 6.14 for the best current terrain models near the expected sites (Runs TER-7 and TER-9). The thrust-vector profiles for the other runs of Table 6.4 are given in Appendix C of this report.

The important points to be seen from the data of Table 6.4 and Figs. 6.12 through 6.14 are the following.

1) The required velocity increment (ΔV) for the landing maneuver is not significantly increased by the lunar terrain-slope variations used as models for the performance study.
2) If the altitude of the terrain below the vehicle during the latter part of the braking phase is appreciably different from the altitude of the site, then significant High-Gate-point altitude errors may occur. When the terrain is high relative to the site (Runs TER-3,5,7,8), the vehicle will pass above the desired High-Gate point. When the terrain is low relative to the site (Runs TER-2,4,9), on the other hand, the vehicle will go below the desired point. This can be seen from the data of Table 6.4.
3) The DPS thrust during the period of operation in the continuously- throttle-able region remains in all cases well below the maximum permissible value of 6300 pounds.
4) Terrain-slope variations of the the types considered here do not appear to adversely affect either the visibility-phase thrust-vector profiles or the errors in attaining Low-Gate-point conditions.

Table 6.4: Effect of Terrain Characteristics on PGNCS Performance
(no initial-condition errors or DPS uncertainties)

Run No.	Fig. No.	Terrain Model	ΔV (f/s)	Max Thrust Throttleable Region (lbs)	Maximum Deviations in Braking Phase		High-Gate Point Errors		Low-Gate Point Errors	
					El. Angle(deg)	Thrust(lbs)	Alt. (ft)	Vel (f/s)	Alt. (ft)	Vel (f/s)
TER-1	6.12	T-9	6283	5469	4.8	130	+ 89	4.1	+ .29	.47
TER-2	C.1	T-4 (+)	6284	6015	7.2	497	-667	2.3	-2.7	.33
TER-3	C.2	T-4 (-)	6286	5692	8.6	205	+785	4.9	+9.3	.78
TER-4	C.3	T-1 (+)	6291	5802	15.1	484	-857	8.2	-3.2	.65
TER-5	C.4	T-1 (-)	6283	5649	4.5	237	+460	8.7	- .01	.50
TER-6	C-5	T-5	6282	5539	3.3	233	+ 97	3.2	-5.4	.42
TER-7	6.13	T-6	6283	5737	7.4	269	+284	3.7	+1.8	.44
TER-8	C.6	T-7	6282	5750	9.5	277	+267	1.7	+1.7	.26
TER-9	6.14	T-8	6283	5590	4.5	198	-201	3.6	+2.4	.61

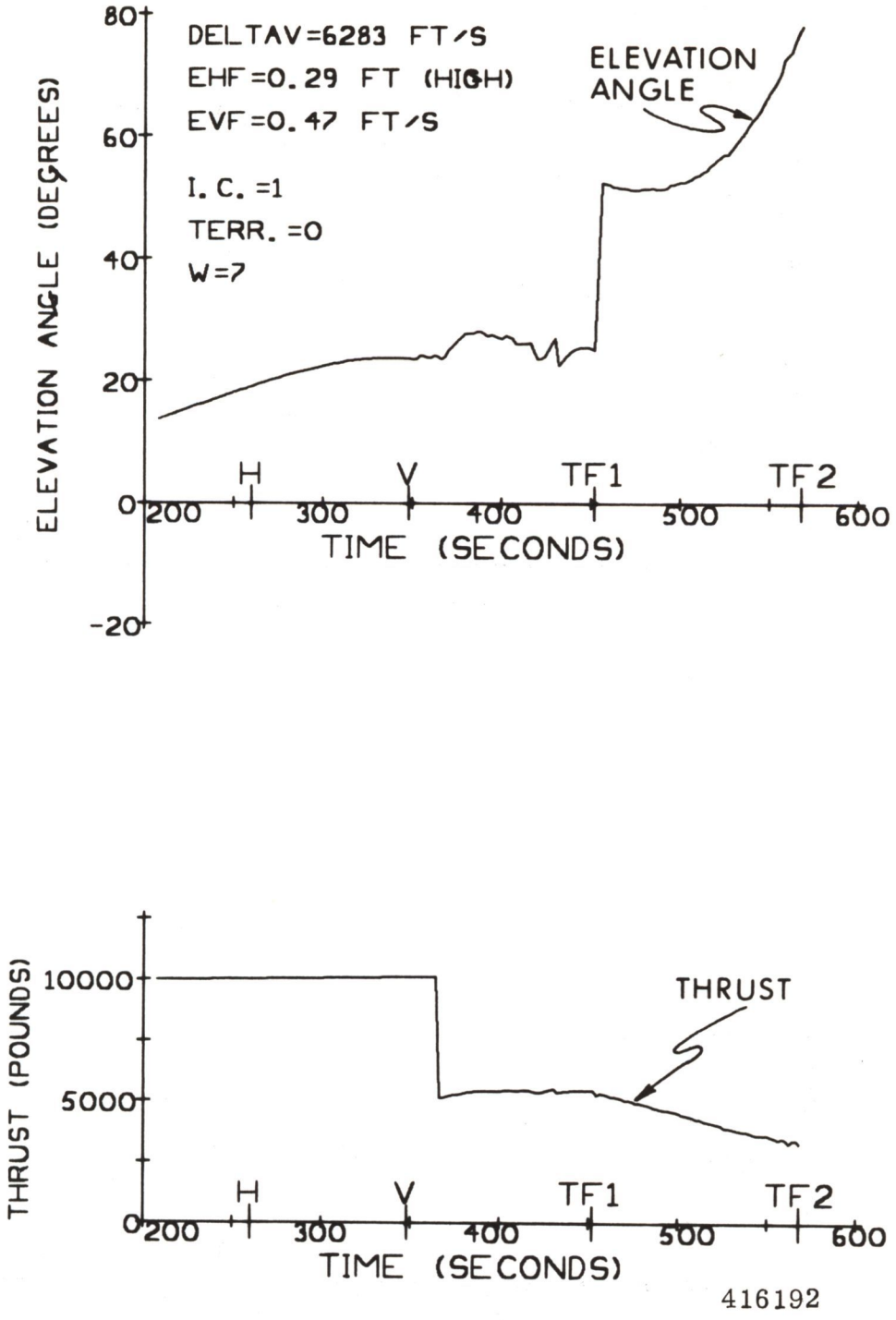

Fig. 6.12 Thrust-Vector Profiles: Smooth Terrain, No Initial Errors or DPS Acceleration Uncertainty
(Case TER-1 of Table 6.4)

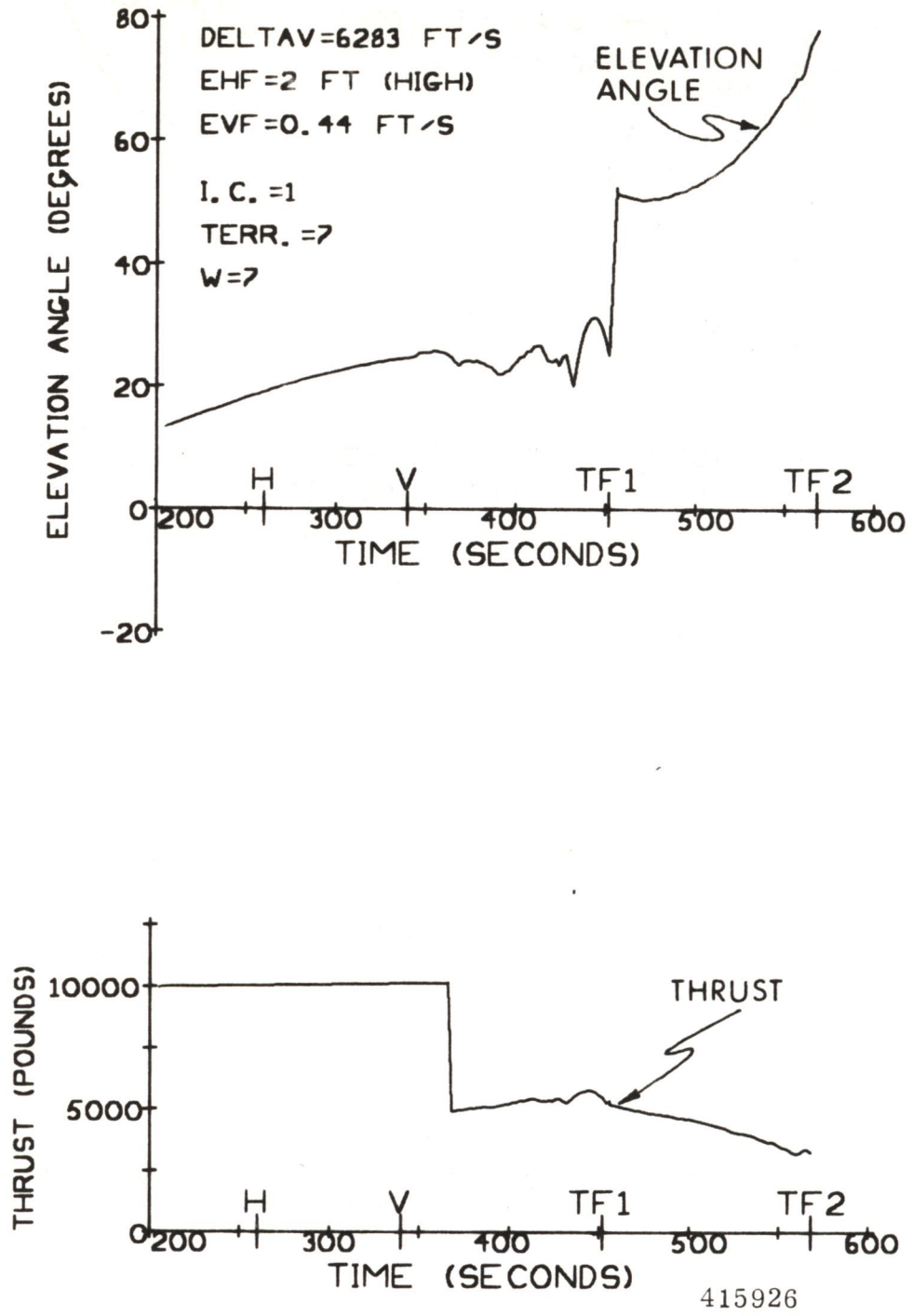

Fig. 6.13 Thrust-Vector Profiles: Terrain Model #6, No Initial Errors or DPS Acceleration Uncertainty (Case TER-7 of Table 6.4)

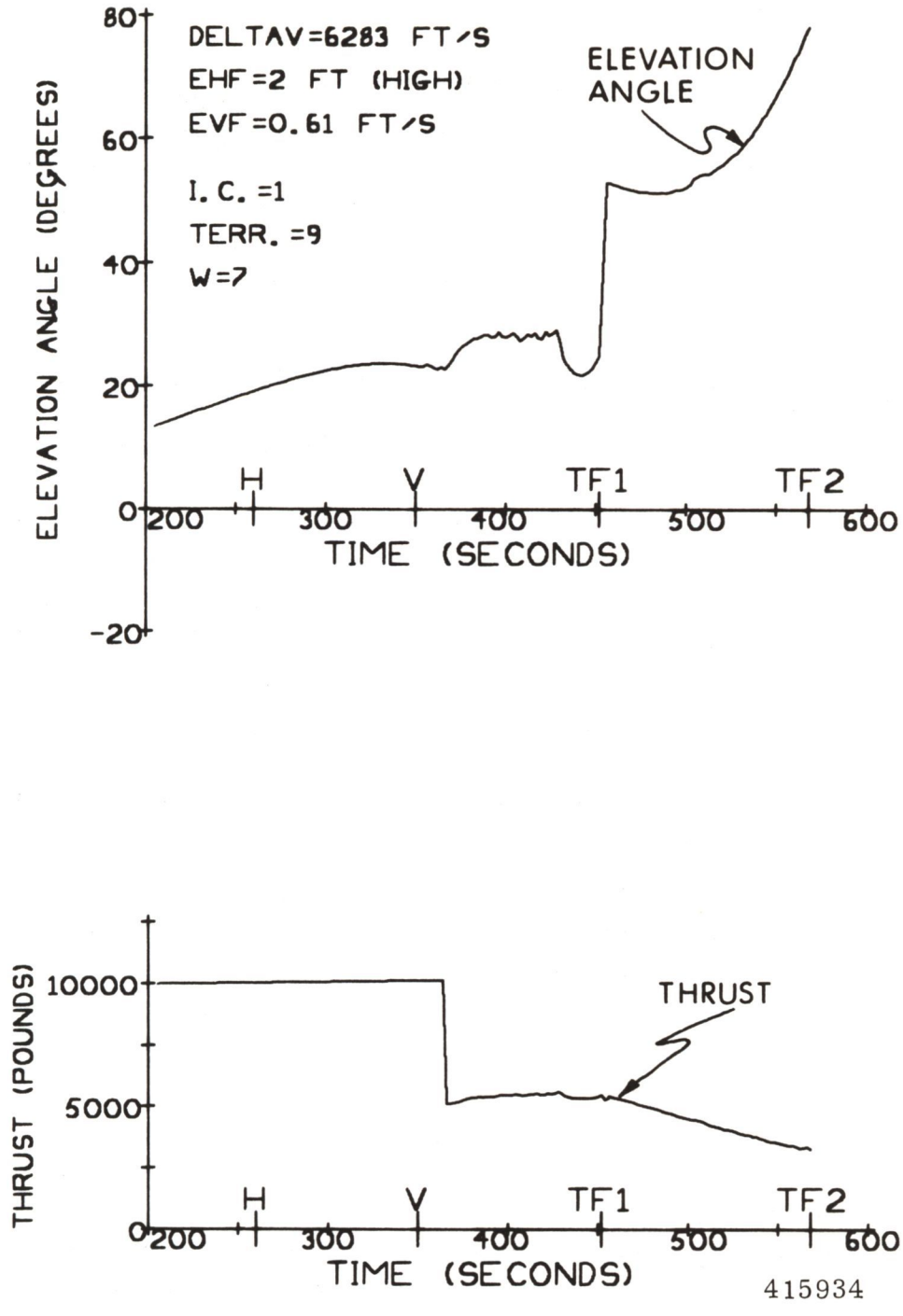

Fig. 6.14 Thrust-Vector Profiles, Terrain Model #8, No Initial Errors or DPS Acceleration Uncertainty. (Case TER-9 of Table 6.4)

5) Terrain-slope variations will cause deviations in the thrust-vector profiles during the latter part of the braking phase. For the cases considered it appears that these deviations are of the same order of magnitude as the deviations to be expected with severe initial-condition errors.

In concluding this section it should be noted that the runs presented here were for cases where no initial-condition errors of DPS throttle-setting uncertainties are present. Additional data showing system performance with terrain variations, severe initial-condition errors, and DPS acceleration uncertainties at maximum throttle are given elsewhere in this report (see for example the data of Figs. 6.5, 6.6, and 6.8 through 6.11).

6.5 Effect of DPS High-Throttle-Setting Acceleration Uncertainties on PGNCS Performance

During the first 350-400 seconds of the braking phase, the DPS is normally operated at a fixed high-throttle setting corresponding to 92.5 percent of the maximum DPS thrust. Under actual operating conditions there will be uncertainties in the DPS acceleration at this maximum throttle setting due to engine and vehicle weight uncertainties. At the time this study was made it was assumed that acceleration uncertainties of maximum thrust of as large as ± 1 percent could reasonably be expected.

Acceleration uncertainties at the high-throttle setting of this magnitude have an extremely important effect on PGNCS performance. This can be seen from the simulation runs of Figs. 6.15 and 6.16, where the only errors present are the DPS high-throttle acceleration uncertainties. The same effects are shown in Figs. 6.8 through 6.11 with normal navigation-system errors, severe initial-condition errors, and realistic terrain variations present.

The effects of positive and negative DPS acceleration deviations during the braking phase on PGNCS performance are quite different. A positive deviation (e.g. +1 percent) will cause the DPS to throttle-down earlier than for the nominal or standard case. This can be seen by comparing the thrust-vector profiles of Figs. 6.10 and 6.15 with the reference run of Fig. 3.2.

At the same time, the duration of the braking phase (which is computed to satisfy a specified horizontal, terminal, second-derivative of velocity at High-Gate) will also increase. The net result is that the interval of time during the braking phase for which the DPS is in the continuously-throttleable region is significantly increased. A negative deviation (e.g. -1 percent), on the other hand, will cause the DPS to throttle-down later after the start of the landing maneuver. At the same time, the duration of the braking phase will be decreased. As a result, in this case the interval of time during the braking phase that the DPS is in the throttleable region will be decreased under typical operating conditions for the PGNCS. It has been found that the sensitivity

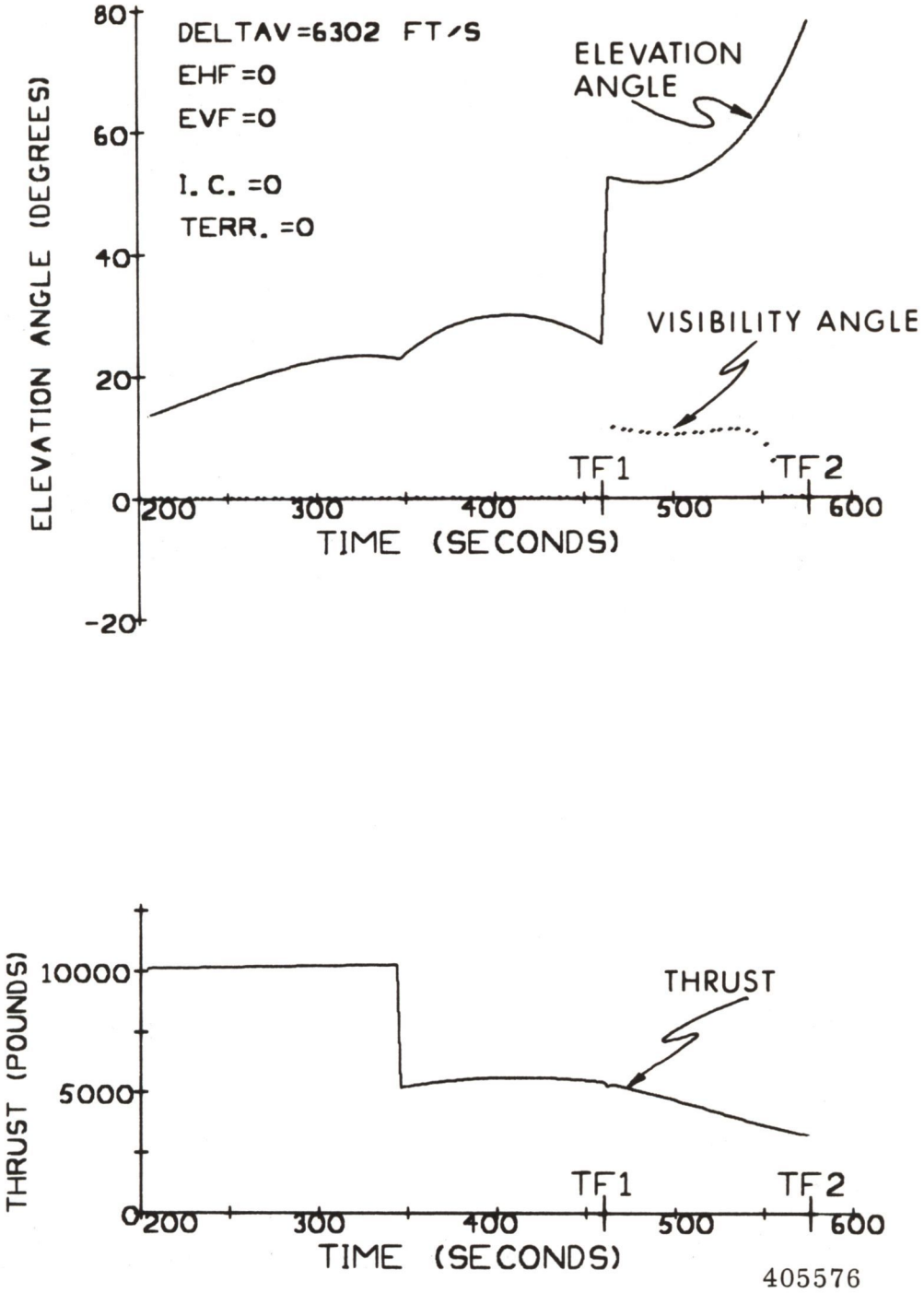

Fig. 6.15 Thrust-Vector Profiles: +1% DPS Acceleration Uncertainty, No I.C. Errors or Terrain Variations

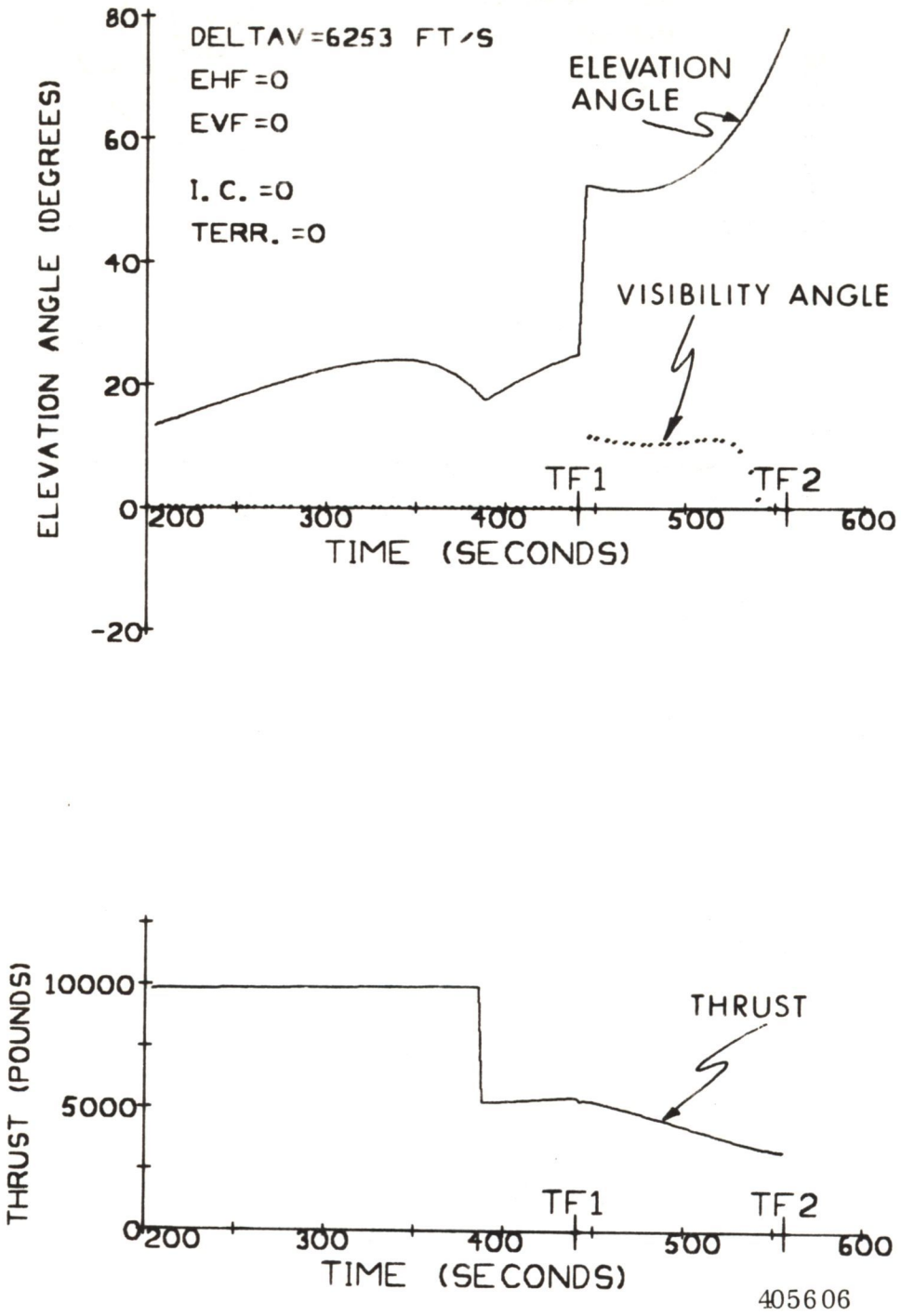

Fig. 6.16 Thrust-Vector Profiles: -1% DPS Acceleration Uncertainty, No I. C. Errors or Terrain Variations.

of the braking-phase throttleable interval to high-throttle-setting acceleration variations is about 30 sec/percent acceleration uncertainty.

For the case where the fixed-throttle acceleration deviation is positive, the length of time required for the vehicle to achieve the High-Gate conditions will be longer than in the nominal error-free case. For an acceleration deviation of +1 percent it has been found that the duration of the total braking phase is increased by about 10 seconds from the nominal case. The corresponding increase in required velocity increment (ΔV) for the braking phase has been found to be about 25 ft/sec.

For the case where the fixed-throttle acceleration deviation is negative, on the other hand, the required ΔV will be less than on the nominal trajectory, and as such it is not a major factor here. The major problem in this case is to design the basic landing trajectory in such a way that a reasonable interval of time is obtained during the braking phase with the DPS in the continuously-throttleable region. If such an interval is not provided, the vehicle will not meet High-Gate conditions with acceptable accuracy. In the present PGNCS, moreover, no steering-coefficient recomputations (c_0, c_1, ---c_8) are made during the last 20 seconds of the braking phase in order to minimize attitude transients. With the above considerations in mind and in view of the expected DPS performance uncertainties, initial-condition errors, and terrain variations at the time this study was made, the reference landing trajectory was designed to throttle-down the DPS 80 seconds before the end of the braking phase. It was found that this was necessary to insure reasonable accuracy in meeting High-Gate conditions.

In concluding this section, it should be noted that the maximum ΔV requirements for the PGNCS are, in effect, set by the case where the high throttle-setting acceleration deviation is positive. The minimum interval of continuously-throttleable DPS operation during the braking phase, on the other hand, is determined by the maximum expected negative deviation in the throttle setting. In regard to the latter case, it should be noted that there is a ΔV penalty for designing the reference trajectory to throttle down at an earlier time. In the cases investigated this penalty has been found to be about 1 ft/sec/sec.

6.6 Effect of Altitude Errors at High-Gate Point on Landing-Site Visibility

An important objective for the landing maneuver, as mentioned in Chapter 1, is that the selected landing site be visible to the astronaut at least 10 degrees above the edge of the LEM window for a minimum of 75 seconds. In order to accomplish this objective efficiently, the PGNCS first guides the LEM to a preselected High-Gate point. The LEM is then guided from the High-Gate point to the Low-Gate point via a trajectory designed to meet the visibility requirements.

The effect of errors in altitude at the High-Gate point on landing-site visibility is shown in Fig. 6.17. This figure presents data on the location of the landing site above the edge of the LEM window (as seen by the astronaut) as a function of time during the visibility phase of the landing. No other PGNCS errors other than altitude are assumed to be present here, e.g. there are no down-range position errors present.

From the curves shown in Fig. 6.17, it can be seen that the landing site will be visible to the astronaut for at least 75 seconds with High-Gate altitude errors as large as 2000 feet. If the landing-site must at the same time be 10 degrees or more above the edge of the window, then the maximum permissible High-Gate altitude error is 100 feet. If, on the other hand, the site were required to be only 8 degrees above the window's edge, then the permissible High-Gate altitude error would be increased to 500 feet.

The data presented in Fig. 6.17 assume that there are no down-range position errors present in the PGNCS. Under actual operating conditions, however, down-range position errors will be present, since the landing-radar does not update the horizontal components of estimated position. Under these conditions the vehicle may miss the Low-Gate and High-Gate points by as much as several thousand feet in down-range position. This will cause the astronaut to lose visibility of the initially-selected site earlier in the visibility phase as indicated in Fig. 6.18. The visibility of the site below the Low-Gate point actually reached by the vehicle at the end of the visibility phase, however, will be the same as shown in Fig. 6.17.

6.7 Comparison of PGNCS Performance with Different Landing-Radar Weighting Functions

6.7.1 Introduction

The performance of the PGNCS has been investigated with several different types of landing-radar weighting functions. The characteristics of these weighting functions have been described in Chapter 4. This section will compare PGNCS performance with the different weighting functions. Both statistical and Monte-Carlo results will be presented. The major emphasis here will be on uncoupled weighting functions of the type being planned for use in the PGNCS.

6.7.2 Navigation-System Accuracy with Coupled Weighting Functions

The rms values of the navigation errors during the landing maneuver are presented in Fig. 6.19 for the various coupled weighting functions W-1, W-2, W-3, and W-4, whose characteristics were described in Chapter 4. The primary differences between weighting functions, as may be recalled, arise from the manner in which doppler-velocity bias errors and terrain-slope variations are handled in the estimation process. In the weighting-function set W-1, these errors are ignored completely. In set W-2, these errors are represented as white noise. In set W-3, these errors are accounted for as bias errors in the

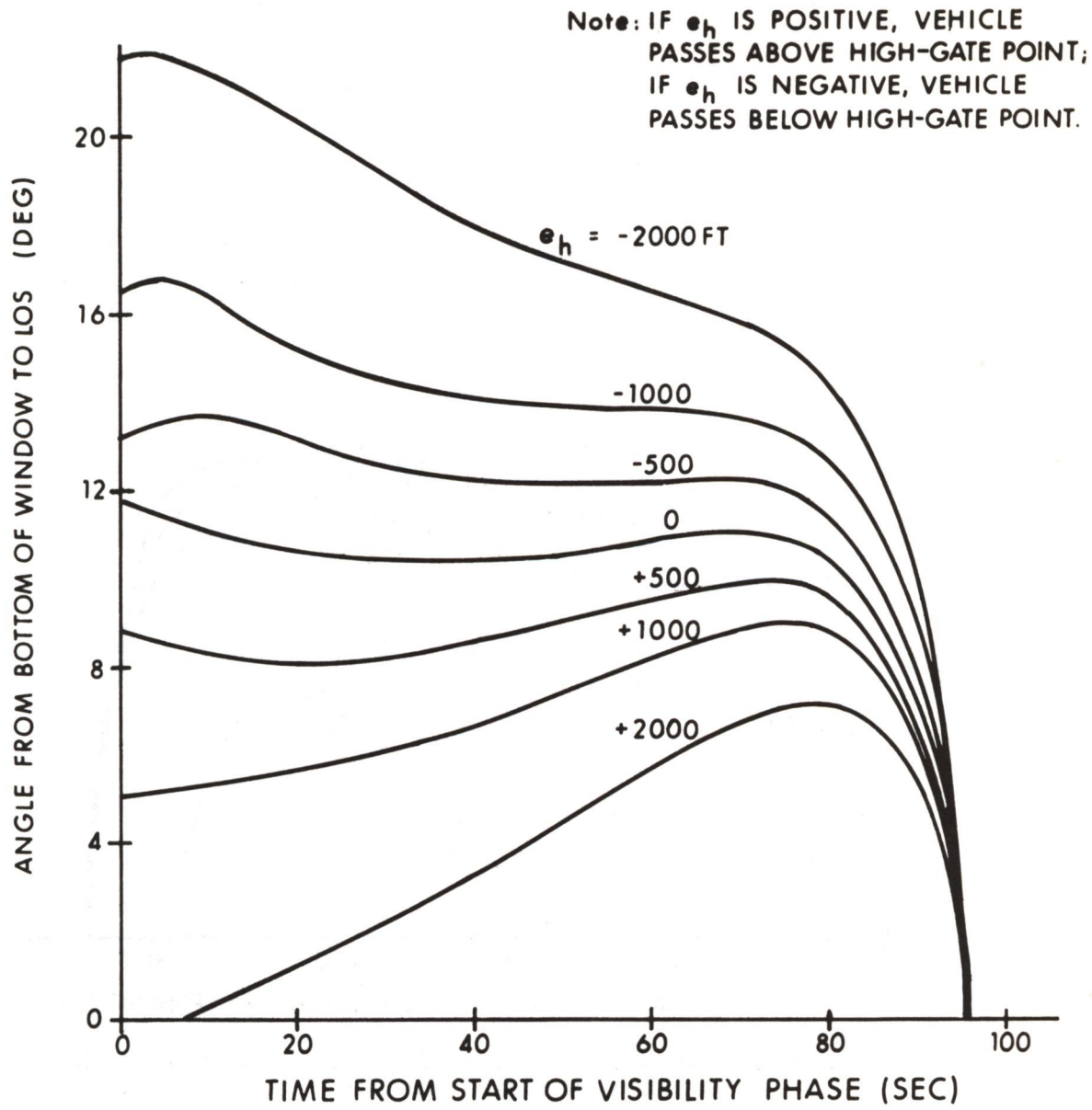

Fig. 6.17 Effect of High-Gate Point Altitude Errors On Landing Site Visibility.

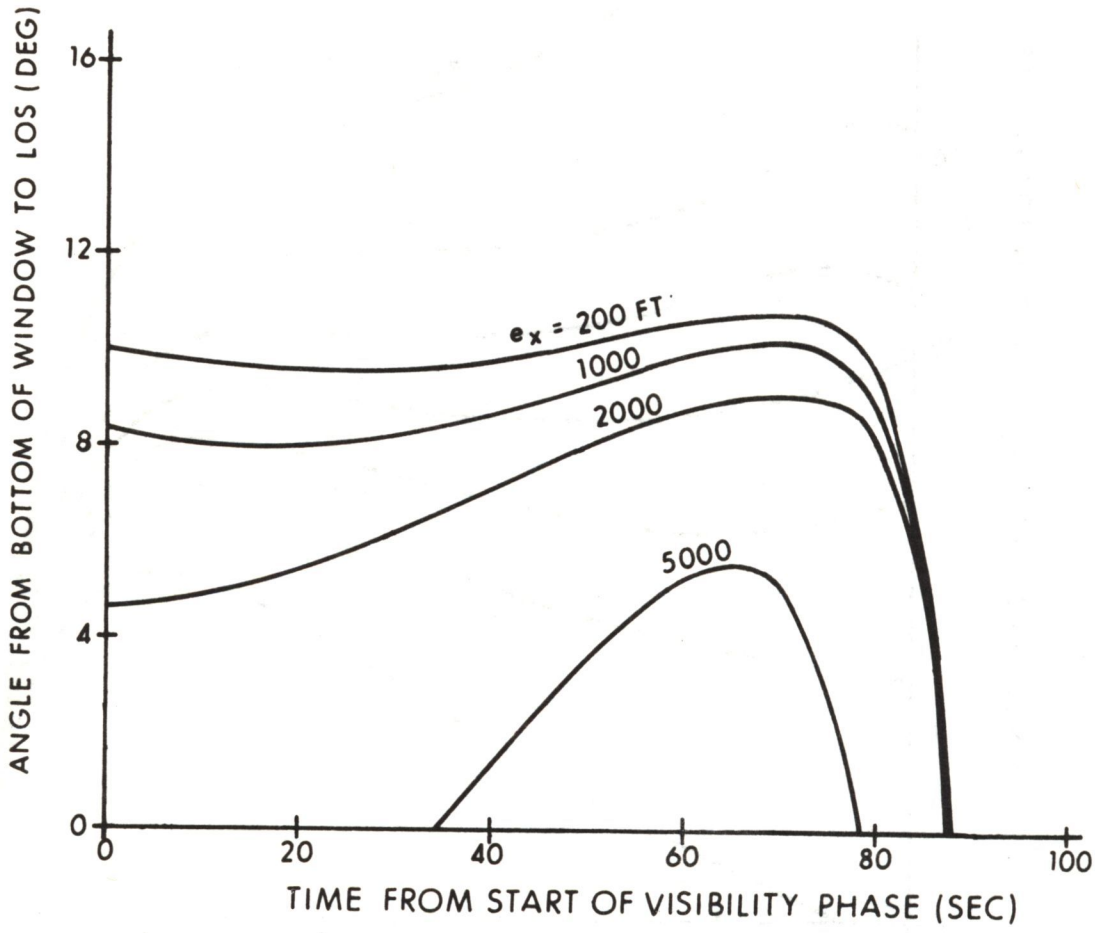

Fig. 6.18 Effect of Down-Range Position Errors at High-Gate Point on Landing-Site Visibility.

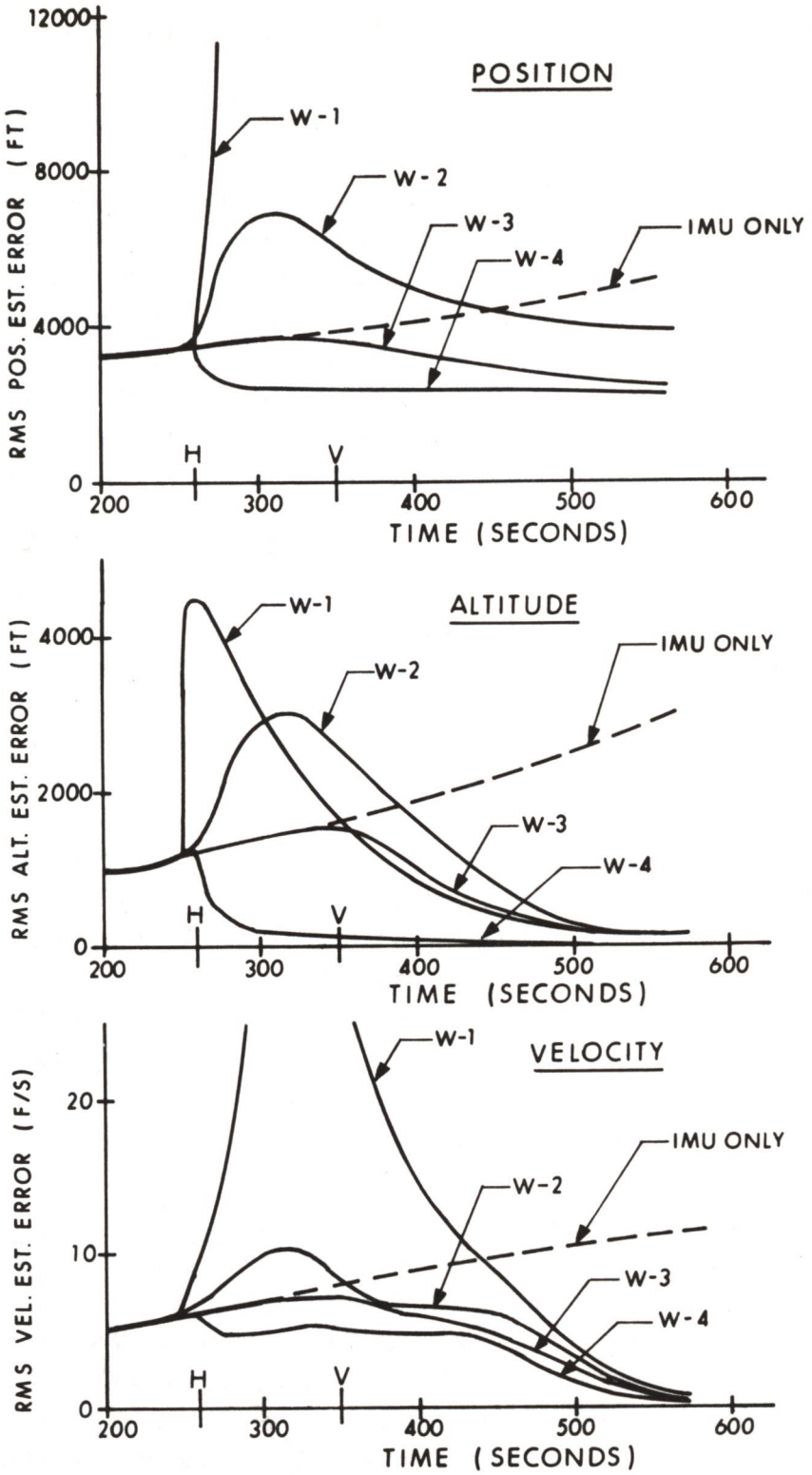

Fig. 6.19 Navigation-System Performance with Various Coupled Weighting Functions.

covariance-matrix computations, but no bias estimates are made. Finally, in set W-4, the terrain variations are estimated as a constant-slope bias error. Also shown in Fig. 6.19 are the rms errors for the case where no radar-updating takes place, i.e. the IMU is the sole navigation sensor.

There are several points of interest in the data of Fig. 6.19. The most important of these are the following.

1) The performance of the radar-updated navigation system becomes significantly better than the non-updated system (IMU only) as time increases during the landing maneuver. This is to be expected since the landing-radar altitude and velocity measurement errors decrease, as the vehicle's altitude and velocity are decreased.
2) As the quality of the model used to represent velocity-bias errors and terrain variations is improved, the accuracy of the navigation information improves, particularly during the early part of the landing maneuver.
3) The navigation errors for the case where velocity-bias errors and terrain variations are ignored completely (W-1) are excessively large and unacceptable.
4) The best navigation accuracy is obtained for the case where a constant-slope bias is estimated for the terrain-slope variations (W-4). It should be recognized, however, that in this latter case the actual terrain-slope variations have also been assumed to follow a constant slope.
5) Improvements in the rms position accuracy of the navigation system are obtained with weighting functions W-3 and W-4. These improvements are obtained even though the basic radar measurements are of vehicle velocity and altitude.
6) Fairly good navigation accuracies are obtained with set W-3 wherein bias errors and terrain variations are accounted for, but not estimated, in the weighting-function computations. At no time during the landing maneuver are the rms errors with these weighting functions greater than those of the non-updated system.

6.7.3 Navigation-System Accuracy with Uncoupled Weighting Functions

Navigation-system performance data are presented in Figs. 6.20 and 6.21 for the uncoupled weighting functions described in Table 4.2. The data in Fig. 6.20 are for various constant-valued weighting functions: set W-6 represents weighting functions of 0.1, set W-7 represents weighting functions of 0.5, and set W-8 represents weighting functions of 0.9. Included in Fig. 6.21 are data on the original set of uncoupled landing-radar weighting functions (W-5), and data on

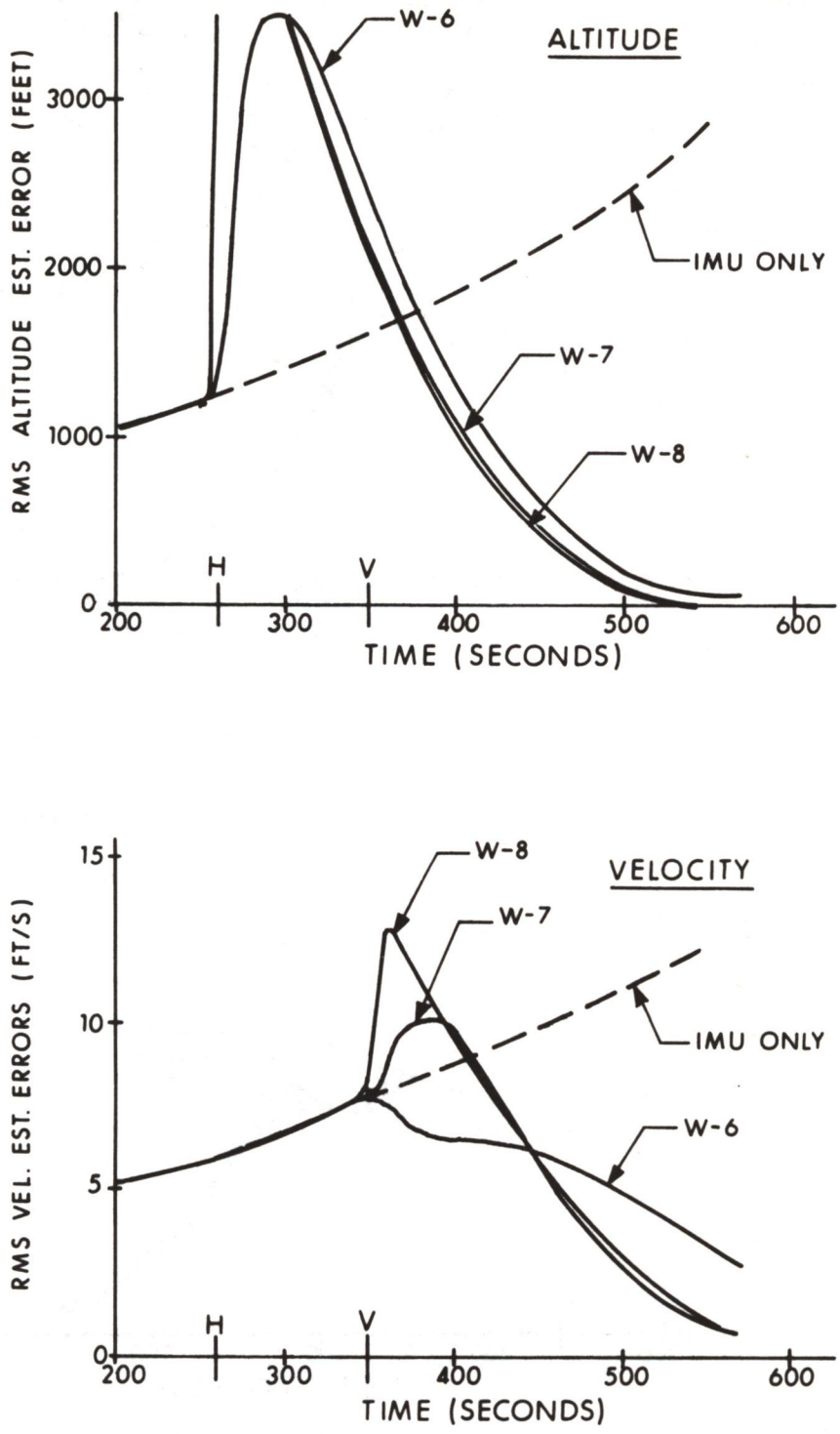

Fig. 6.20 Navigation-System Performance with Constant Uncoupled Weighting Functions.

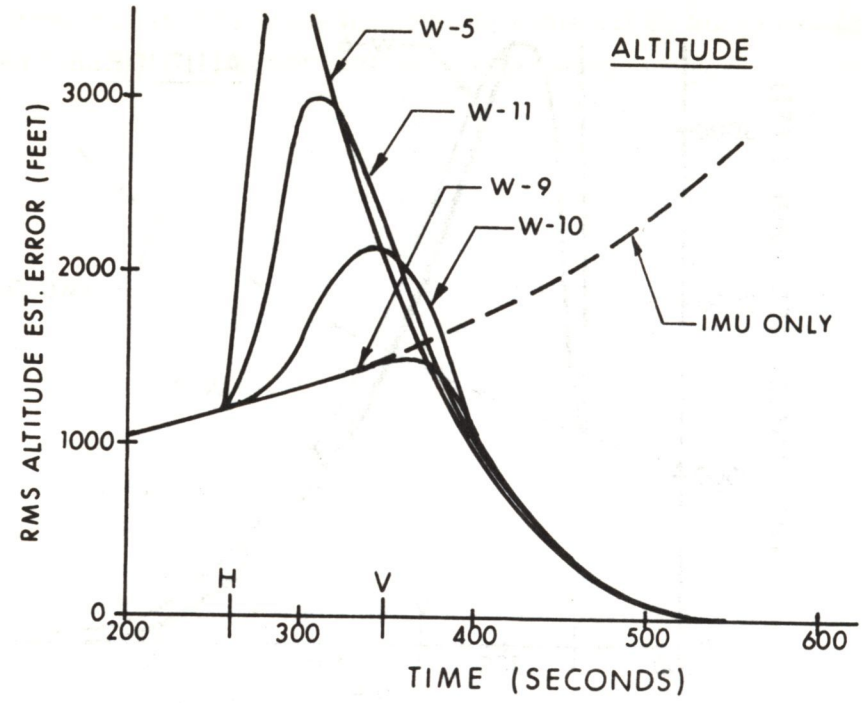

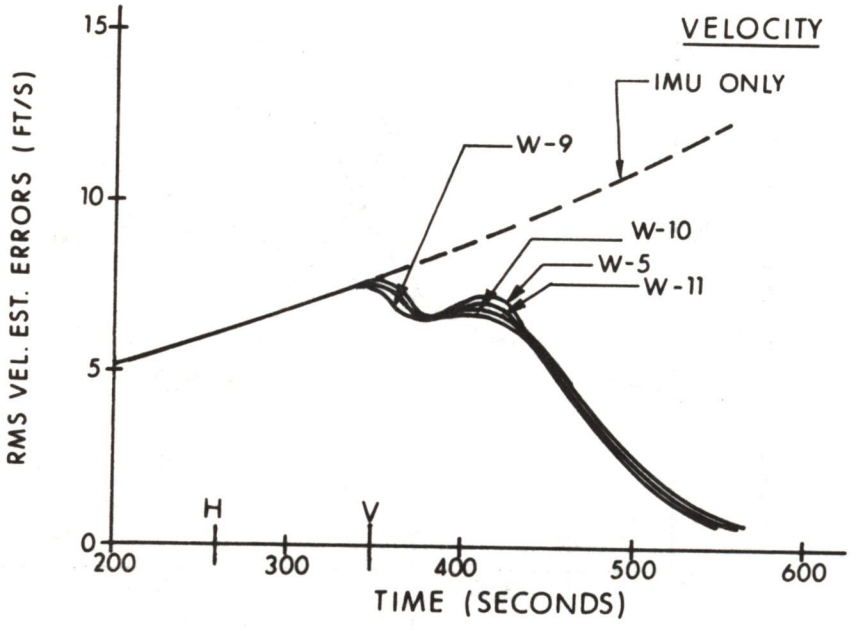

Fig. 6.21 Navigation-System Performance with Various Uncoupled Weighting Functions.

the optimum uncoupled set wherein velocity bias and terrain-variations are accounted for in the weighting-function calculations (W-9). Also included here are data for weighting functions W-10 and W-11, which are linear approximations to the set W-9. Inasmuch as these uncoupled weighting functions update only altitude and velocity estimates, the data of Figs. 6.20 and 6.21 are concerned only with altitude and velocity estimate errors.

The important points to be seen from the data of Fig. 6.20 are the following.

1) During the first 100 seconds after the initial altitude updating (260 seconds from the start of the landing maneuver) the rms altitude errors are significantly larger than for the non-updated system. The largest errors occurs with the constant weighting functions of 0.9 (set W-8)
2) The rms altitude-estimate errors at the end of the landing maneuver are significantly larger with the constant 0.1 weighting functions (W-6) than with either the weighting functions of 0.5 (set W-7) or 0.9 (set W-8). For the low-weighting functions (set W-6) these errors are about 50 feet; for the high-weighting functions (sets W-7 and W-8) they are about 10 feet.
3) The rms velocity-estimate errors at the end of the landing maneuver are also significantly larger for the weighting functions of 0.1 than for 0.5 or 0.9. The corresponding rms velocity errors in this case are about 3 ft/sec and 0.75 ft/sec.
4) From the viewpoint of minimizing rms velocity errors, it appears that in the interval immediately after the initial-velocity updating, low weighting functions should be employed. During the latter part of the landing maneuver it appears that high weighting functions should be used.

With regard to the data for the uncoupled weighting functions shown in Fig. 6.21, the following points are important:

1) The rms altitude and velocity errors at the end of the landing maneuver are acceptably low for all four weighting functions. The rms errors at this time are significantly smaller than for the non-updated system.
2) The lowest rms altitude errors are obtained for the optimum uncoupled weighting functions (set W-9). The rms altitude errors in this case are at all times equal to or smaller than those for the non-updated system.

3) During the first 100-120 seconds after the initial-altitude updating, the original weighting functions (W-5) and the linear approximations (W-10 and W-11) give rms altitude errors significantly larger than the optimum weighting functions (W-9). In this regard it should be recalled that the data of Figs. 6.19 through 6.21 are based on the assumption of a constant-slope terrain, with the slope-coefficient having an rms value of 100 ft/nmi.

4) The rms velocity errors are not significantly different for the four weighting functions investigated in Fig. 6.21

6.7.4 Monte-Carlo Performance Data with Uncoupled LR Weighting Functions

In the preceding two sections of this chapter, statistical data were presented on navigation-system performance for several different LR weighting functions. In the present section, Monte-Carlo data are presented to show PGNCS performance with the various uncoupled LR weighting functions that have been considered for the landing maneuver. The basic reference trajectory for these data is as shown in Figs. 3.2 through 3.5. The ignition, High-Gate, and Low-Gate points are as given in Tables 1.1 and 3.1. The LR updating schedule used here is as shown in Fig. 2.2. The IMU and LR performance characteristics are as given in Table 5.1.

An important objective in this Monte-Carlo study was to investigate the performance of the PGNCS under the most severe conditions that could reasonably be expected at the time of this study. In order to accomplish this objective with a reasonable number of runs, two different initial-error vectors were chosen to represent severe initial-condition errors. The selected error vectors, whose elements are given in Table 6.2, were Nos. 212 and 1191. Both of these error vectors contain large altitude and vertical-velocity components with the same algebraic signs. In error-vector 212 both of these components have negative signs, in No. 1191 both components are positive. Error-vector 212 terminates on a 99.64-percent equiprobability ellipsoid; error-vector 1191 terminates on a 99.84-percent ellipsoid. To limit the number of Monte-Carlo runs, two lunar terrain models suggested by MSC were selected to represent terrain variations in the vicinity of probable landing sites. The selected models were T-6 and T-8 of Table 5.7. The terrain of interest in T-6, as indicated in Fig. 5.2, is generally higher in altitude than the landing site. The terrain of interest in T-8, on the other hand, as can be seen in Fig. 5.2, is generally lower in altitude than the site.

Using the above-mentioned initial-error vectors in combination with the selected terrain models, sets of Monte-Carlo runs were made for the different LR weighting functions with DPS thrust-acceleration uncertainties of ± 1 percent. In this way a total of 8 different runs were obtained for each LR weighting-function set, corresponding to the various combinations of initial error vectors, terrain models, and DPS uncertainties.

To simplify the presentation of data in this section, the key results from the Monte-Carlo runs are presented in tabular form for each weighting function of interest. The thrust-vector profiles, for the runs for which data are tabulated, are given for convenience in Appendix D.

The Monte-Carlo data are tabulated as follows.

1) Original uncoupled weighting-function data (set W-5) are presented in Table 6.5.
2) Data for constant-weighting functions of 0.1 (set W-6) are given in Table 6.6.
3) Data for constant weighting functions of .9 (set W-8) are given in Table 6.7.
4) Optimum uncoupled weighting-function data (set W-9) are given in Table 6.8.
5) Data for linearized weighting functions (set W-11) are given in Table 6.9.

In regard to the data presented in these tables for maximum thrust-vector deviations, it should be noted that these deviations are measured relative to error-free reference trajectories with ± 1 percent DPS thrust-acceleration uncertainties (Figs. 6.15 and 6.16). It should also be noted that the maximum permissible thrust for the DPS in the 10-60 percent region is assumed in this study to be 6300 pounds. Finally, in the tabulated values of ΔV are included the velocity increments required for DPS ullage, the DPS trim phase, the effects of lunar rotation, and all maneuvers required to the Low-Gate conditions.

The most important points to be seen from the data of Table 6.5 through 6.9 and their associated thrust-vector profiles are the following

1) The thrust-vector profiles during the visibility phase are relatively smooth in all cases, i.e. the maximum elevation-angle deviations during this period are less than 1 degree.
2) The major deviations in the thrust-vector profiles occurred during the latter part of the braking phase when the primary trajectory corrections were made.
3) The maximum permissible DPS thrust in the 10-60 percent region (6300 pounds) was not exceeded in any of the runs.
4) The required velocity increments (ΔV), the maximum thrust-vector deviations, and the High-Gate-point errors were not significantly different for the weighting functions considered.
5) Excessively large Low-Gate-point errors were obtained on certain runs with the constant-weighting functions of 0.1 (set W-6). The Low-Gate errors for all other weighting functions considered were acceptably small.

Table 6.5: Monte-Carlo Study for Original Uncoupled LR Weighting Functions

Error Vector Number	Fig. No.	Terrain Model	DPS Accel. Uncert. %	ΔV (f/s)	Max. Thrust 10-60% region (lbs)	Max. Thrust Vector Deviations during Braking Phase		High-Gate Point Errors		Low-Gate Point Errors	
						El. Angle (deg)	Thrust (lbs)	Alt. (ft)	Vel. (f/s)	Alt. (ft)	Vel. (f/s)
212	D. 1	T-6	+1	6305	6136	8.2	511	+358	2.6	- .3	.5
212	6.24	T-8	+1	6308	5879	3.8	346	-263	2.1	-10.6	1.1
1191	6.25	T-6	+1	6310	5914	12.5	516	+261	5.2	- .7	.6
1191	D. 2	T-8	+1	6308	5671	7.4	301	-167	3.5	- 1.7	1.0
212	D. 3	T-6	-1	6258	5784	8.1	333	+326	4.0	- .2	.9
212	D. 4	T-8	-1	6253	5796	3.6	110	-258	2.7	- 1.4	.7
1191	D. 5	T-6	-1	6262	5481	12.5	324	+305	5.2	-13.2	.9
1191	D. 6	T-8	-1	6261	5457	8.6	362	-143	3.5	- 9.0	.8

Table 6.6: Monte-Carlo Study Results for Constant LR Weighting Functions of 0.1

Error Vector Number	Fig. No.	Terrain Model	DPS Accel. Uncert. %	ΔV (f/s)	Max. Thrust 10-60% region (pounds)	Max. Thrust Vector Dev. during Braking Phase		High-Gate point Errors		Low-Gate Point Errors	
						El. Angle(deg)	Thrust(lbs)	Alt.(ft)	Vel.(f/s)	Alt.(ft)	Vel.(f/s)
212	E.1	T-6	+1	6309	5902	5.2	309	+345	5.7	+32	.9
212	6.22	T-8	+1	6305	5799	3.5	195	-305	7.5	+21	1.2
1191	6.23	T-6	+1	6307	5638	10.0	450	- 56	10.5	-112	4.2
1191	E.2	T-8	+1	6306	5499	7.1	286	-383	2.0	- 1.4	.5
212	E.3	T-6	-1	6266	5960	6.2	478	+341	18.8	+ 26	1.0
212	E.4	T-8	-1	6255	5475	5.0	549	-338	1.4	+ 36	.8
1191	E.5	T-6	-1	6271	5685	10.5	275	+489	5.3	+17.7	1.2
1191	E.6	T-8	-1	6261	5458	15.2	577	-256	4.1	+24.6	1.1

Table 6.7: Monte-Carlo Study Results for Constant LR Weighting Functions of 0.9

Error Vector Number	Fig. No.	Terrain Model	DPS Accel. Uncert. %	ΔV (f/s)	Max. Thrust 10-60% region (lbs)	Max. Thrust Vector Deviations during Braking Phase		High-Gate Point Errors		Low-Gate Point Errors	
						El. Angle (deg)	Thrust (lbs)	Alt. (ft)	Vel. (f/s)	Alt. (ft)	Vel. (f/s)
212	F.1	T-6	+1	6312	5885	7.4	644	+ 47	28.5	- .76	2.2
212	F.2	T-8	+1	6308	6087	7.7	507	-360	1.4	+10.0	2.4
1191	F.3	T-6	+1	6324	5811	18.5	439	+ 11	18.2	- .5	1.1
1191	F.4	T-8	+1	—	*6300	—	—	—	—	—	—
212	F.5	T-6	-1	6257	5819	7.0	412	+408	6.4	4.1	1.3
212	F.6	T-8	-1	6258	5676	8.1	274	-430	6.3	10.4	3.2
1191	F.7	T-6	-1	6266	5458	13.6	402	+221	6.8	-15.0	2.3
1191	F.8	T-8	-1	6254	5569	13.2	504	+ 30	19.3	-19.3	4.3

* Maximum thrust level of 6300 pounds in throttleable region was violated in this run.

Table 6.8: Monte-Carlo Study Results for Optimum Uncoupled LR Weighting Functions

Error Vector Number	Fig. No.	Terrain Model	DPS Accel. Uncert. %	ΔV (f/s)	Max. Thrust 10-60% region (lbs)	Max. Thrust Vector Deviations during Braking Phase		High-Gate Point Errors		Low-Gate Point Errors	
						El. Angle (deg)	Thrust (lbs)	Alt. (ft)	Vel. (f/s)	Alt. (ft)	Vel. (f/s)
212	6.8	T-6	+1	6306	6194	11.1	590	+442	4.8	+1.8	.5
212	G.1	T-8	+1	6306	6042	7.4	1002	-245	4.6	+2.1	.5
1191	6.10	T-6	+1	6317	5973	10.8	805	- 29	9.4	-4.7	.6
1191	G.2	T-8	+1	6322	6059	20.0	462	-561	10.6	+1.9	.5
212	6.9	T-6	-1	6261	6000	12.9	330	+453	5.0	+1.6	.5
212	G.3	T-8	-1	6259	6004	8.2	296	-277	4.1	+6.6	.6
1191	6.11	T-6	-1	6278	5458	26.0	575	- 38	9.6	-2.8	.6
1191	G.4	T-8	-1	6277	5611	25.6	302	-532	8.9	+4.3	.8

Table 6.9: Monte-Carlo Study Results for Linearized LR Weighting Functions

Error Vector Number	Fig. No.	Terrain Model	DPS Accel. Uncert. %	ΔV (f/s)	Max.Thrust 10-60% region (lbs)	Max.Thrust Vector Deviations during Braking Phase		High-Gate Point Errors		Low-Gate Point Errors	
						El. Angle (deg)	Thrust (lbs)	Alt. (ft)	Vel. (f/s)	Alt. (ft)	Vel. (f/s)
212	H.1	T-6	+1	6306	6030	8.5	507	+435	4.5	+4.0	.6
212	6.26	T-8	+1	6307	5848	5.2	229	-331	1.4	-1.0	.3
1191	6.27	T-6	+1	6311	5837	12.2	538	+296	4.1	-4.6	.3
1191	H.2	T-8	+1	6309	5561	6.9	278	-149	5.3	+5.6	1.0
212	H.3	T-6	-1	6258	5863	9.0	440	+442	4.6	+1.9	.4
212	H.4	T-8	-1	6252	5514	5.7	132	-289	4.2	- .34	.5
1191	H.5	T-6	-1	6266	5475	12.1	356	+266	2.7	+ .98	.9
1191	H.6	T-8	-1	6264	5467	14.4	396	-139	1.4	-5.2	.5

6) From an examination of the thrust-vector profiles with constant-weighting functions of 0.1, it is apparent that the updating process and the correction of the vehicle's trajectory are accomplished at a relatively slow rate. This can be seen from the relatively smooth, noise-free, long-period characteristics of the elevation angle, as indicated in Figs. 6.22 and 6.23. In some of the runs made with these LR weighting functions, the vehicle actually hit the surface of moon with a significant impact velocity.

7) The original uncoupled weighting functions (set W-5) tend to produce thrust-vector profiles that are somewhat noisier than those for the other weighting functions considered. The high-frequency trajectory deviations are noticeable in the visibility phase as well as in the braking phase, as can be seen in Figs. 6.24 and 6.25.

8) The best choice of weighting functions of those considered appears to be the linearized set (W-11). These weighting functions are the simplest to mechanize in the computer, and in the Monte-Carlo runs did not give performance results significantly different from the optimum uncoupled (W-9). Data for these weighting functions are given in Figs. 6.26 and 6.27 for the same initial-error vectors, DPS uncertainties, and terrain models as in Figs. 6.22 through 6.25.

6.8 Effect of Initial Altitude Errors on System Performance

Under certain conditions it is possible that extremely large deviations may occur in the altitude of the vehicle at the start of the landing. Insofar as the landing guidance problem is concerned, the important altitude of interest is that of the vehicle with respect to the selected landing site. At the start of the landing maneuver this altitude difference is about 50,300 feet under ideal conditions.

In the event that the estimated altitude of the vehicle relative to the moon is not updated by CSM optical tracking measurements to the desired landing site prior to ejection of the vehicle from the 80-mile parking orbit, significant initial altitude errors may result. Terrain-slope variations may also contribute to this relative altitude error.

Initial altitude deviations can adversely affect PGNCS performance in any of three different ways.

1) The required ΔV is increased, as shown in Fig. 6.28. No initial errors other than altitude, no DPS uncertainties, and no terrain variations are included in these data.

2) Significant deviations in thrust-vector elevation angle may be required to correct the altitude deviations during the braking phase. This can be seen from the data of Figs. 6.29 through 6.30 where the deviations in

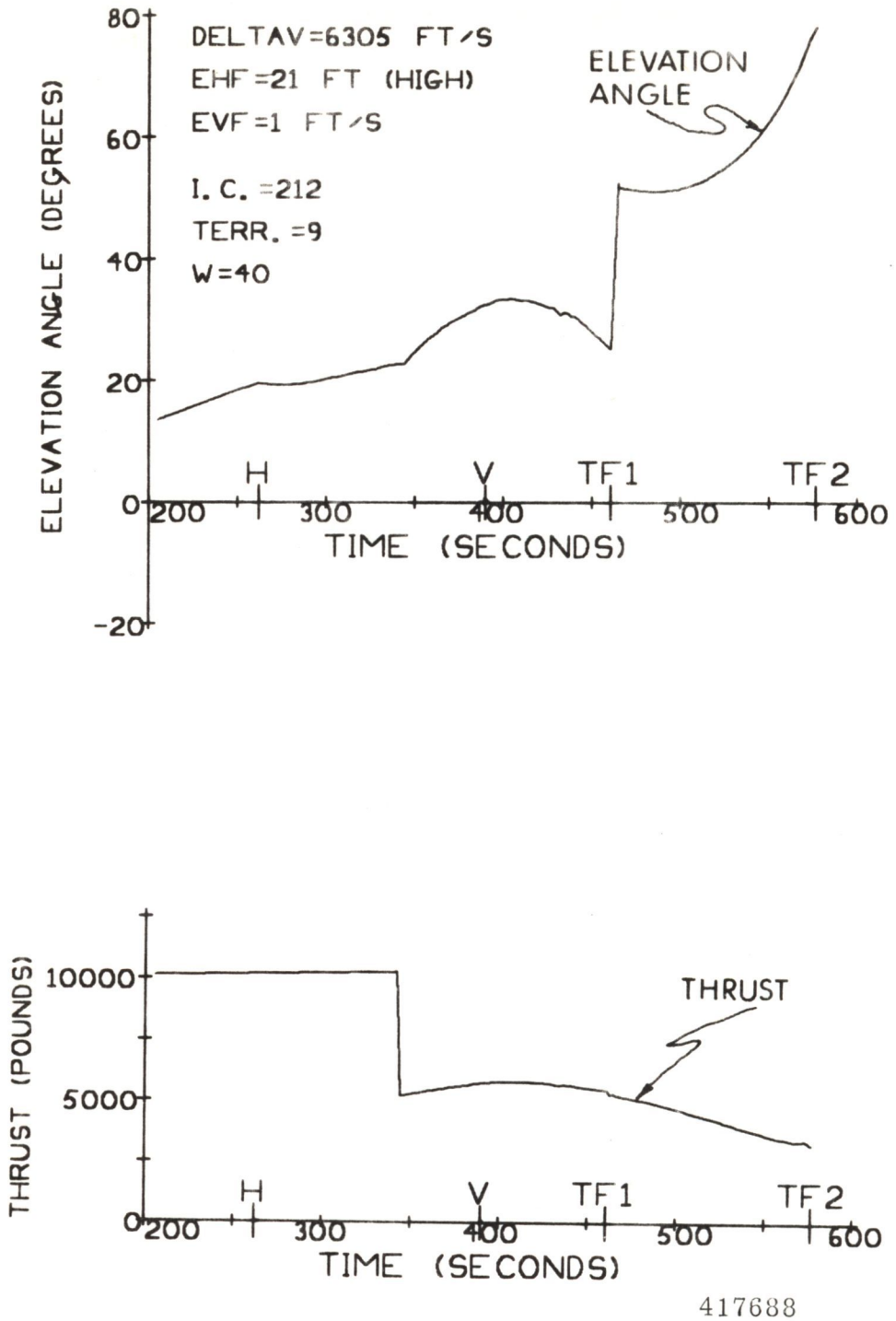

Fig. 6.22 Thrust-Vector Profiles: Constant Weighting Functions of .1. (See Table 6.6)

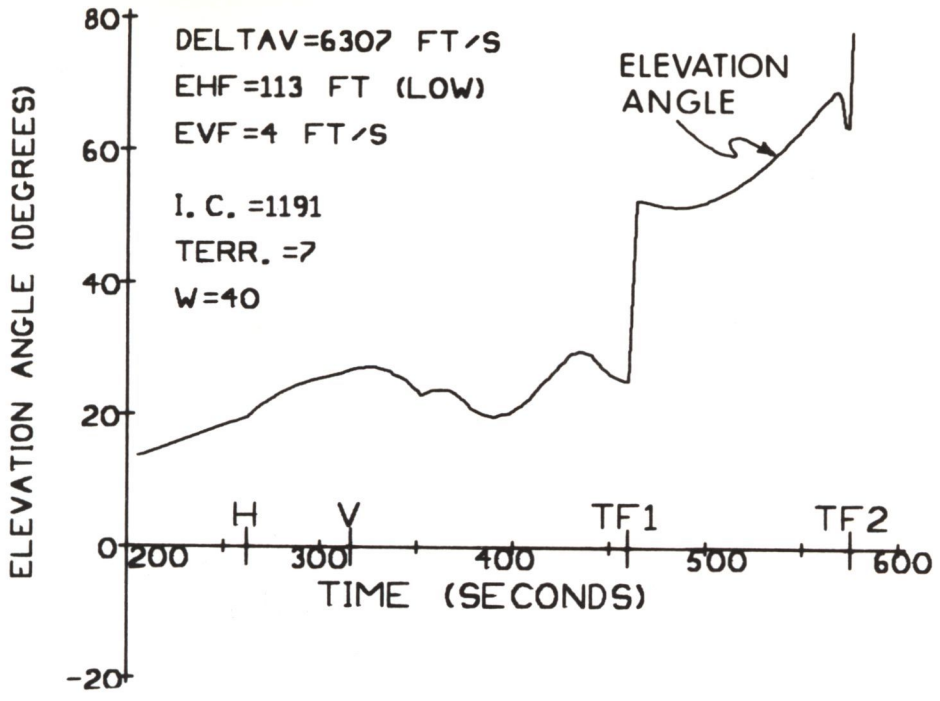

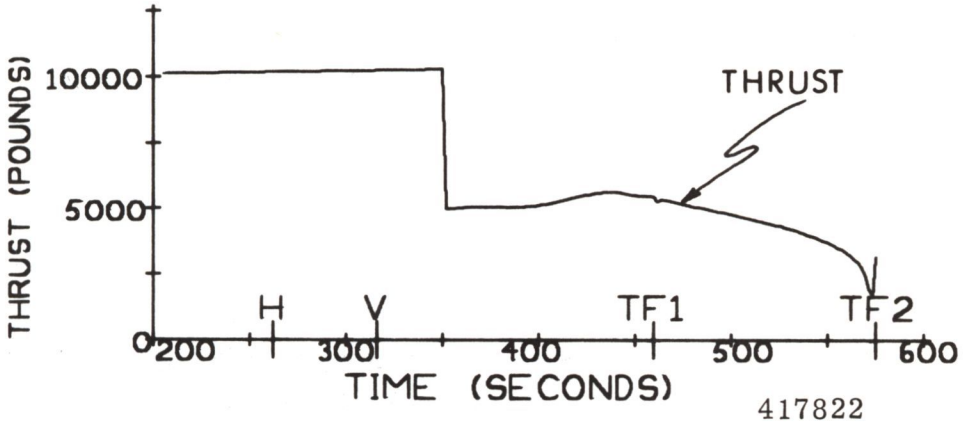

Fig. 6.23 Thrust-Vector Profiles: Constant Weighting Functions of .1. (See Table 6.6)

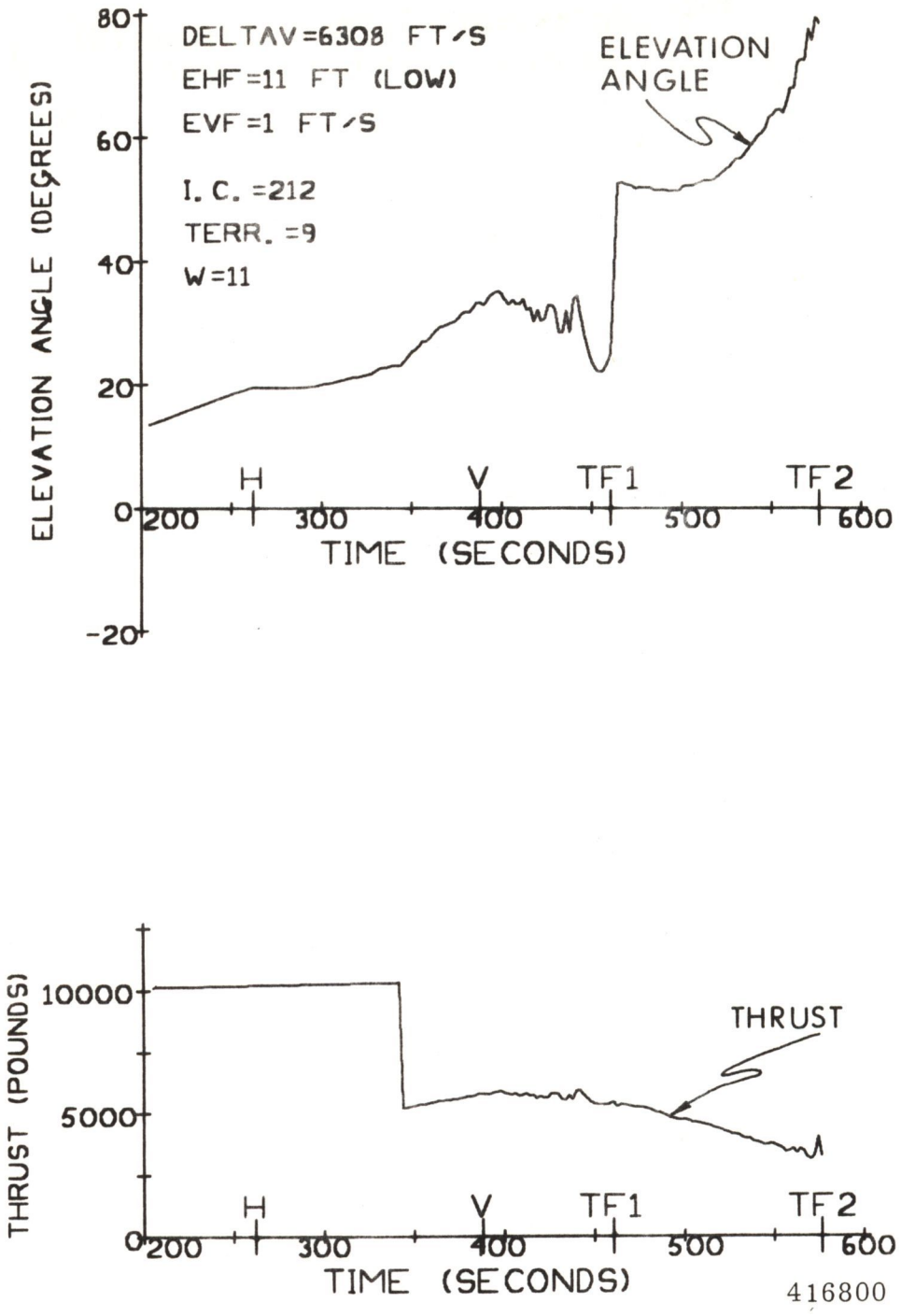

Fig. 6.24 Thrust-Vector Profiles: Original Uncoupled Weighting Functions. (See Table 6.5)

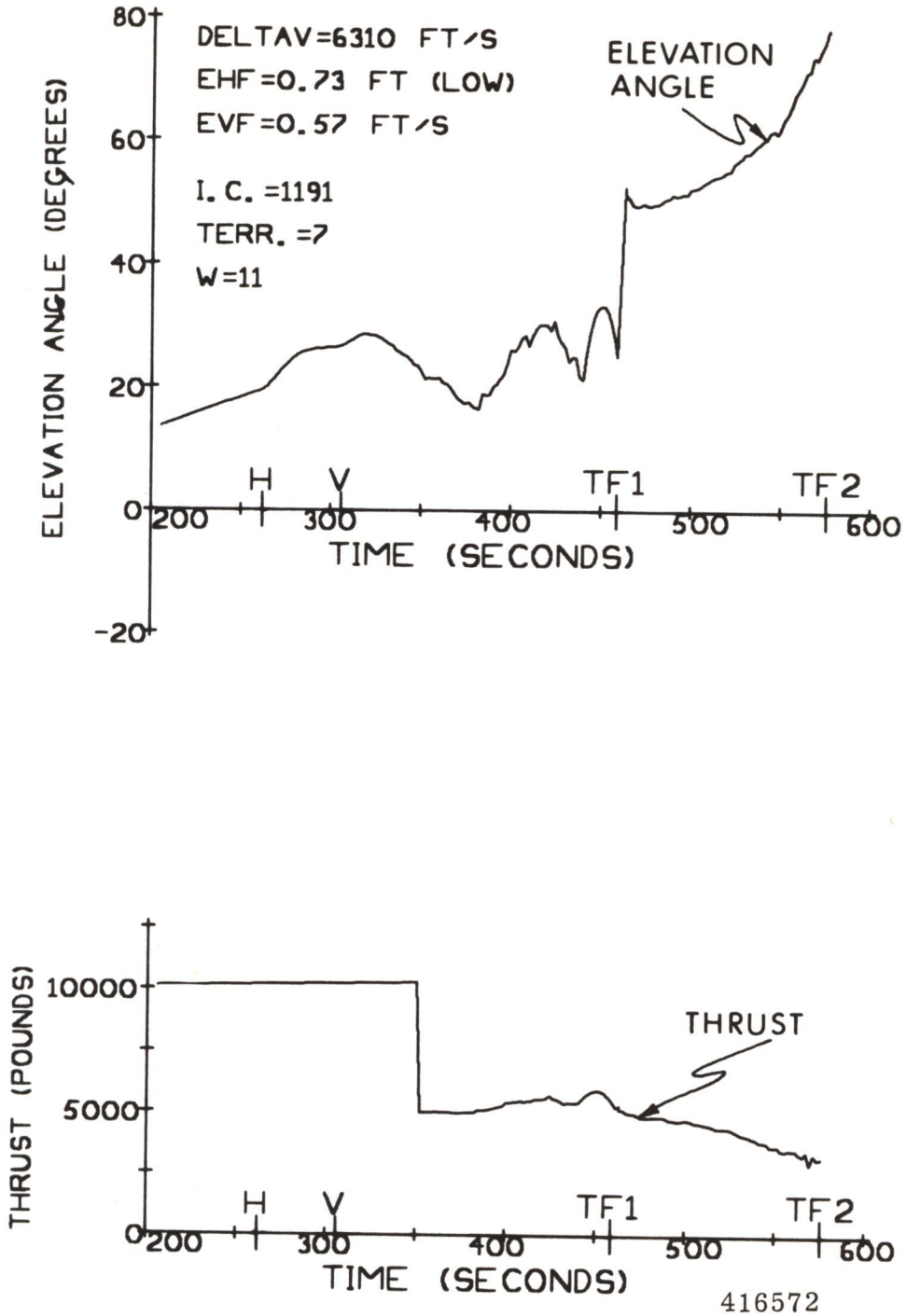

Fig. 6.25 Thrust-Vector Profiles: Original Uncoupled Weighting Functions. (See Table 6.5)

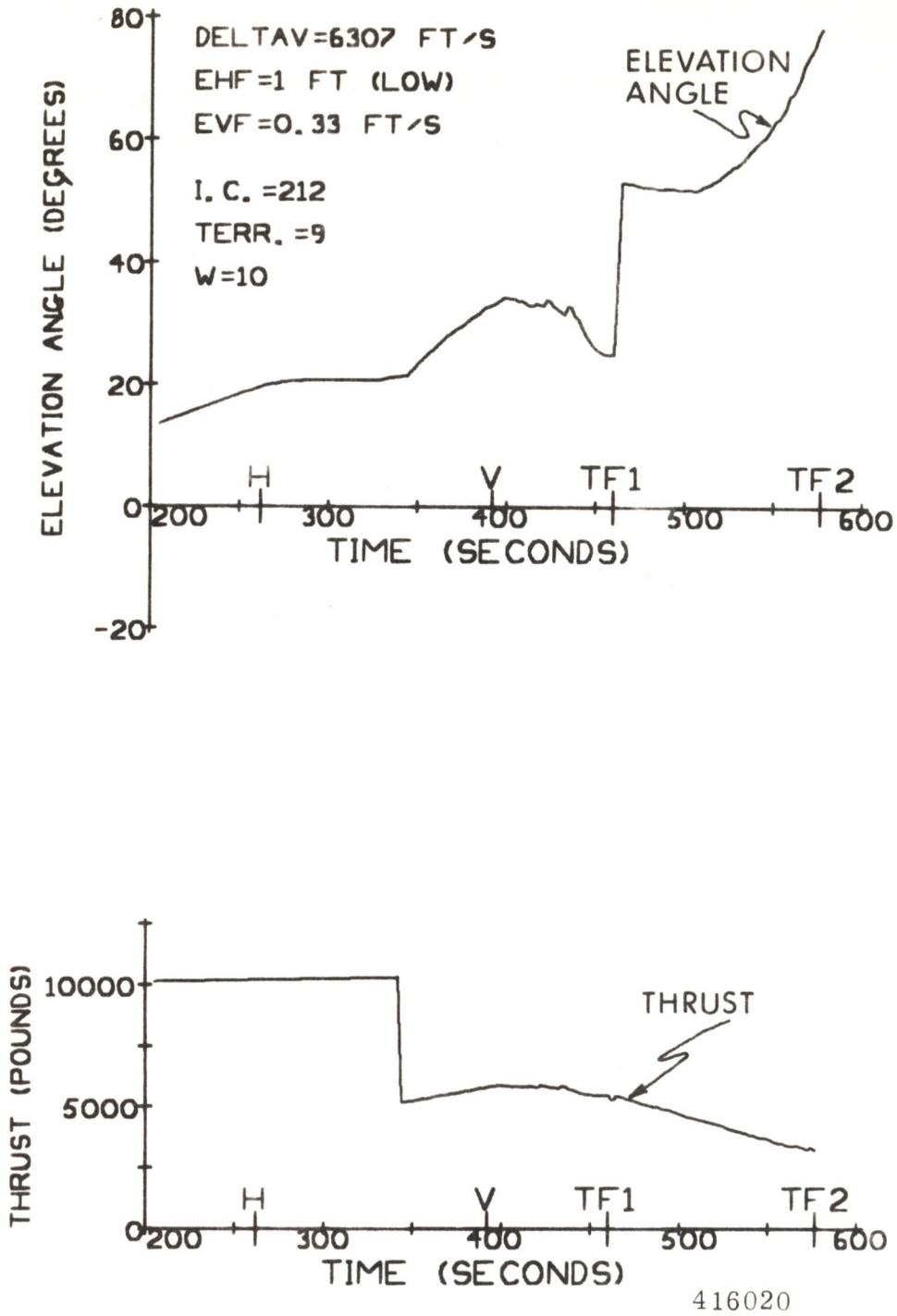

Fig. 6.26 Thrust-Vector Profiles: Linear Uncoupled Weighting Functions. (See Table 6.9)

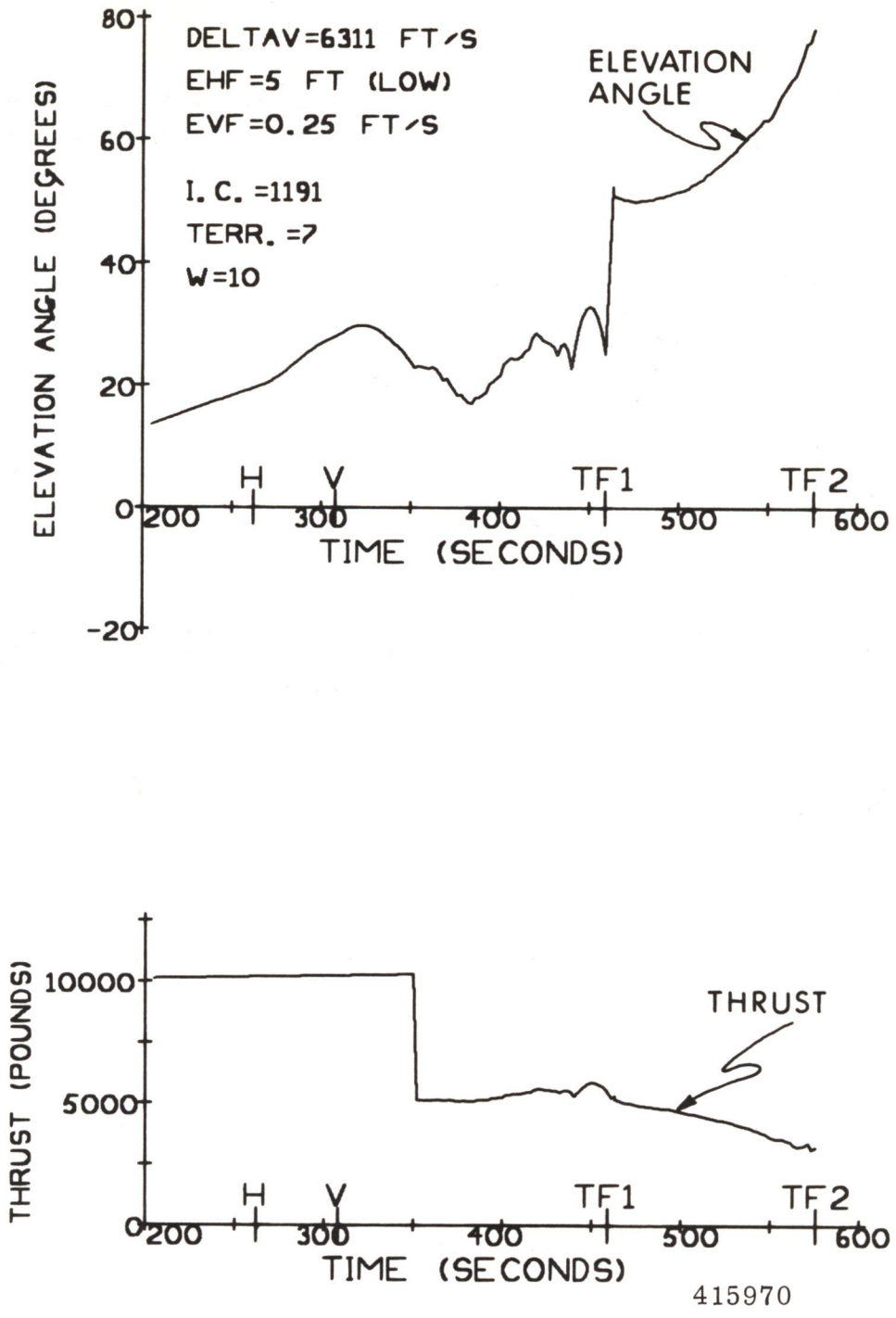

Fig. 6.27 Thrust-Vector Profiles: Linear Uncoupled Weighting Functions. (See Table 6.9)

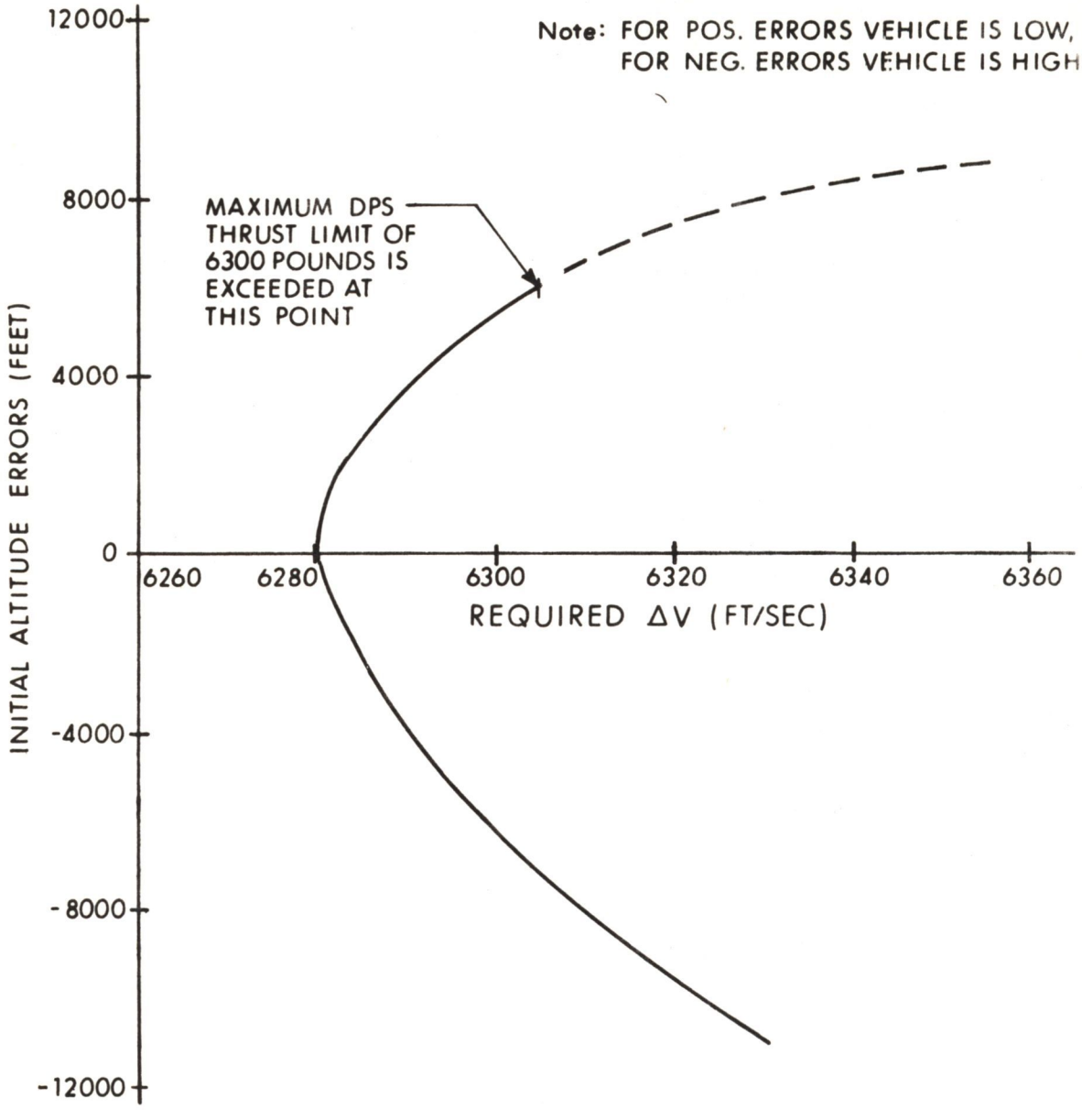

Fig. 6.28 Effect of Initial Altitude Errors on Required ΔV.

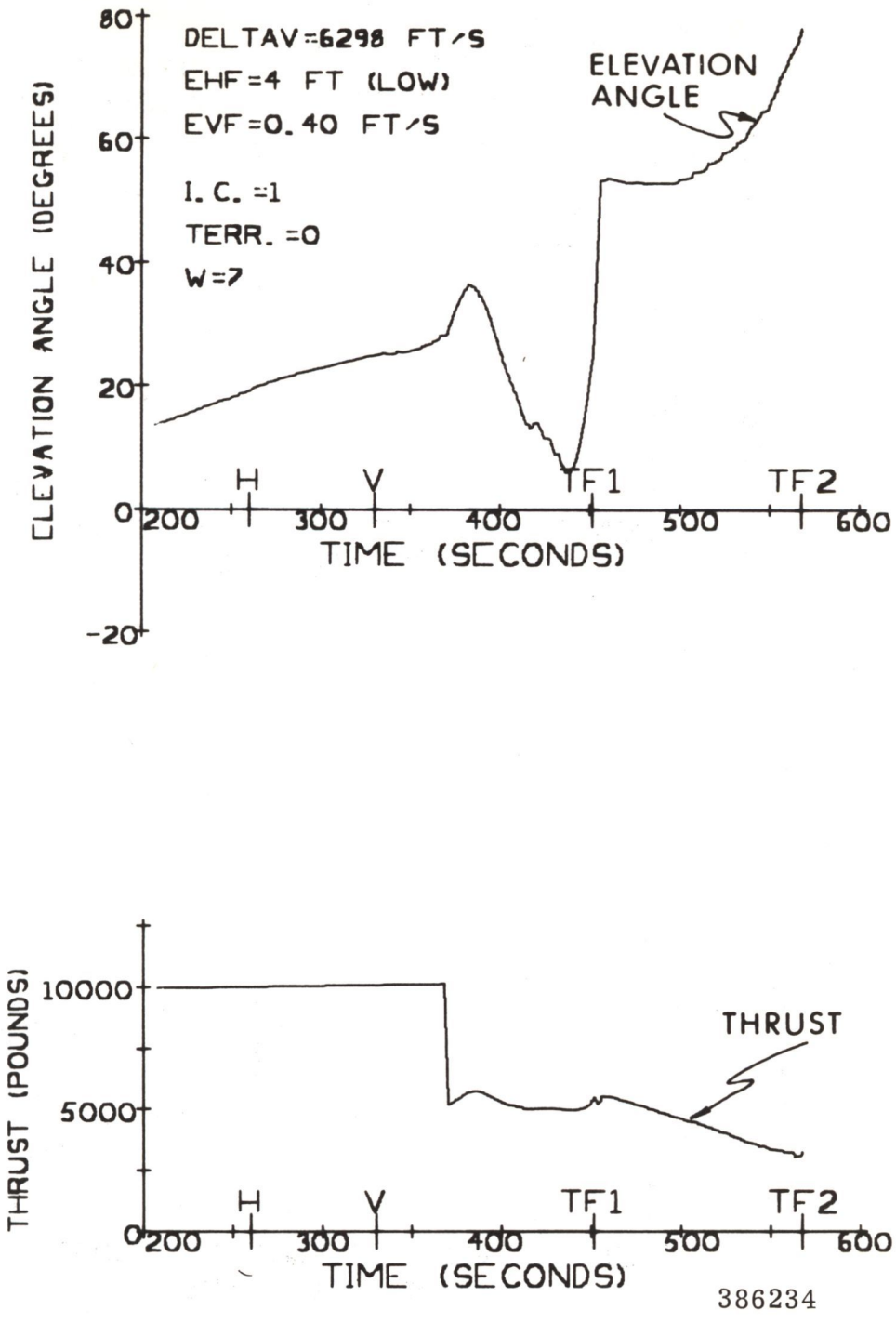

Fig. 6.29 Thrust-Vector Profiles: Initial Altitude Error of +6000 Feet. (+ Altitude Error = LEM low Initially)

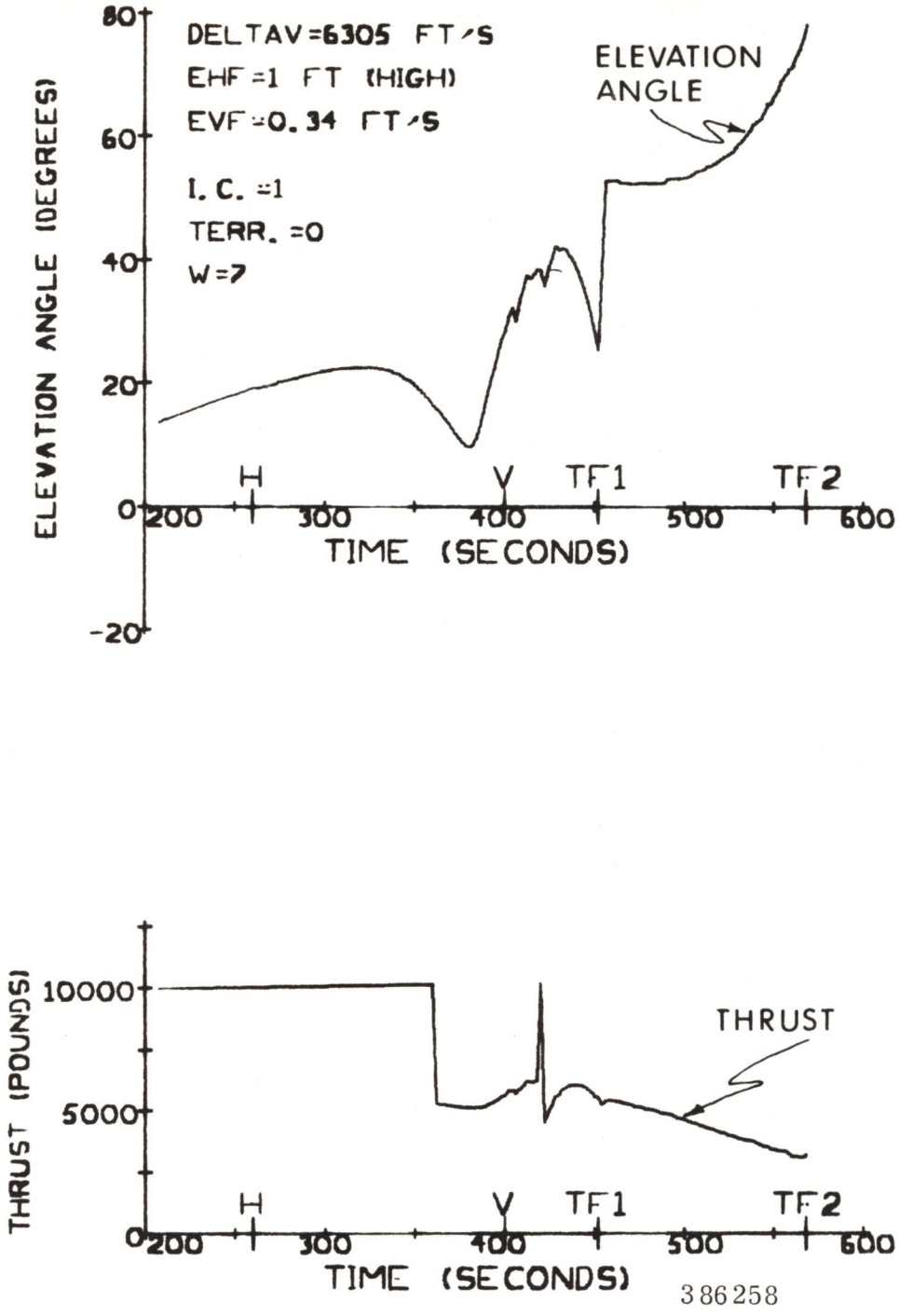

Fig. 6.30 Thrust-Vector Profiles: Initial Altitude Error of -6000 Feet. (←Altitude Error = LEM High Initially)

altitude are 6000 feet low and high respectively. It is interesting to note that when the vehicle is low, the thrust vector will experience a positive (upward) deviation in elevation angle followed by a negative (downward) deviation, as shown in Fig. 6.29. When the vehicle is high, on the other hand, the order of the elevation-angle deviations is reserved, as shown in in Fig. 6.30.

3) The maximum permissible thrust value for the throttleable region (6300 pounds) may be exceeded when the initial-altitude errors are large, as indicated in Fig. 6.30. In the case shown in Fig. 6.30, the throttle was switched to the 92.5-percent position when the command thrust exceeded 6300 pounds. It was then held in this position until the command thrust was below 5460 pounds. This throttle-switching procedure is not recommended for actual operation of the DPS.

6.9 Effect of Errors in Assumed Radar-Parameter Values

The LR weighting functions have been developed under the assumption that the navigation sensors were modeled as described in Chapter 4. The performance numbers assumed for the LR have been given in Table 5.1. An investigation has been made of the effects of errors in these performance numbers, i.e. the actual rms errors are different from the assumed numbers. This section presents the important results of this study.

Consider first of all the case where the random errors in the LR altitude and velocity measurements are larger than their normal assumed values. Under these conditions the rms values of the altitude and velocity errors during the landing maneuver will vary as shown in Fig. 6.31. The LR measurements are assumed to update the PGNCS here according to the schedule of Fig. 2.2, using the uncoupled linear weighting functions (set W-11 of Table 4.2). Data are presented for two different cases in Fig. 6.31: 1) the actual LR parameters have the values assumed in Table 5.1, and 2) the rms values of the actual random LR errors are 3 times larger than their values in Table 5.1 (all other errors as in Table 5.1).

From the data of Fig. 6.31 it can be seen that an increase by a factor of 3 in the rms LR random errors does not significantly affect the rms altitude errors. The predominant source of error here is the variation in the altitude of the lunar terrain. In regard to the velocity-estimate errors, on the other hand, there is a significant increase in the rms error as a result of the increased magnitude of the random measurement errors. This is particularly important during the latter part of the landing maneuver.

Two typical Monte-Carlo runs, for the conditions where the rms random LR errors are 3 times their assumed values in Table 5.1, are shown in Figs. 6.32 and 6.33. As can be seen, the random deviations in both elevation angle and thrust

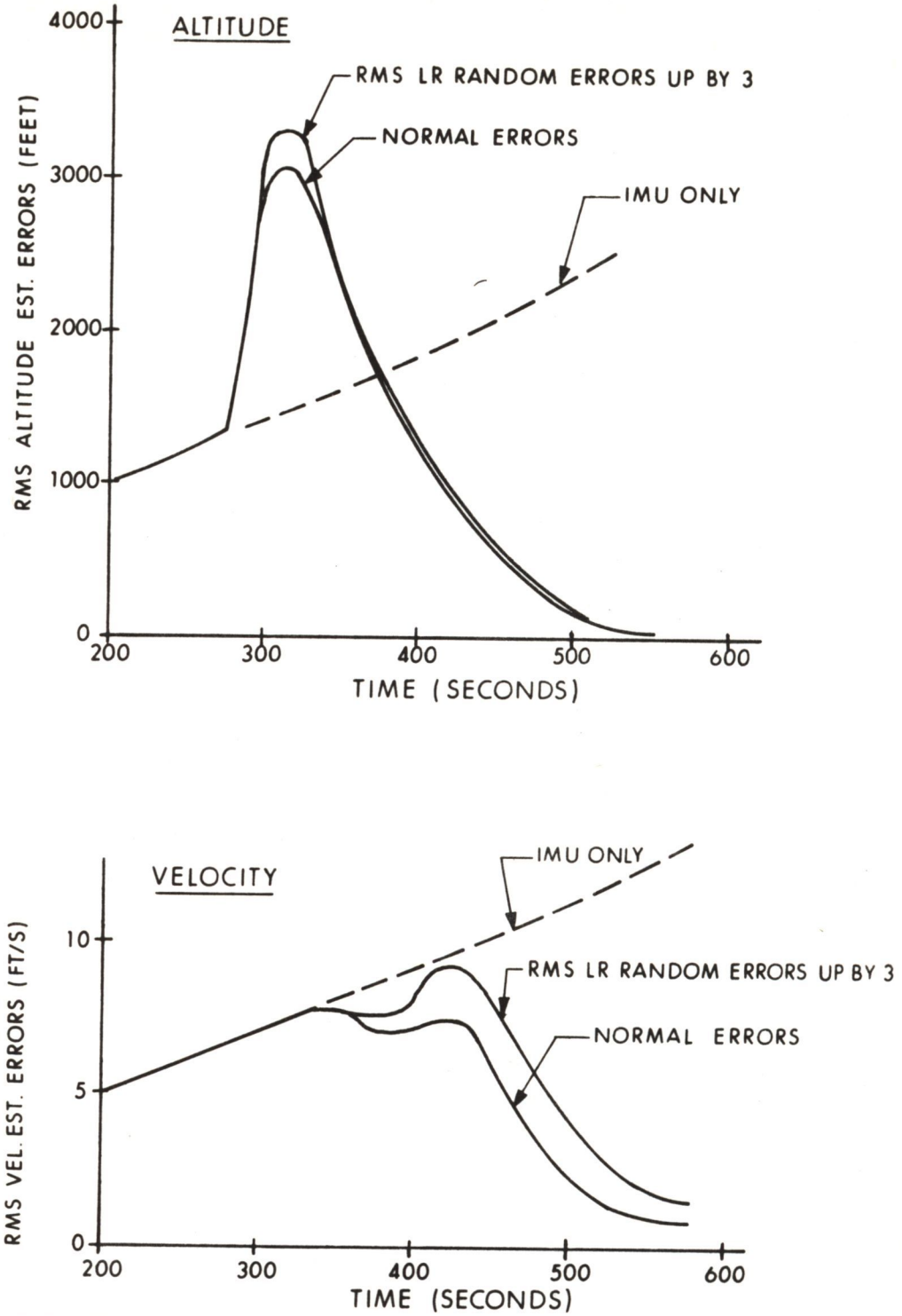

Fig. 6.31 Effect of LR Parameter Errors on Navigation System Accuracy.

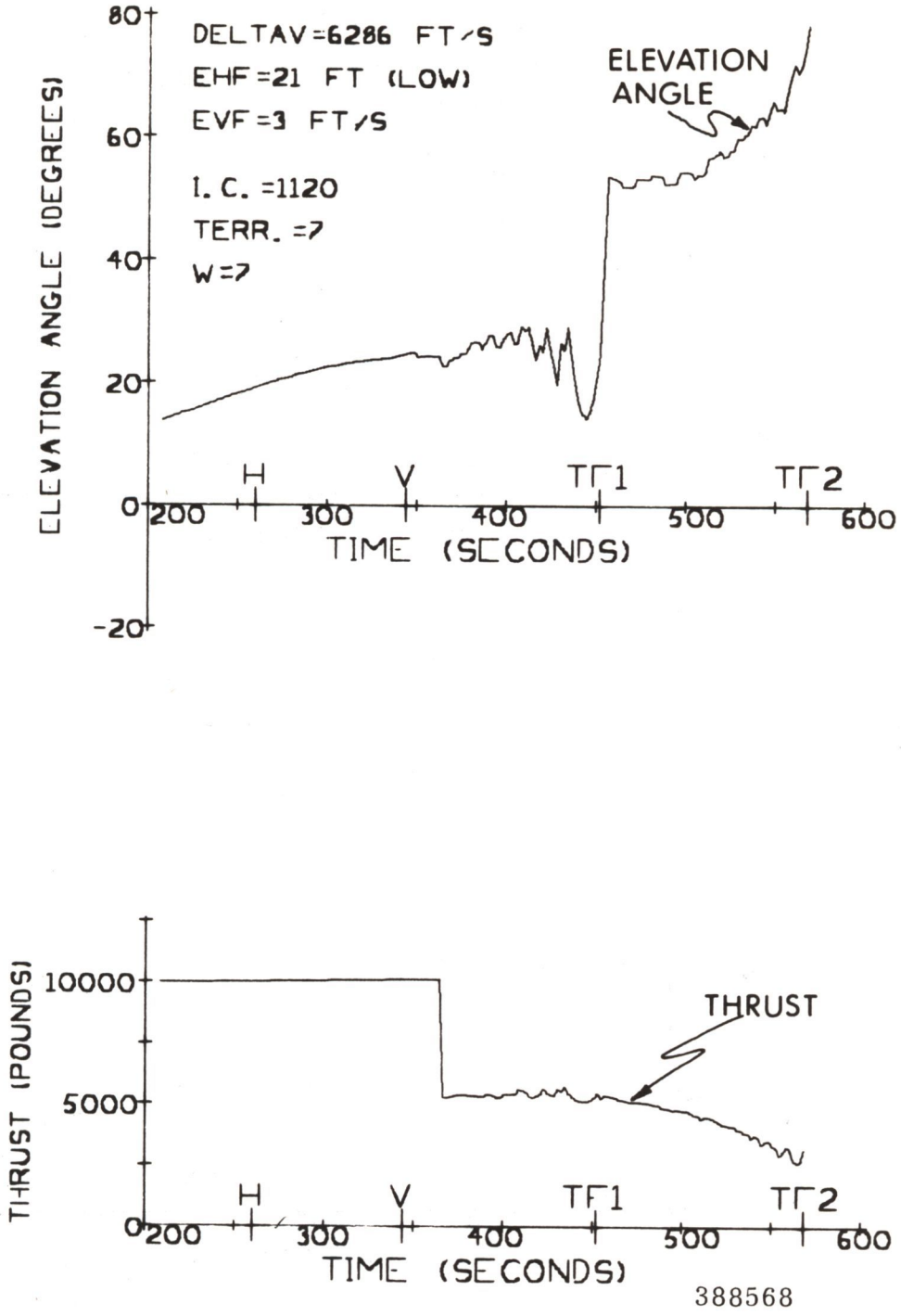

Fig. 6.32 Thrust-Vector Profiles: RMS Random LR Errors Up by Factor of 3.

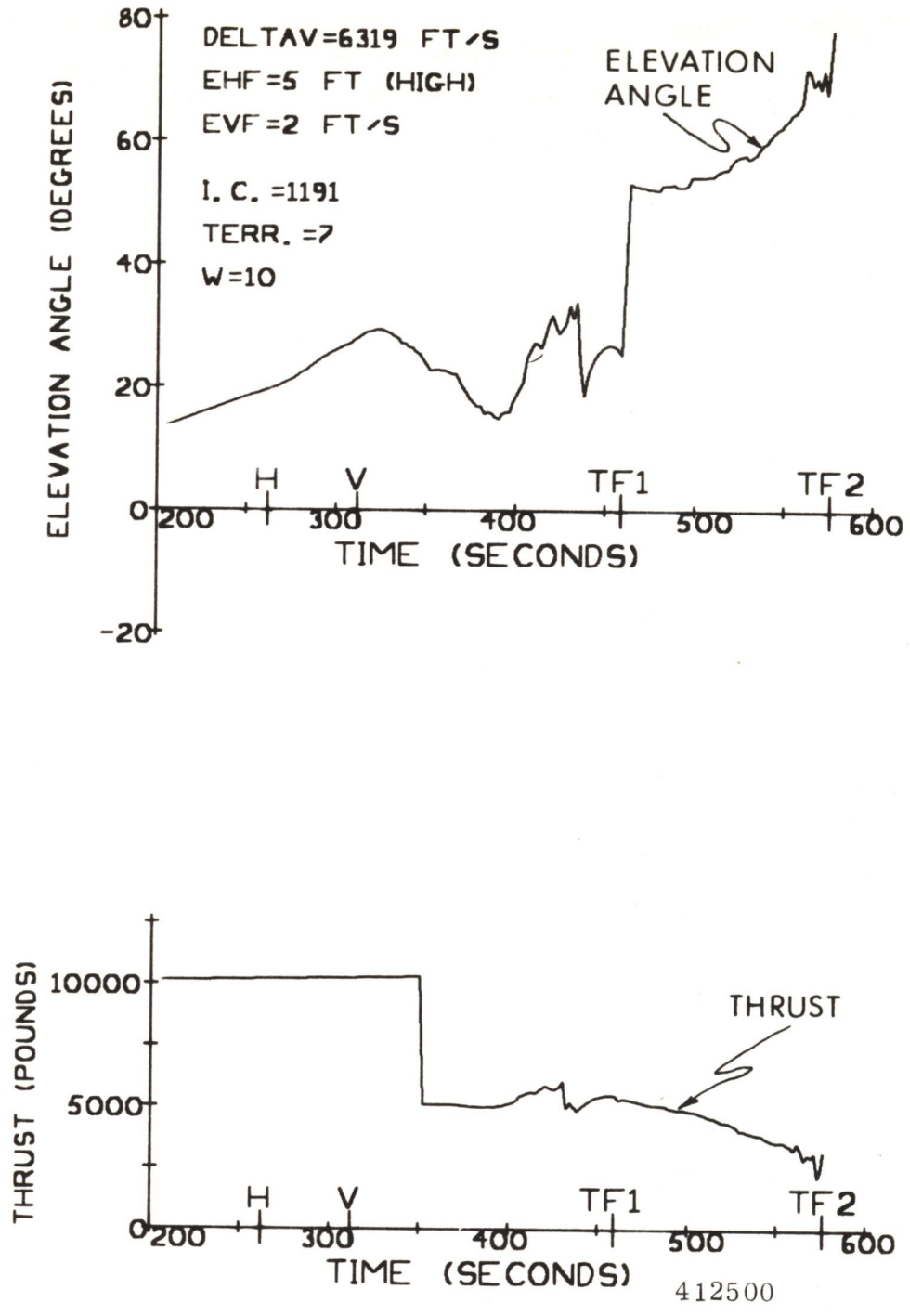

Fig. 6.33 Thrust-Vector Profiles: RMS Random LR Errors Up by Factor of 3.

magnitude are greater than under normal conditions. This is particularly noticeable during the visibility phase. Also, the Low-Gate-point velocity errors in both of these runs are larger than the normally-expected errors of less than 1 ft/sec. It is important to note that the major objective of the landing-radar weighting-function development was to provide relatively small commanded thrust-attitude deviations during the visibility phase of the landing maneuver. Figures 6.32 and 6.33 illustrate the need for accurate LR performance data to achieve this objective such that the LPD can be used effectively.

The effect of errors in the assumed rms value of the LR velocity-bias errors, i.e. the orientation of the LR-antenna axes with respect to the inertial-reference axes, is shown in Fig. 6.34. The rms velocity errors in this case, as can be seen, are quite sensitive to errors in the assumed rms orientation uncertainty of the LR. From these data it is evident that the orientation-uncertainty bias error is a major source of navigation-system error and must be properly considered in the derivation of LR weighting functions. In the event that the rms error is not well known, it is best to estimate a high value rather than a low one for this error in the development of LR weighting functions. This will tend to limit the maximum rms errors during the landing maneuver.

6.10 Effect of Increasing High-Gate Altitude

In earlier studies of the landing maneuver it was suggested that the High-Gate-point altitude be raised to about 9200 feet. This section presents data to show the effect on system performance of increasing the High-Gate altitude. The same visibility requirements are assumed here as in the 6600-foot High-Gate data presented elsewhere in this report. The basic reference trajectory used here is designed to throttle-down the DPS at 80 seconds before the end of the braking phase. Also, the DPS is switched to the continuously-throttleable operating region (10-60 percent of nominal thrust) when the command thrust is less than 52 percent of nominal thrust.

The important results of the study are summarized in Table 6.10. The linearized weighting functions (set W-11 of Table 4.2) are used in all these data. The particular initial errors used in the data of Table 6.10 represent extremely severe initial errors, both in vehicle altitude and vertical velocity. A typical set of thrust-vector profiles for the 9200-foot High-Gate point are shown in Fig. 6.35.

There are two important points to be seen from the data of Table 6.10.

1) The required ΔV with the 9200-foot High-Gate altitude is about 40 ft/sec higher than for the 6600-foot High-Gate point. This can be seen by comparing the data in Tables 6.9 and 6.10. This increase in ΔV is to be expected since the vehicle is operating at lower thrust (10-60 percent region) for a greater part of the landing maneuver.

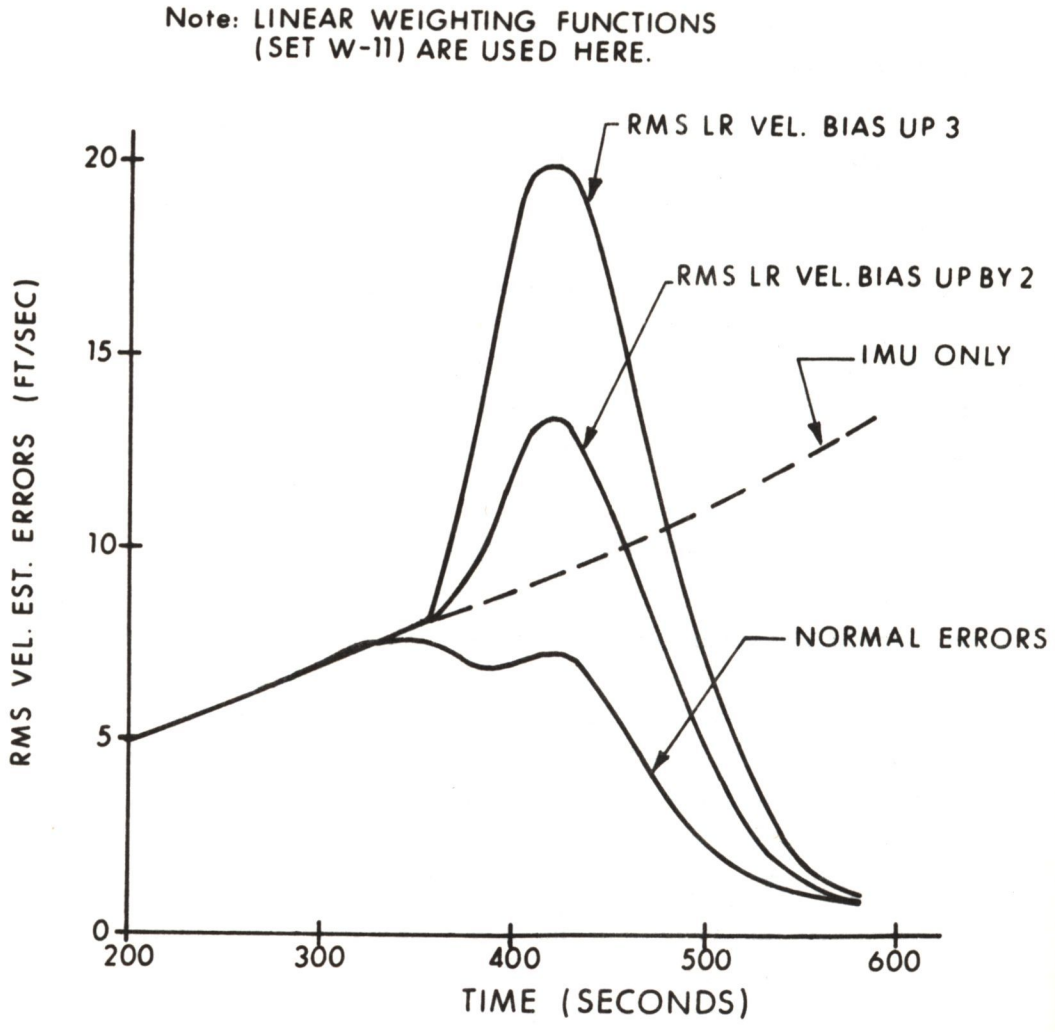

Fig. 6.34 Effect of LR Parameter Errors on Navigation-System Accuracy

Table 6.10: Monte-Carlo Data for 9200-foot High-Gate Altitude with LR Weighting Functions W-11

Error Vector Number	Fig. No.	Terrain Model	DPS Accel. Uncert. %	ΔV (f/s)	Max. Thrust 10-60 % region (pounds)	High-Gate Point Errors		Low-Gate Point Errors	
						Alt.(ft)	Vel.(f/s)	Alt.(ft)	Vel.(f/s)
212	I.1	T-6	+1	—	* 6300	—	—	—	—
212	I.2	T-8	+1	6343	6298	-477	4.4	-1.7	.42
1191	I.3	T-6	+1	6352	5806	+ 99	7.3	-4.5	.60
1191	6.35	T-8	+1	6345	5637	-690	7.5	+1.9	.70
212	I.4	T-6	-1	—	* 6300	—	—	—	—
212	I.5	T-8	-1	6299	5931	-477	2.4	+2.5	.42
1191	I.6	T-6	-1	6323	5546	+ 81	8.1	- .9	.55
1191	I.7	T-8	-1	6307	5695	-770	9.1	-4.0	.86

* Maximum thrust level of 6300 pounds in throttleable region was violated in this run.

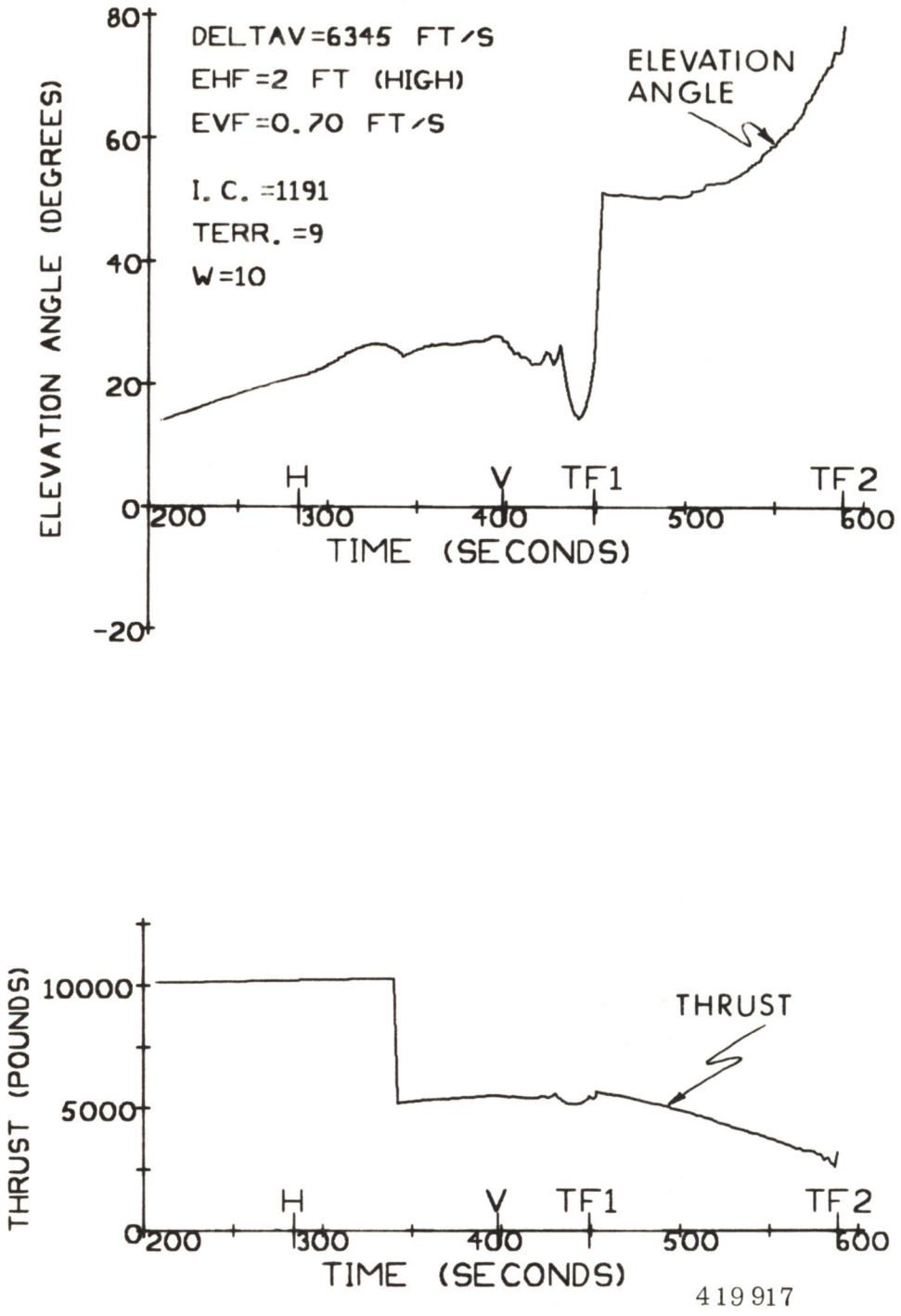

Fig. 6.35 Thrust-Vector Profiles: 9200-Foot High-Gate Altitude. (See Table 6.10)

2) The maximum permissible thrust level of 6300 pounds for the throttleable region is violated on certain severe initial-condition trajectories. This problem can be corrected by adjusting the thrust level at which the DPS is throttled down, and also the final braking-phase thrust level. The required ΔV will be increased by these changes.

6.11 Interruption of LR Measurements

6.11.1 Introduction

Under certain conditions it is possible that good LR measurements may not be available to the PGNCS throughout the landing maneuver. This section presents the results of a study on PGNCS performance of the effects of interrupting various combinations of LR measurements at different times during the landing maneuver.

In the first subsection the case will be considered where no LR measurements at all are provided during the braking phase. Then, in the next two subsections, data will be presented first for the situation where no LR velocity measurements are used in the braking phase, and next for the case where no LR altitude data are used. In the final subsection, the situation is investigated wherein LR measurements are interrupted whenever any LR velocity beam is within ± 5 degrees of the plane normal to the vehicle's velocity vector. This is intended to represent the zero-doppler situation.

The results to be presented are primarily from Monte-Carlo runs using the optimum uncoupled weighting functions (W-9) and the linearized weighting functions (W-11). The normal LR updating schedule is as shown in Fig. 2.2. The sensor performance characteristics are as given in Table 5.1.

6.11.2 No LR Measurements in Braking Phase

A series of Monte-Carlo runs were made to investigate PGNCS performance under the conditions that no LR measurements were processed during the braking phase. The weighting functions used in the runs were the linearized set W-11. Several different combinations of initial-error vectors, terrain models, and DPS uncertainties were used. These are indicated in Table 6.11. The maximum permissible DPS thrust in the continuously-throttleable region was taken as 6300 pounds. Whenever this limit was reached in a given run after the initial throttling-down, the run was automatically terminated.

The key results from the series of Monte-Carlo runs are presented in Table 6.11. The important points to be seen from these data are the following.

1) In the absence of LR measurements during the braking phase, High-Gate-point altitude errors as large as 6000 feet may occur when severe initial-condition errors are present.

Table 6.11: No LR Measurements at all in Braking Phase

Error Vector Number	Terrain Model	DPS Accel. Uncert. %	ΔV (f/s)	Max. Thrust 10-60% region (pounds)	High-Gate Errors		Low-Gate Errors		Error-Vector Prob. Ellipsoid %
					Alt. (ft)	Vel. (f/s)	Alt. (ft)	Vel. (f/s)	
1191	6	+1	—	* 6300	—	—	—	—	99.4
1191	8	+1	—	* 6300	—	—	—	—	99.4
212	6	+1	6317	5598	+5346	12.2	-4.0	.7	99.6
212	8	+1	6317	5598	+5346	12.2	-3.7	.5	99.6
739	6	0	—	* 6300	—	—	—	—	69.2
887	6	0	—	* 6300	—	—	—	—	99.7
1597	6	0	6281	5523	+221	4.5	3.0	.9	94.1
862	6	0	—	* 6300	—	—	—	—	97.2
616	8	+1	—	* 6300	—	—	—	—	80.3
223	8	+1	—	* 6300	—	—	—	—	79.9
-786	8	0	—	* 6300	—	—	—	—	80.0

* Maximum thrust level of 6300 pounds in throttleable region was violated.

2) Under conditions where the High-Gate-altitude errors are positive, i.e. the vehicle passes over the High-Gate point, the vehicle will get to the Low-Gate point without hitting the lunar surface and without requiring a thrust magnitude in excess of 6300 pounds. The landing-site visibility during the early part of the visibility phase will suffer in this case, because of the lower thrust-vector elevation angles required in this interval to meet Low-Gate conditions.

3) Under conditions where the High-Gate-altitude errors are negative, on the other hand, i.e. the vehicle passes below the High-Gate point, the effects are quite different from the cases with positive altitude errors. In the runs where the errors were large, the required DPS thrust exceeded the maximum-permissible value of 6300 pounds early in the visibility phase, and the runs were terminated unsuccessfully. The particular runs referred to here are where the High-Gate-altitude errors vary between 3000 and 6000 feet.

A typical case where the High-Gate-altitude error was negative, i.e. the vehicle was high, is shown in Fig. 6.36. As should be expected, the thrust-vector profile is very smooth during the braking phase because no LR updatings are made here. The important point to be seen from Fig 6.36 is that during the early part of the visibility phase, the elevation angle is significantly smaller than for the error-free reference run (Fig. 6.15). As a result of this, the astronaut's visibility of the landing sight will be greatly degraded, and the interval of visibility will be reduced.

A case where the High-Gate-altitude error was negative, i.e. the vehicle was low, is shown in Fig. 6.37. In this particular case, as can be seen, the command thrust exceeded the maximum permissible value of 6300 pounds early in the visibility phase. When this occured in the simulation run, the throttle was switched to the 92.5-percent position and held there until the command thrust was below 52 percent of the nominal thrust (5460 pounds). This procedure is not recommended for actual operation of the PGNCS.

In concluding this section it should be noted that the cases illustrated in Figs. 6.36 and 6.37 represent cases with very severe initial-condition errors and large High-Gate-altitude errors. In certain cases where the combination of initial-condition errors and terrain variations lead to relatively small High-Gate-altitude errors, the PGNCS will perform reasonably well with no LR measurements during the braking phase. An example of such a case is shown in Fig. 6.38, but it should be noted that even in this case the resulting angle deviations may make effective LPD operation questionable.

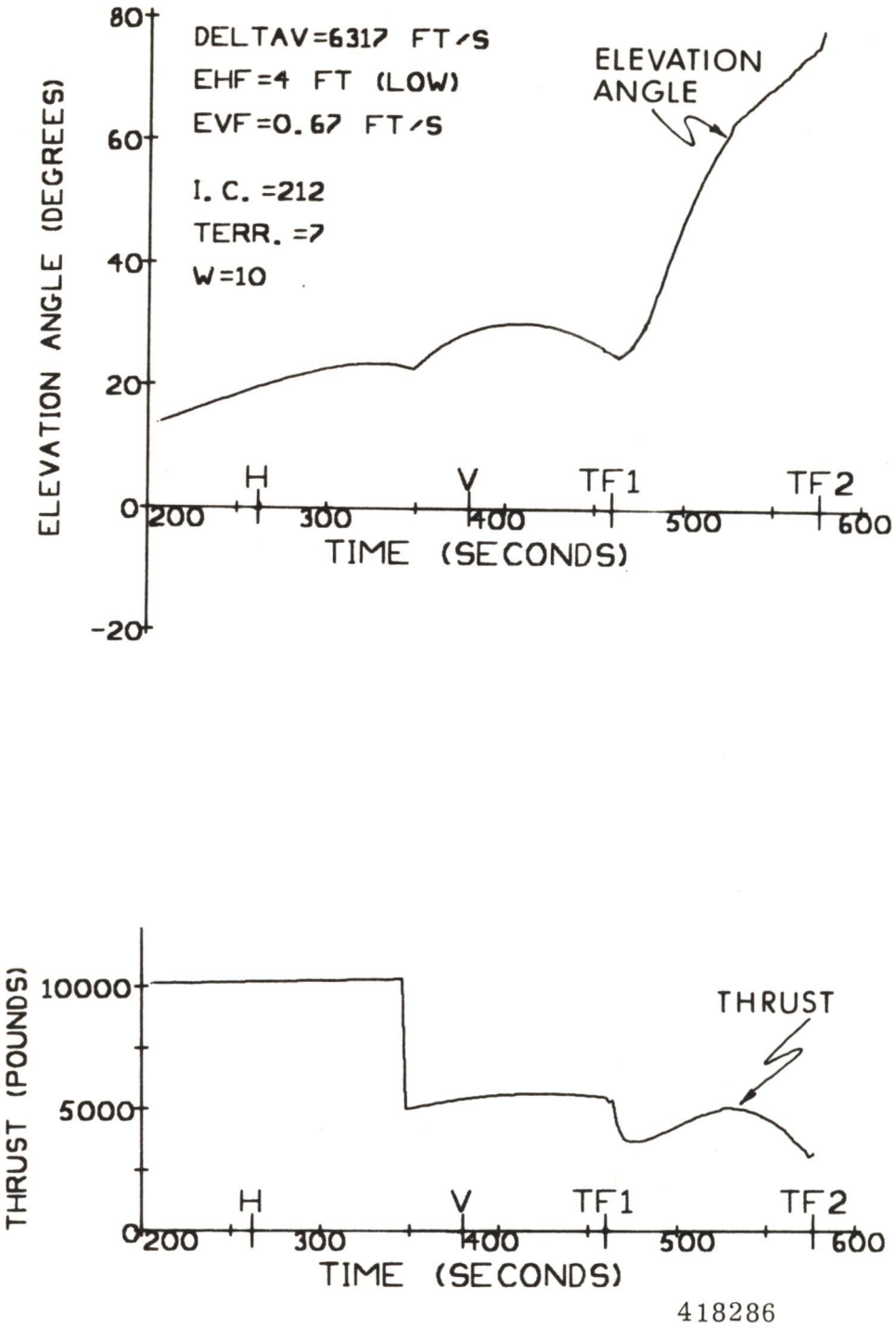

Fig. 6.36 Thrust-Vector Profiles: No LR Measurements in Braking Phase.

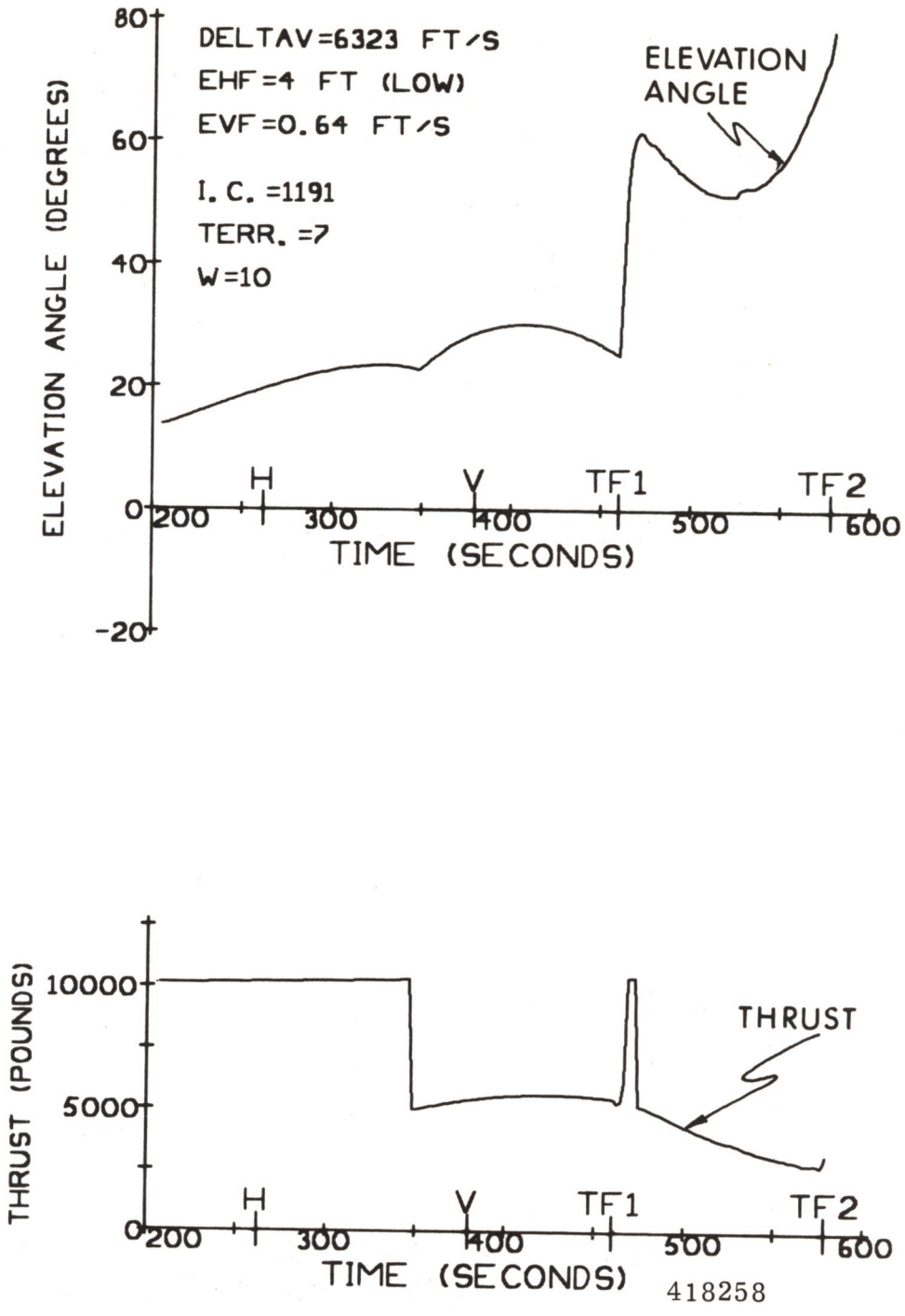

Fig. 6.37 Thrust-Vector Profiles: No LR Measurements in Braking Phase.

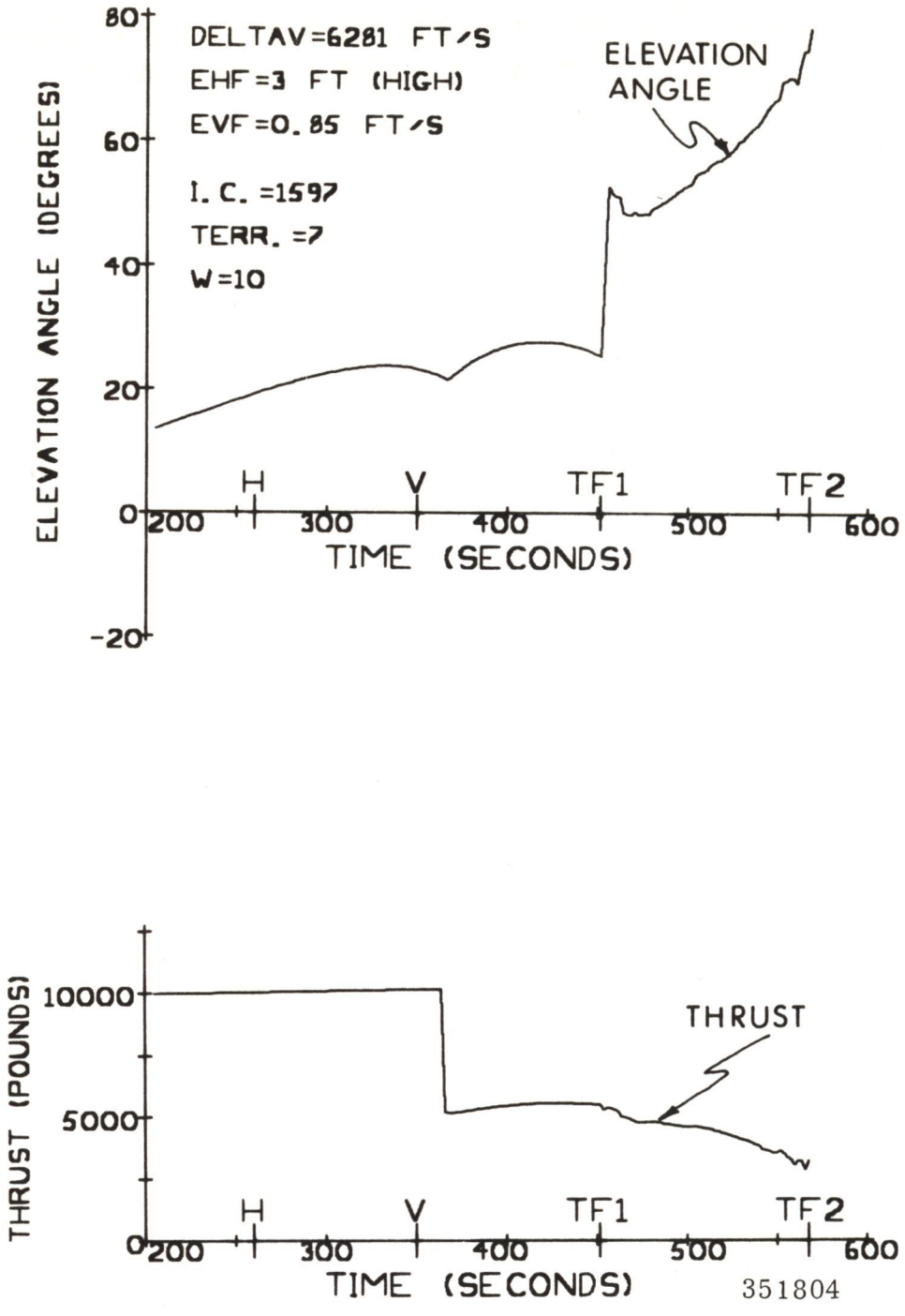

Fig. 6.38 Thrust-Vector Profiles: No LR Measurements in Braking Phase.

6.11.3 No LR Velocity Measurement Used during Braking Phase

A series of Monte-Carlo runs were made for the conditions where no LR velocity measurements were used during the braking phase. Only LR altitude measurements were used during this interval. The same combinations of initial-error vectors, terrain models, and DPS uncertainties, that led to unsatisfactory PGNCS performance when no LR measurements were taken during the braking phase, were investigated here.

The important results from these Monte-Carlo runs are presented in Table 6.12. On the basis of these runs it is evident that LR altitude measurements are necessary during the braking phase to obtain satisfactory PGNCS performance for the initial errors, terrain models, and DPS uncertainties investigated. If LR altitude measurements are not taken, large High-Gate-point altitude errors may result. These altitude errors will either prevent the DPS from operating within the desired 10-60 percent range during the visibility phase, or will reduce the astronaut's visibility of the landing site, depending upon the direction of the error.

A typical Monte-Carlo run for which satisfactory performance was obtained with LR altitude measurements in the braking phase (but not velocity measurements) is shown in Fig. 6.39. The conditions here are the same as in Fig. 6.37, wherein the DPS thrust limit was exceeded.

Under certain conditions, however, the PGNCS will not operate without violating the DPS thrust limit (6300 pounds), even though altitude updatings are taken in the braking phase. This is indicated by the third and eighth runs in Table 6.12. It is interesting to compare the results of the third runs in Tables 6.11 and 6.12. In the case where no measurements are taken during the braking phase, the DPS thrust limit is not violated; the landing-site visibility, however, is very poor. On the other hand, in the particular case here where altitude measurements are made during the braking phase, the DPS thrust limit (6300 pounds) is violated.

In concluding this section it should be emphasized that in most situations the PGNCS will perform much better with altitude updatings during the braking phase than without them.

6.11.4 No LR Altitude Measurements Used during Braking Phase

In the preceding subsections it was found that PGNCS performance was adversely affected if no LR updatings were made during the braking phase. It was also found that if only altitude updatings (but not velocity) were made during the braking phase, the system performance was essentially the same for nominal conditions as if both altitude and velocity updates were used.

Table 6.12: No Velocity Measurements in Braking Phase

Error Vector Number	Terrain Model	DPS Accel. Uncert. (percent)	ΔV (ft/s)	Max.Thrust 10-60% region (pounds)	High-Gate Errors		Low Gate Errors	
					Alt.(ft)	Vel.(f/s)	Alt.(ft)	Vel.(f/s)
1191	6	+1	6310	5710	+ 46	6.6	-1.8	.53
1191	8	+1	6311	5662	-445	5.8	-6.0	.58
212	6	+1	——	* 6300	——	——	——	——
212	8	+1	6306	5832	-153	10.5	-1.0	.56
739	8	0	6286	5586	-265	4.5	-1.2	.35
-887**	8	0	6306	5523	-611	7.8	+5.8	.75
862	8	0	6289	5553	-358	8.7	+2.3	.79
-786**	8	0	6289	5626	-356	7.8	+ .92	.53
616	8	+1	——	* 6300	——	——	——	——

* Maximum thrust level of 6300 pounds in throttleable region was violated in this run.
** Negative sign indicate all components of vector have opposite signs from those in Table.5.6.

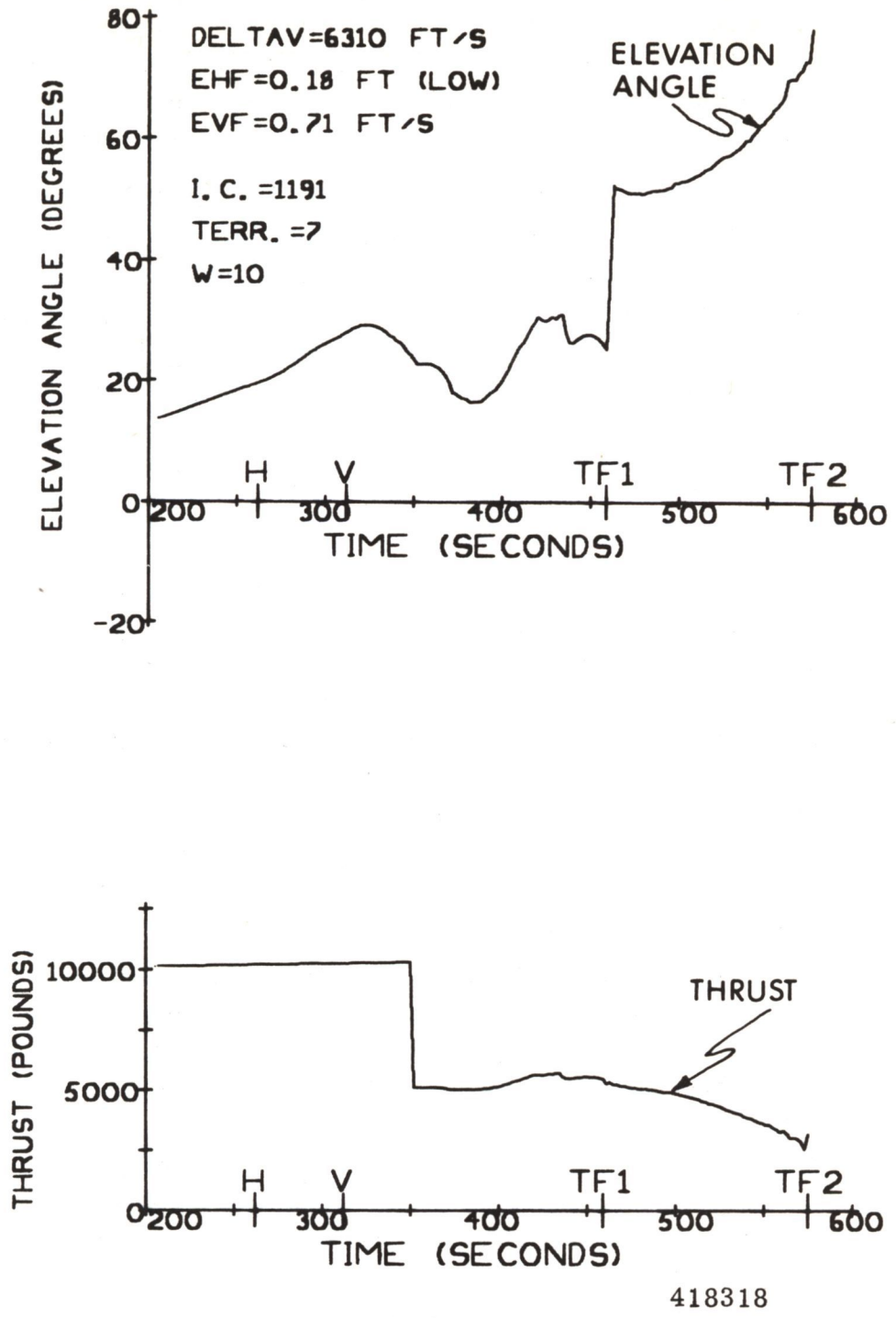

Fig. 6.39 Thrust-Vector Profiles: No LR Velocity Measurements in Braking Phase.

A series of Monte-Carlo runs were made to investigate the case where only velocity updatings were made during the braking phase. On the basis of these runs it was found that the PGNCS performance was not significantly different from the cases where no LR measurements at all are used during the braking phase. In effect, this implies that the important and necessary LR measurement during the braking phase is altitude,not velocity.

6.11.5 Interrupt Measurements when Zero Doppler Shift Is Obtained

A series of Monte-Carlo runs were made to simulate PGNCS operation under conditions where certain of the beams experience zero doppler-frequency shift. The criterion used in the simulation to test for zero doppler shift was that if any beam axis were within 5 degrees of being normal to the velocity vector, then that beam would experience zero doppler shift. Furthermore, if a rear beam experienced zero doppler shift, it was assumed that no useful altitude or velocity data would be provided by the LR. If, on the other hand, the forward beam experienced zero doppler shift, only the velocity measurements were interrupted.

With the present LR antenna arrangement, the longitudinal axis of the vehicle is about 105 degrees above the plane containing the 3 rear beams of the LR. During the latter part of the braking phase, when LR measurements are taken, the vehicle's velocity vector is typically 3-5 degrees below the local horizontal plane. Under these conditions, when the orientation of the thrust vector is about 20 degrees above the local horizontal, it is highly probable that at least one rear beam will be in the zero doppler region. From an examination of the thrust-vector profiles presented in this report it is evident that thrust-vector elevation angles of about 20 degrees during significant intervals of the braking phase are not unlikely.

The primary results from these Monte-Carlo runs are presented in Table No. 6.13. From these runs it was found that in several cases no useful velocity or altitude LR data were obtained during the major part of the braking phase. In such cases, large High-Gate-altitude errors could result, which may adversely effect PGNCS operation as discussed in Sec. 6.11.3. In many cases, on the other hand, the LR measurements were not interrupted for a significant interval during the braking phase. The duration of time for which LR measurements were interrupted, in a given run, was primarily a function of the thrust-vector profile for the particular run. This in turn is strongly dependent on the initial-condition errors and DPS thrust-acceleration uncertainties.

An example of a run where a large number of measurements are lost, i.e. are not used, during the braking phase is shown in Fig. 6.40. In this particular

Table 6.13: Measurements Interrupted when Zero Doppler Shift is Obtained

Error Vector Number	Terrain Model	DPS Uncert. %	ΔV (ft/sec)	Max. Thrust 10-60% region (pounds)	High-Gate Errors		Low-Gate Errors	
					Alt (ft)	Vel (f/s)	Alt (ft)	Vel(f/s)
1191	6	+1	6314	5433	+851	6.8	- .8	.24
1191	8	+1	6313	5630	-832	8.5	+5.5	.66
212	6	+1	——	*6300	——	——	——	——
212	8	+1	——	*6300	——	——	——	——
212	6	-1	6264	5469	+402	9.2	+4.4.	.39
212	8	-1	6261	5494	+329	9.4	- .9	.79

* Maximum thrust level of 6300 pounds in throttleable region was violated in this run.

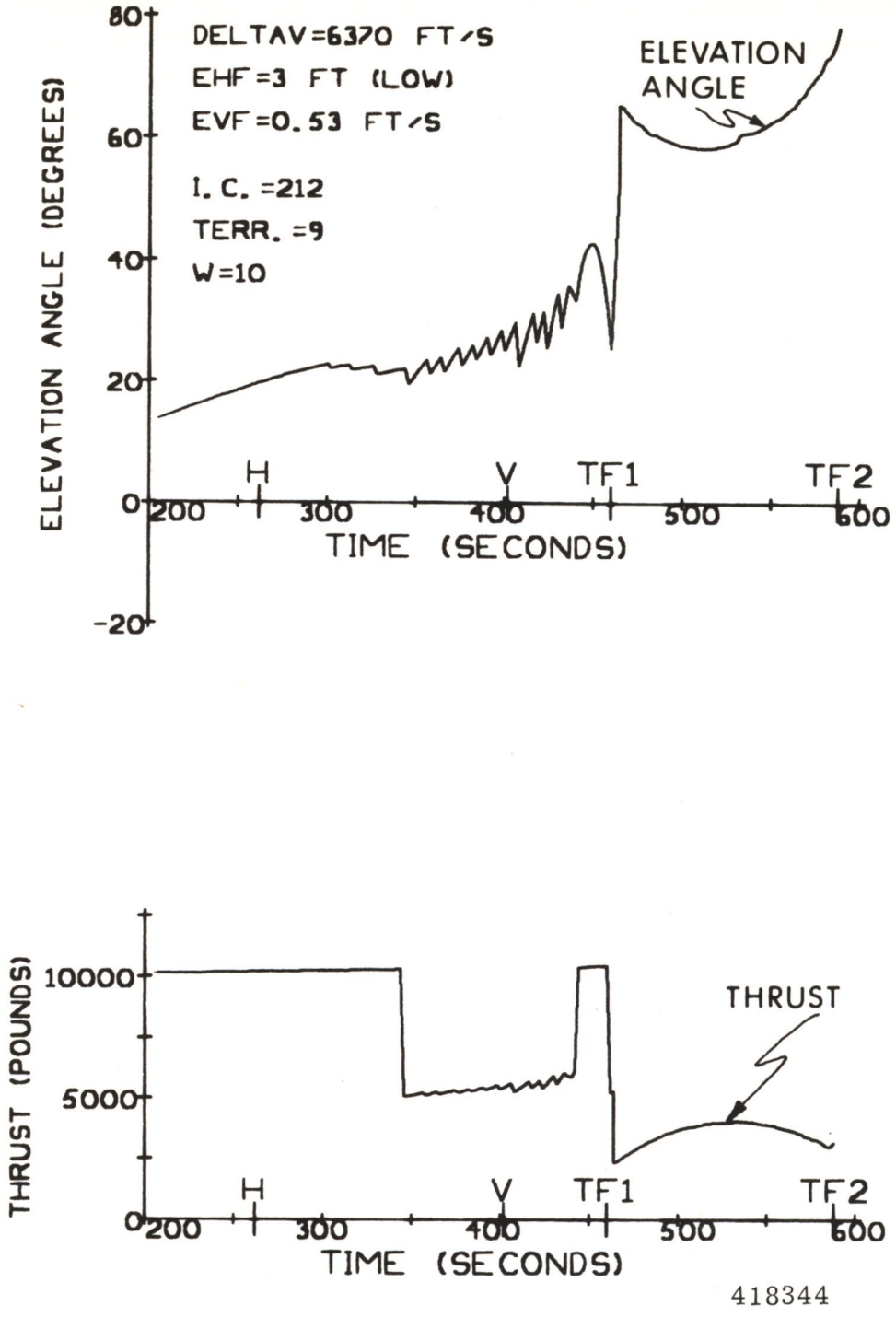

Fig. 6.40 Thrust-Vector Profiles: Interrupt Measurements When Zero-Doppler Condition Occurs

case more than 80 altitude updatings were bypassed during the braking phase (normally updating would be made at 2-second intervals). The interval between successive updatings during the braking phase was typically 8-10 seconds or more. As a result of this, the trajectory corrections at the few times that updatings were made were quite large, as indicated by the sawtooth-like changes in the elevation-angle profile. In this particular run the required thrust exceeded the throttleable-region upper limit of 6300 pounds at about 20 seconds before the end of the braking. The throttle was then moved to the 92.5-percent position and held there until the required command thrust was below 52 percent of nominal thrust. The required velocity increment in this run was excessively large (6370 ft/sec). Under conditions where no measurements are lost, the trajectory would have had the characteristics shown in Fig. 6.26.

In concluding this section it should be noted that, for the LR-antenna orientation and landing-maneuver trajectories assumed in this study, the zero doppler-shift condition occurred on several trajectories for a significant part of the braking phase. The resultant loss of altitude updatings in such cases adversely affected PGNCS performance.

CHAPTER 7

CONCLUSIONS

The important conclusions from this study are the following.

1) In order to achieve the objectives of the landing maneuver it is necessary to update the navigation data from the IMU with altitude and velocity measurements from the landing radar.
2) The best choices of landing-radar weighting functions were found to be simple, linearized, uncoupled functions which could be precomputed and then stored in the LGC. Consideration was given here to computational simplicity as well as to navigation accuracy.
3) The PGNCS was found to perform satisfactorily with LR updatings. It was tested in the study for operation with extremely severe initial errors, realistic terrain profiles, and ± 1-percent DPS acceleration uncertainties at the high-throttle setting.
4) The PGNCS makes the major trajectory corrections (for factors such as initial errors) during the latter part of the braking phase. As a result, there may be significant deviations in the magnitude and elevation angle of the thrust vector at this time. The deviations during the visibility phase, however, are extremely small, e.g. typically less than 1 degree in elevation angle.
5) The maximum permissible thrust level for DPS operation in the continuously-throttleable region was not normally exceeded on any of the trajectories studied, provided that the linear, uncoupled LR functions were used. This included cases with very severe initial errors, realistic terrain models, and ± 1-percent DPS acceleration uncertainties.
6) The maximum required velocity increment (ΔV) occurs when the DPS acceleration uncertainty is positive (e.g. + 1%). For the severe initial errors and terrain models investigated, the maximum ΔV was about 6315 ft/sec.
7) Lunar-terrain variations can significantly increase the vehicle's altitude errors at the High-Gate point by as much as several hundred feet, using realistic terrain models. In order to satisfy the landing-site visibility requirements it is necessary to hold this error down to about 100 feet. If

the requirement for visibility is relaxed so that the site need only be visible and 8 degrees above the window edge (instead of 10), then the permissible error can be increased to about 500 feet.

8) Increasing the High-Gate-point altitude from 6700 to 9200 feet resulted in a ΔV increase of about 35 ft/sec.

9) In the absence of LR updatings during the braking phase, the maximum DPS thrust level for operation during the throttleable region was exceeded in many of the cases investigated.

10) The PGNCS performed satisfactorily with initial-altitude errors as large as 6000 feet. With larger positive initial errors (vehicle high) the maximum DPS thrust level was exceeded.

APPENDIX A

DESIGN OBJECTIVES FOR GUIDANCE LOGIC, ATTITUDE CONTROL LOGIC, AND TRAJECTORIES

The following list of design objectives has been used as a starting point from which to approach the design of the guidance and attitude control logic and to choose the parameters for a first cut at trajectory design. The numbers quoted are in all cases arbitrary, they have no official sanction. They are listed here only to demonstrate that, given a reasonable set of specifications in this format, the guidance and attitude control logic makes it possible to design trajectories that meet the specification.

Figure A.1 shows a landing footprint which was chosen as an arbitrary objective for steering capability. This footprint shows that if a landing maneuver were initiated at some altitude H_0, and at a ground range of 4 H_0 from the current landing site, then the objective is to be able to reach any landing point in an ellipse extending 3 H_0 in front of the current site and 5/8 H_0 to either side. Any trajectory produced by redesignation at this initial point and landing anywhere in the ellipse should meet all the objectives. Trajectories can be flown which land outside of the footprint, but they may fail to meet one or more of the constraints.

It may be noticed from Fig. A.1 that the entire landing footprint lies forward from the unredesignated landing site. This permits the preplanned trajectory (unredesignated) to use minimum fuel consistent with visibility constraints, i.e. visibility is barely within the required limits on the preplanned trajectory. Forward steering would improve visibility; backward steering would degrade visibility below the visibility limits.

A.1 Characteristic Velocity Objectives

The characteristic velocity shall be near the minimum consistent with meeting the other objectives.

A.2 Steering Objectives

1) It shall be possible to select and steer to a new landing site anywhere within the landing footprint of Fig. A.1 with the resulting trajectory meeting all of the design objectives, provided that the gross targeting correction is completed in the first 15 seconds of the approach phase.

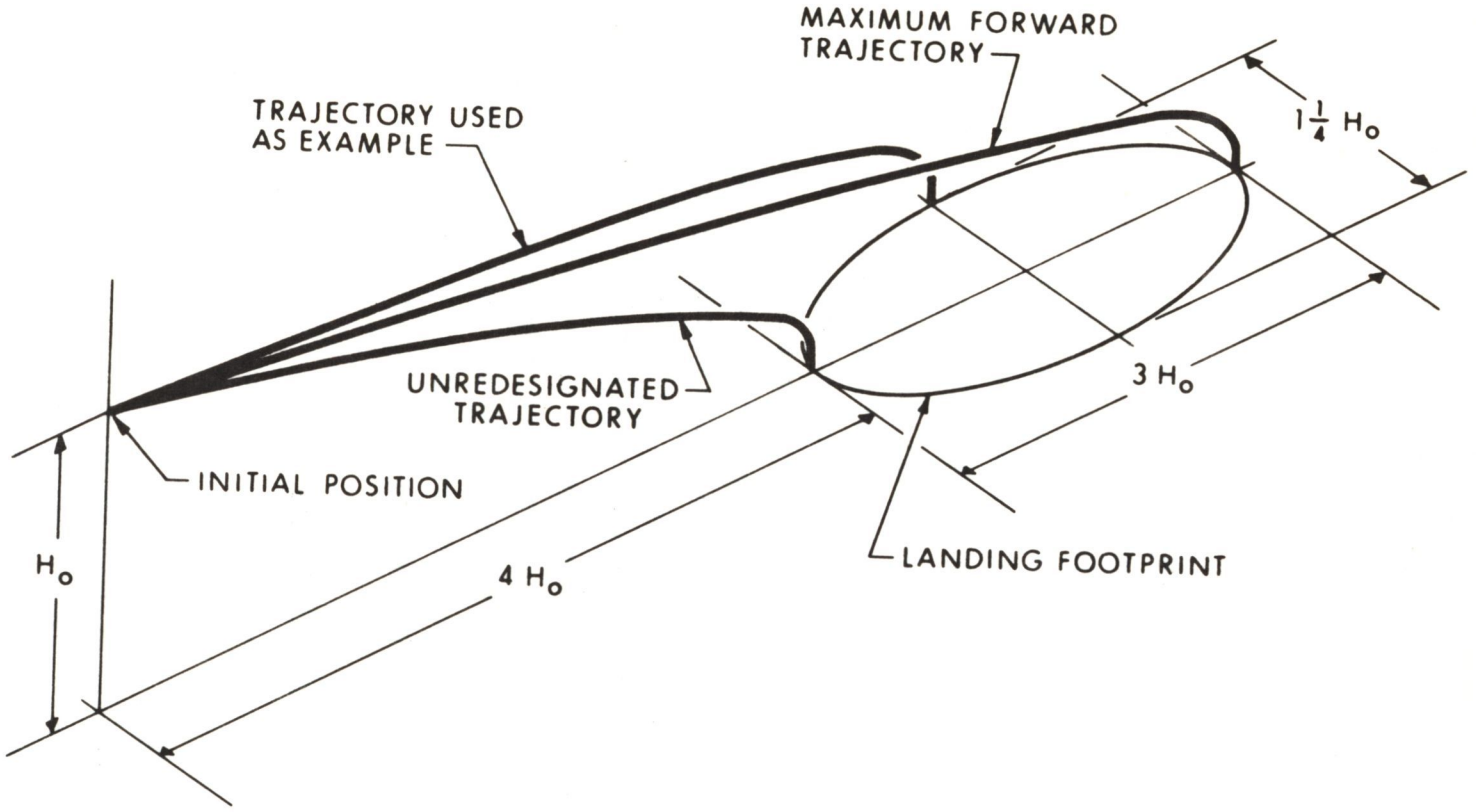

Fig. A.1 Landing Footprint - An Objective for Steering Capability

2) It shall be possible to select and steer to a new landing site at any time during the approach phase, but it shall be the responsibility of the Commander to use proper judgement in the magnitude and rate of application of the site redesignation such as to maintain adequate visibility and attitude excursion limits.

3) It shall be possible to steer to convergence upon a previously selected site throughout the approach phase so long as the site is visible.

A.3 Visibility Objectives

1) The landing site shall lie at least 10^{o} above the bottom edge of the window (the look angle shall be at least 35^{o}) from the beginning of the approach phase, for a minimum of 75 seconds, and until it recedes from view at the bottom of the window just prior to phase terminus.

2) The landing site shall not recede from view at greater than 300-ft slant range.

3) No site redesignation within the conditions of objective A.2 shall cause the landing site to disappear.

4) The angle of depression of the landing (the angle between the local horizontal and the vector to the site) shall be greater than 15^{o} for at least 15 seconds prior to loss of visibility.

A.4 Attitude Objectives

1) The attitude shall be controlled such as to keep the landing site in the plane of the LEM X and Z axes at all times when thrust-pointing requirements permit site visibility, as shown in Fig. A.2. It shall also be controlled in such a way as to minimize the angle between the normal to the trajectory plane and the LEM Y axis* when thrust-pointing requirements do not permit visibility. Transition between these two control criteria shall be smooth.

2) Attitude limits during the approach phase, including the effects of site redesignation, shall be 0^{o} to 50^{o} in pitch, and $\pm 30^{o}$ in bank.

3) As the phase terminus is approached, the LEM pitch axis shall approach horizontal and the pitch angle shall approach a value not exceeding 15^{o}.

A.5 Path and Velocity Objectives

1) In the plan view of the path from the redesignation point to the landing site, the center of curvature shall lie to the same side of the path at all points along the path, i.e. no S turns in the plan view.

* The LEM Y axis is normal to the plane of the X and Z axis, and directed so as to form a right-handed coordinate system.

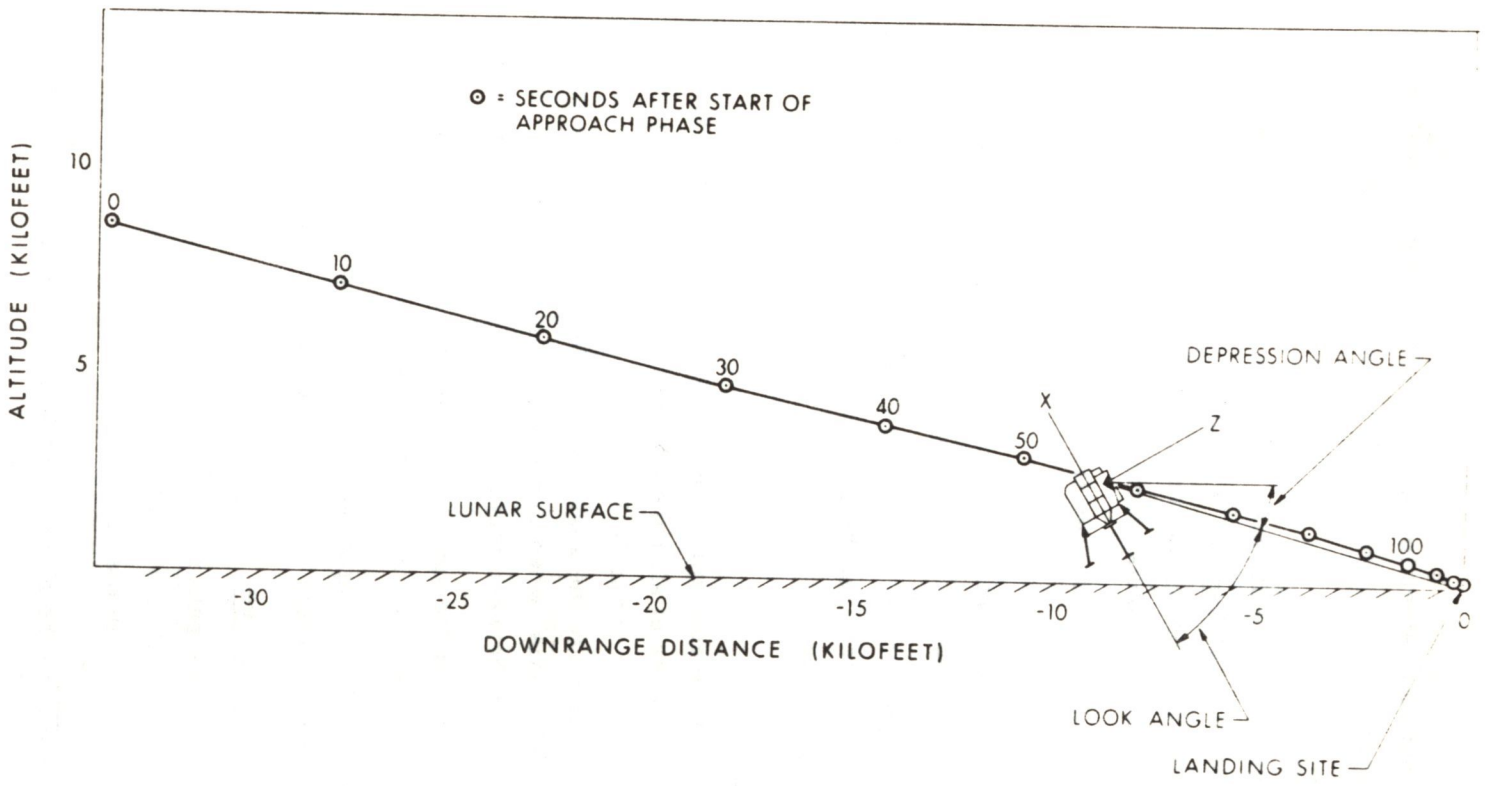

Fig. A.2 Trajectory Illustrating Approach Phase Geometry and LEM Coordinate Axes

2) The rate of descent as a function of altitude shall be a smooth curve from a point at 400-ft altitude not exceeding 20 ft/sec, to nominally 0 ft/sec (hover) at an altitude of at least 100 feet.

3) The forward velocity as a function of altitude shall be a smooth curve between points at 400-ft altitude not exceeding 70 ft/sec, at 200-ft altitude not exceeding 30 ft/sec, and nominally 0 ft/sec at hover altitude and below.

APPENDIX B

THRUST-VECTOR PROFILES FOR VARIOUS INITIAL-CONDITION ERRORS

Thrust-vector profiles are presented in this appendix to show the effects of initial-condition errors on PGNCS performance. A discussion of these effects has been given in Section 6.3 of this report. The numerical values for the different error vectors referred to here are given in Tables 5.6 and 6.3.

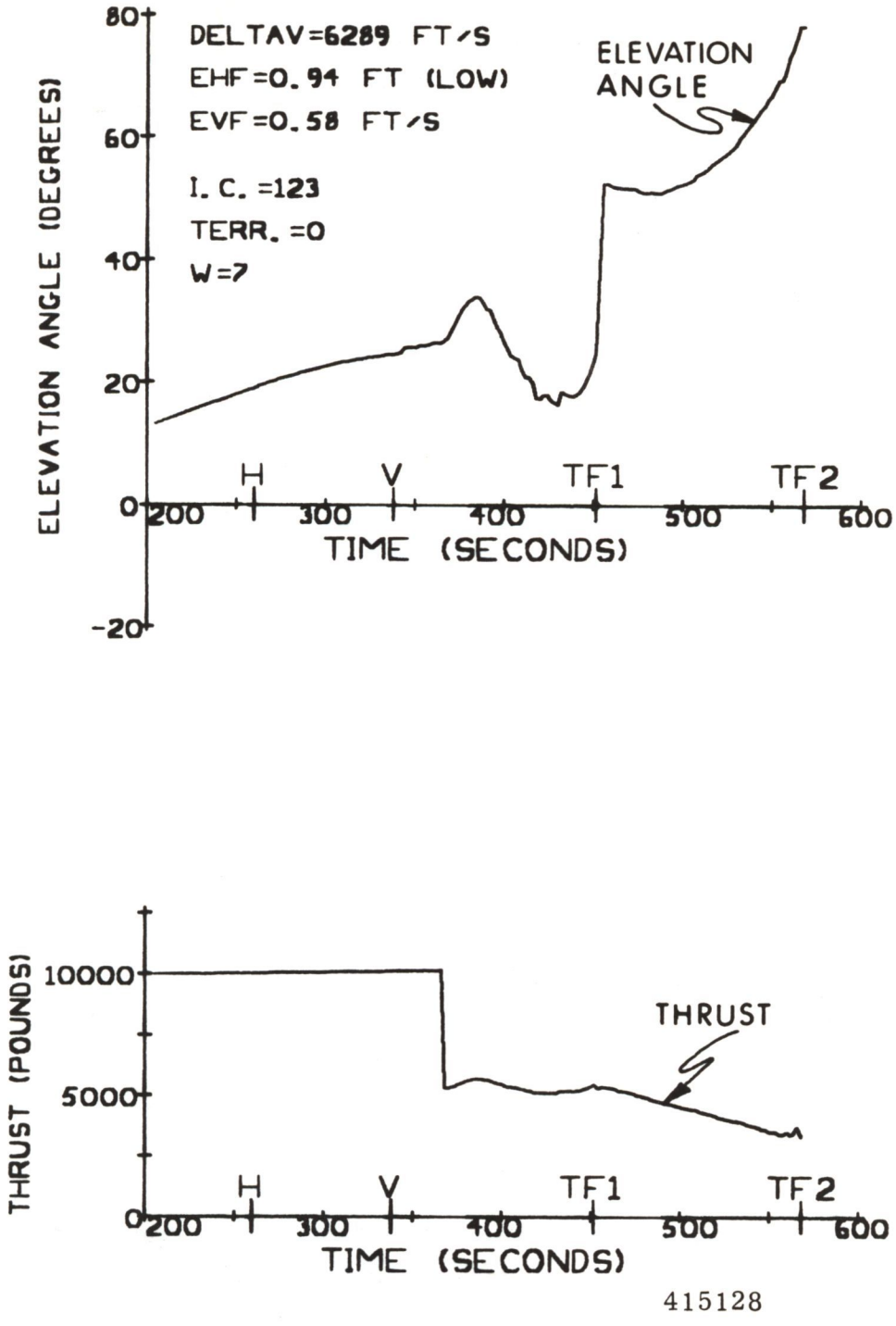

Fig. B.1 Thrust-Vector Profiles: **Severe** Initial Errors in VY, Smooth Terrain.

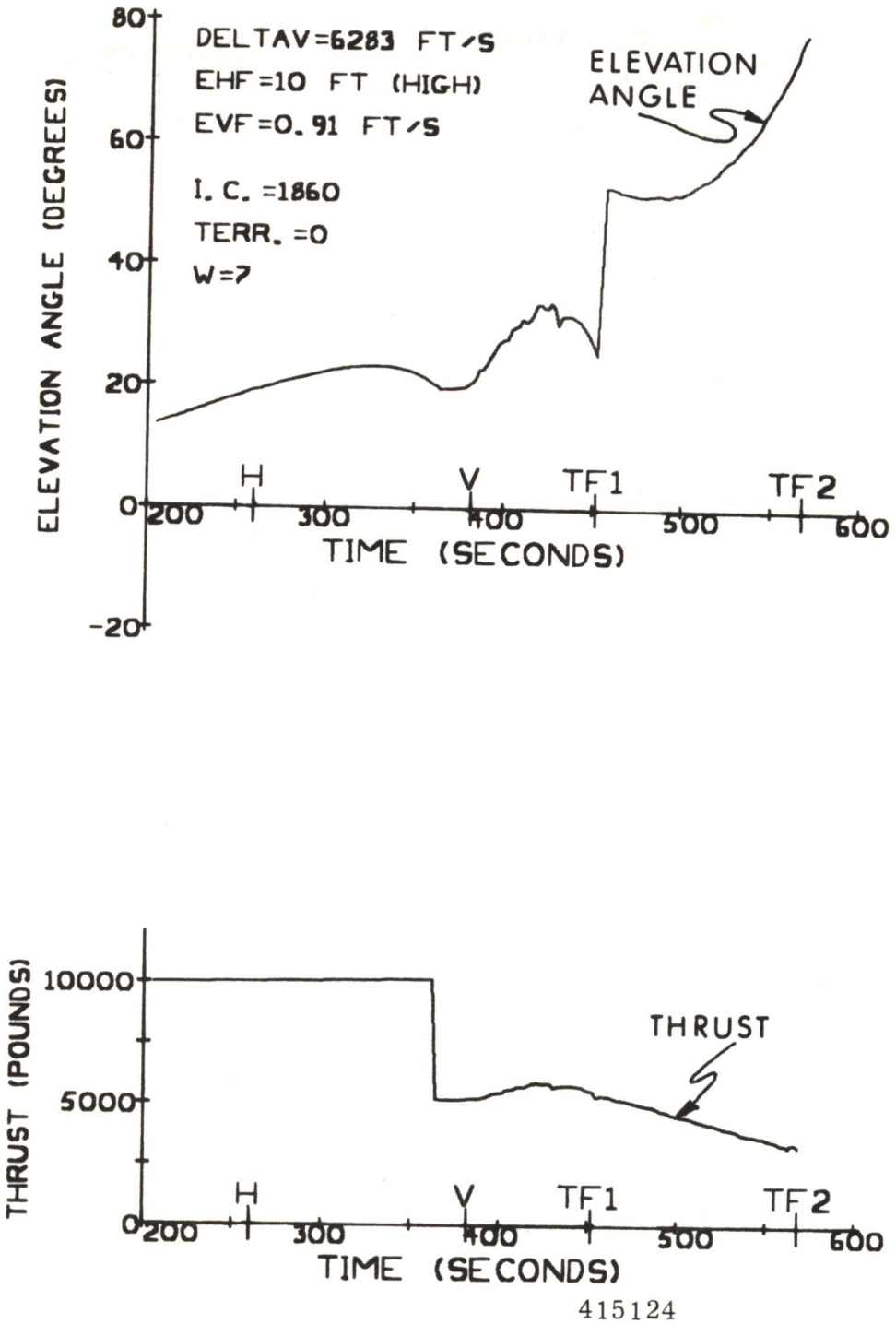

Fig. B.2 Thrust-Vector Profiles: Severe Initial Errors in VY, Smooth Terrain.

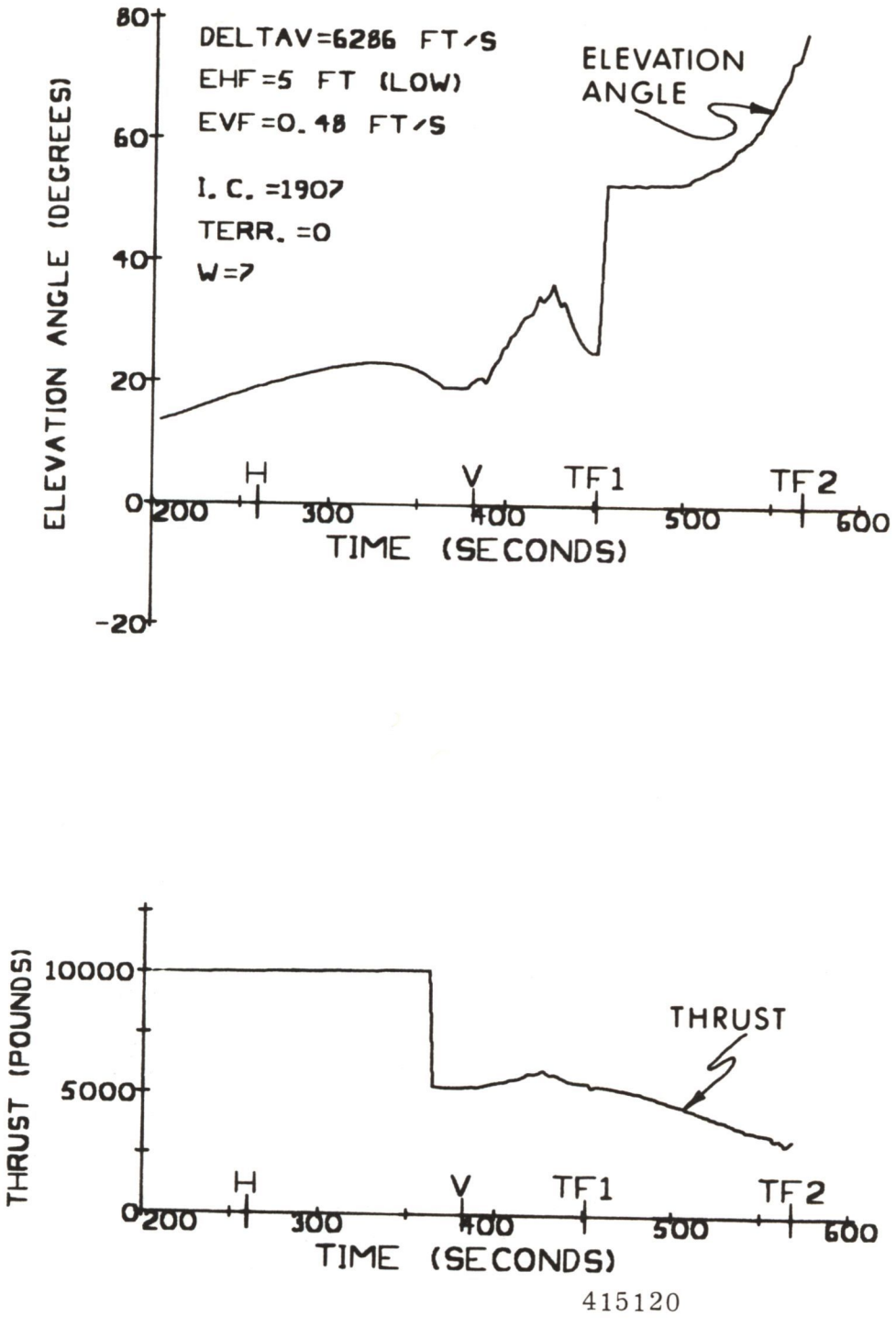

Fig. B. 3 Thrust-Vector Profiles: **Severe** Initial Errors in **RY,** Smooth Terrain

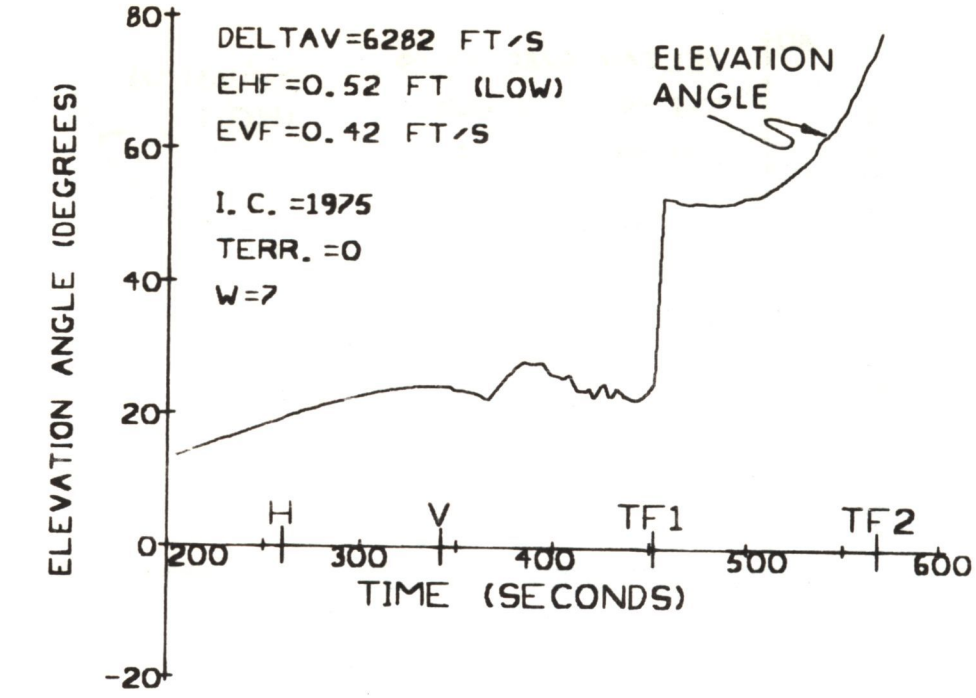

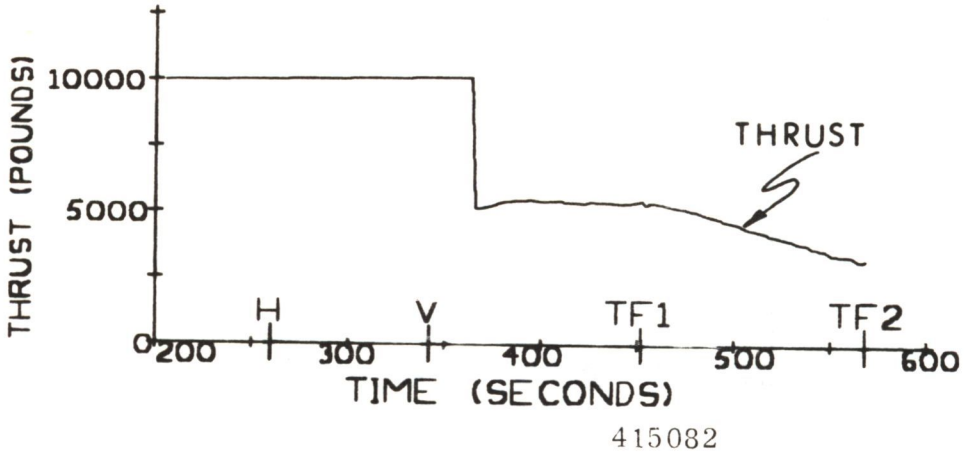

Fig. B.4 Thrust-Vector Profiles: **Severe** Initial errors in RY, Smooth Terrain.

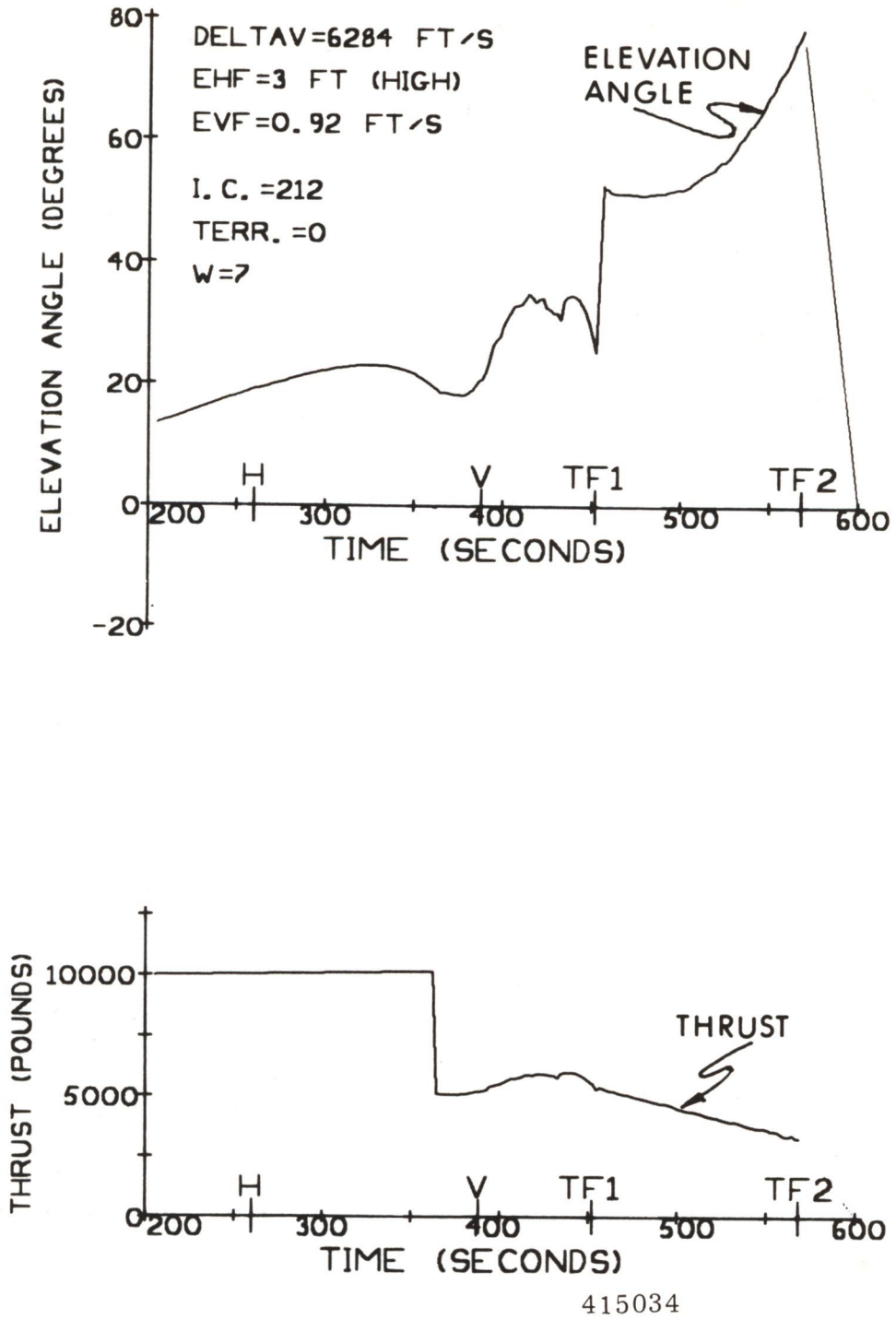

Fig. B.5 Thrust-Vector Profiles: Severe Initial Errors in RY,and VY, Smooth Terrain.

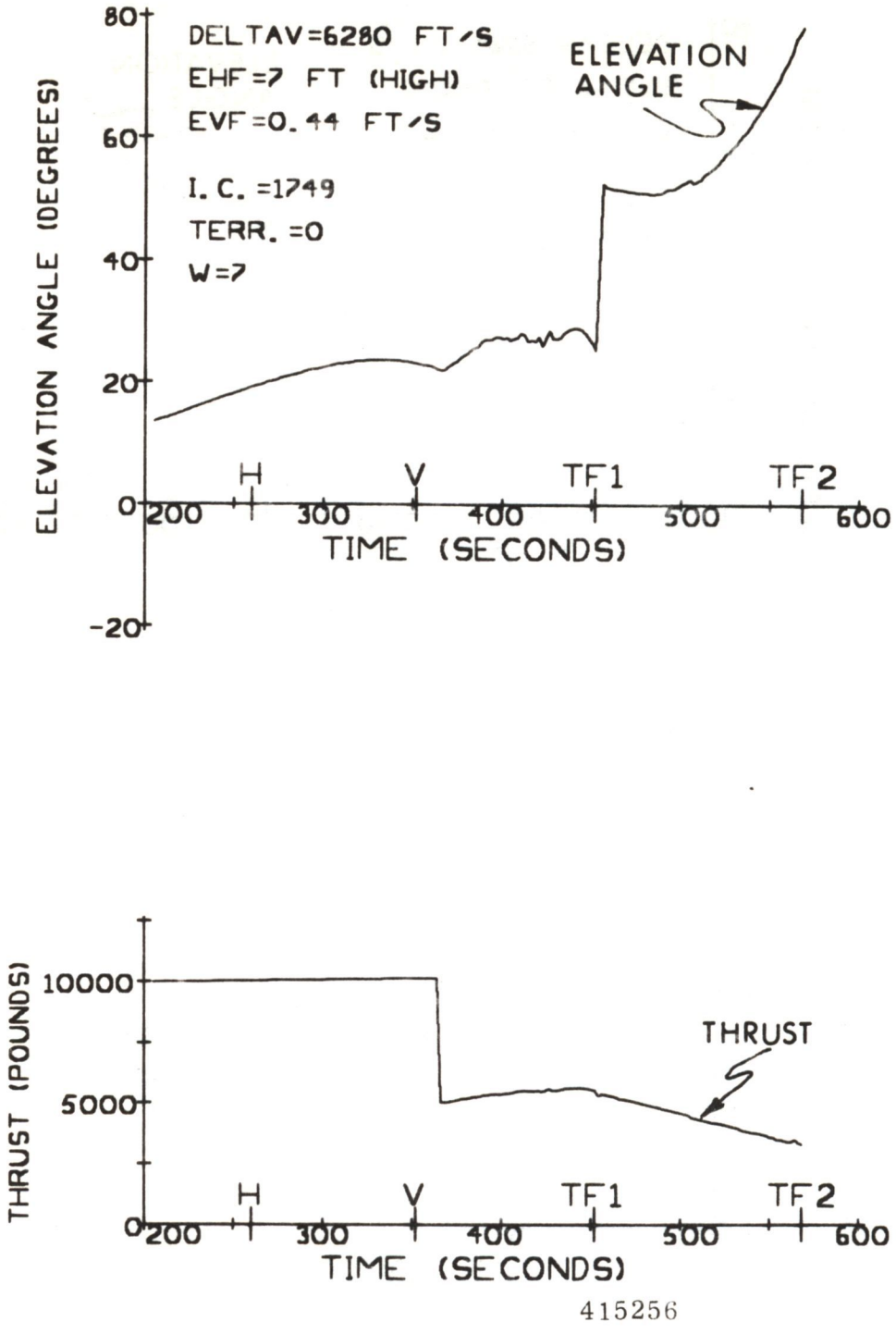

Fig. B.6 Thrust-Vector Profiles: Severe Initial Errors in RY and VY, Smooth Terrain.

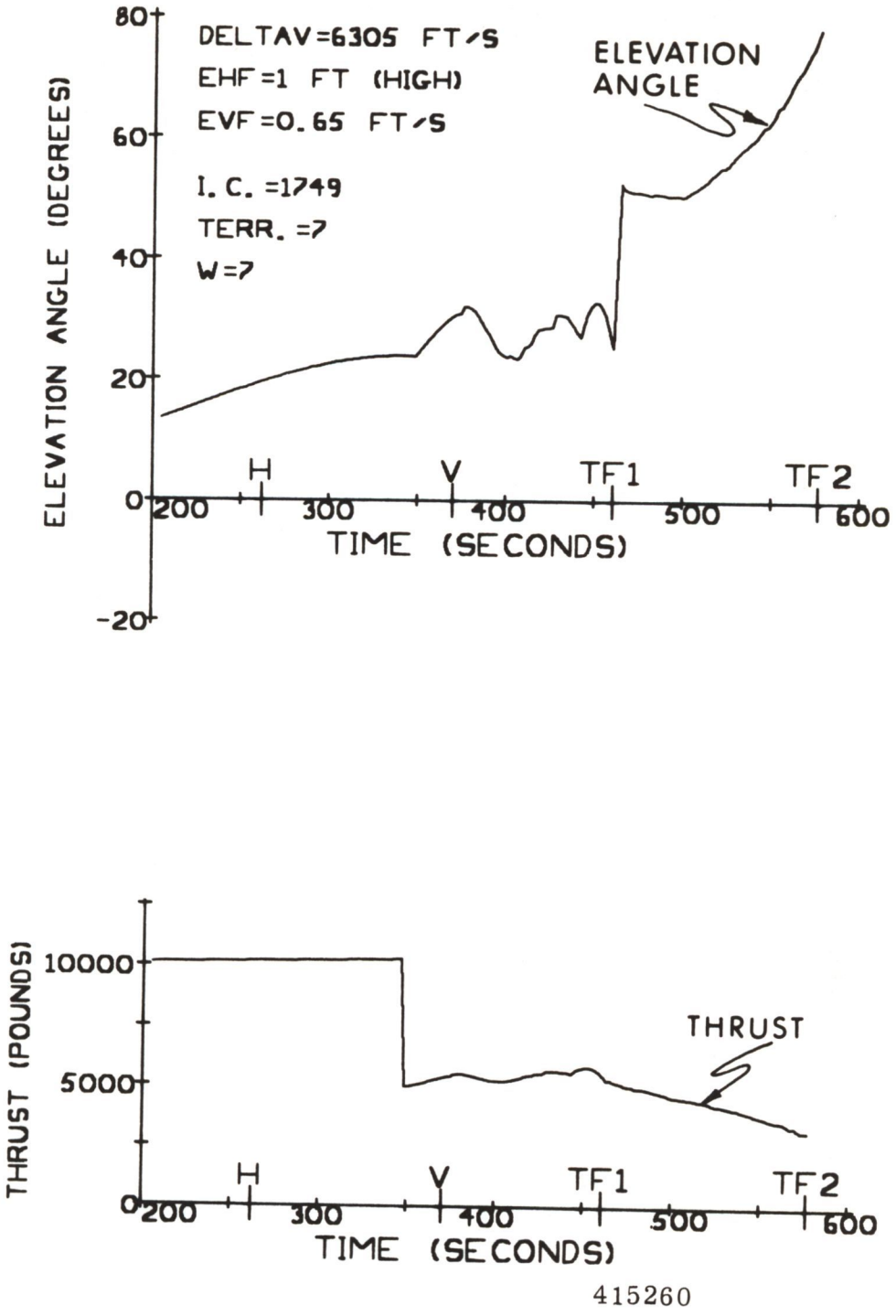

Fig. B.7 Thrust-Vector Profiles: Severe Initial Errors in RY and VY, +1% DPS Uncertainty, Realistic Terrain.

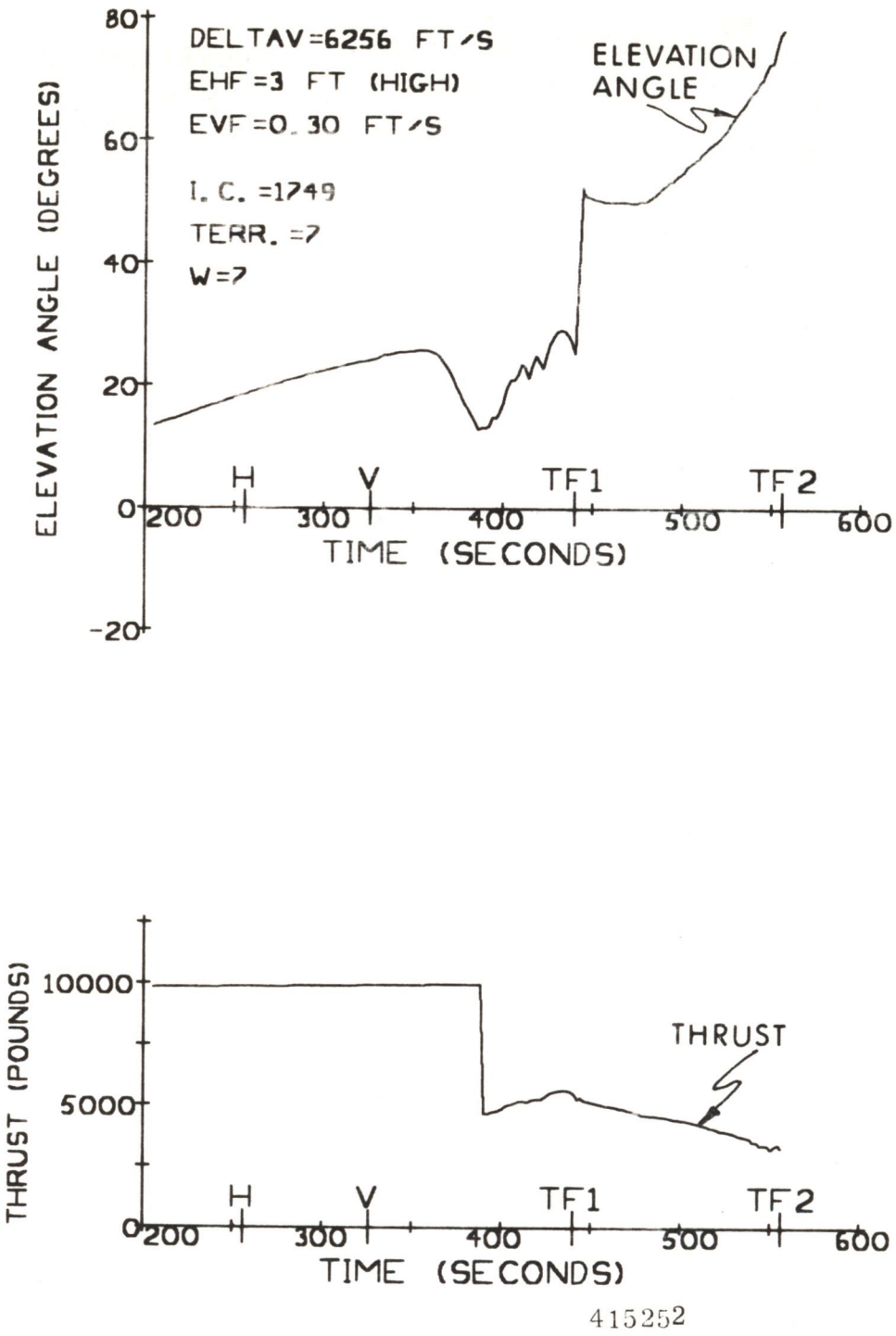

Fig. B.8 Thrust-Vector Profiles: Severe Initial Errors in RY and VY, -1% DPS Uncertainty, Realistic Terrain.

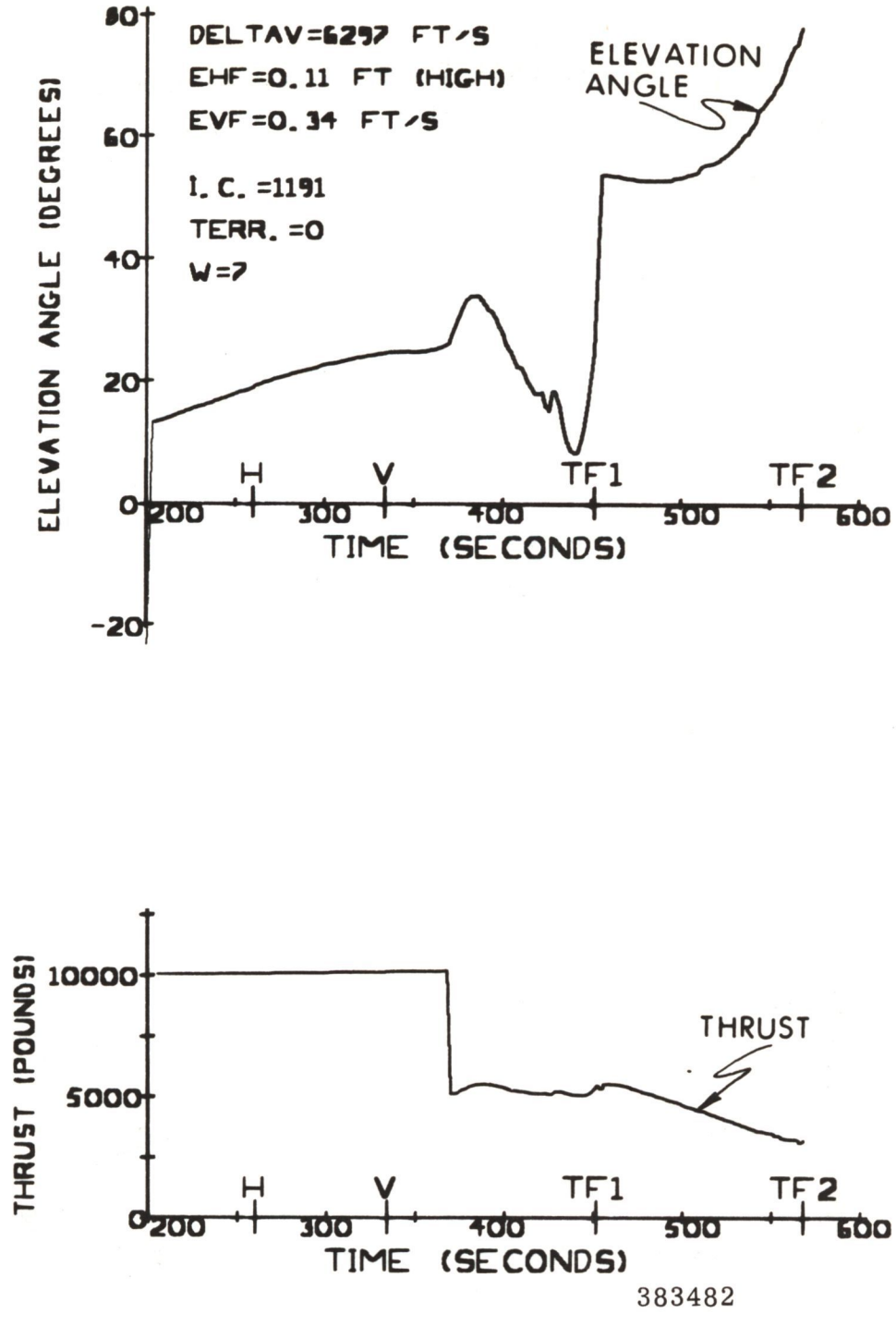

Fig. B.9 Thrust-Vector Profiles: Severe Initial Errors in RY and VY, Smooth Terrain.

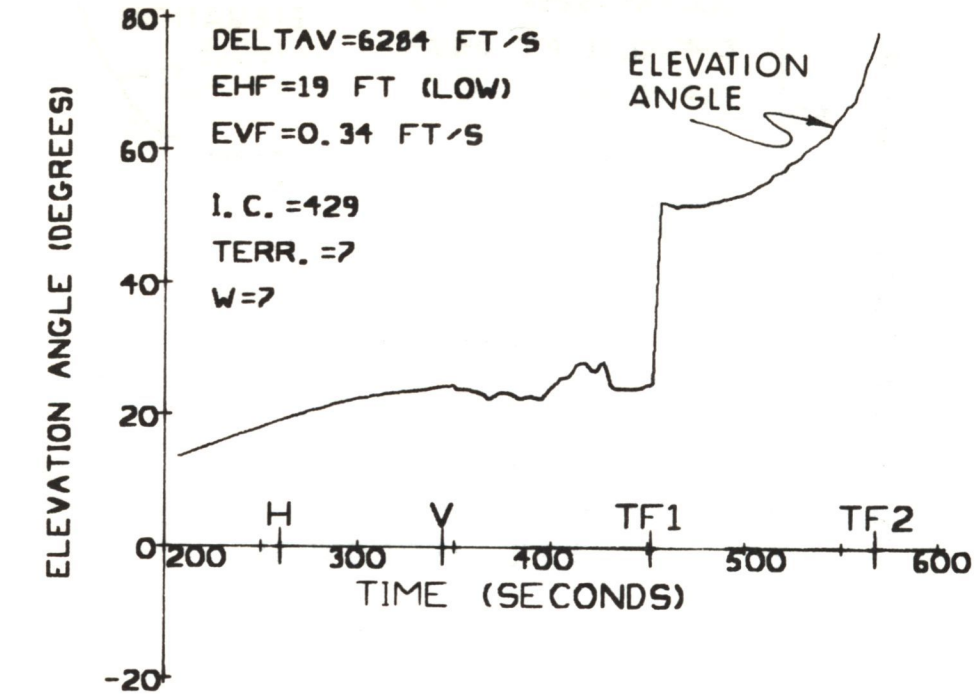

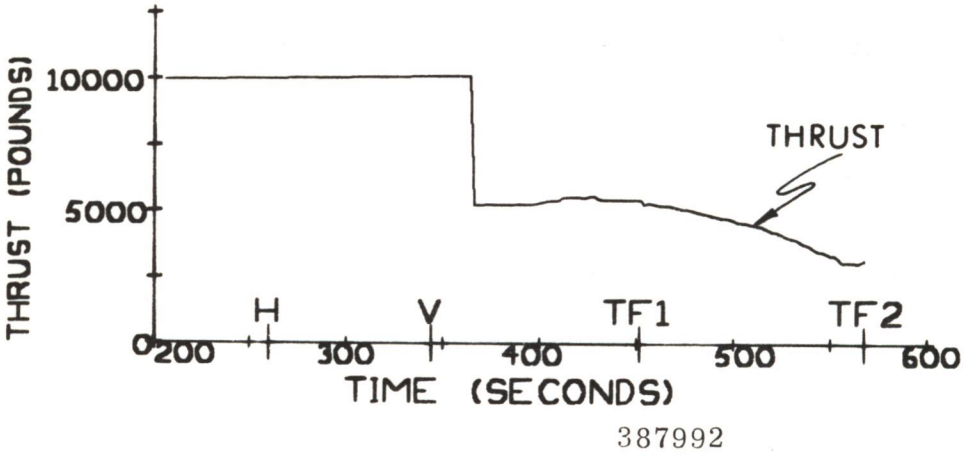

Fig. B.10 Thrust-Vector Profiles: Mild Initial Errors, Realistic Terrain.

APPENDIX C

THRUST-VECTOR PROFILES FOR VARIOUS TERRAIN MODELS

Thrust-vector profiles are presented in this appendix to show the effects of terrain-slope variations on PGNCS performance. A discussion of these effects has been given in Section 6.4 of this report. Key numerical results corresponding to these data are given in Table 6.4.

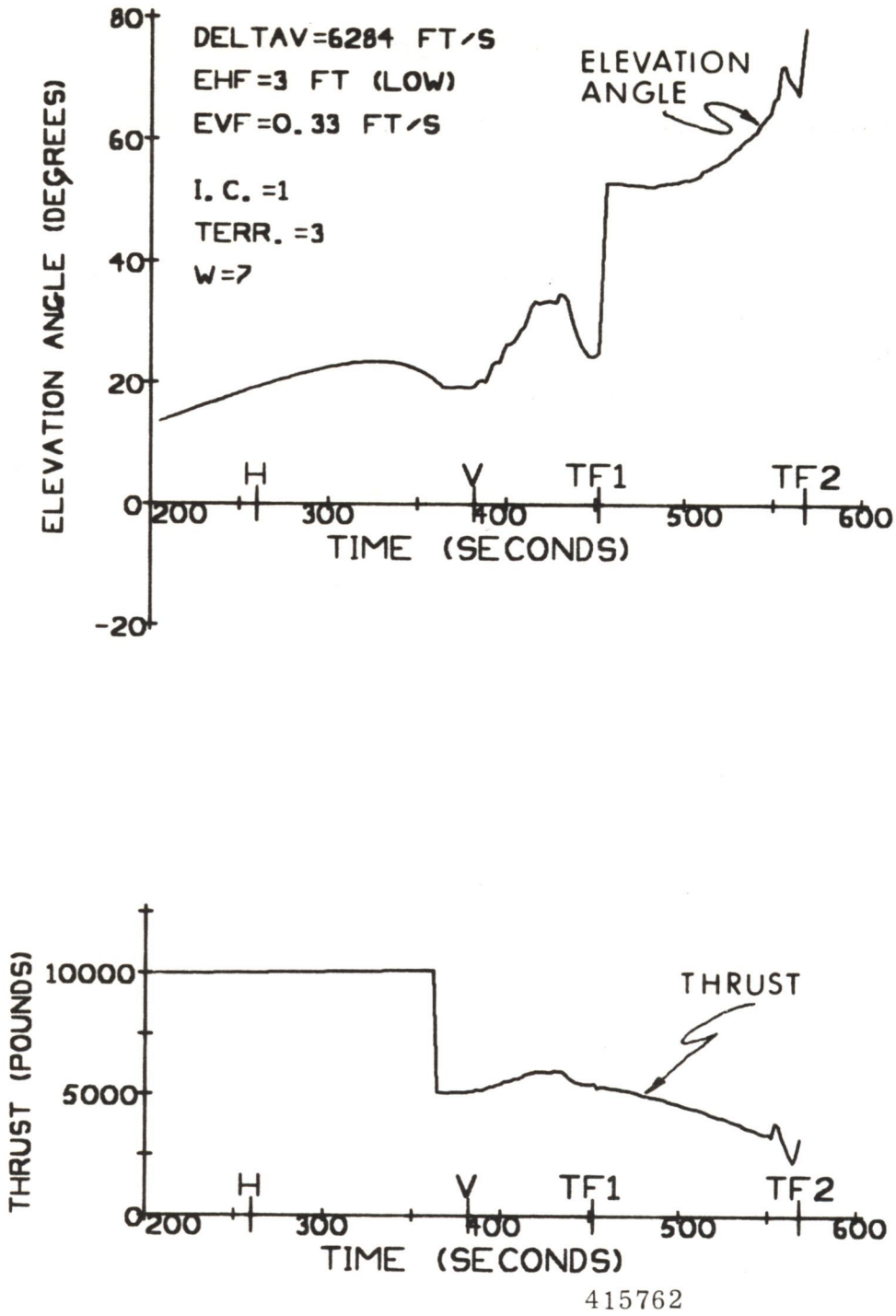

Fig. C.1 Thrust-Vector Profiles: Exponential Terrain Variations, No Initial Errors, No DPS Uncertainty, Optimum.Uncoupled Weighting Functions.

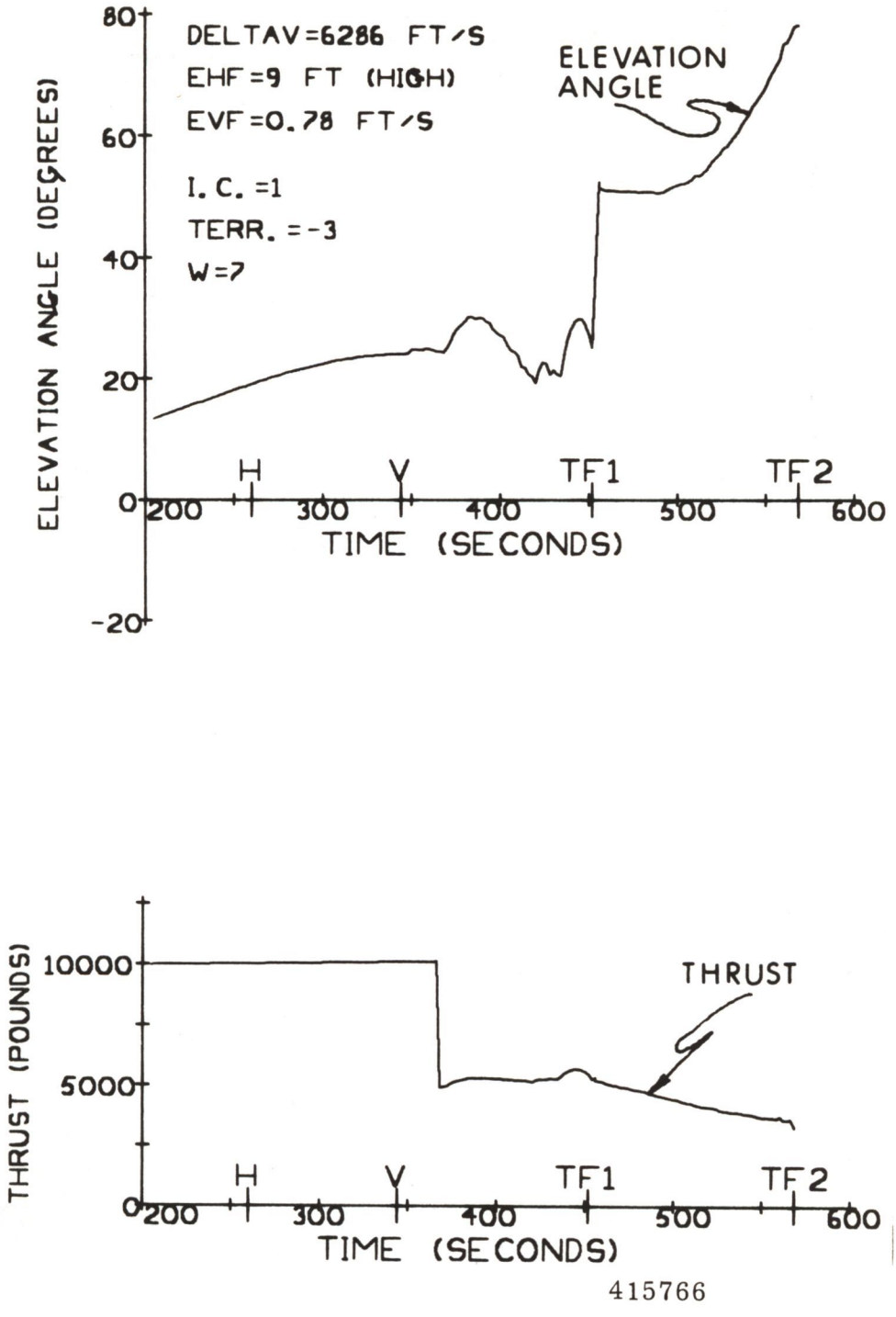

Fig. C.2 Thrust-Vector Profiles: Exponential Terrain Variation, No Initial Errors, No DPS Uncertainty, Optimum Uncoupled Weighting Functions.

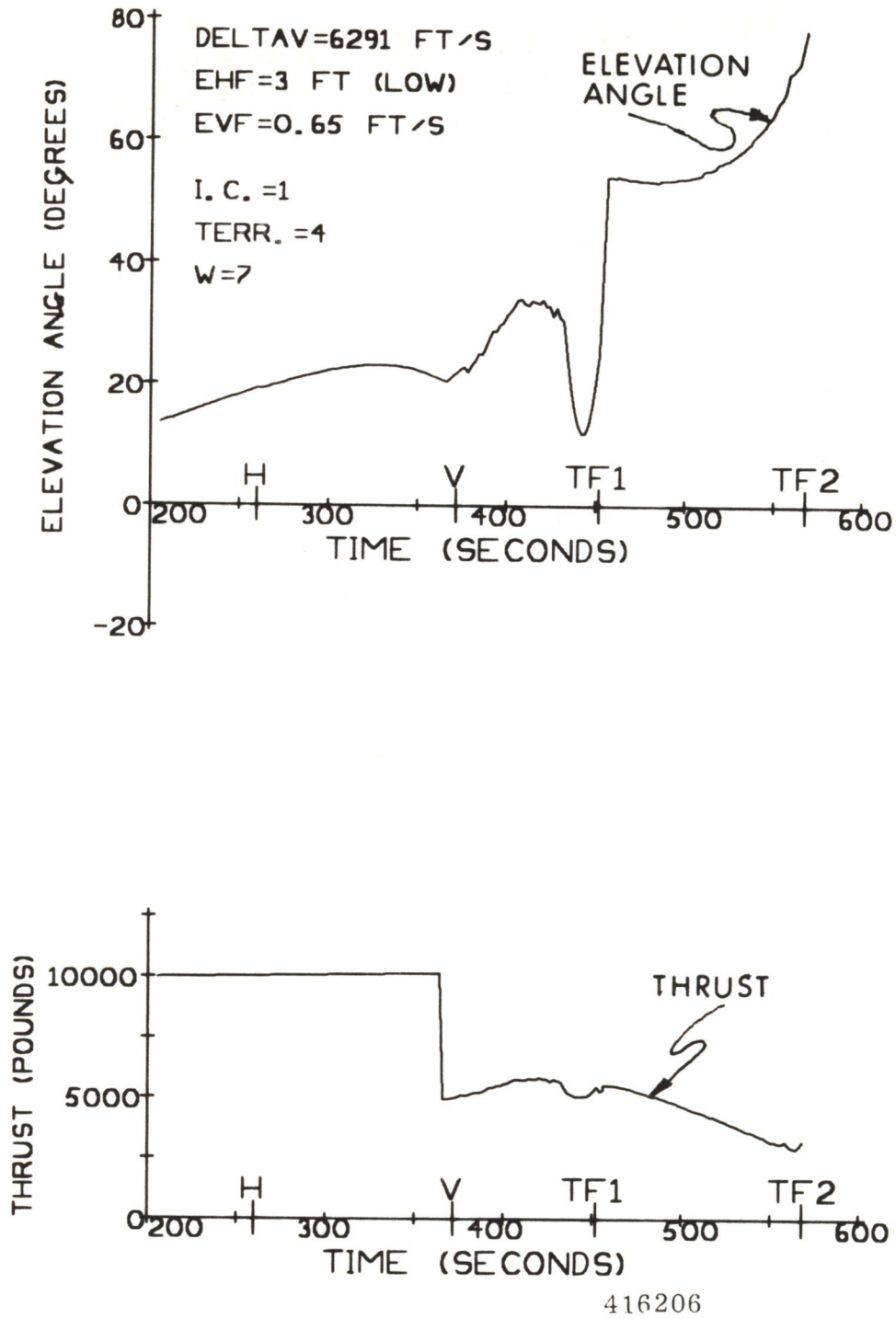

Fig. C. 3 Thrust-Vector Profiles: 100 ft/nmi Terrain Slope, No Initial Errors, No DPS Uncertainty, Optimum Uncoupled Weighting Functions.

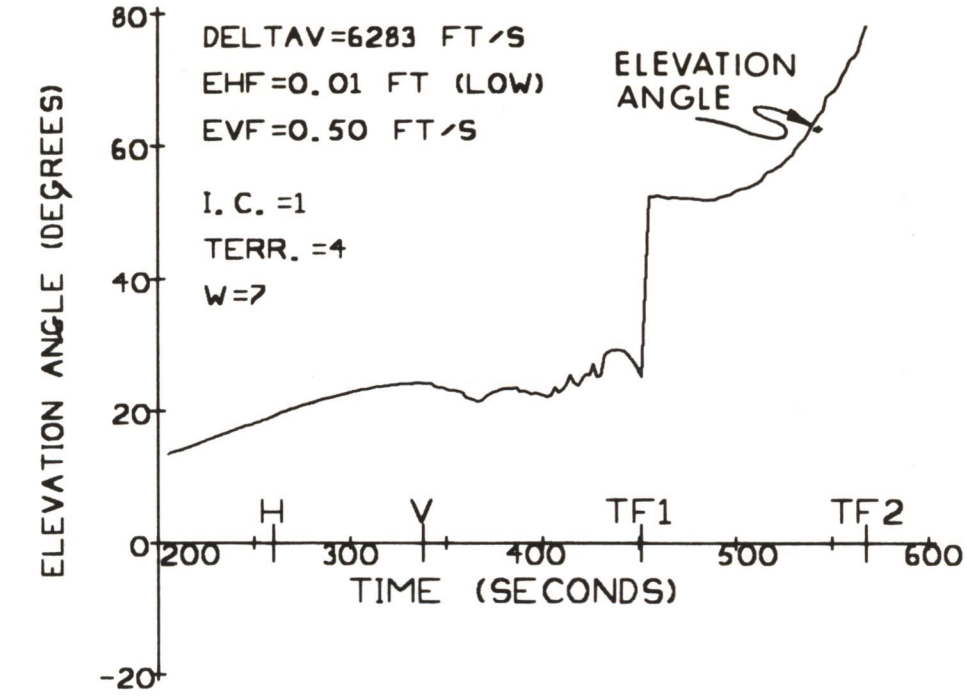

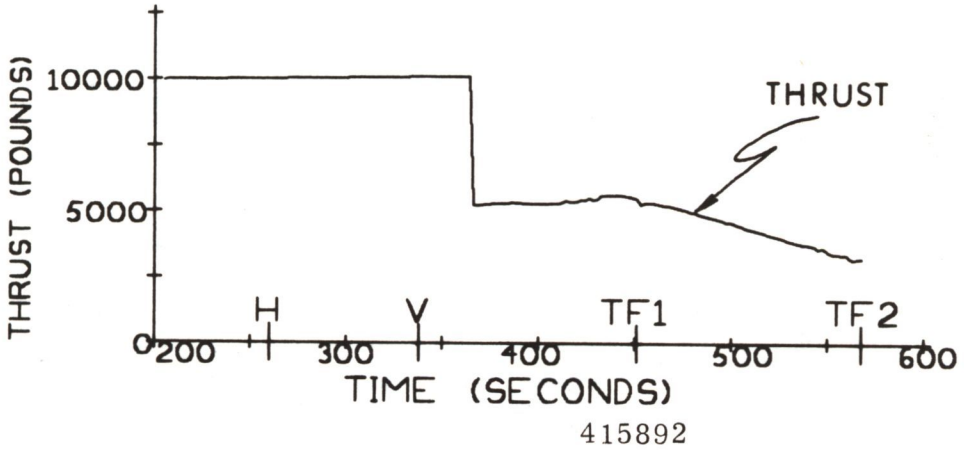

Fig. C.4 Thrust-Vector Profiles: -100 ft/nmi Terrain Slope, No Initial Errors, No DPS Uncertainty, Optimum Uncoupled Weighting Functions.

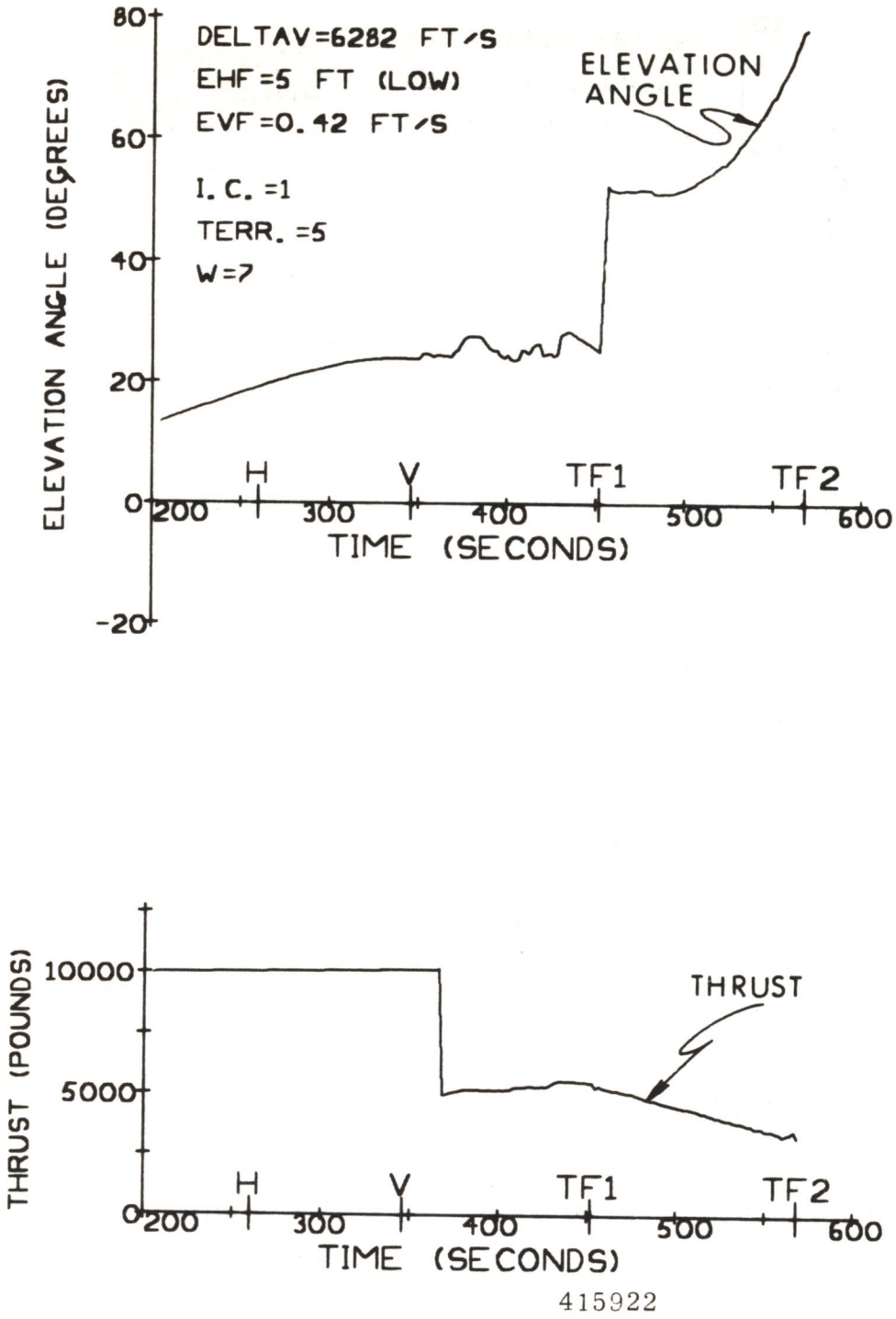

Fig. C.5 Thrust-Vector Profiles: Realistic Terrain, No Initial Errors, No DPS Uncertainty, Optimum Uncoupled Weighting Functions.

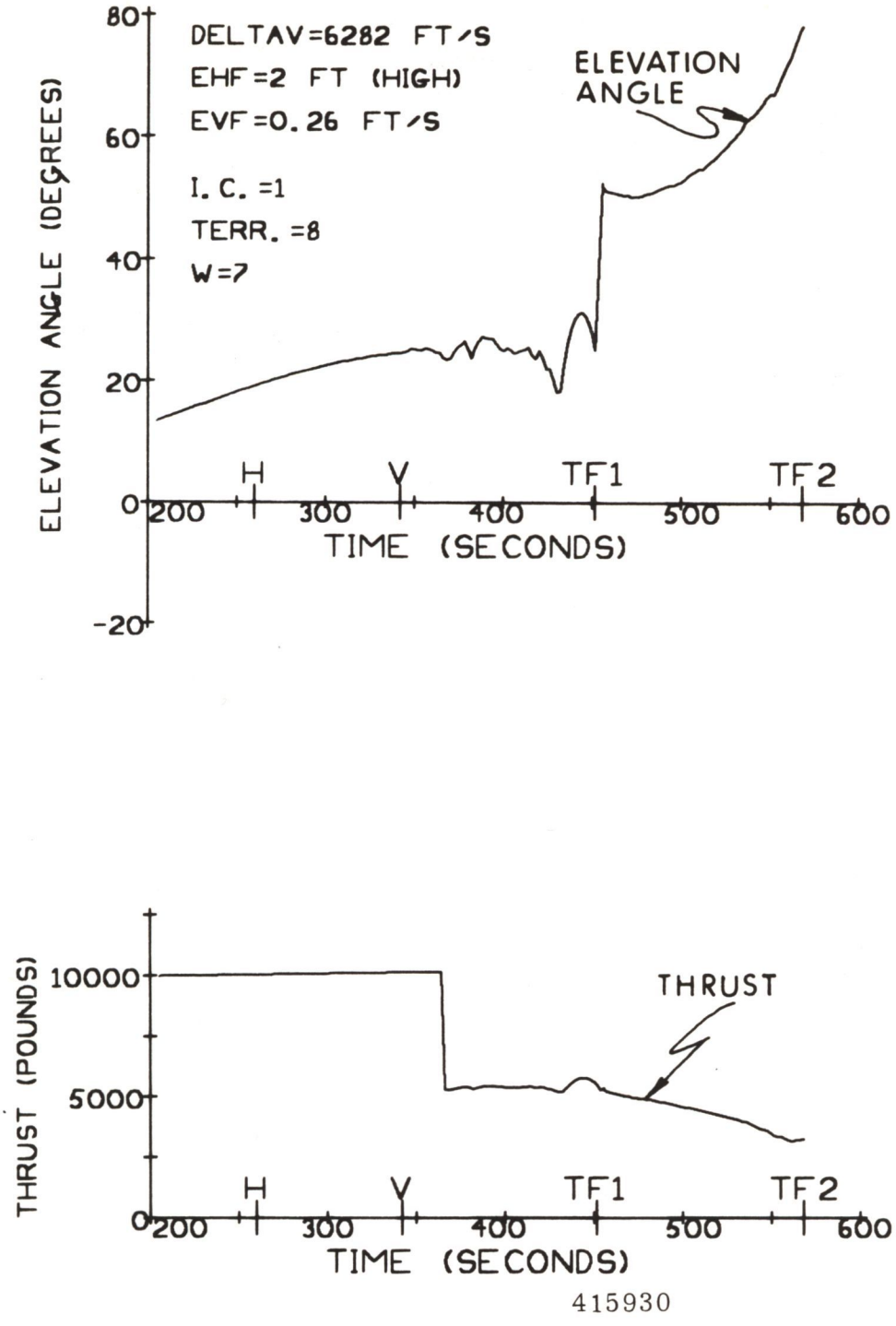

Fig. C.6 Thrust-Vector Profiles: Realistic Terrain, No Initial Errors, No DPS Uncertainty, Optimum Uncoupled Weighting Functions,

APPENDIX D

THRUST-VECTOR PROFILES FOR ORIGINAL EMPIRICAL LR WEIGHTING FUNCTIONS

Thrust-vector profiles are presented in this appendix for landing trajectories wherein the original empirically determined landing-radar weighting functions were used. These weighting functions are shown in Fig. 4.2 of this report. The important numerical results for these data are given in Table 6.5 and are discussed in Section 6.7.

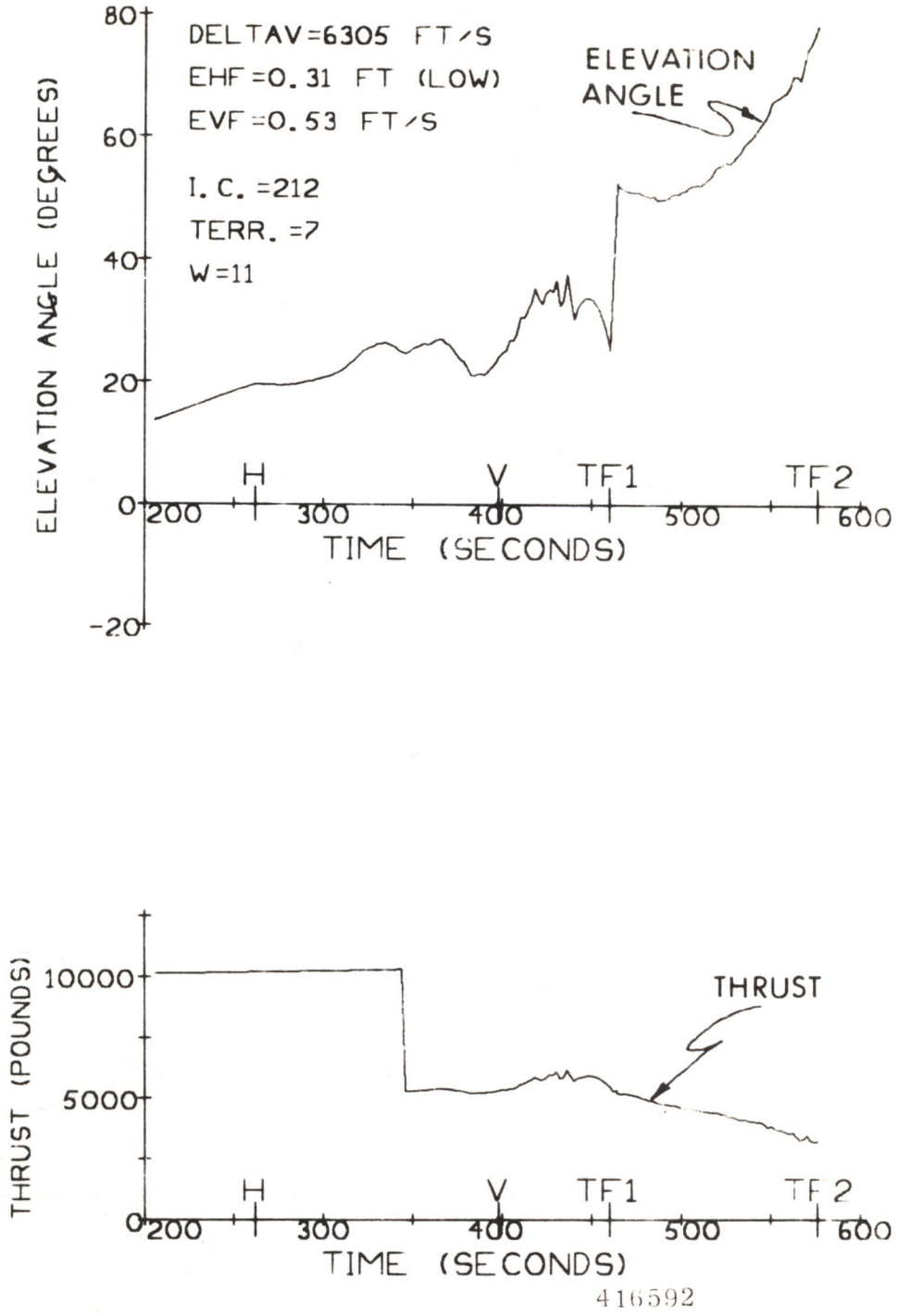

Fig. D.1 Thrust-Vector Profiles: Severe Initial Errors, +1% DPS Uncertainty, Realistic Terrain, Original Empirical Weighting Functions.

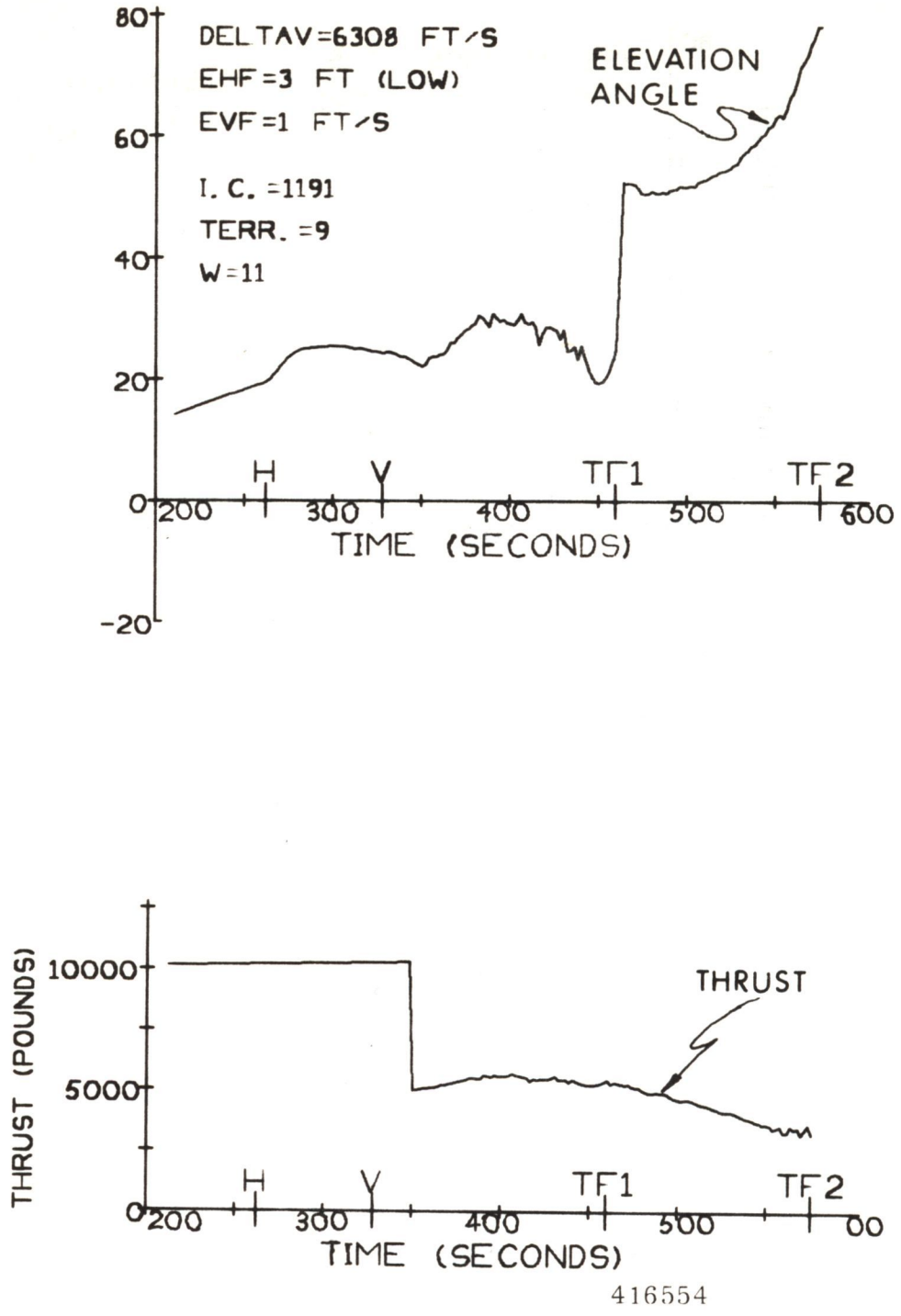

Fig. D. 2 Thrust-Vector Profiles: Severe Initial Errors, +1% DPS Uncertainty, Realistic Terrain, Original Empirical Weighting Functions.

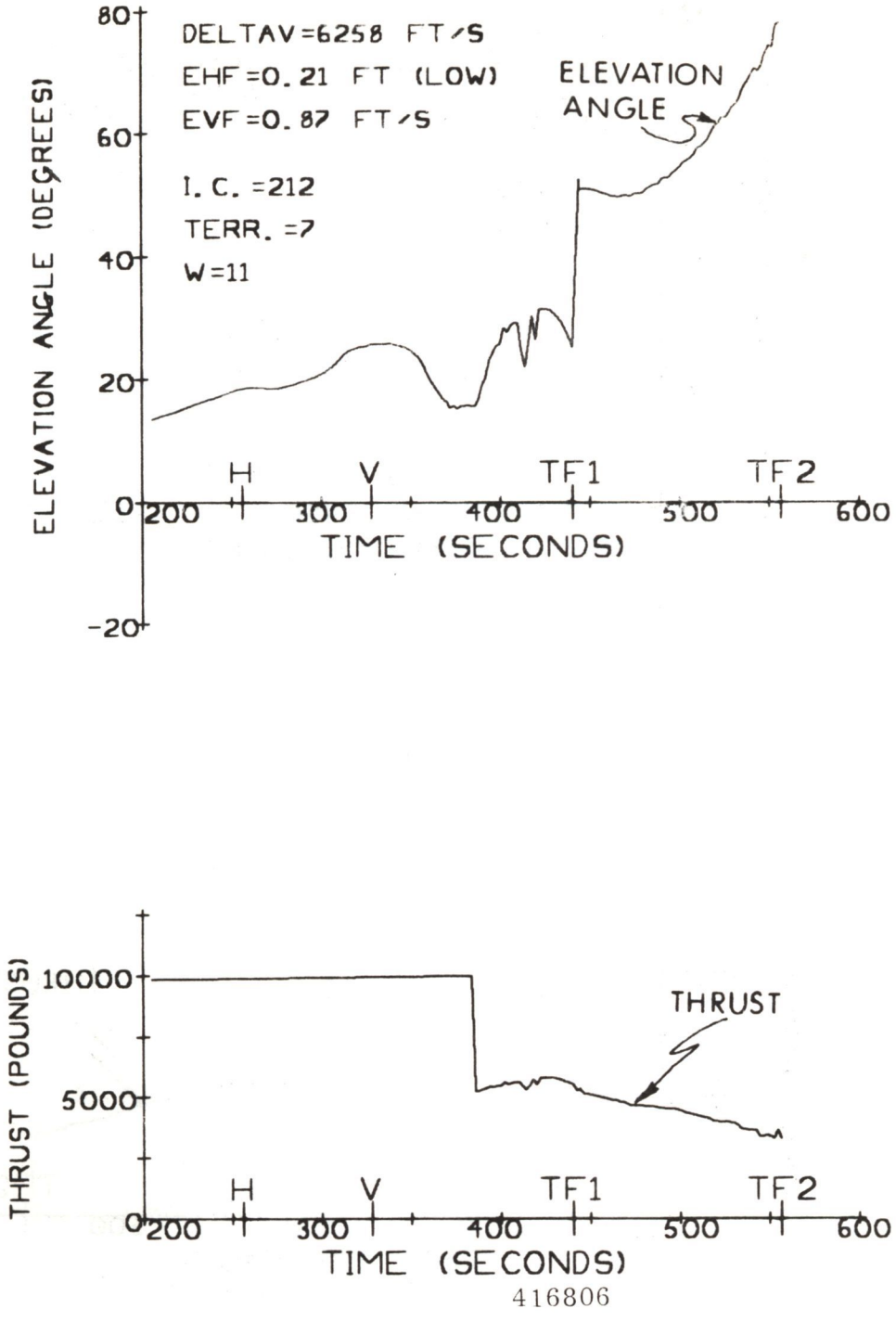

Fig. D.3 Thrust-Vector Profiles: Severe Initial Errors, -1% DPS Uncertainty, Realistic Terrain, Original Empirical Weighting Functions.

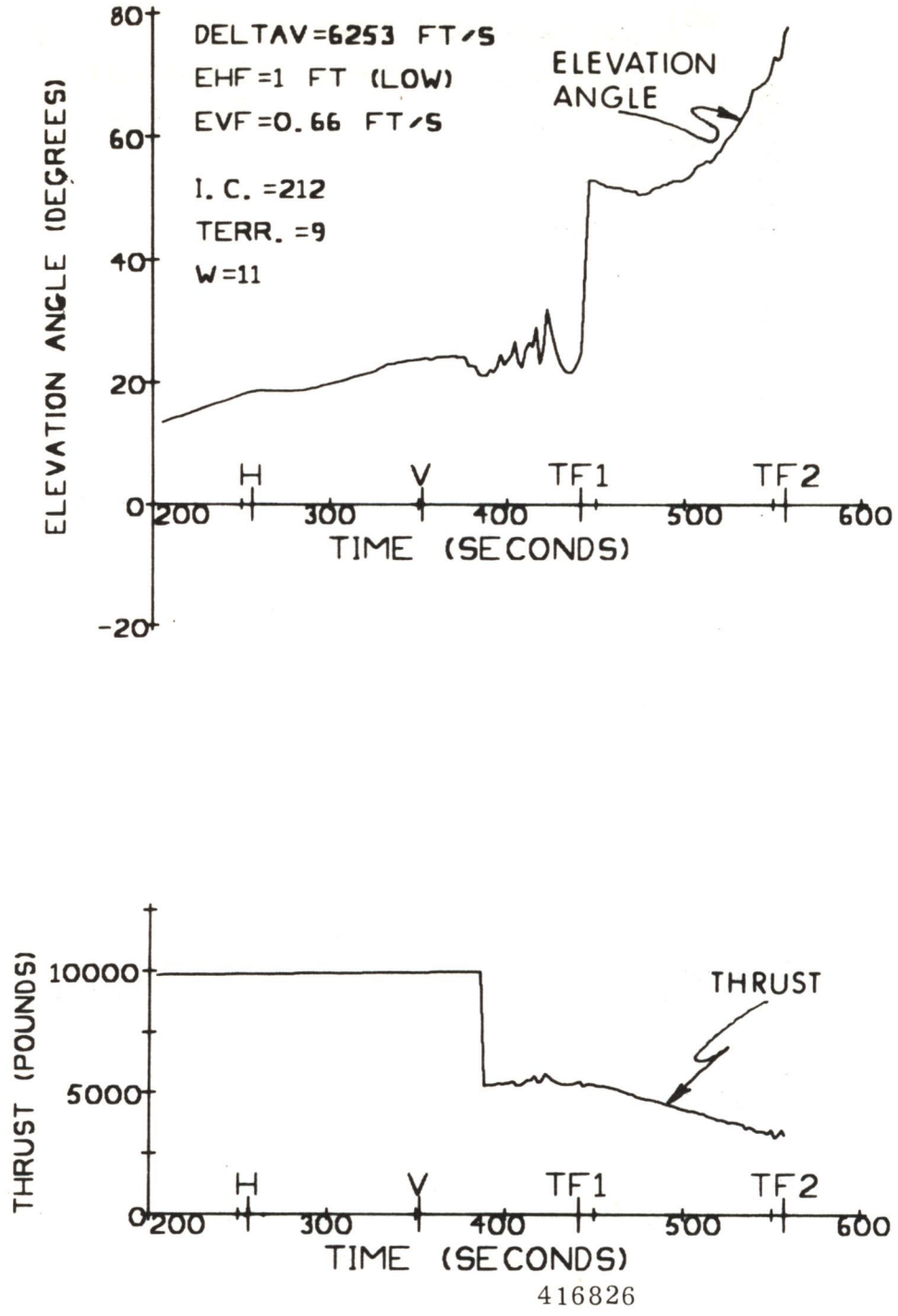

Fig. D.4 Thrust-Vector Profiles: Severe Initial Errors, -1% DPS Uncertainty, Realistic Terrain, Original Empirical Weighting Functions.

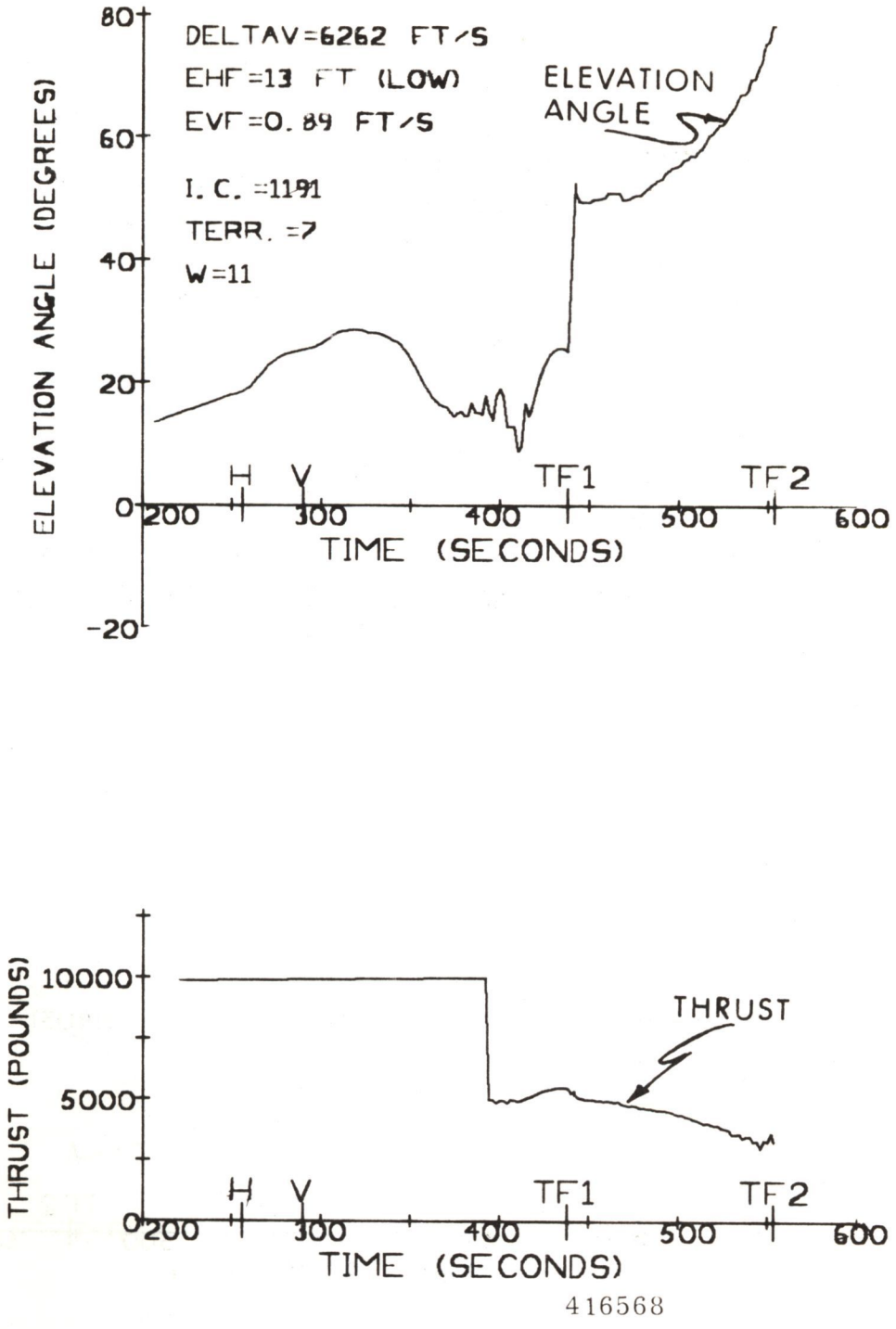

Fig. D. 5 Thrust-Vector Profiles: Severe Initial Errors, -1% DPS Uncertainty, Realistic Terrain, Original Empirical Weighting Functions.

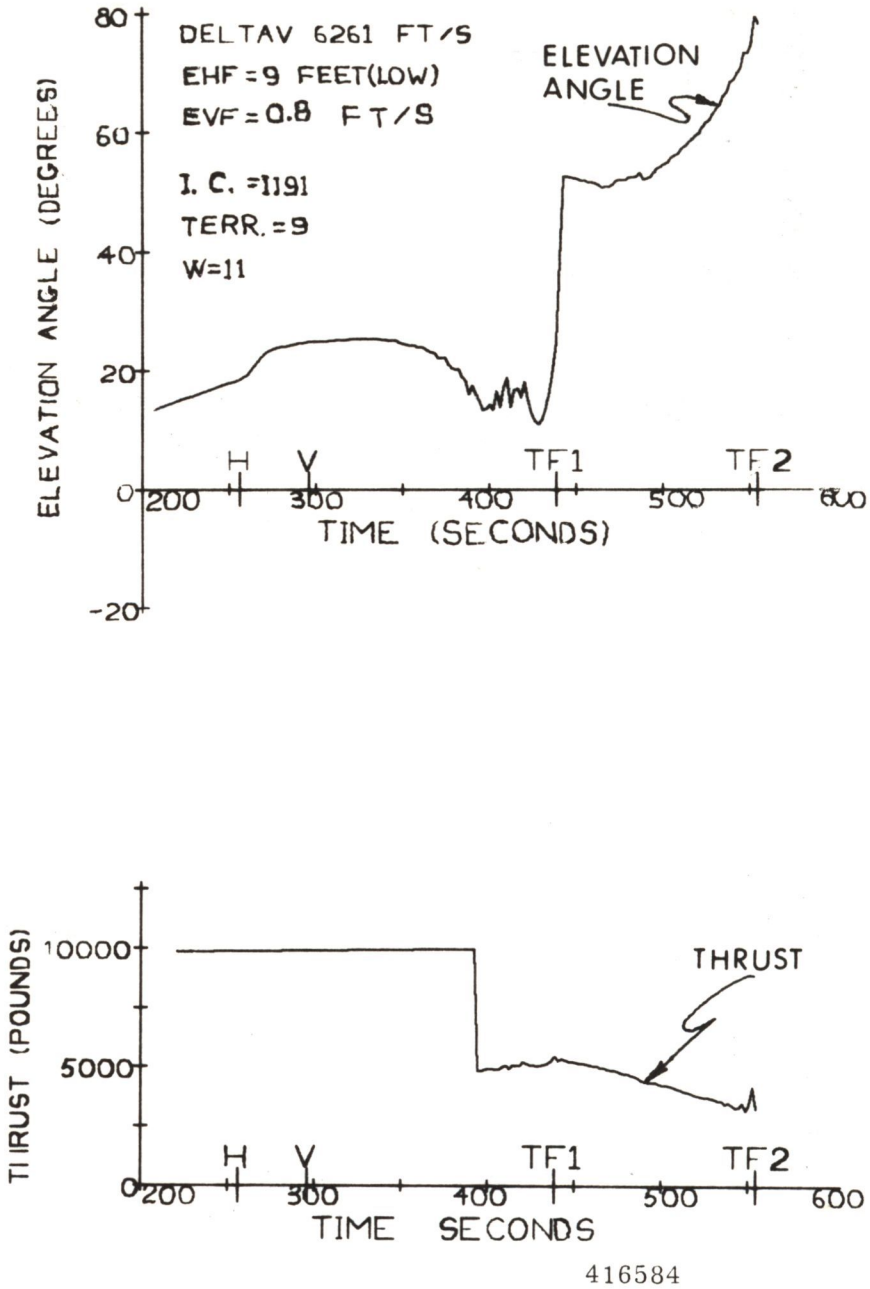

Fig. D. 6 Thrust-Vector Profiles: Severe Initial Errors, -1% DPS Uncertainty, Realistic Terrain, Original Empirical Weighting Functions.

APPENDIX E

THRUST-VECTOR PROFILES FOR LR WEIGHTING FUNCTIONS OF 0.1

Thrust-vector profiles are presented in this appendix for landing trajectories wherein LR weighting functions of 0.1 are used for all the LR altitude and velocity-component updatings. The important results from these data are given in Table 6.6 of this report and are discussed in Section 6.7.

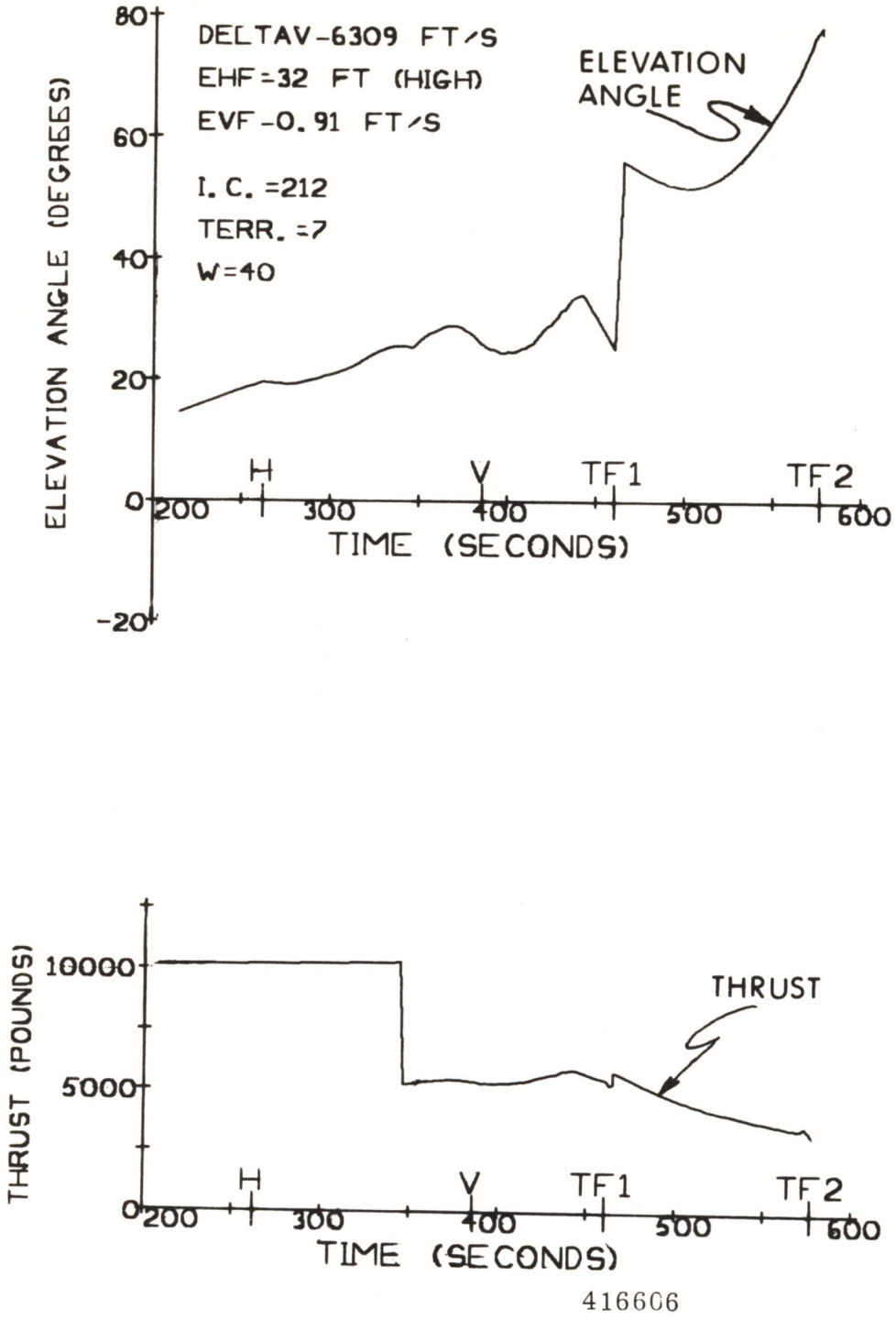

Fig. E.1 Thrust-Vector Profiles: Severe Initial Errors, +1% DPS Uncertainty, Realistic Terrain, Constant LR Weighting Functions of 0.1.

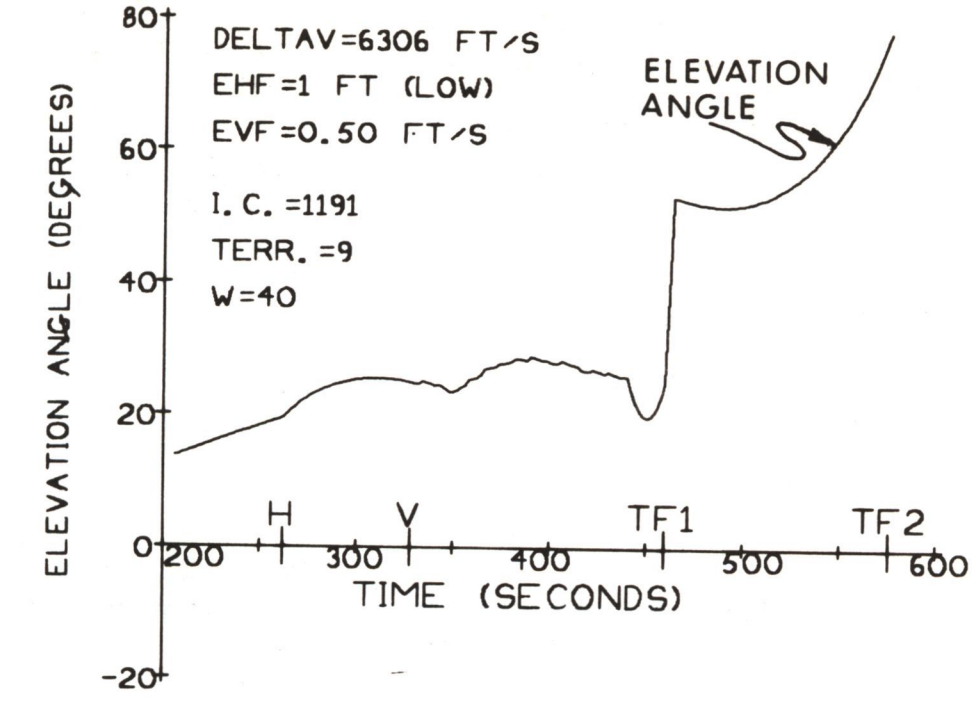

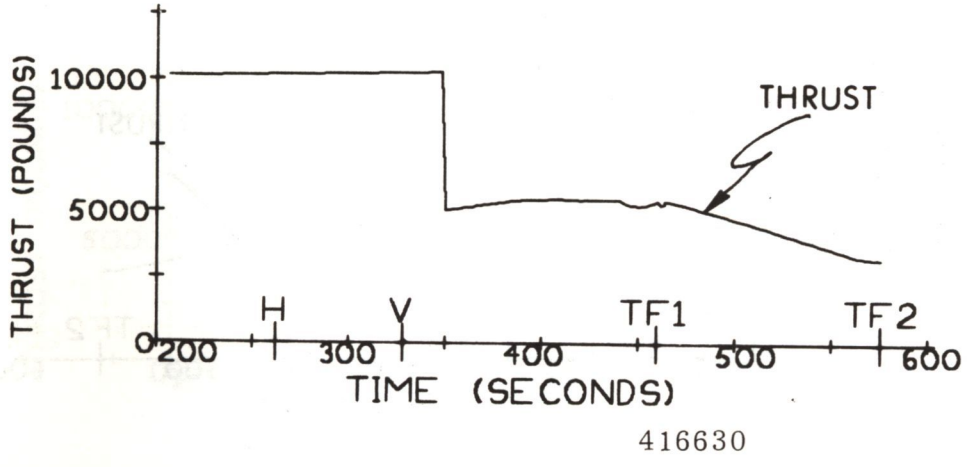

Fig. E.2 Thrust-Vector Profiles: Severe Initial Errors, +1% DPS Uncertainty, Realistic Terrain, Constant LR Weighting Functions of 0.1.

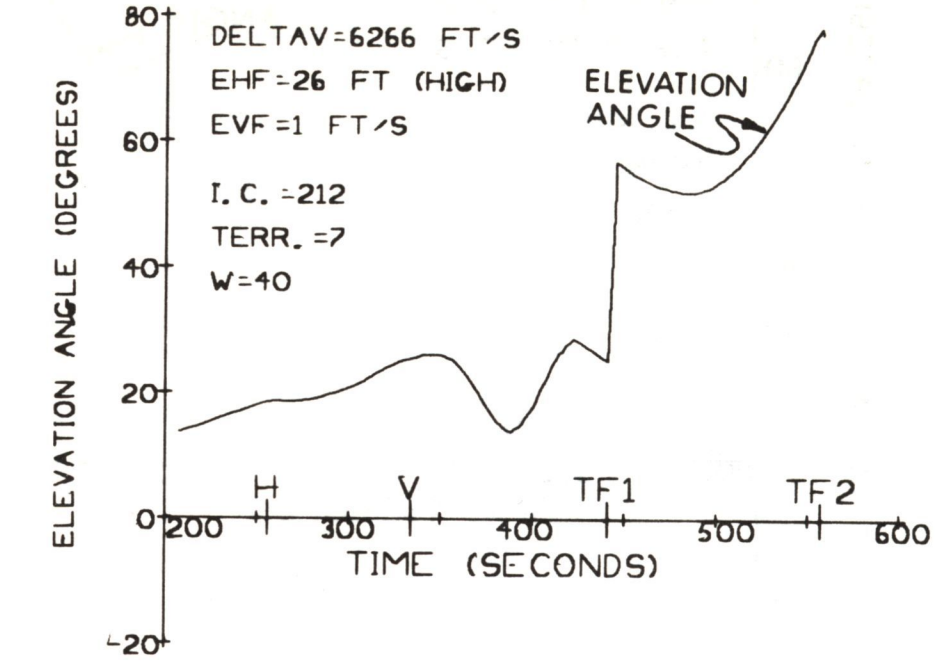

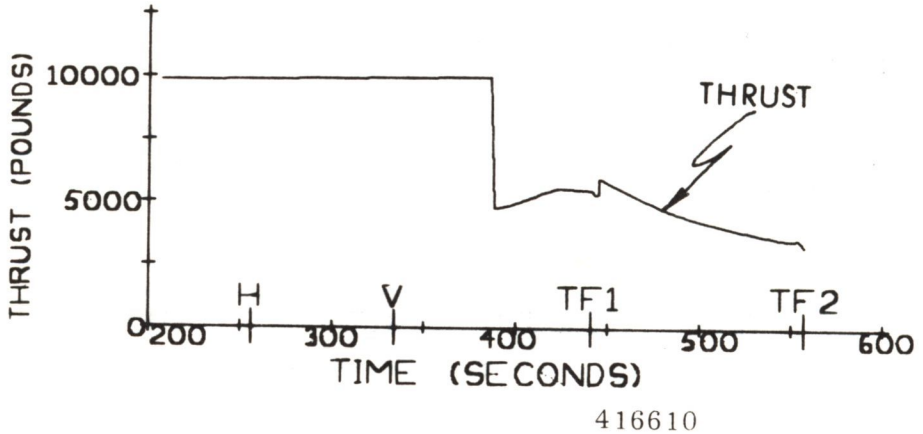

Fig. E. 3 Thrust-Vector Profiles: Severe Initial Errors, -1% DPS Uncertainty, Realistic Terrain, Constant LR Weighting Functions of 0. 1.

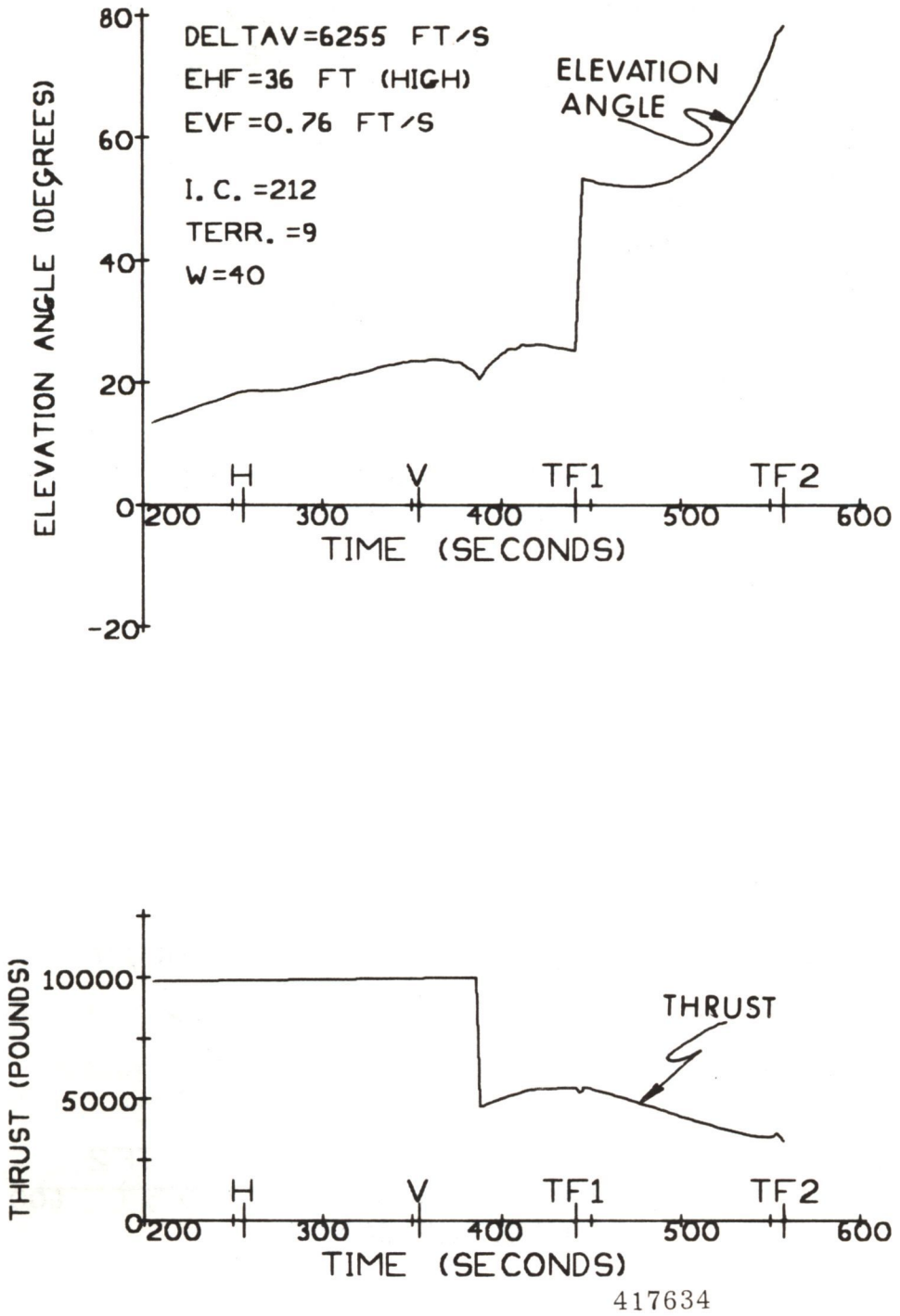

Fig. E.4 Thrust-Vector Profiles: Severe Initial Errors, -1% DPS Uncertainty, Realistic Terrain, Constant LR Weighting Functions of 0.1.

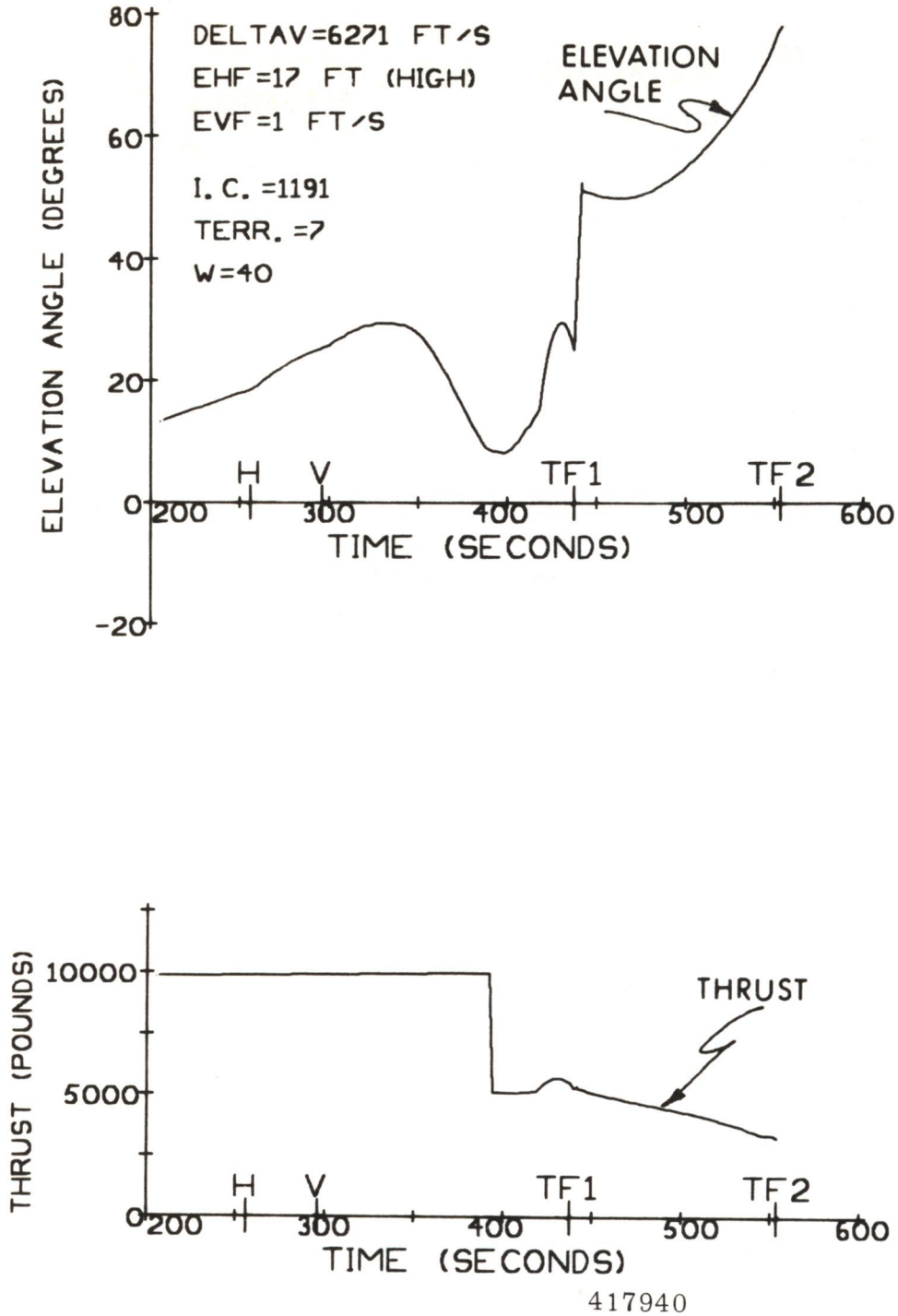

Fig. E. 5 Thrust-Vector Profiles: Severe Initial Errors, -1% DPS Uncertainty, Realistic Terrain, Constant LR Weighting Functions of 0.1.

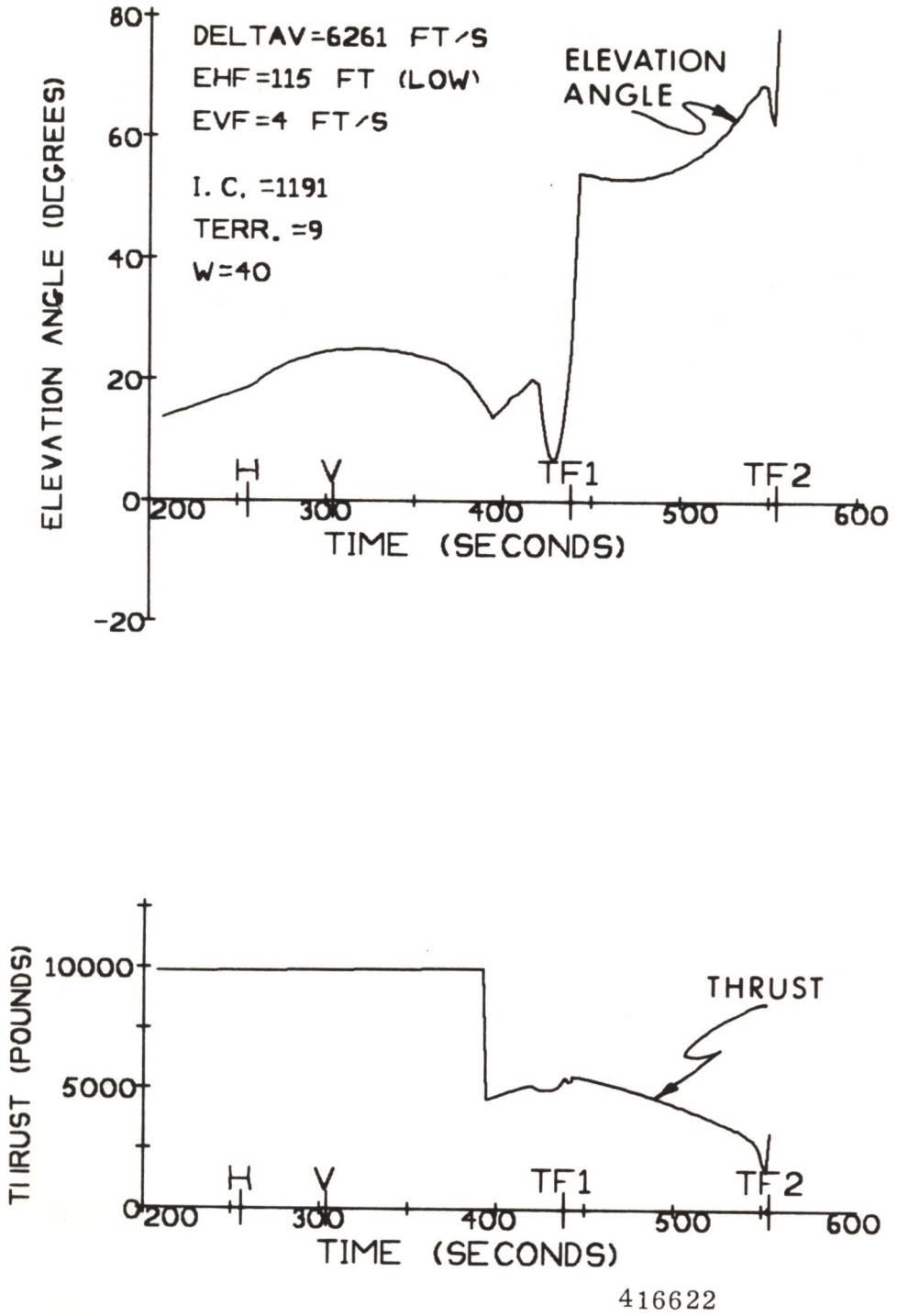

Fig. E.6 Thrust Vector Profiles: Severe Initial Errors, -1% DPS Uncertainty, Realistic Terrain, Constant LR Weighting Functions of 0.1.

APPENDIX F

THRUST-VECTOR PROFILES FOR LR WEIGHTING FUNCTIONS OF 0.9

Thrust-vector profiles are presented in this appendix for landing trajectories wherein LR weighting functions of 0.9 are used for all the LR and velocity-component updatings. The important results from these data are given in Table 6.7 of this report and are discussed in Section 6.7.

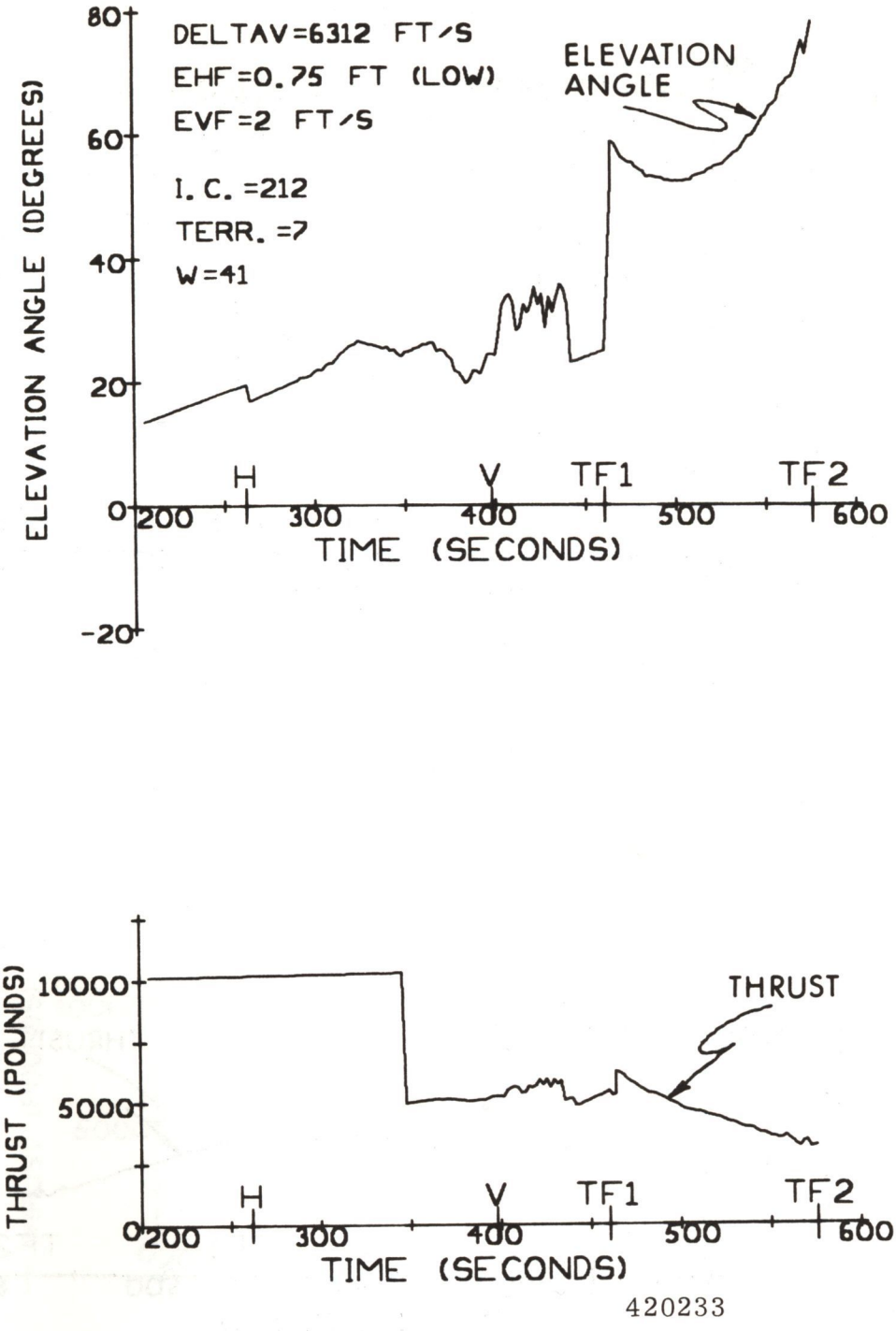

Fig. F.1 Thrust-Vector Profiles: Severe Initial Errors, +1% DPS Uncertainty, Realistic Terrain, Constant LR Weighting Functions of 0.9

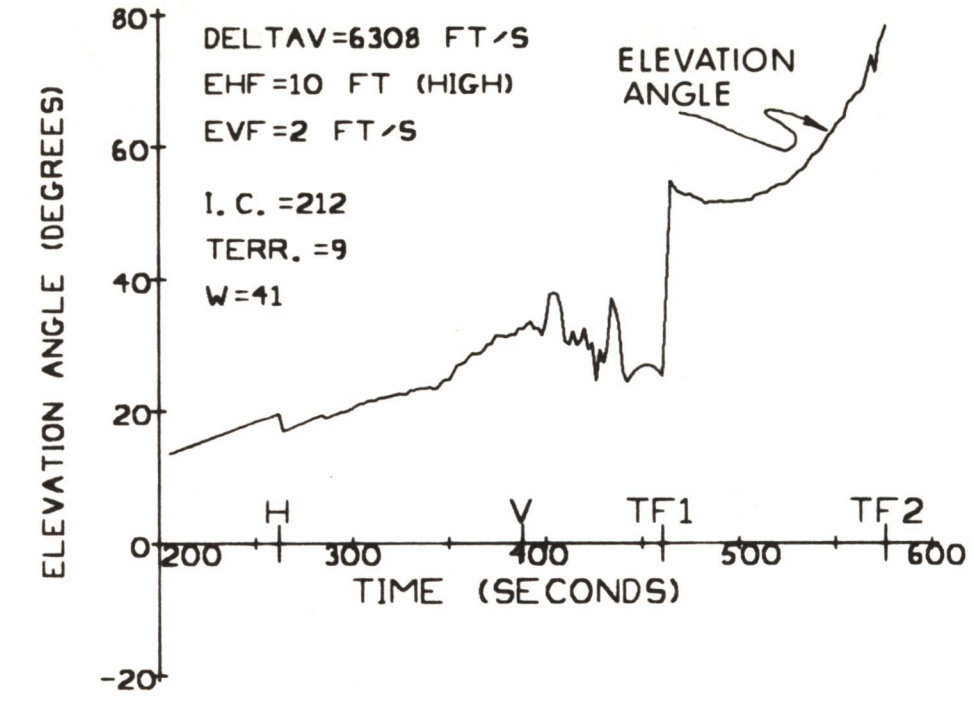

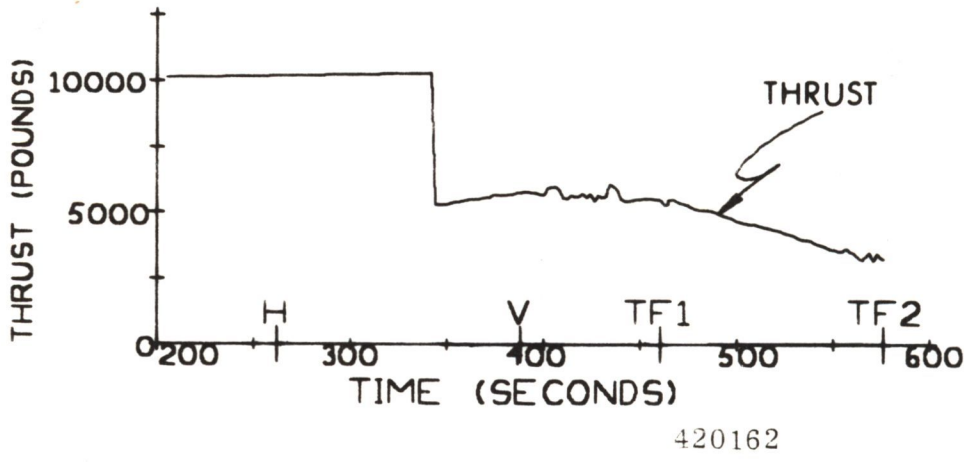

Fig. F.2 Thrust-Vector Profiles: Severe Initial Errors, +1% DPS Uncertainty, Realistic Terrain, Constant LR Weighting Functions of 0.9.

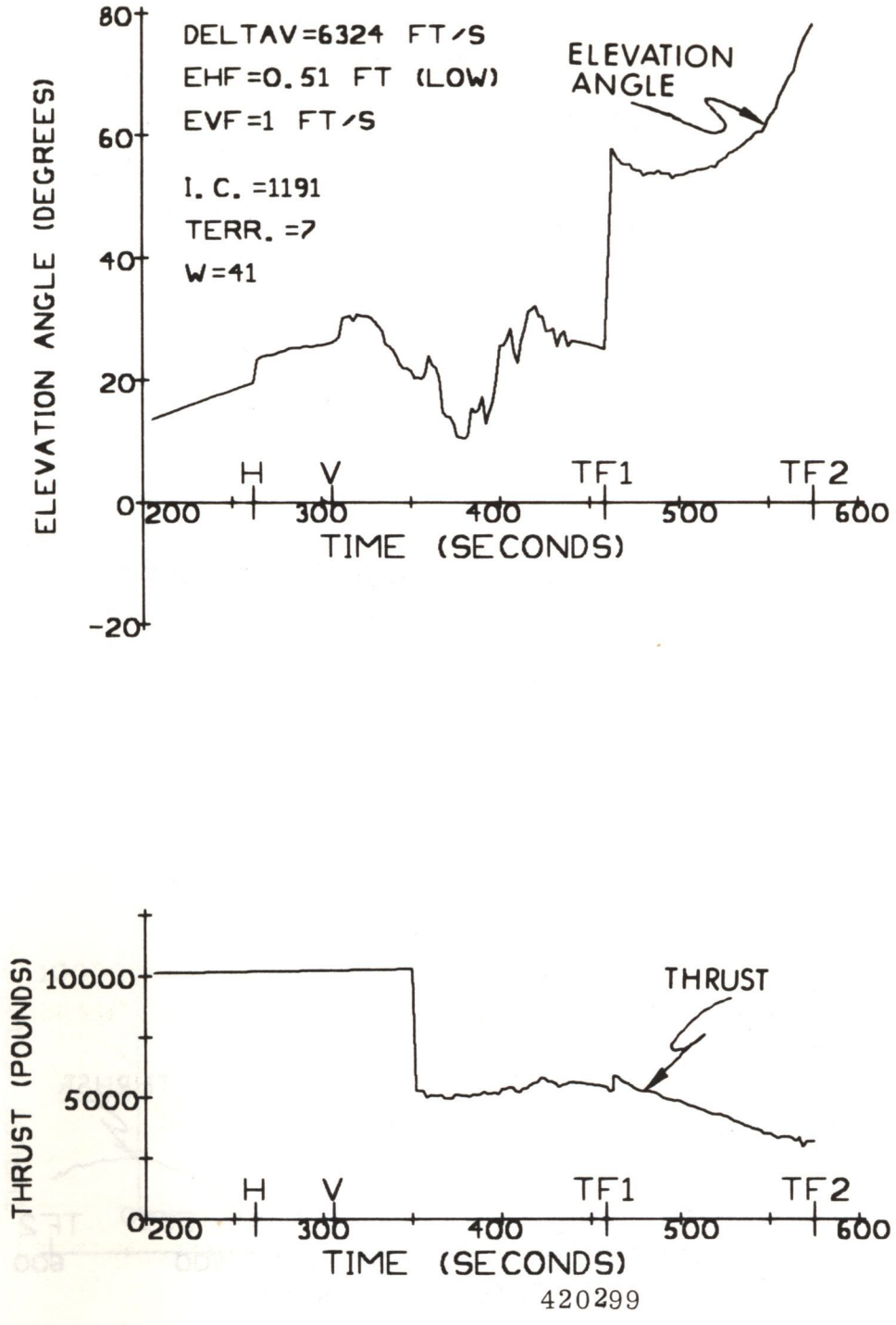

Fig. F.3 Thrust-Vector Profiles: Severe Initial Errors, +1% DPS Uncertainty, Realistic Terrain, Constant LR Weighting Functions of 0.9.

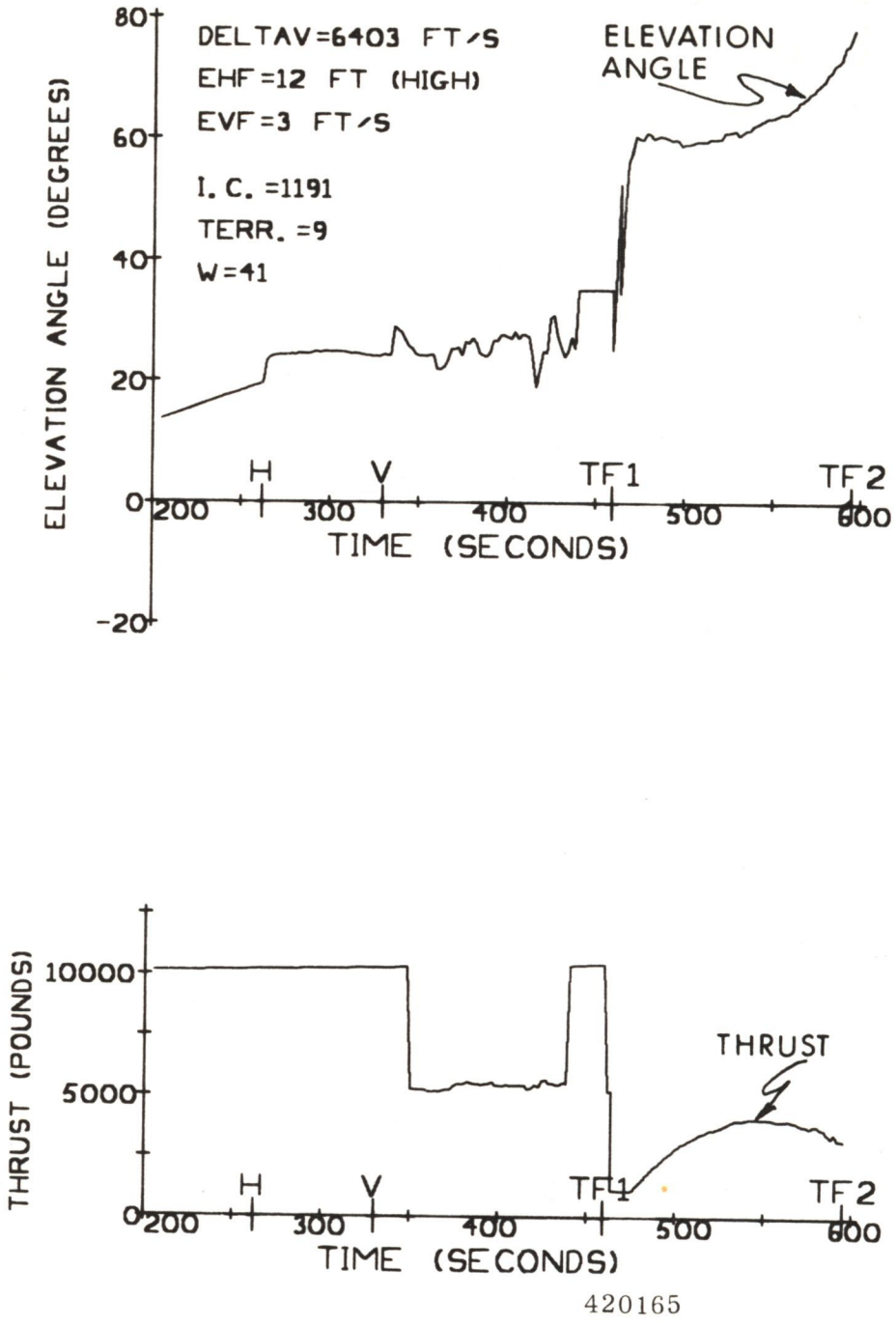

Fig. F.4 Thrust-Vector Profiles: Severe Initial Errors, +1% DPS Uncertainty, Realistic Terrain, Constant LR Weighting Functions of 0.9.

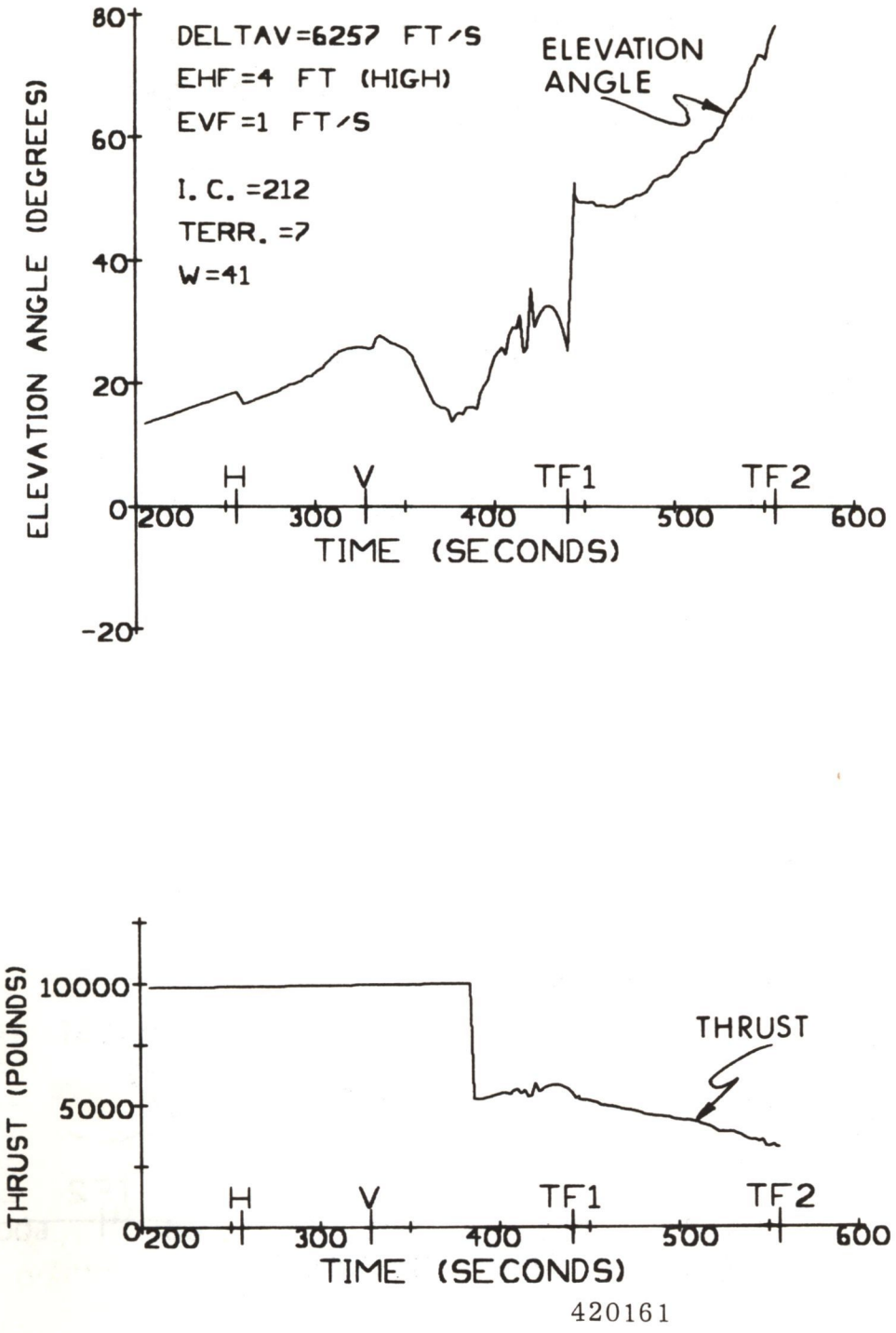

Fig. F.5 Thrust-Vector Profiles: Severe Initial Errors, -1% DPS Uncertainty, Realistic Terrain, Constant LR Weighting Functions of 0.9.

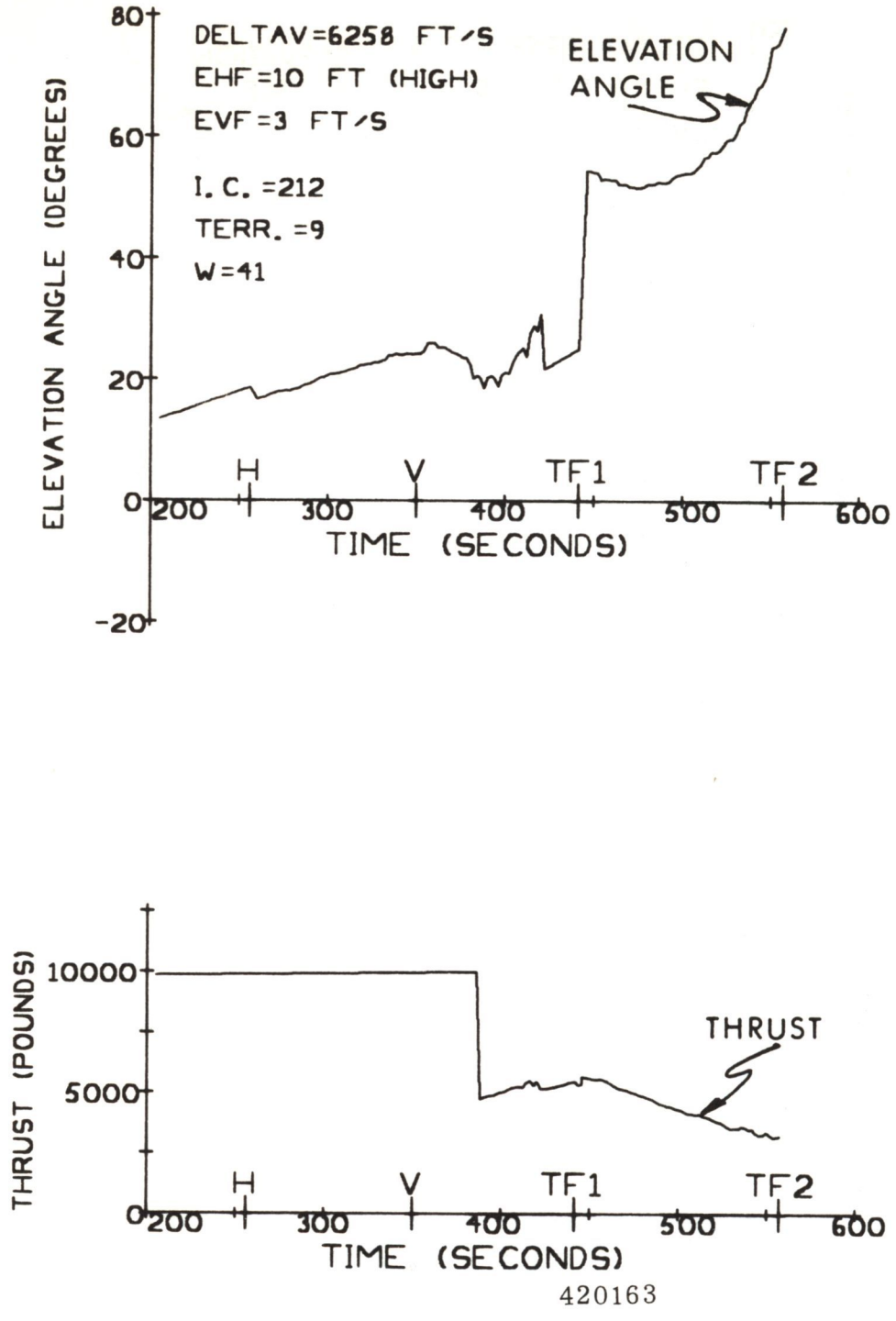

Fig. F.6 Thrust-Vector Profiles: Severe Initial Errors, -1% DPS Uncertainty, Realistic Terrain, Constant LR Weighting Functions of 0.9.

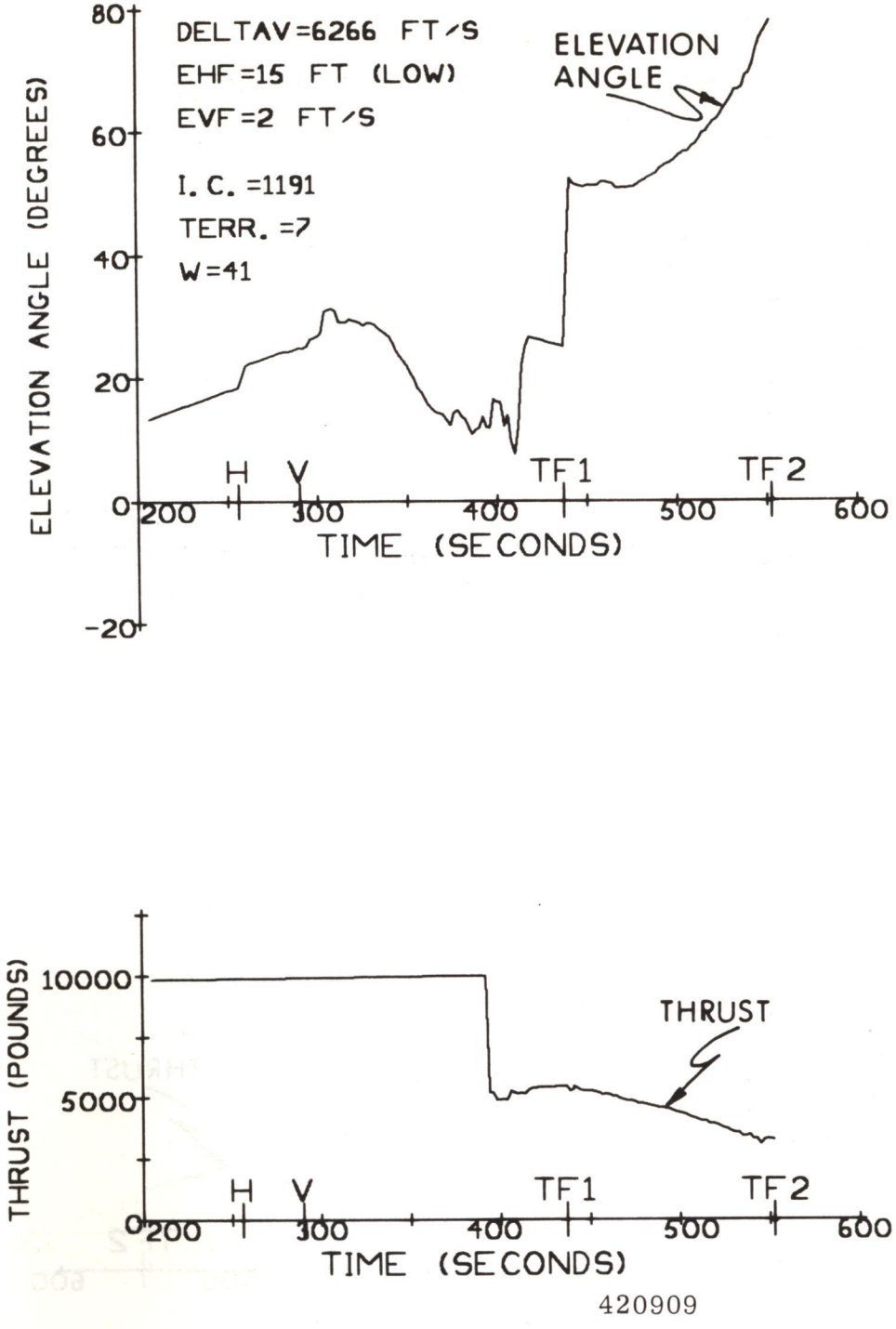

Fig. F.7 Thrust-Vector Profiles: Severe Initial Errors, -1% DPS Uncertainty, Realistic Terrain, Constant LR Weighting Function of 0.9.

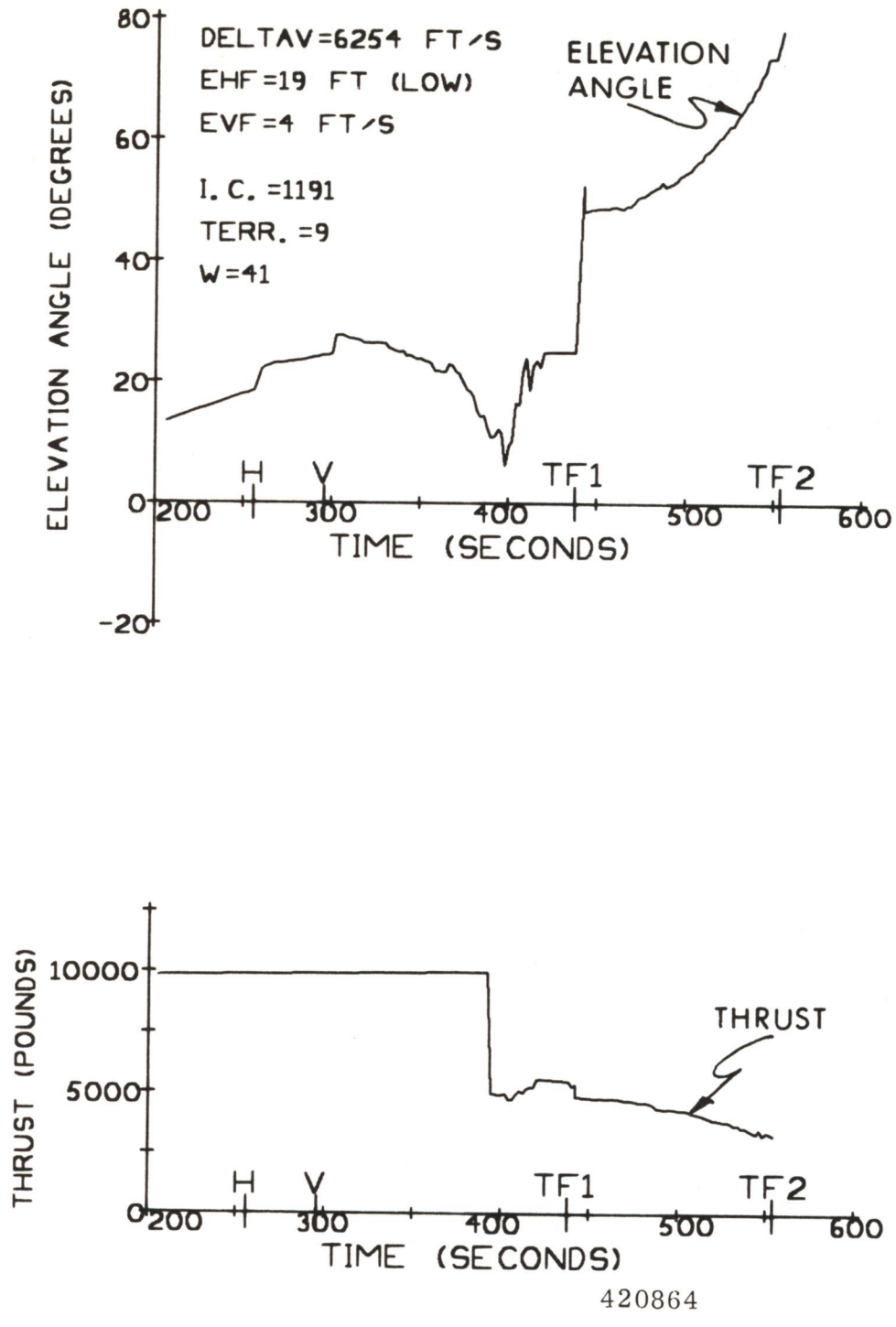

Fig. F.8 Thrust-Vector Profiles: Severe Initial Errors, -1% DPS Uncertainty, Realistic Terrain, Constant LR Weighting Functions of 0.9.

APPENDIX G

THRUST-VECTOR PROFILES FOR OPTIMUM UNCOUPLED LR WEIGHTING FUNCTIONS

Thrust-vector profiles are presented in this appendix for landing trajectories wherein the optimum uncoupled landing-radar weighting functions were used. These weighting functions are given in Fig. 4.3 of this report. The key numerical results for these trajectories are given in Table 6.8 and are discussed in Section 6.7.

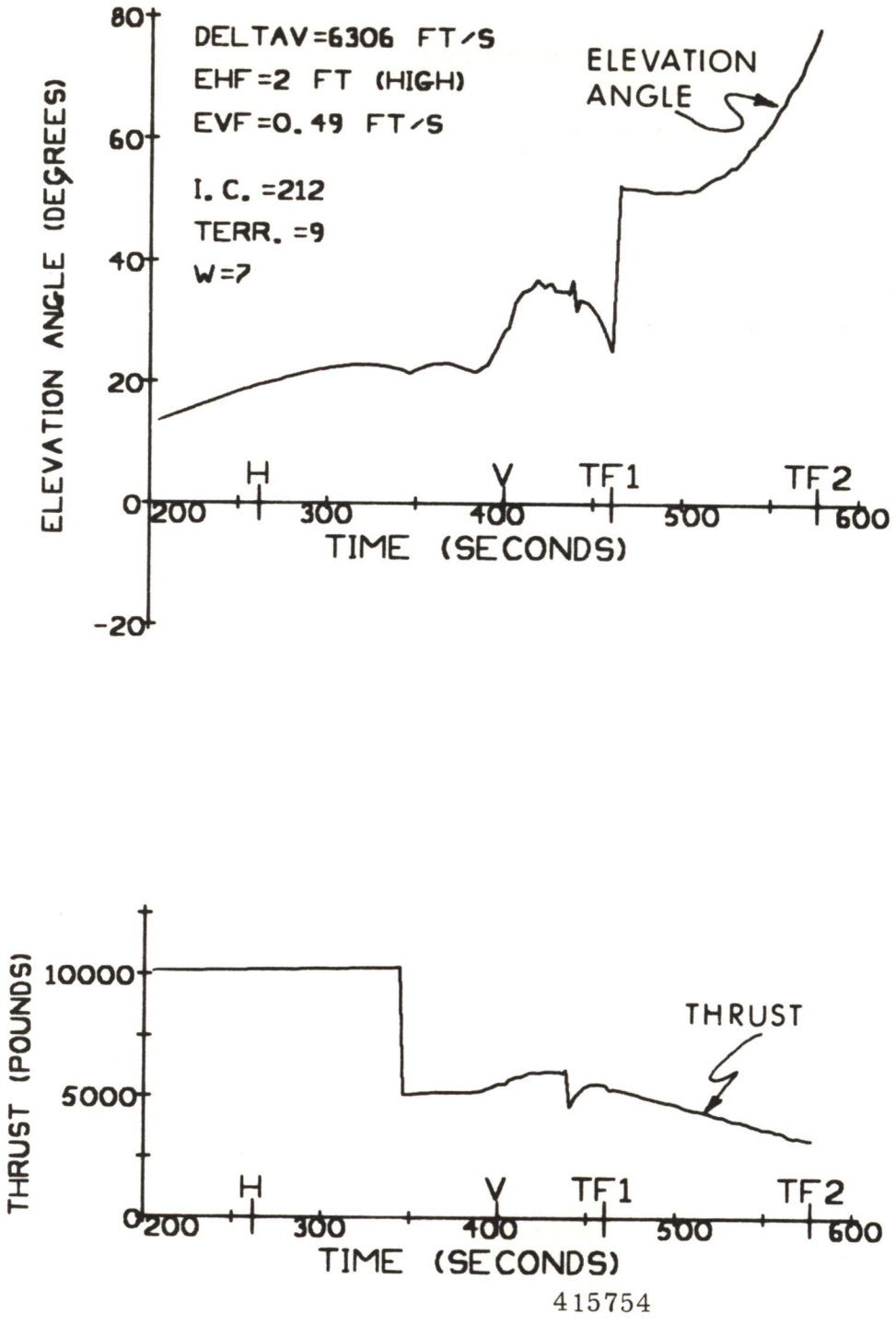

Fig. G.1 Thrust-Vector Profiles: Severe Initial Errors, ±1% DPS Uncertainty, Realistic Terrain, Optimum Uncoupled LR Weighting Functions.

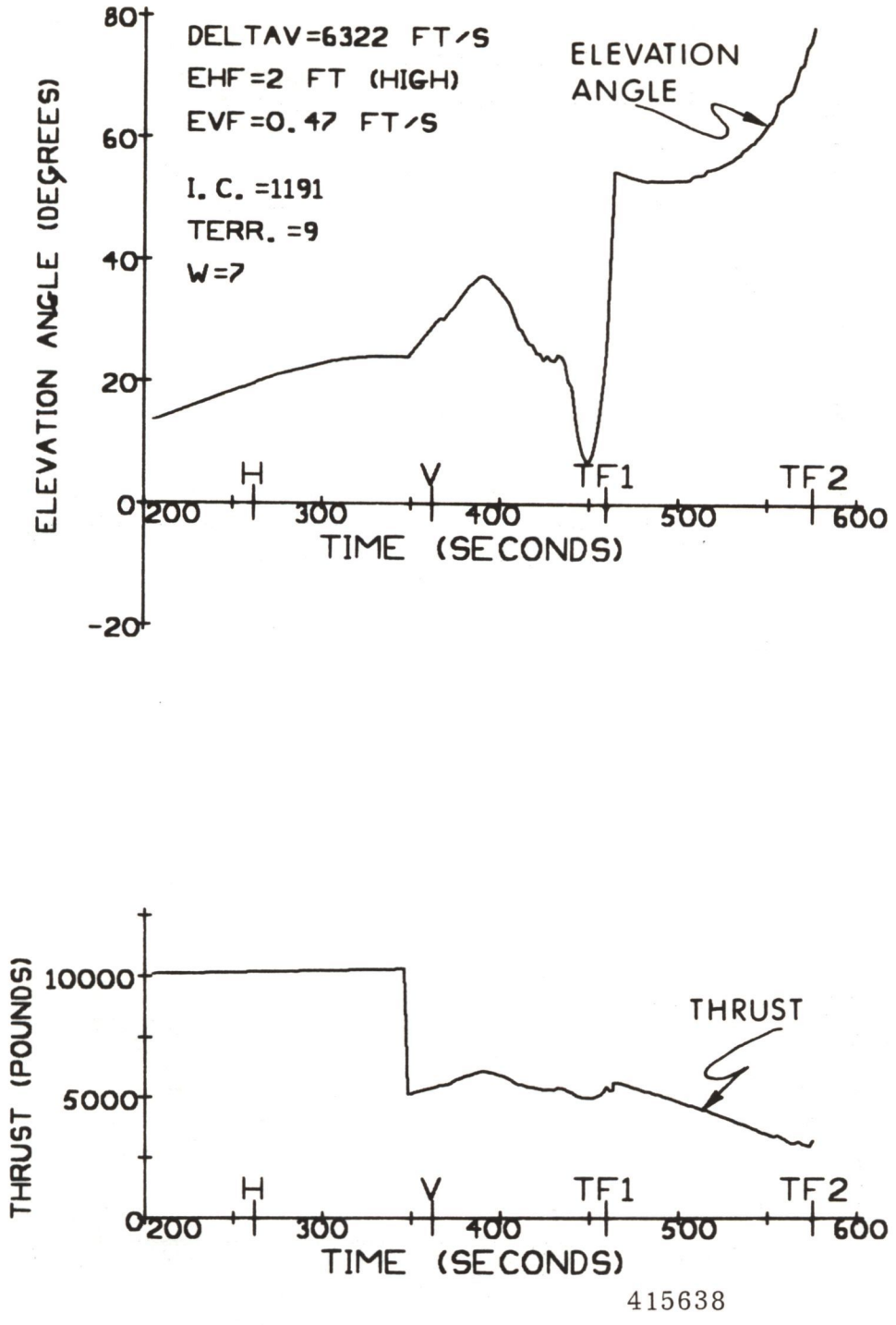

Fig. G. 2 Thrust-Vector Profiles: Severe Initial Errors, +1% DPS Uncertainty, Realistic Terrain, Optimum Uncoupled LR Weighting Functions.

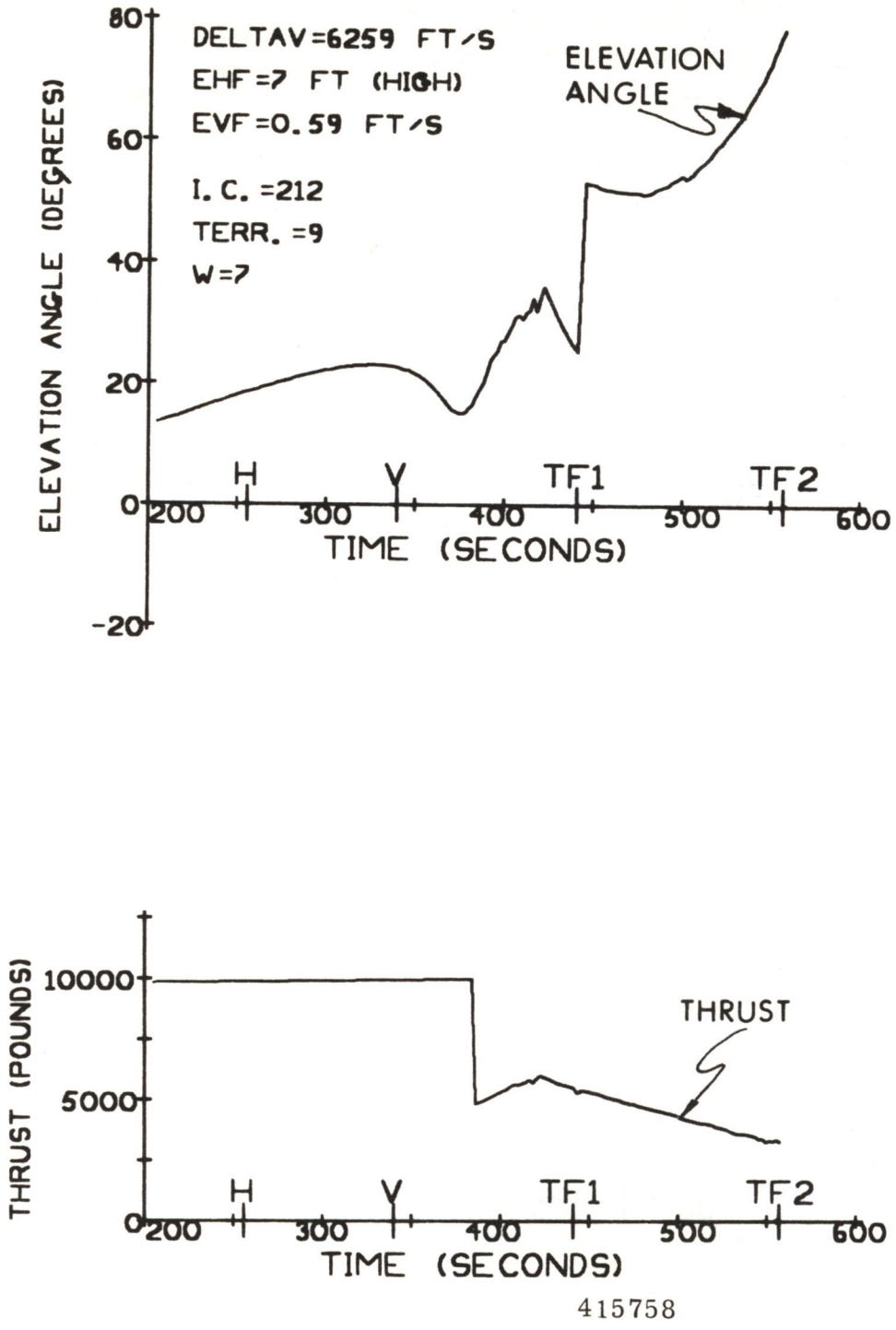

Fig. G. 3 Thrust-Vector Profiles: Severe Initial Errors, -1% DPS Uncertainty, Realistic Terrain, Optimum Uncoupled LR Weighting Functions.

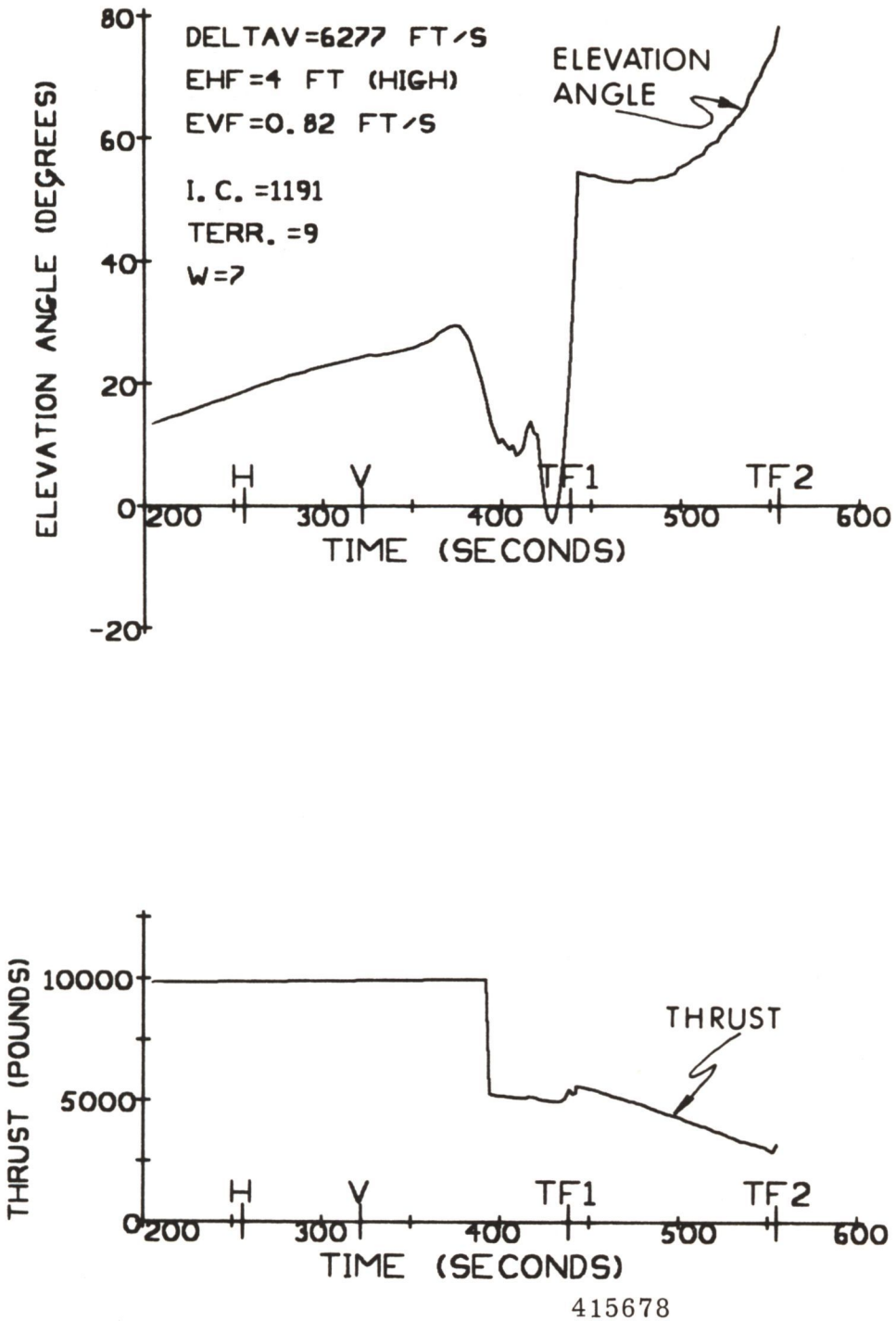

Fig. G.4 Thrust-Vector Profiles: Severe Initial Errors, -1% DPS Uncertainty, Realistic Terrain, Optimum Uncoupled LR Weighting Functions.

APPENDIX H

THRUST-VECTOR PROFILES FOR LINEARIZED WEIGHTING FUNCTIONS 6667-FOOT HIGH-GATE ALTITUDE

Thrust-vector profiles are presented in this appendix for landing trajectories wherein the landing-radar weighting functions used are linear approximations to the optimum uncoupled ones. These weighting functions are given in Fig. 2.3 of this report. The important results from these data are summarized in Table 6.9 and Section 6.7.

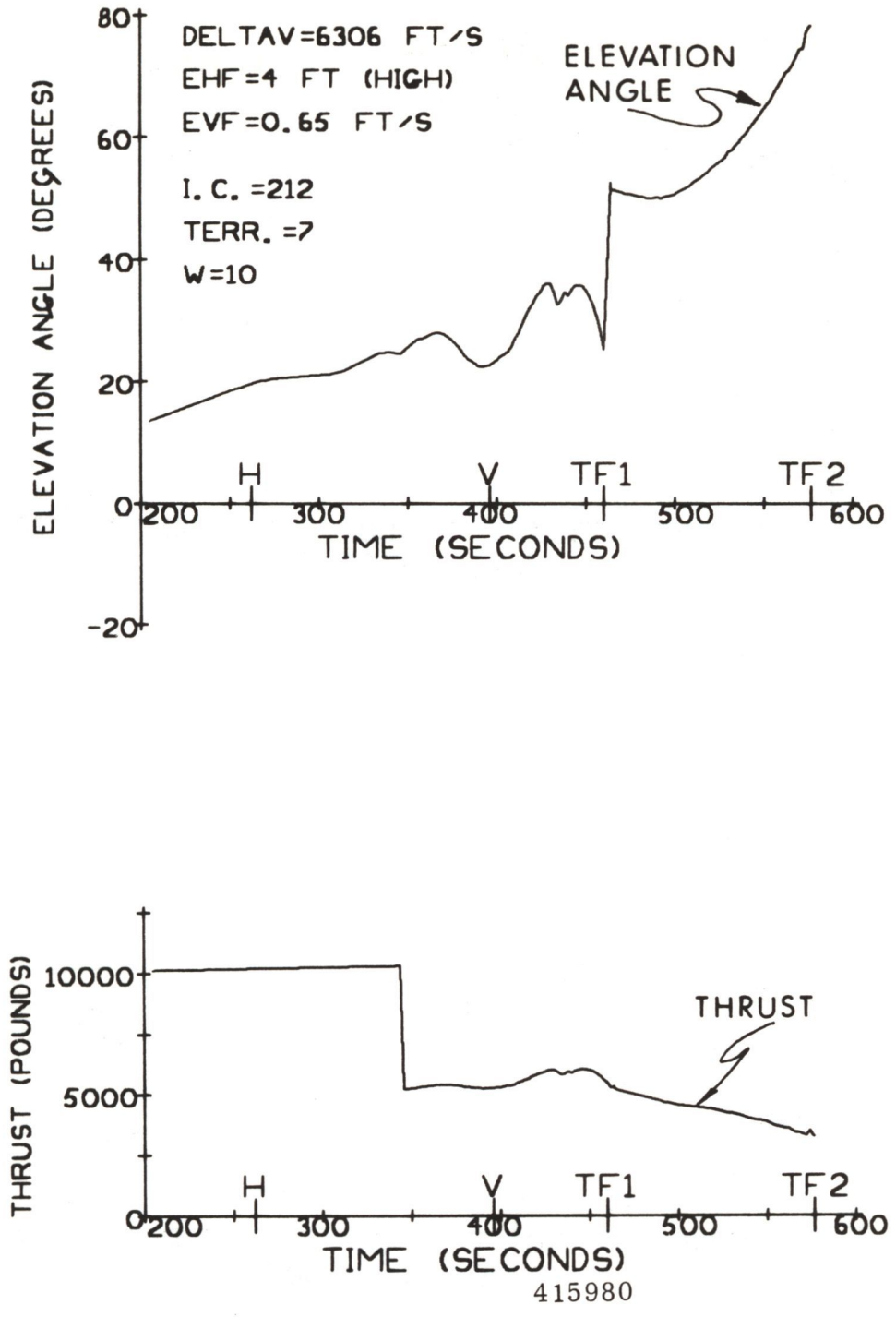

Fig. H.1 Thrust-Vector Profiles: Severe Initial Errors, +1% DPS Uncertainty, Realistic Terrain, Linearized LR Weighting Functions.

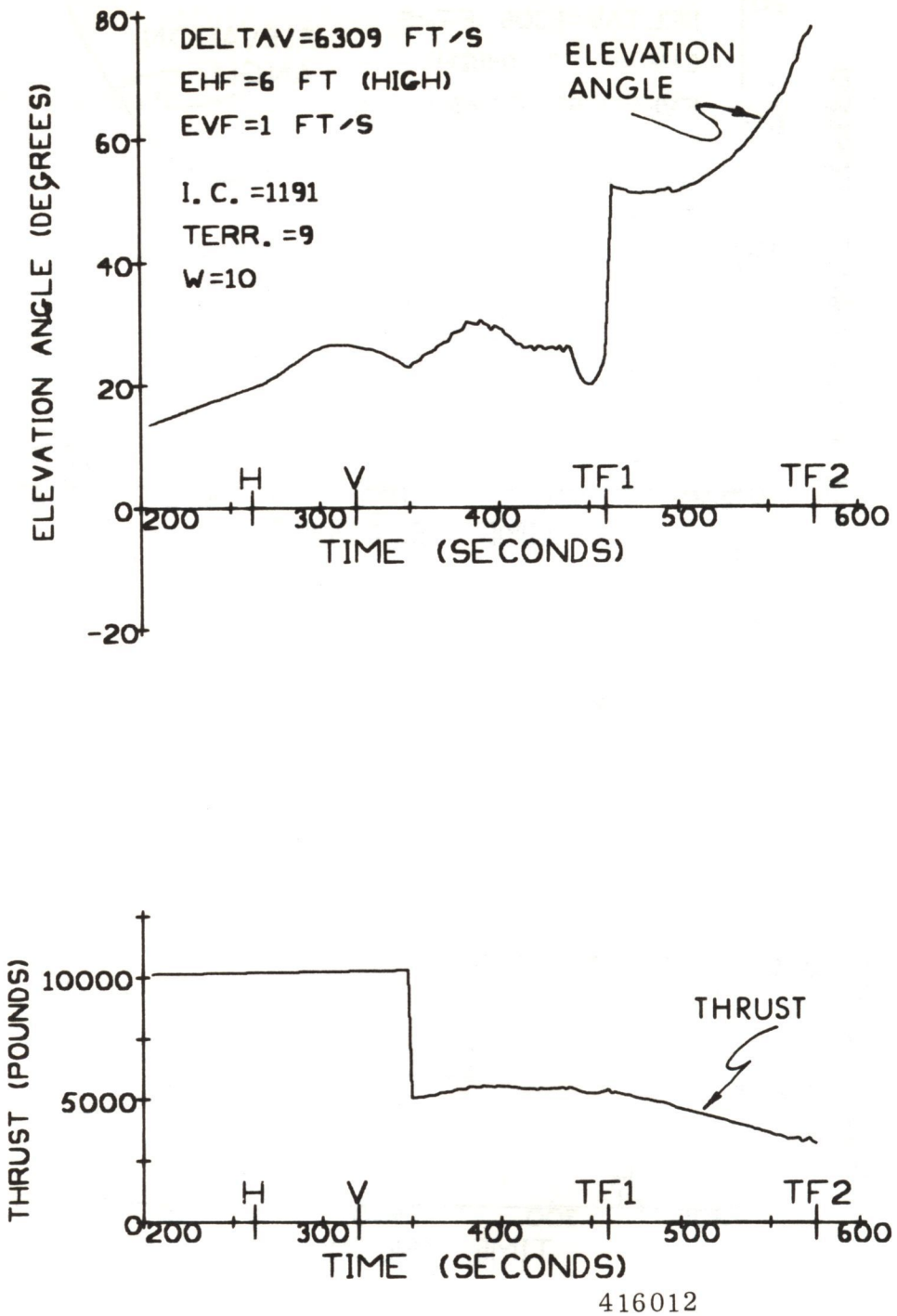

Fig. H.2 Thrust-Vector Profiles: Severe Initial Errors, ±1% DPS Uncertainty, Realistic Terrain, Linearized LR Weighting Functions.

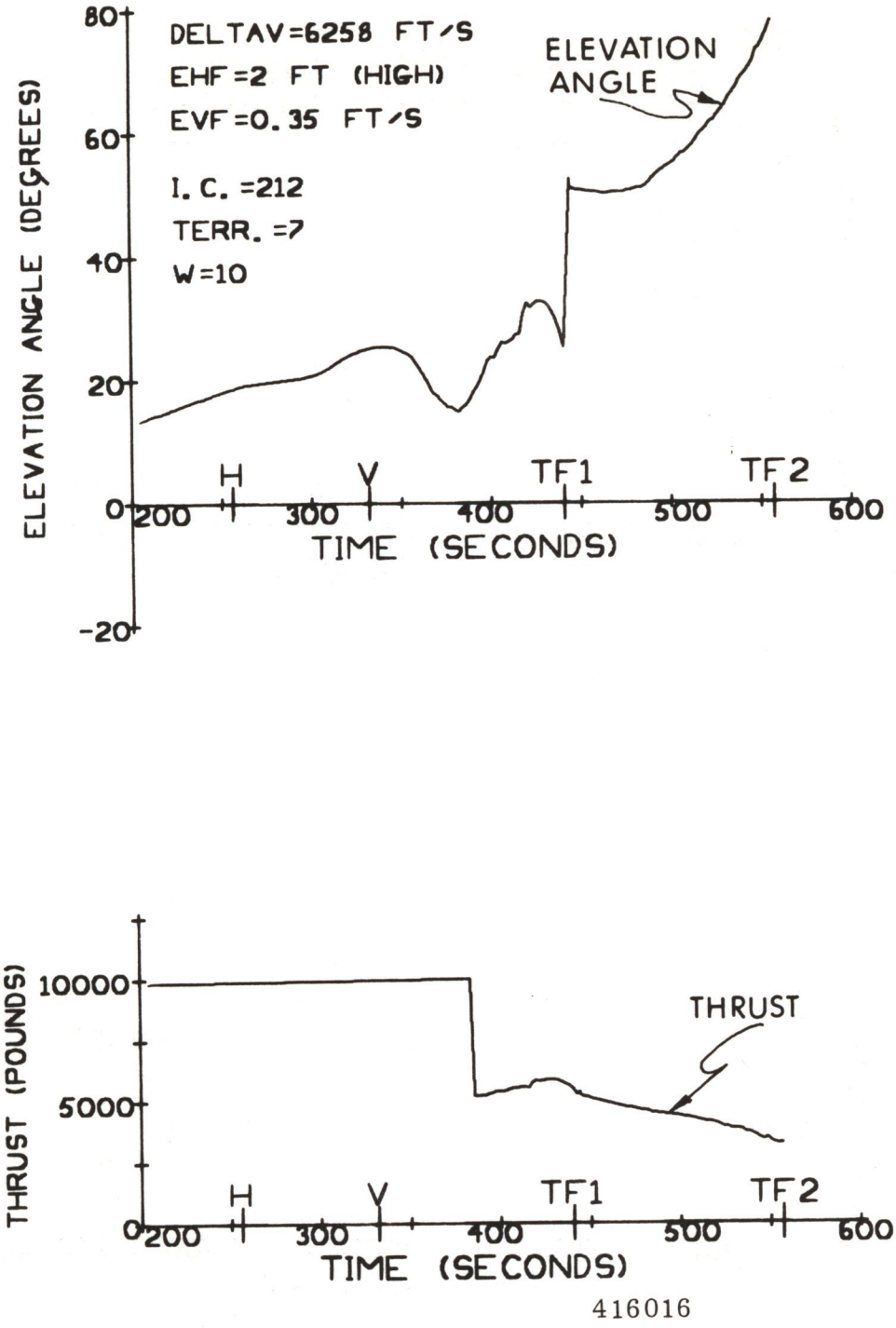

Fig. H.3 Thrust-Vector Profiles: Severe Initial Errors, -1% DPS Uncertainty, Realistic Terrain, Linearized LR Weighting Functions.

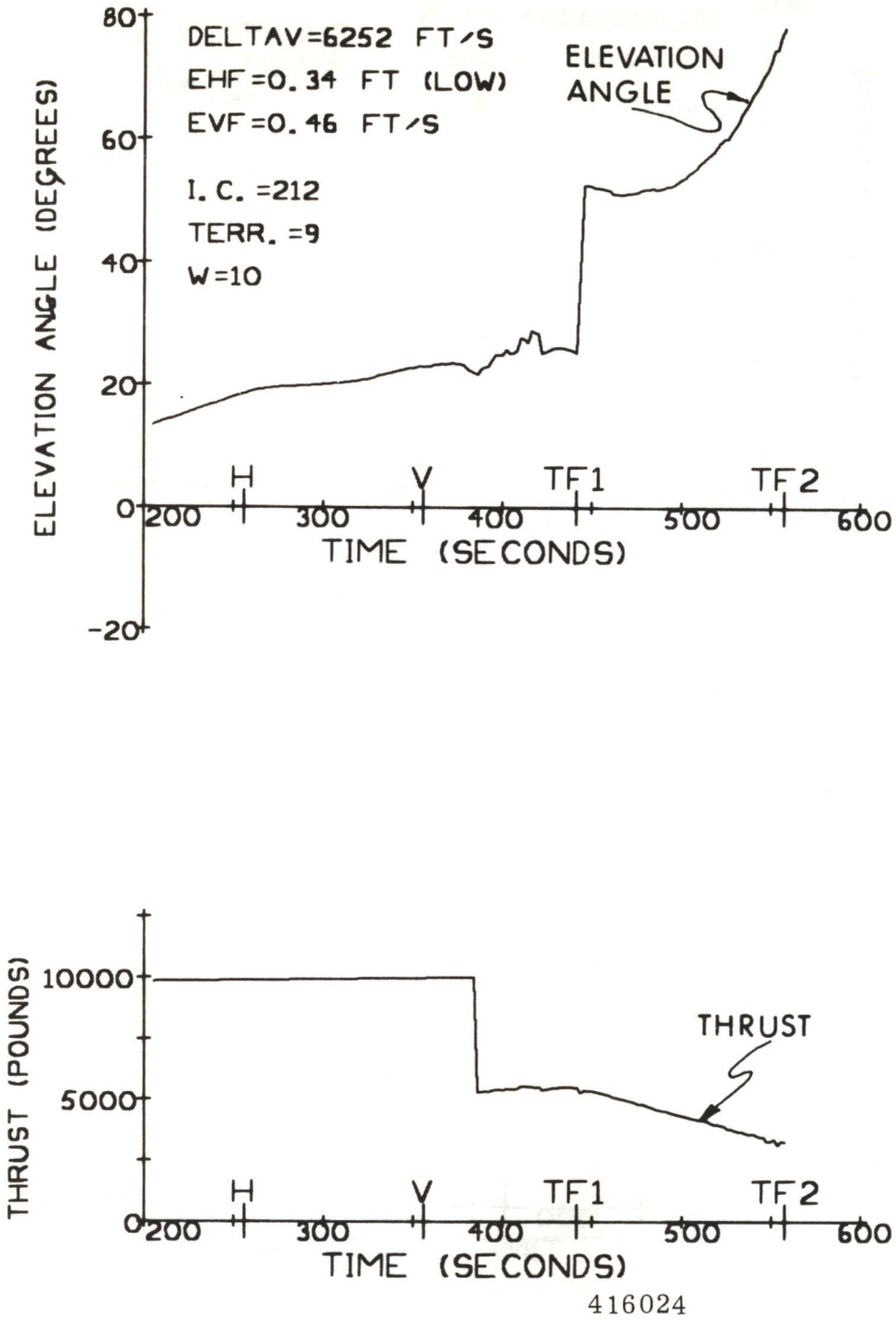

Fig. H.4 Thrust-Vector Profiles: Severe Initial Errors, -1% DPS Uncertainty, Realistic Terrain, Linearized LR Weighting Functions.

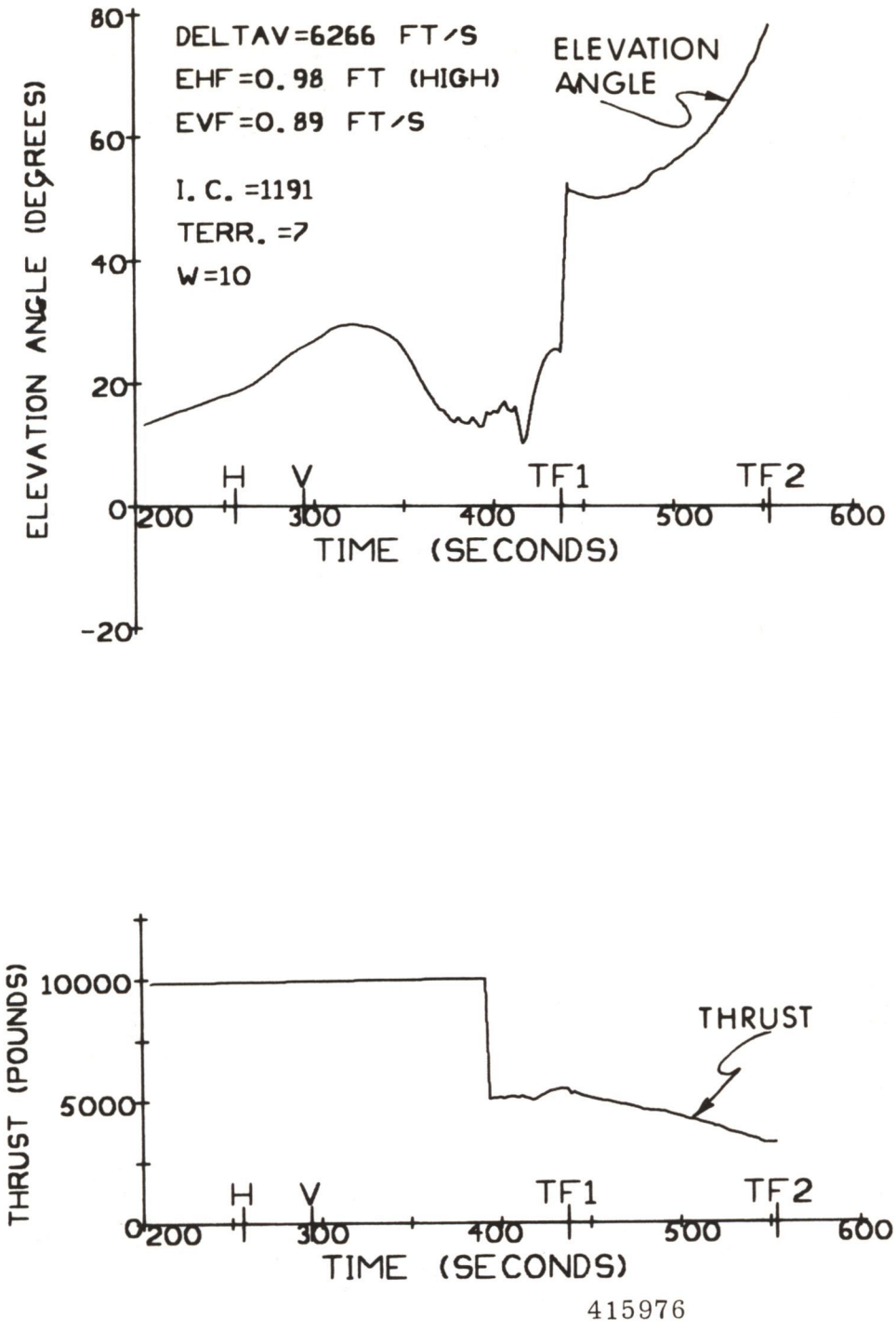

Fig. H.5 Thrust-Vector Profiles: Severe Initial Errors, -1% DPS Uncertainty, Realistic Terrain, Linearized LR Weighting Functions.

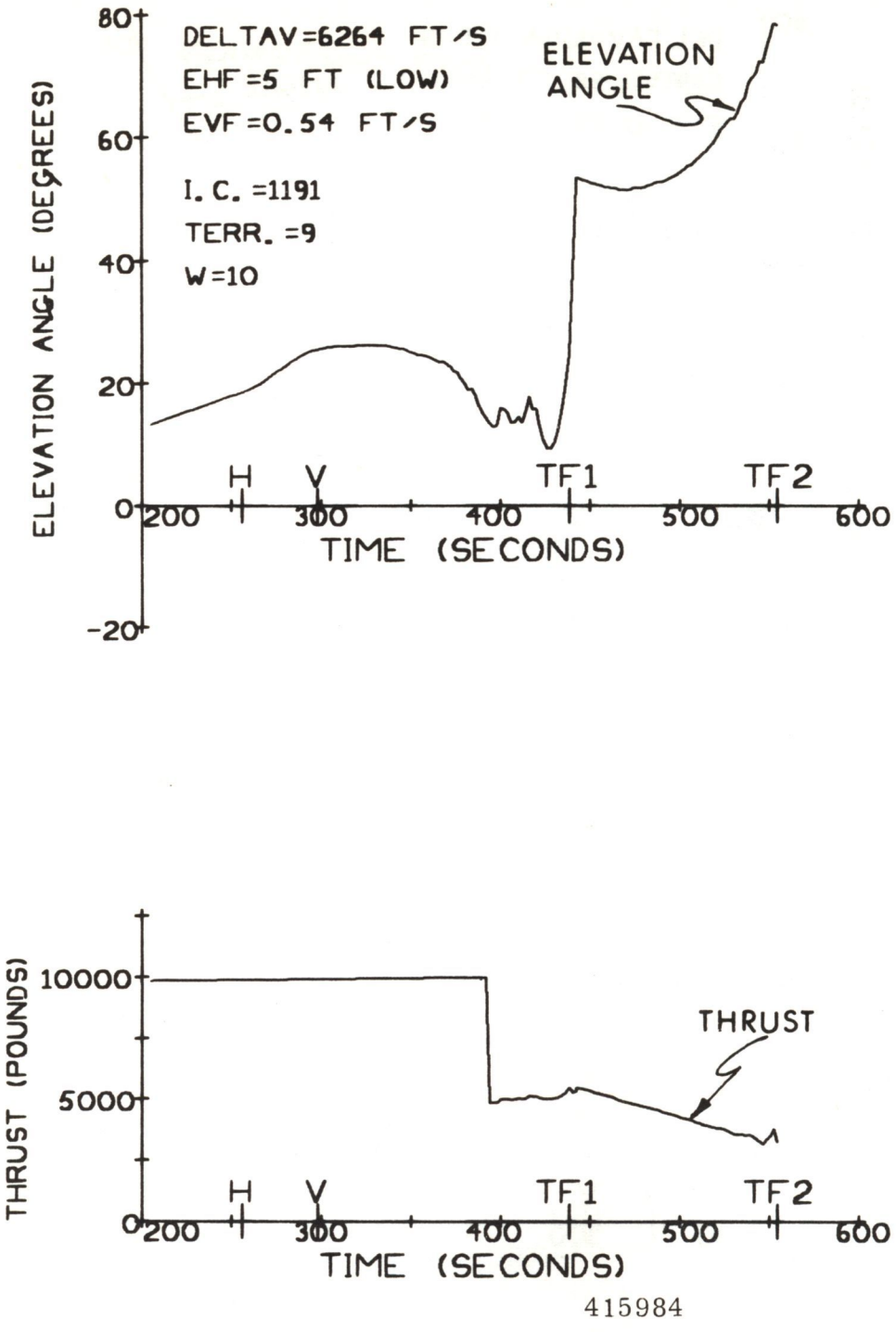

Fig. H.6 Thrust-Vector Profiles: Severe Initial Errors, -1% DPS Uncertainty, Realistic Terrain, Linearized LR Weighting Functions.

APPENDIX I

THRUST-VECTOR PROFILES FOR LINEARIZED WEIGHTING FUNCTIONS, 9200-FOOT HIGH-GATE ALTITUDE

Thrust-vector profiles are presented in this appendix for landing trajectories to a 9200-Foot High-Gate altitude. The DPS is nominally throttled down 80 seconds before the end of the visibility phase in these runs. The landing-radar weighting functions used here are linear approximations to the optimum uncoupled ones. These weighting functions are given in Fig. 2.3 of this report. The important results from these data are summarized in Table 6.9 and Section 6.10.

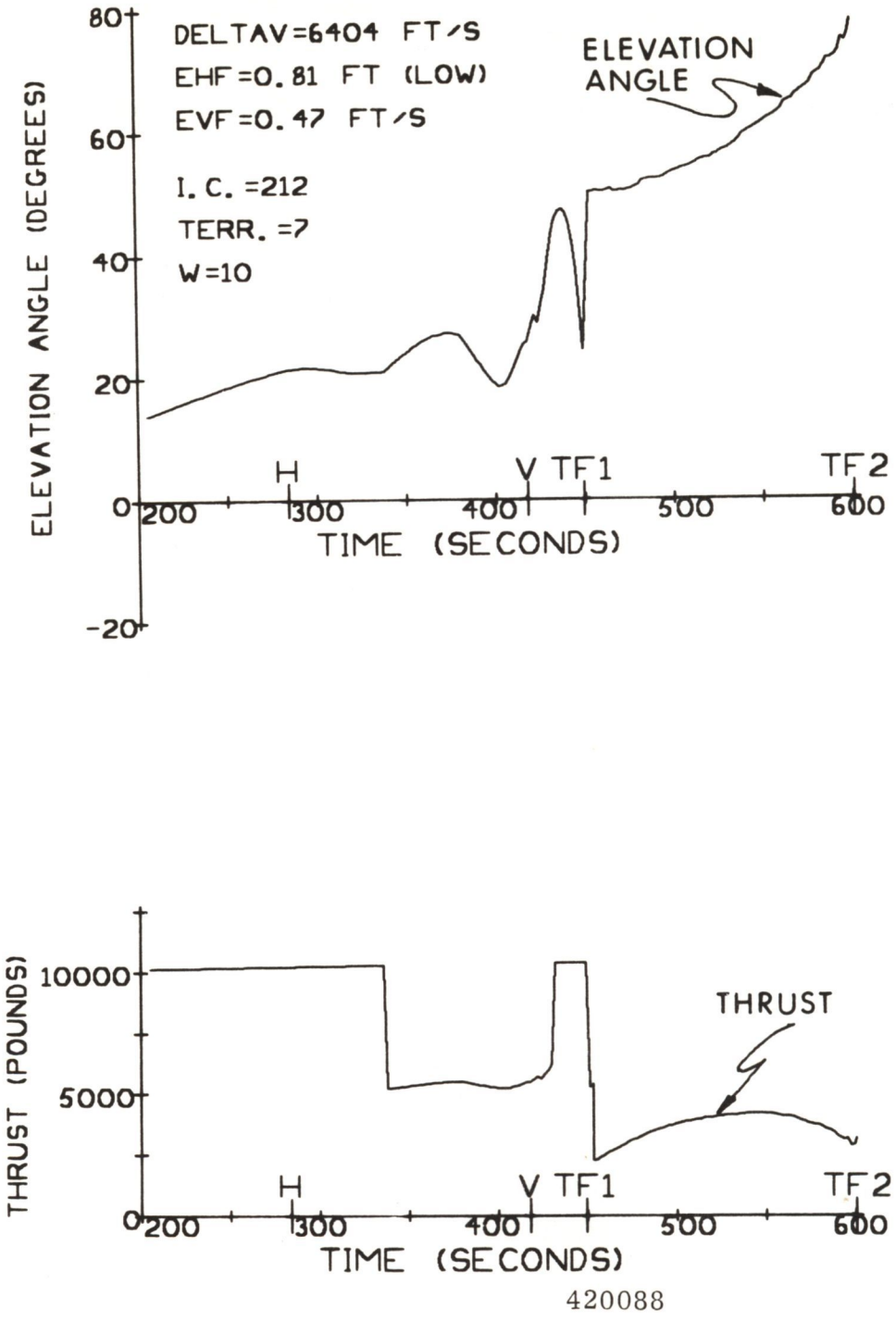

Fig. I.1 Thrust-Vector Profiles: Severe Initial Errors, +1% DPS Uncertainty, Realistic Terrain, Linearized LR Weighting Functions.

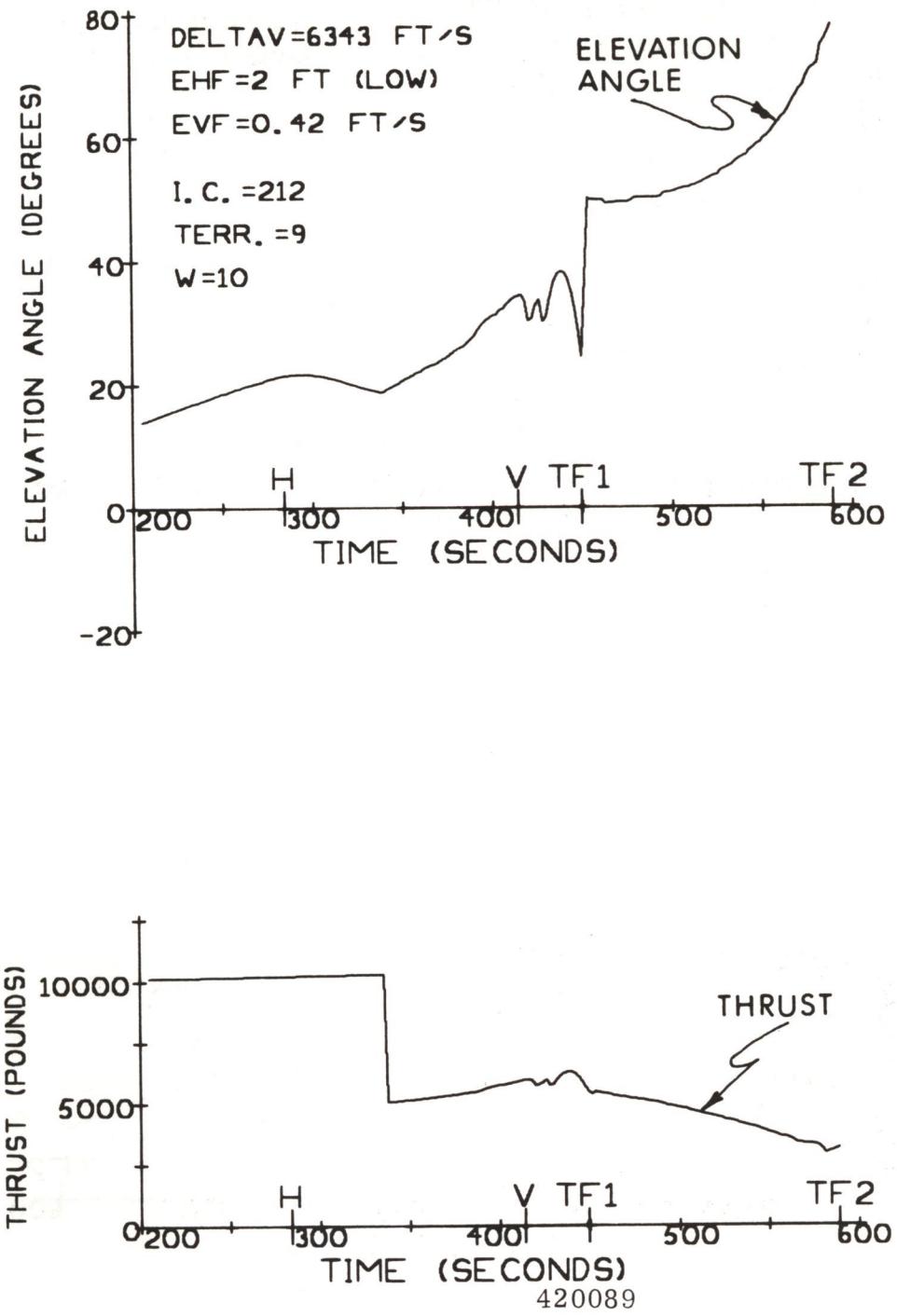

Fig. I.2 Thrust-Vector Profiles: Severe Initial Errors, +1% DPS Uncertainty, Realistic Terrain, Linearized LR Weighting Functions.

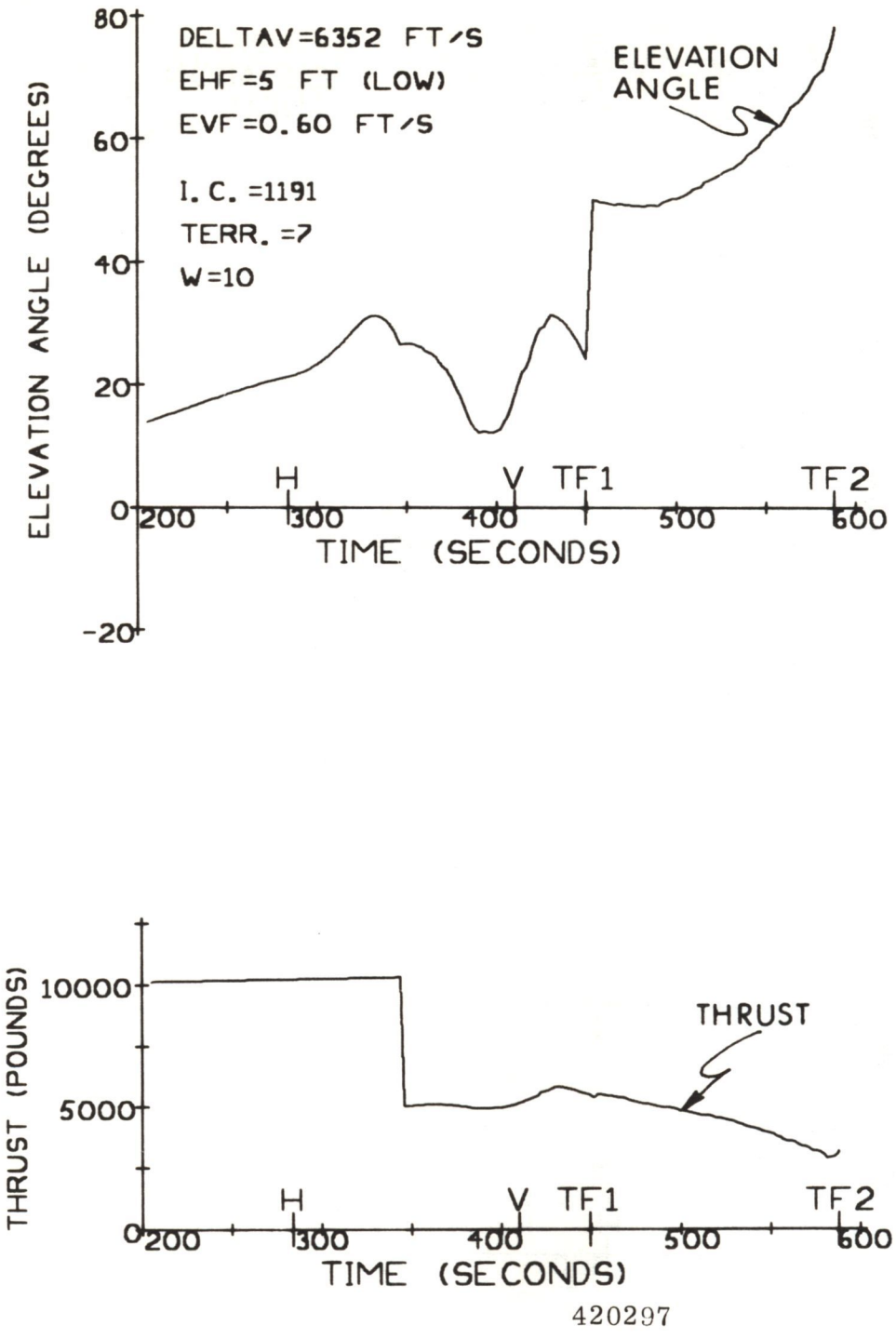

Fig. I. 3 Thrust-Vector Profiles: Severe Initial Errors, +1% DPS Uncertainty, Realistic Terrain, Linearized LR Weighting Functions.

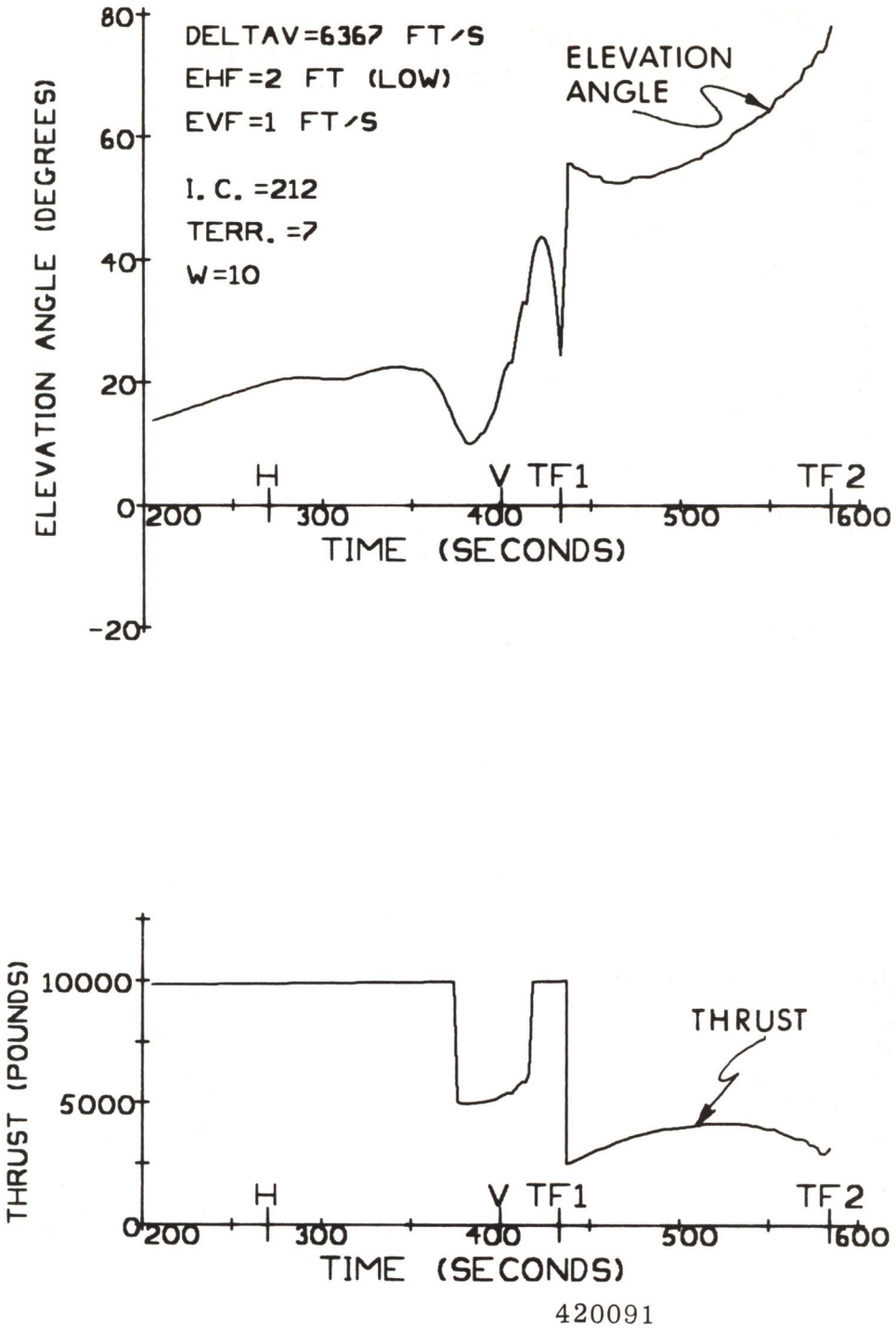

Fig. I.4 Thrust-Vector Profiles: Severe Initial Errors, -1% DPS Uncertainty, Realistic Terrain, Linearized LR Weighting Functions.

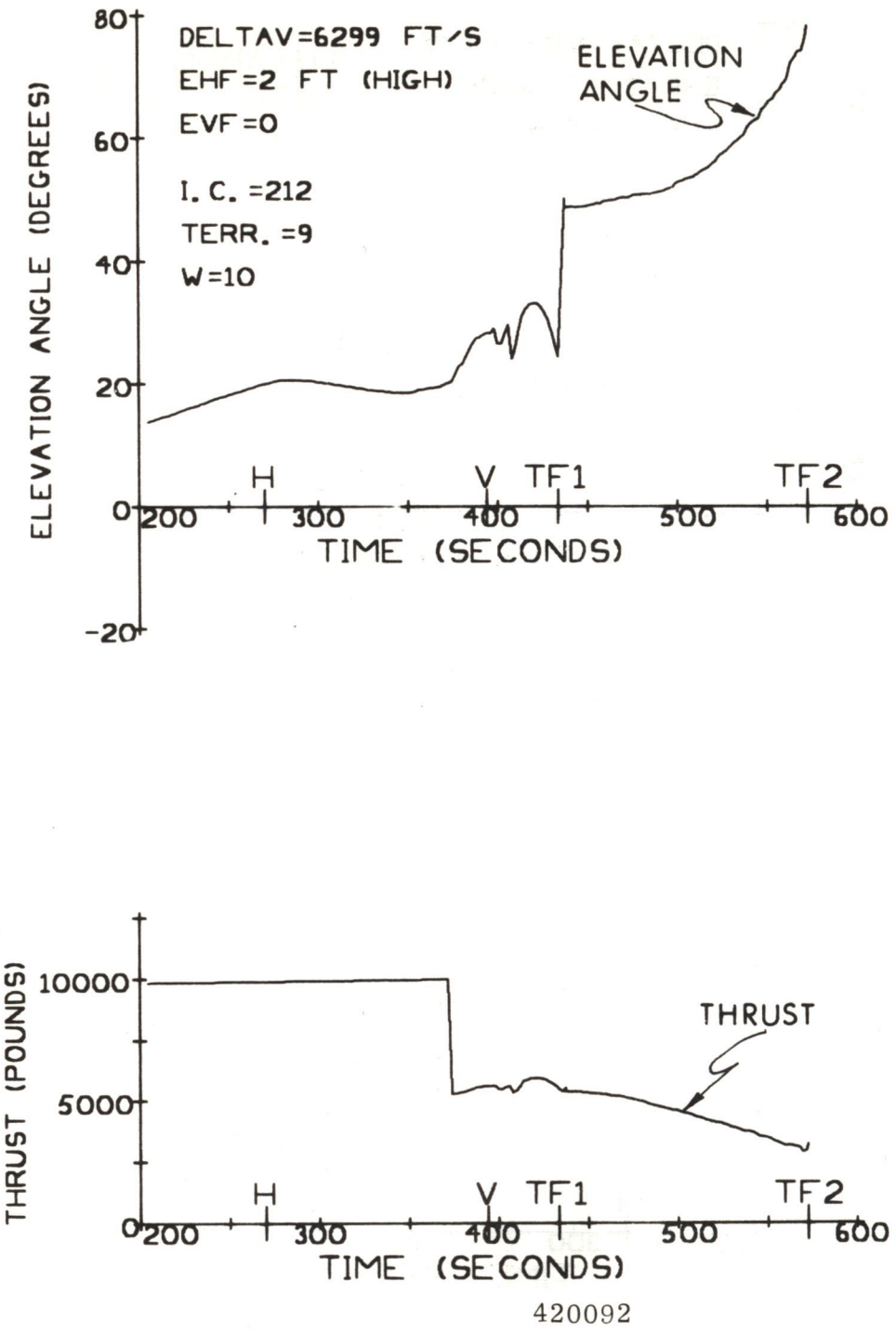

Fig. I.5 Thrust-Vector Profiles: Severe Initial Errors, -1% DPS Uncertainty, Realistic Terrain, Linearized LR Weighting Functions.

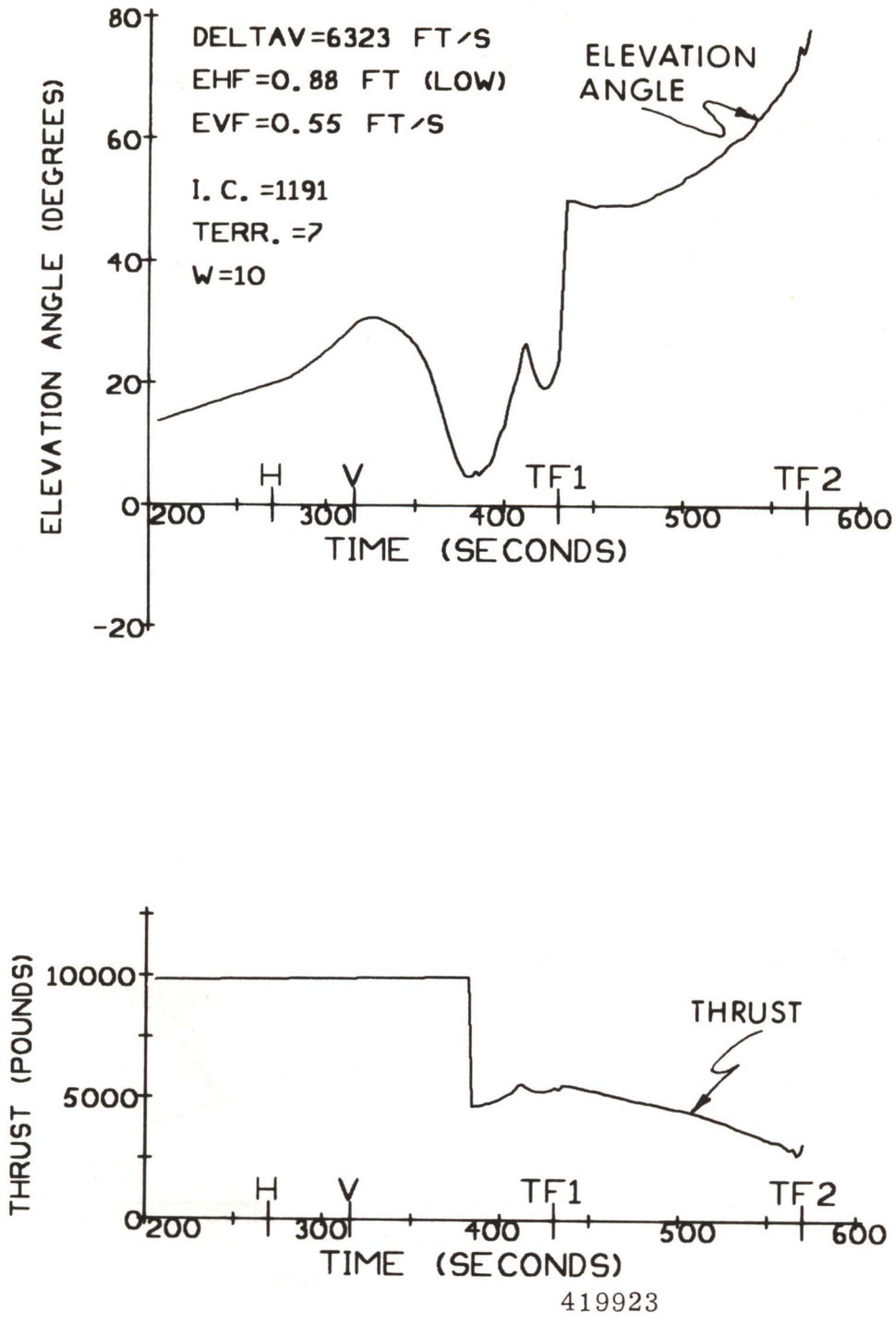

Fig. I.6 Thrust-Vector Profiles: Severe Initial Errors -1% DPS Uncertainty, Realistic Terrain, Linearized LR Weighting Functions.

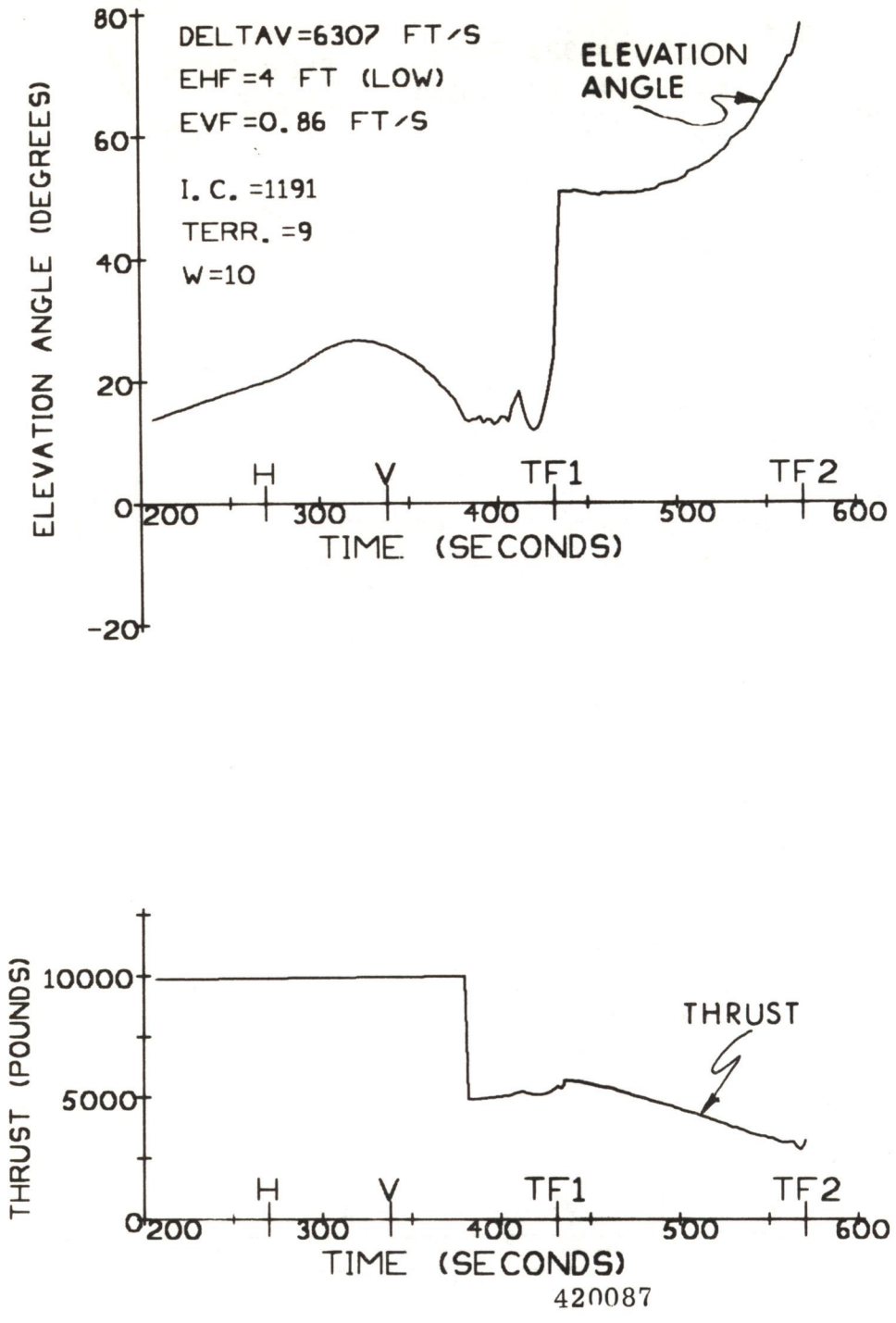

Fig. I.7 Thrust-Vector Profiles: **Severe** Initial Errors, -1% DPS Uncertainty, **Realistic** Terrain, Linearized LR Weighting Functions.

REFERENCES

1. Klumpp, A. R., A Manually Retargeted Automatic Descent and Landing System for LEM, MIT Instrumentation Laboratory Report No. R-539, March 1966.

2. Kalman, R. E., "A New Approach to Linear Filtering and Prediction Problems", Journal Basic Eng., March 1960.

3. Battin, R. H., Astronautical Guidance, McGraw-Hill Inc., New York, 1964.

4. Cherry, G. W., A General, Explicit, Optimizing Guidance Law for Rocket-Propelled Spaceflight, AIAA Paper No. 64-638.

5. Hoffman, P. F., and Sears, N. E., LEM-PGNCS Guidance Equations for a Nominal Lunar Landing Mission, MIT Instrumentation Laboratory Report No. E-1981, May 2, 1966.

6. Klumpp, A. R.,"New LEM Landing Equations and Trajectories", SGA Memo 24-65, MIT Instrumentation Laboratory, October 1965.

7. Bryson, A. and Ho, Y. E., "Optimal Programming, Estimation, and Control", Notes from Course Eng. 204 at Harvard University, (to be published in near future).

8. Kriegsman, B. A., "Radar-Updated Inertial Navigation of a Continuously Powered Space Vehicle", IEEE Aerospace Systems Conf., Seattle, Washington, July 11-15, 1966.

9. Fried, W. R., "Doppler Radar for Guidance-Design Techniques and Performance", ARS Journal, pp. 957-966, December 1959.

10. Fried, W. R., "Principles and Performance Analyses of Doppler Navigation Systems", IRE Transactions, Vol. ANE-4, pp 176-196, December 1957.

11. Berger, F. B., "The Design of Airborne Velocity Measuring Systems", IRE Transactions, Vol. ANE-4, pp. 157-175, Dec. 1957.

12. Berger, F. B., and Henf, G., "The Application of Doppler Techniques to Lunar Missions", Progress in Astronautics and Aeronautics, Academic Press, New York, N.Y., Vol. 13, June 1964.

13. Fitzgerald, R.J., Measurement and Filtering Techniques for Orbital Navigation, Raytheon Company, Space and Information Systems Division, Report FR-65-226-1, July 30, 1965.

14. Bryson, A.E. Jr., and Johansen, D.E., "Linear Filtering for Time-Varying Systems Using Measurements Containing Colored Noise", IEEE Transactions on Automatic Control, Vol. AC-10, No. 1, January 1965, pp. 4-10.

15. Sears, N.E., and Johnson, L.B., PGNS Landing Radar Functional and Performance Specifications, MIT Instrumentation Laboratory Report No. E-1904, February 1965.

16. Muller, E.S., and Goss, R.D., "Deriving Random Error Vectors from Covariance Matrix", SGA Memo No. 56, MIT Instrumentation Laboratory, August 1963.

17. Potter, J.E., "Error Ellipsoids", SGA Memo No. 29, MIT Instrumentation Laboratory, November 1962.

18. Eggleston, J.E., "Lunar Terrain Variations", NASA Internal Memo, January 25, 1965.

E-1982

DISTRIBUTION LIST

Internal

M. Adams (MIT/GAEC)
J. Alexshun
R. Battin (20)
P. Bowditch/F. Siraco
G. Cherry
E. Copps
R. Crisp
J. Dahlen
J. DeLisle
J. B. Feldman
P. Felleman
S. Felix
J. Flanders (MIT/KSC)
J. Fleming
J. Gilmore
Eldon Hall
T. Hemker (MIT/NAA)
D. Hoag
L. B. Johnson
M. Johnston
A. Koso
A. Laats
L. Larson
S. Laquidara (MIT/FOD)
J. Lawrence (MIT/GAEC)
T. J. Lawton
T. M. Lawton (MIT/MSC)
D. Lickly
G. Mayo
J. McNeil
R. McKern
James Miller
John Miller
J. Nevins
J. Nugent
E. Olsson
R. Ragan
J. Rhode
R. Scholten
J. Sciegienny
N. Sears (20)
J. Shillingford
W. Shotwell (MIT/AC)
W. Stameris
J. Suomala
R. Weatherbee
R. White
L. Wilk
R. Woodbury
W. Wrigley
Apollo Library (2)
MIT/IL Library (6)

External:

W. Rhine (NASA/MSC) (2)

NASA/RASPO (1)

L. Holdridge (NAA/MIT) (1)

T. Heuermann (GAEC/MIT) (1)

AC Electronics (3)

Kollsman (2)

Raytheon (2)

Major H. Wheeler (AFSC/MIT) (1)

MSC: (25 + 1R)

National Aeronautics and Space Administration
Manned Spacecraft Center
Apollo Document Distribution Office (PA2)
Houston, Texas 77058

LRC: (2)

National Aeronautics and Space Administration
Langley Research Center
Hampton, Virginia
Attn: Mr. A. T. Mattson

GAEC: (5 + 1R)

Grumman Aircraft Engineering Corporation
Data Operations and Services, Plant 25
Bethpage, Long Island, New York
Attn: Mr. E. Stern (3 + 1R)
Mr. P. Hoffman (1)
Mr. J. Eichler (1)

NAA: (18 + 1R)

North American Aviation, Inc.
Space and Information Systems Division
12214 Lakewood Boulevard
Downey, California
Attn: Apollo Data Requirements AE99
Dept. 41-096-704 (Bldg 6)

NAA RASPO: (1)

NASA Resident Apollo Spacecraft Program Office
North American Aviation, Inc.
Space and Information Systems Division
Downey, California 90241

ACSP RASPO: (1)

National Aeronautics and Space Administration
Resident Apollo Spacecraft Program Officer
Dept. 32-31
AC Electronics Division of General Motors
Milwaukee 1, Wisconsin
Attn: Mr. W. Swingle

Defense Contract Administration (1)
Service Office, R
Raytheon Company
Hartwell Road
Bedford, Massachusetts 01730

Mr. S. Schwartz (1)
DOD, DCASD, Garden City
605 Stewart Avenue
Garden City, L.I., New York
Attn: Quality Assurance

Mr. D. F. Kohls (1)
AFPRO (CMRKKA)
AC Electronics Division of General Motors
Milwaukee 1, Wisconsin 53201